UNIVERSITY OF CANTERBURY

Department of Mechanical Engineering

Christchurch New Zealand

Grinding Sludge Oil Recovery Transportation System Development

by

C. Chen

A thesis submitted in partial fulfillment of the

requirements for the Degree

of

Master of Engineering

at the University of Canterbury

25th July 2003

ABSTRACT

Patience & Nicholson (NZ) Limited, a Canterbury based drill bits manufacturing company is currently suffering heavy losses of grinding oil from their recycling facility. With the high production rate, approximately 80 tons of waste sludge is produced after the recycling process every year, and 20-30% of the weight of the swarf is the entrapped oil. This waste product from the fluke grinding process is currently discarded. An estimated saving of $40000 can be achieved if this oil from the swarf can be recovered, then the remaining steel powder can be sold to the material supplier in France. With this unnecessary loss of material is why Patience & Nicholson wish to understand the feasibility of the development of a recovery system to recycle the oil and steel from the swarf.

The aim of this work was to develop a transportation system which copes with both the current and new extraction facility. The clean swarf was required to be loaded into 200 gallon barrels. The flow property was determined and the physical limitation from the entry port of the barrel was perceived. With the understanding of M2 steel property, several transportation methods were investigated to reduce abrasion during transportation. A transportation method via a multi linkage was selected.

A full scale flow channel were designed and constructed to simulate the discharge from hopper to barrel in the actual system. Formation of lumps and unexpected moisture resulted as flow obstruction from dome formation was experienced within the flow channel. The dried, sieved powder was found to flow well with the currently design. Hence, enlargement of the current design is required to compensate the unpredictable humidity contained within the clean swarf after extraction. A direct injection of compressed air can then be implemented for arch destruction at the predicted locations.

ACKNOWLEDGEMENTS

I would like to express my appreciation to a number of people whose support and encouragement made this thesis possible.

Firstly, to my supervisor **Dr David R. Aitchison** without whom the opportunity to undertake this project would not have existed. Secondly, to **Dr Shane D. Gooch** AND **Dr S. Ilanko** on the excellent guidance and technical support on my thesis, and **Dr Keith Alexander** for the consultations on the test rig design, while my supervisor is on leave.

Thanks to the workshop staff: **Scott Amies** for the scheduling of the production, **Paul Wells** for the construction and modification of the test rig and manufacturing suggestions, **Ken Brown** for unlimited quick access to all the parts in the storeroom, and **Rodney Elliott** on the purchase of pneumatic components. Thanks to **Kelvin Stobbs** and **Eric Cox** on the suggestion of particle size measurements and the available space for testing. Also, many thanks to **Julian Murphy** and **Julian Phillips** on the expertise and guidance on the selections of sensor and limit switch.

Thanks to the staff in Chemical & Process Engineering (CAPE): **Professor John Abrahamson** for his guidance on the investigation of the cyclone separation, and also Miss **Christine A. Nichol** on both the technical and information support associated with this project.

Thanks to the staff in **Chalston Engineering** for their admirable patience and valuable suggestions when consulted on the details.

Thanks to all the staff in the **Academic Skill Centre: Writing and Study Skills (WASS)**, for their patience and grammatical support.

Thanks to all the friends, **Angelo C. Garcia, Ben Low, Andrew Tsai, Eric Hung, Siew King Hung, Angela Chen, Dean Kirk** my room mates **Amanda Batchelor, Allan Saville** for all their support, encouragement and wonderful times during the difficult period.

Finally, to my family, many thanks to my parents both the financial support and encouragement on the research, and also my girl friend, **Biddy O**, for being there for me all the time.

Table of Contents:

6. Design Validation

6.1

7. Prototype Valve Testing

8. Discussion

9. Conclusion & Recommendation

10. Reference

10.1 Journals

10.2 Final Year Reports

10.3 Textbooks & Other Source of Information

Appendix

1. INTRODUCTION

1.1 Company Overview

The Canterbury based company Patience & Nicholson, a fully owned subsidiary of Sutton Tool Pty Ltd of Australia, is a main supplier of high-speed steel drill bits for the national and international market. Several renowned brands include Evacut, P&N, Sutton Tools, as shown in Figure 1.1; these quality products are well-distributed into the industrial supply network throughout Australasia and Southeast Asia.

(a) **(b)** **(c)**

Figure 1.1, Different variety of cutting and drilling tools produced by Patience & Nicholson, (a) stub drills, (b) tool bits, and (c) reduced shank drills (Source: Patience & Nicholson website)

1.2 Material and Manufacturing Process

Tool materials first developed in the 1900s largely focused on use in high-speed cutting tool application, and was then named High Speed Steels (HSS); they were the most highly alloyed tool and die steels, which were able to maintain their hardness and strength at elevated operating temperature. With the properties of high toughness and resistance to fracture, high-speed steels are suitable for high positive-rake-angle tools (small included angles), interrupt cut, and for machine tools with low stiffness, which are subject to vibration and chatter **[13,17]**. High-speed steel tools may also be subject to surface treatments, such as case hardening for improved hardness and wear resistance. Improved performance in machining such as reducing built-up edge formation can be achieved by developing a black oxide layer from steam treatment at elevated temperature, and coating with titanium nitride and titanium carbide for better wear resistance.

There are two basic types of high-speed steel: the molybdenum (M-series) type and the tungsten (T-series) type. Generally the M-series have slightly higher toughness than T-series at the same hardness; otherwise, the mechanical properties of these two types are similar and equivalent in performance. However the main difference is in cost approximately 40% lower for M-series than that of similar T-series steels. This results from the lower atomic weight of molybdenum, about one-half that of tungsten, therefore, based on weight percent, to achieve the same atom ratio, only about one-half as much molybdenum as tungsten is required **[18]**.

The M-series generally has higher abrasion resistance than the T-series, undergoes less distortion during heat treating, and is less expensive; therefore they are the most widely used tool material today, and dominate about 95% of the tool products in US. All the drills manufactured from Patience & Nicholson are produced from M2 tungsten-molybdenum high-speed steel, which has very good toughness and wear-resistant properties, and Table 1.1 shows the composition limits of principle of M2 type tool steel.

Table 1.1, Composition limits of principle of M2 type tool steel (Source: ASTM International Handbook Committee [18])

Designation		**Composition (%)**								
AISI	UNS	C	Mn	Si	Cr	Ni	Mo	W	V	Co
M2	T11302	0.78-0.88: 0.95-1.05	0.15-0.40	0.20-0.45	3.75-4.50	0.30 max	4.50-5.50	5.50-6.75	1.75-2.20	…

The increase of the carbon and vanadium contents of M-series steels increases wear resistance; increasing the cobalt content improves red hardness (that is, the capability of certain steels to resist softening at temperatures high enough to cause the steel to emit radiation in the red part of the visible spectrum) but simultaneously lowers toughness **[18]**. The general properties of the M2 tool steel are listed in Table 1.2.

Table 1.2, Properties of M2 tool steel (Source: ASM International Handbook Committee [18])

Designation	**Major factors (a)**			**Hardness, HRC**				
AISI	Wear resistance (b)	Toughness (c)	Hot hardness	25°C	315°C	425°C	540°C	650°C
M2	7	3	8	65	62	59	55	36

Note: Rating range from 1 (low) to 9 (high) for (a), (b) and (c).

The material for all the high speed steel drill bits made by Patience & Nicholson is supplied by **Erasteel, Champagnole Cedex, Frence [10]**. These high-speed steels are available in wrought, cast and sintered forms, therefore further machining is required.

The manufacturing process involved in drill bits production is a conventional pendulum fluke grinding. The wheel depth of cut is small with a relatively high working speed; hence only a thin layer of material can be removed with each pass; in order to achieve the demand dimension, the wheel is cycled back and forth across the work, hence described as having pendulum motion. This process has been applied mainly to the materials which are difficult to grind in the circular surface grinding or profile surface grinding modes **[15]**. Grinding fluid must be introduced at the point at which the wheel enters the work. With a precise location and orientation of the nozzle, the fluid provides a uniform coverage over the wheel-work contact area and reduces the high temperature generated from the creep feed grinding process. As demonstrated, the cutting fluid has three main functions in the contact zone: (1) conducting heat away, (2) reducing friction, and (3) carry away chips.

The material is fed automatically into the grinding machine and pendulum fluke grinded with the abrasive medium such as Al_2O_3 or cubic boron nitride (CBN). Grinding fluid with particles removed from the work piece is flushed into the onboard filter medium which entraps the solid particles and drains the fluid away. The swarf is collected regularly and separated with the existing separation system; approximately 70~80% weight (% wt) of the fluid can be recycled from the facility, and the rest remains entrapped in the swarf and disposed as waste.

1.3 Current Oil Recycling Process

Currently a coopermatic filtration system is employed in Patience & Nicholson to recycle the grinding oil from the swarf. A diatomaceous earth filter aid is coated on the pipes within the filter. The grinding particles and oil mixture are first deposited on those pipes from the circulating stream, when sufficient volume has reached; it is then transferred by compressed air to a pressure chamber which is attached to a collection pot. The collection hopper (pot) and pressure chamber are jointed by the locking devices located outside the chamber wall. The mixture of grinding particles and oil is then landed on a bed located inside the hopper, where the Dacron mat is, as shown in Figure 1.2.

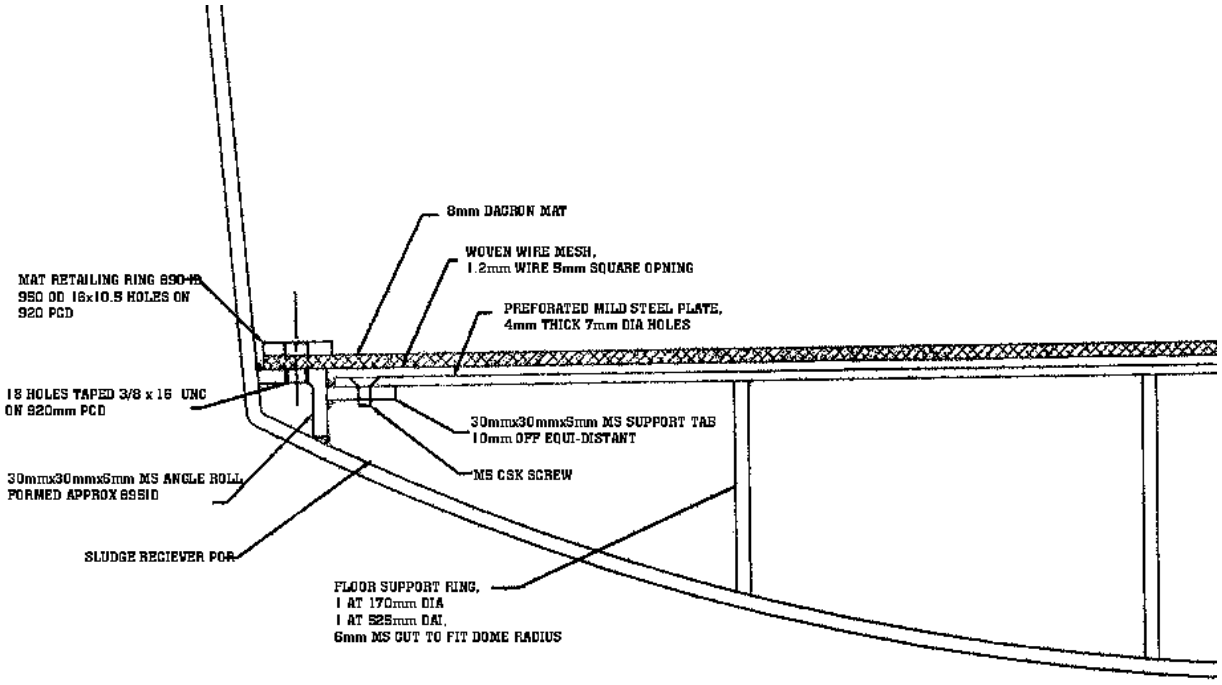

Figure 1.2, Detail hopper (pot) bed description (Source: C. A. Nichol)

Compressed air is blown at high pressure through the sludge bed from the inlet located on the pressure chamber above the hopper, and forces most of the oil from the sludge to drain out. This oil is then returned to the intake of the filter then reused in the factory. The overall oil recovery process takes approximately 24 hours, or until filter cleaning requirement occurs. The amount of oil remaining within the sludge after this recycling process will heavily depends on the operation pressure and time, and also the particle size. A dry cake is formed after the filtration process, however, it is still oily to the touch, since there is 20~30% wt of oil still entrapped in the swarf.

1.4 Sludge Recycling Potential

Patience & Nicholson Christchurch based head office and manufacturing facility currently has a problem with high losses of cutting oil. The oil would be reusable but unfortunately it gets trapped in with the waste steel swarf given off during machining. The oily grinding sludge contains fine steel grindings, grinding media (non-metallic particulates such as silicon carbide and aluminium oxide), and other non-hazardous solids, all of which are covered with a residue of adsorbed cutting oil.

At the moment, the grinding sludge is filtered in a diatomaceous earth filter to recover most of the oil. However, after the first stage of the oil recovering process, about 20~30%wt **[1, 10]** of oil is still entrapped, further extraction is difficult with the available facility, and so the dried sludge is currently discarded along with the residual oil. The company currently discards approximately 80 tonnes of grinding waste per year, and it was predicted that savings of $25,000 **[1]** on purchasing fresh oil could be achieved if the oil can be recovered and re-used. This unnecessary loss of material is why Patience & Nicholson have put this project to the Mechanical and Chemical & Process Engineering Department at University of Canterbury. They wish to understand the feasibility of the development of a recovery system to recycle the oil and steel after the first stage separation process.

A literature research showed that a complete recovery and recycling procedure for the oily waste must involve a multi-stage separation process, and this project focuses mainly on the removal of oil (and if possible also the phosphorous) remaining in the solid matrix after first stage separation with the existing facility within the company. At the outset of the project the technical criterion for the oil in the sludge content was set at 1%wt, set by **Grigor, J. E. [1]**; as for the phosphorous acceptable recycled level, it is 0.003% wt or less, which was set by **Matthews, M. A.** *et al* **[2]**.

The counter-current leaching process developed by Chemical & Process Engineering at the University of Canterbury **[1]** was found to be able to successfully remove the oil to less than 1%; however, the phosphorous content is still over the acceptable level. Subsequent recovery of the steel by-product is achievable with the use of an aqueous cleaning method **[2]** to remove the phosphorous, but an additional separation process is required, which will further increase the capital spending on the recovering system.

1.4.1 Grinding Oil

A mineral oil with additives was selected as the grinding fluid for the manufacturing process by the Patience and Nicholson. The oil acts as a grinding lubricant along with additives such as fatty acids, phosphorus compounds, and sulphur compounds to form easily-shearable boundary layers through chemical reaction to prevent metal asperity contact and the accompanying instantaneous local welding. The fatty acids react with the freshly-exposed metal surface at normal temperature forming soaps, and this soap film ensures adequate lubricant performance under light cutting conditions. The phosphorus compound reacts with iron at temperature between 500-700°C and forms surface layers of iron phosphide. Low quantities of free sulphur are suitable for difficult steel cutting operations, and the effectiveness of these substances starts about 700°C and the boundary layers produced can maintain stability to about 1200°C **[11]**.

With the health and safety issue on the application of the water-insoluble coolants in the manufacturing process, minimum exposure of operators to odours and oil mist is required, therefore the temperature of the coolants supplied to the working zone was suggested to be kept near 20° and not exceeding 30° **[11]**. Regarding the life time of the oil, it was found that a low oil temperature results in a definite increase in the operating life of the oil fill. A rough estimation value is that above 70°C, each 10°C temperature rise doubles the reaction speed of oxidation, hence reduce the life time. These temperature limits will have a significant implication on designing the recycling process.

1.4.2 Environmental Issue & Cost Benefit

With heightened awareness of environmental issues and production costs, it is important to be able to recycle this grinding oil. The increasingly strict environment regulations have resulted in an elevated landfill cost, therefore recycling will not only reduce industrial waste that can be damaging to the environment but also reduce the cost of production. From the landfill census conducted by the Ministry for the Environment in New Zealand, and the figure provided by Patience & Nicholson in Table 1.3, a dramatic increase in the landfill cost was observed over the 5 year period.

Table 1.3, Landfill cost (Source: Ministry for the Environment in New Zealand at 1995 [23], and Patience & Nicholson (NZ) Ltd in 1999 [1], and 2000 [10].)

Information Provider & Date	Cost per ton
Ministry for the Environment, New Zealand (1995)	$27.62
Patience & Nicholson (NZ) Ltd (1999)	$150.00
Patience & Nicholson (NZ) Ltd (2000)	$187.50

With the cost of $15,000 annual spending on disposing the grinding waste the from drill bits manufacturing process, the total saving after a complete recycle of oil can bring a net saving of approximately $40,000 per year, plus the additional trading on the by-product with the high-speed steel manufacturer. Hence, a significant environmental and financial long term benefit will be a consequence for the company when a complete recycling system is implemented.

The payoffs from the recycling system can be significant and include: reduced liability, more efficient use of natural resources, reduced treatment and disposal costs, lower environmental impacts, reduced regulatory costs, and improved public relations. Short-term waste disposal costs have increased dramatically in recent years and will continue to increase. Potential long-term costs of waste disposal associated with the liability for environmental damage cannot be estimated and have no financial ceiling. Therefore, these short-term disposal costs and the potential for long-term liability have combined to make minimization of waste economically attractive.

1.4.3 Alternative Solutions

The supercritical carbon dioxide extraction process developed by Chemical Engineering at the University of South Carolina **[2]** can remove up to 80%wt of the oil without going through the diatomaceous earth filter, and bring the phosphorous level to as low as 0.014%wt. Further extraction of oil can then be done with hexane; however, this will raise the capital investment by a huge amount, which could be uneconomical.

1.5 Overview of Background

Eventually the steel, which raises other problems in waste disposal terms, will be able to be recycled. The clean dried swarf will be loaded into a standard 200 gallon barrel and returned to the manufacturer. At this stage, the continuing development of the counter-current leaching system and other associated hexane recycling systems is underway, therefore material handling and transportation mechanisms for these systems are required. The feasibility of the recovering process at this stage is clear, and further development of the recovery system will be weighted out on an economic basis by the company.

This project is offered in conjunction with Chemical & Process Engineering at the University of Canterbury; hence the workload has been evenly shared between both parties involved. An oil recovery system is required to be designed by Chemical and Process Engineering, and powder transportation system from Mechanical Engineering. The solution from each individual party is required to cope with both the work partner and the existing company facilities, and together to form a complete system for Patience & Nicholson (NZ) Ltd.

1.5.1 Development of Oil Recovery System

A laboratory experiment has been conducted by **Nichol, C. A. [10]** from Chemical & Process Engineering at the University of Canterbury associated with the implementation of hexane in the oil recovery process and the outcome of a preliminary recovery system design as shown in Figures 1.3 and 1.4 respectively.

(a) **(b)**

Figure 1.3, Oil recovery experiment conducted by C. A. Nichol from Chemical and Process Engineering at the University of Canterbury, (a) the leaching experiment, and (b) the separation of oil and hexane mixture.

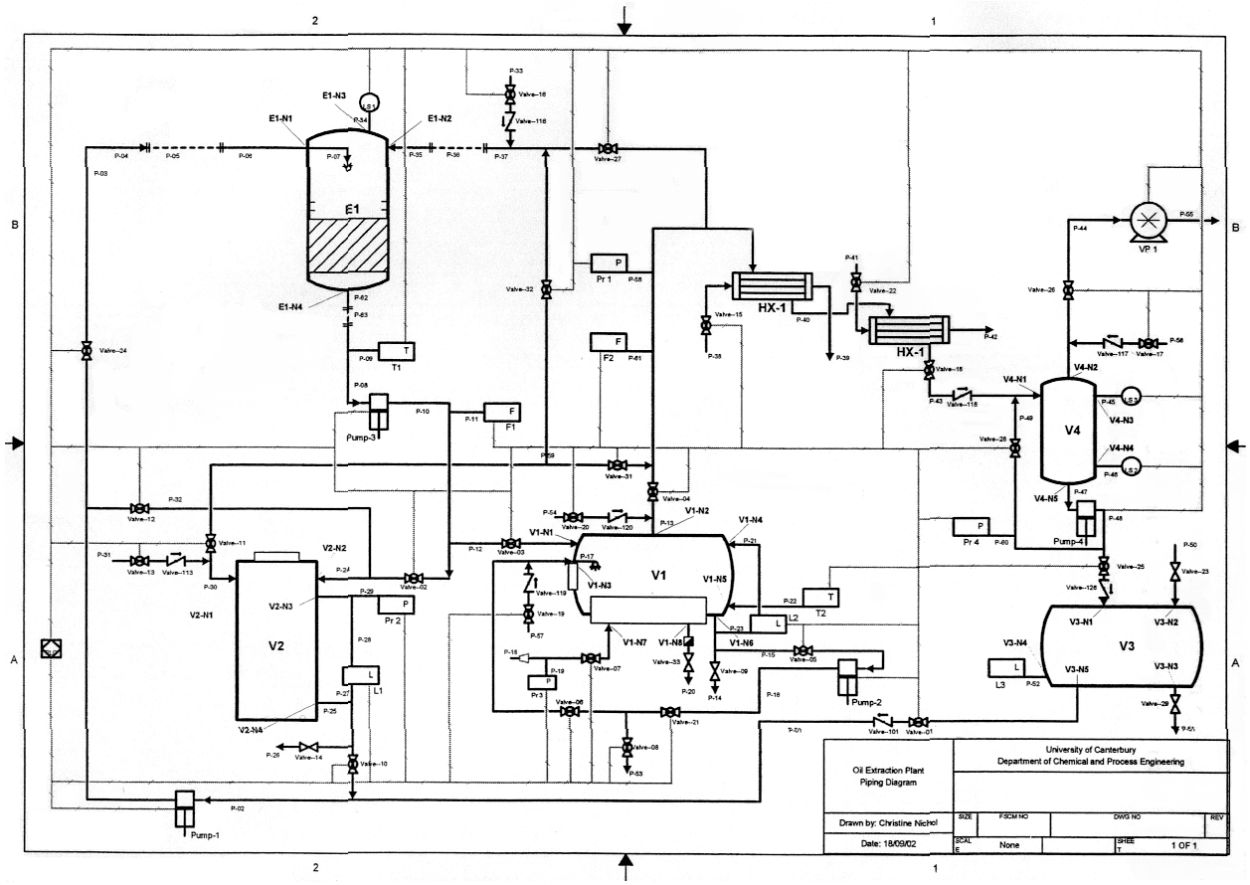

Figure 1.4, Preliminary design of the secondary recovery system (Source: Nichol, C. A. [10])

The oily swarf was located inside the hopper after the first stage oil recovery process with the diatomaceous filter. The hopper is then placed onboard the existing trolley designed by the company, and transported to the newly designed oil recovery system.

From **Grigor's [1]** experiment, to achieve the acceptable swarf recycling criteria, the residual oil level contained within the swarf needed to be washed twice with hexane. The first stage wash takes place by flushing the hexane from Tank V2 to the extraction chamber. The solvent percolates through the swarf bed by gravity and then drains out from the hose connected at the bottom of the hopper and collects in evaporator V1. Tank V2 has a charge of slightly oily hexane left over from the previous charge of swarf, therefore after two washes, the oil contained within the hexane is saturated, and ready for separation. The second stage leaching process is similar to the first stage wash; however, hexane drained from the extractor chamber is stored in Tank V2 for the next charge of swarf.

Since the boiling point of hexane if far lower than the oil, with additional heat to the hexane-oil mixture, hexane can be vaporised and extracted from the evaporator chamber then condensed for storage in Tank V3 and remaining inside Tank V1 is oil. As for the clean

swarf, after washing with hexane, instead of oil trapped within the metal matrix, it is now hexane. With the vapour pump VP1, air is then pulled through the bed, collected and condensed for recycling the hexane at Tank V4 for further use.

1.5.2 Development of Powder Transportation System

After two stages of oil recovery processes, the swarf is now clean and ready to be packed into 200 gallon drums and shipped to the manufacturer in France. With the preliminary understanding of the material properties, and physical restriction of the barrel provided by the company, few problems associated with the current swarf packaging process can be foreseen.

Currently, the swarf is contained inside the hopper onboard the trolley after the first stage oil recovery process with diatomaceous filter. A forklift is used to suspend the trolley and locate it above the waste collection bin then the operator manually rotates the hopper with a lever arm to discharge the swarf. The swarf was in a dense cake form due to the pumping action of the diatomaceous filter which was compressing the swarf together. As a result of the swarf cake being broken during hopper rotation, lumps of swarf can be observed as shown in Figure 1.5.

(a) **(b)**

Figure 1.5, Images of the dirty swarf, (a) dirty swarf in the container, and (b) lumps of dirty swarf

Since the swarf contains approximately 20% wt of oil within the metal matrix, therefore particles are able to keep relatively close together with the viscous oil, and hence flowing of lumps were observed rather than individual flow of particles during discharge. With the current discharging process, workspace safety requirements set by OSHA (Occupational Safety & Health Association) can easily be achieved by employing masks during the discharging operation. This is mainly due to the heavier weight of swarf lumps which are

harder to become airborne, therefore less dust flies in the surrounding environment. However, after the secondary oil recovery process, the absence of oil results in a dramatic change of the swarf properties. Particles are now lighter and can be transported by air easily, which consequently raised the safety concern for the operator.

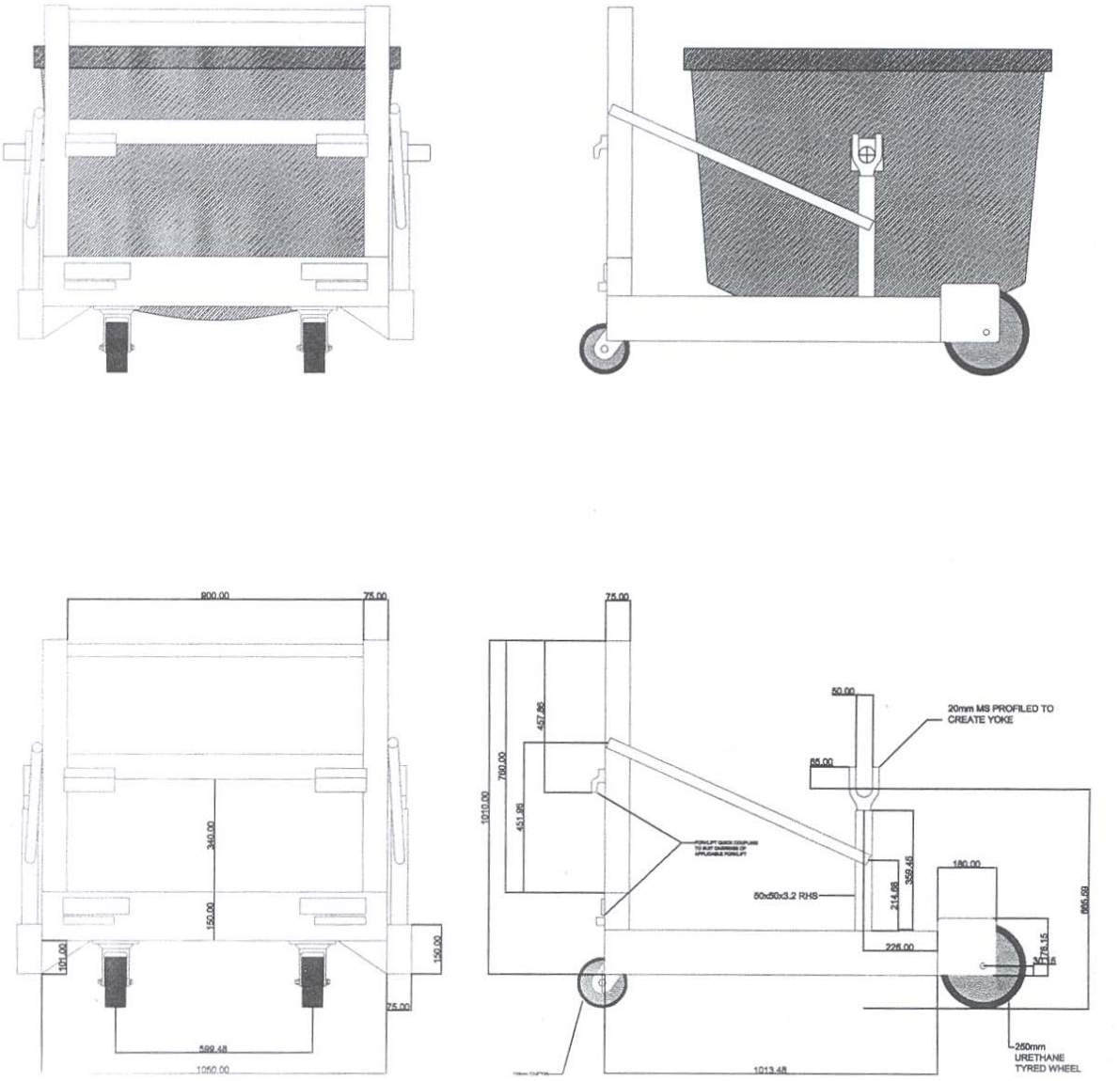

Figure 1.6, Hopper and trolley currently in use by the company (Source: C. A. Nichol)

Moreover, with the physical limitation on the barrels, powder contained within the hopper may not be able to be loaded with the current facility; hence a transportation system is required to be developed to adopt the existing setting of the facility and also the new oil recovery system, as shown in Figure 1.6 and 1.7 respectively.

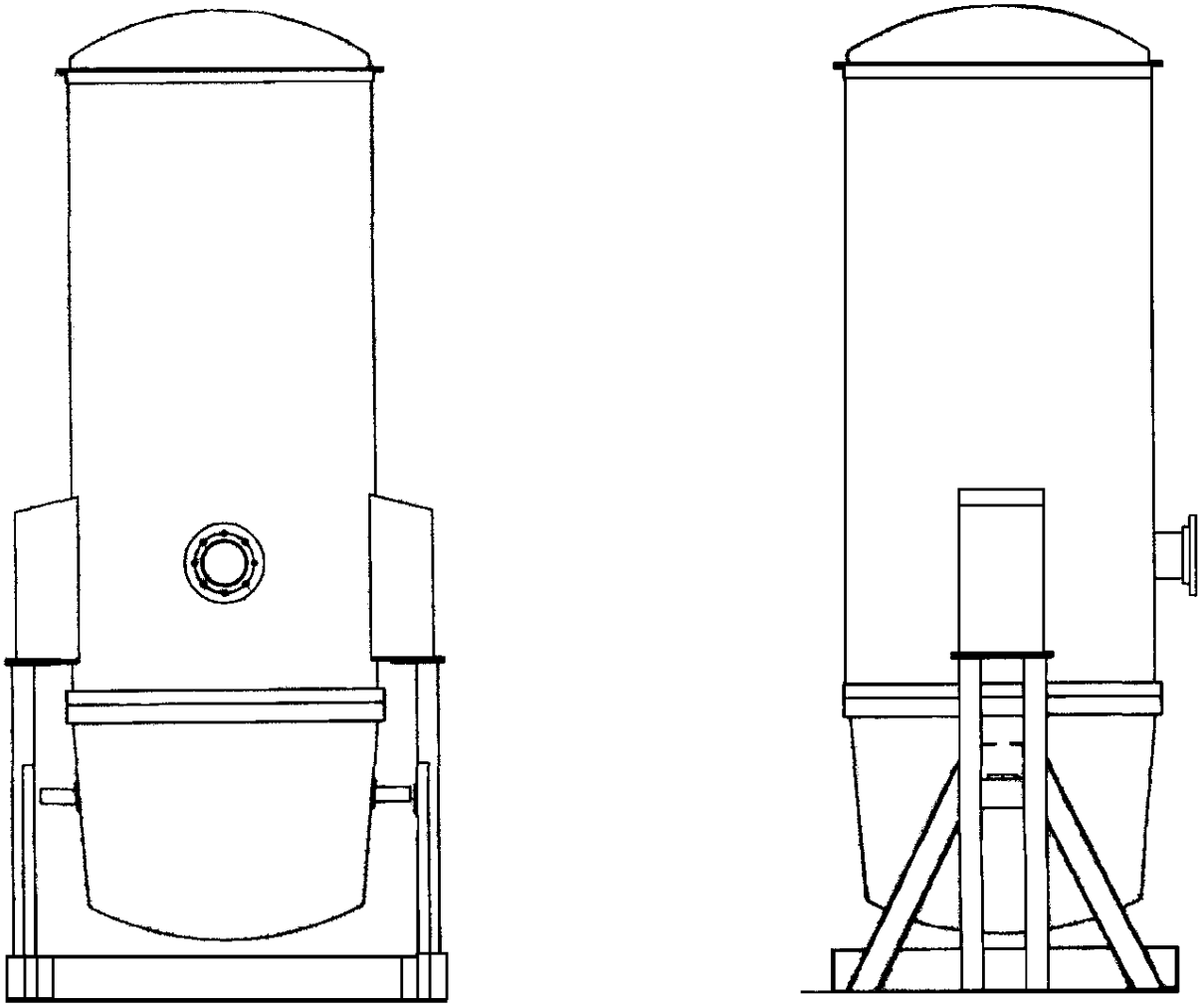

Figure 1.7, Extraction facility developed by Chemical & Process Engineering at University of Canterbury (Source: C. A. Nichol)

1.5.3 Scope of This Project

Currently, there is still 20~30% wt of oil entrained in the sludge after the first stage recovery process. From the research done by the Chemical & Process Engineering Department at the University of Canterbury, a process involving hexane to recover the remaining oil from the sludge, may require two stages of recovering process to keep the oil content to the acceptable level of below 1%. Although this part recovers the oil, the by-product still has a high level of phosphorous content, therefore at this stage the by-product will have to be loaded into barrels and melted down in a furnace for further recycling.

The aim of this project is to develop material transportation systems in conjunction with the separation process developed by Chemical & Process Engineering at the University of

Canterbury. This project focused mainly on the development of material transportation which incorporates with both the existing facility in Patience & Nicholson (NZ) Ltd and the new facility designed by **Nichol, C. A. [10]** from Chemical & Process Engineering. Exploration of different transportation methods and system control methods in order to implement these technologies into a transportation system design will be the goal for this project. Therefore, the chemical separation process design and development will not be taken into account; however, the basic understanding of relative separation techniques and chemical analysing knowledge is essential.

1.5.4 Thesis Outline

This thesis will be presented as follow:

Chapter 2: Background Theories – this section of the thesis outlines the background theories which the project has investigated, and their significance in the process selection and the transportation system design.

Chapter 3: Design Specification – this chapter presents the investigation on the powder properties and understanding of their effect on the physical restriction of the design. A study of the possible processes which can be implemented into the transportation system design were analysed; the advantages and disadvantages were defined for each process involved in the selection.

Chapter 4: Conceptual Design – this chapter shows the concept of the type of transportation system selected previously, and the direction of development towards a converged solution.

Chapter 5: Embodiment Design – further development of the transportation system is conducted and presented as a preliminary solution mainly due to the withdrawal of the industrial sponsorship.

Chapter 6: Design Validation – an experiment was designed and conducted to validate the design work which has been carried out in this project. The results were analysed and the key research findings are summarised with recommendations on the development direction for further work.

2. BACKGROUND THEORIES

In the engineering world, there are many ways to implement the latest technologies to solve a particular task; however, the economic will always become an important priority factor in the final process selection.

In this section, a number of the background theories were carefully studied, and its feasibility for further implementation will not only be judged based on the performance, efficiency, and safety, but also long term operating cost. This chapter will introduce the two main theories which have being considered possible pre-selection processes, they are the ***Powder mechanics*** and ***Cyclone separation***, and are listed below:

1) ***Powder Mechanics*** – study of bulk solid property, and understand the requirement for flow to occur within a discharge funnel, and any possible formation of arch or dome which obstruct the powder flow. This investigation can lead to a successful design of a discharge mass flow bin, and significantly reduce the loading operation time.

2) ***Cyclone Separation Method*** – study of centrifugal separation system with fluid as the transport medium to remove the solid particles in the air stream by the centrifugal force. This is a common industrial separation process, which has been recommended as a simple and economical ways of separating particles from the carried medium.

Additional researches during the project period regarding the implementation of vortex in the transportation system have been documented in Appendix C.

2.1 Powder Mechanics

When the phrase "flow of solid" is mentioned, one is inclined to assume – by association – that the solids dynamically behave much like liquid during motion, due to the fact that the word "flow" is more often used associated with fluids than with solids. Such an assumption is incorrect since the properties of these two phases are quite different.

From **Jenike, A. W., [31],** a bulk solid has to be considered as a plastic rather than a visco-elastic continuum due to the following three major differences:

- Under static conditions, solids form piles whereas liquids form a levelled surface. This is due to solids having a static angle of friction greater than zero, therefore solids can transfer shearing stress under static conditions and liquids cannot.

- Most solids possess cohesive strength which occurred when consolidated – that is after pressure has been applied to them, they retain a shape under loading and form a stable dome or arch; liquids cannot do that.

- Since the shearing stresses occur in a slowly deforming process for bulk solids, therefore they can usually be considered independent of the rate of shear and dependent on the mean pressure acting within the solid. As for liquids, the shearing stresses are dependent on the rate of shear and independent of the mean pressure.

Powder mechanics theories were based on the fundamental of soil mechanics. Due to their cohesive behaviour, powders were regarded as free flowing in soil mechanics. Therefore, powder mechanics is the work based on soil mechanics theory, further evolved in order to cope with the differences. From **Brown, R. L.** *et al* **[32]**, three fundamental principles have then been developed:

1) Principle of Dilatancy: when a tightly packed mass of granules enclosed within a flexible and inextensible envelope with invariably increases in the overall particle numbers, no deformation is possible until the either the applied force ruptures the envelope or fractures the granules. Shearing loosens up the contacted granules and causes some granules to separate and form surfaces of sliding, permitting relative displacement of granules to occur.

2) Principle of Mobilization of Friction: the maximum frictional force for any two adjacent contact granules in a powder at rest can be reached when the granules are about to move relative to each other. When the frictional force due to shear of a powder reaches its limiting value, a surface of sliding is formed, hence angle of repose can then be determined. This leads to a macroscopic picture in which there can be discontinuity in the stresses or in one of their derivatives with respect to displacement.

3) Principle of Minimum Energy of Flowing Granules: since the flow of powder through an aperture accelerates from rest to steady flowing condition, the granules are rearranged progressively; hence the discharge rate through the aperture can be determined from the shape of the sliding surface at the aperture.

In practice, powder mechanics is used to solve powder flow obstruction problems in the discharge bin design. Flow obstruction such as formation of a dome at the discharge opening, and rat-holing are common problems in the industry, as shown in Figure 2.1.1.

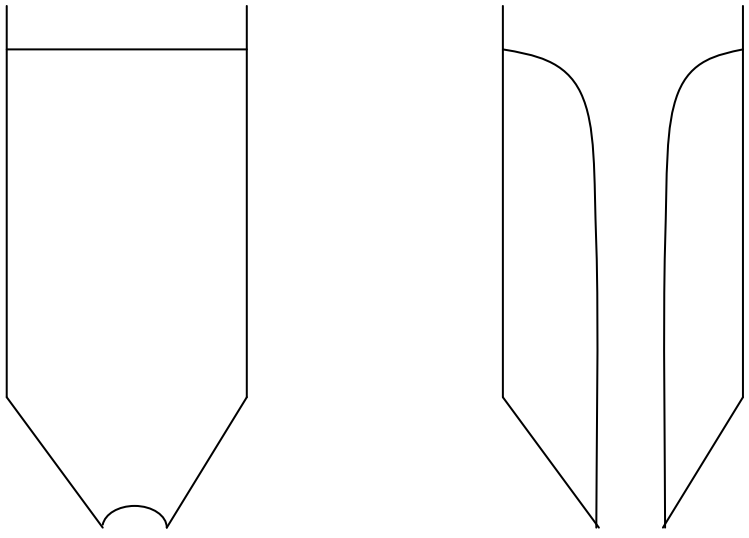

Figure 2.1.1, Type of common flow obstruction occur in the hopper, (a) formation of dome, (b) rat-hole

2.1.1 Coulomb Powder & Yield Locus

For powders contained in a bucket, the stress exerted at any point *P* of the plane has two components; σ is the stress normal to the plane and τ is the stress parallel to the plane, as shown in Figure 2.1.2.

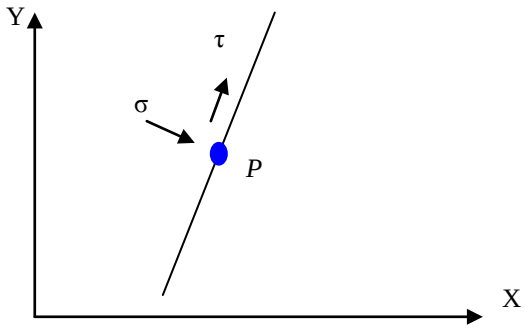

Figure 2.1.2, Normal and shear stress at a point P on a plane

A shear cell is the most widely used instrument designated to measure the bulk material properties, as shown in Figure 2.1.3; a normal force *N* is applied from above, and shear force *S* is applied from the side.

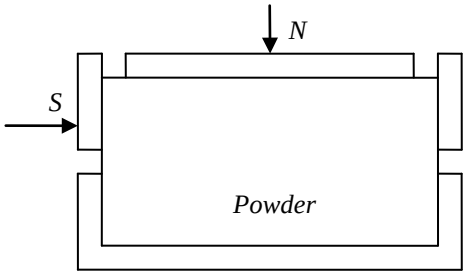

Figure 2.1.3, Force on a powder in base of shear cell

Figure 2.1.4, describes the plane stresses at a point *P* at right angle.

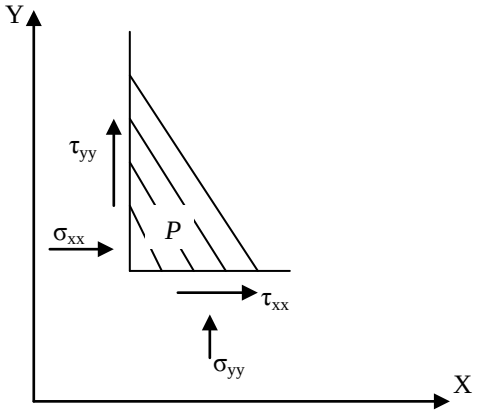

Figure 2.1.4, Plane stress at point P

Consider the small triangle of powder surrounding *P* with the described dimensions in Figure 2.1.5. For plane-stress transformation, the normal stress σ and shear stress τ acting on the point *P* at the hypothetical plane θ, a general equation can be formulated **[32]**,

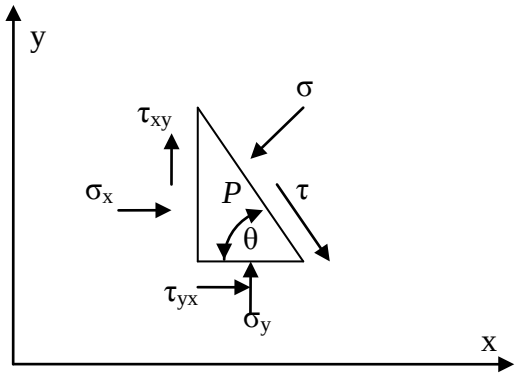

Figure 2.1.5, Stress on a plane at angle θ.

$$\sigma = \frac{(\sigma_{xx} + \sigma_{yy})}{2} - \frac{(\sigma_{xx} - \sigma_{yy})}{2}\cos 2\theta - \tau_{xy}\sin 2\theta \qquad \textbf{(2.1.1)}$$

$$\tau = \frac{(\sigma_{xx} - \sigma_{yy})}{2}\sin 2\theta - \tau_{xy}\cos 2\theta \qquad \textbf{(2.1.2)}$$

Hence, the general equation for the principle stress can be obtained, and Möhr circle can then be constructed as shown in Figure 2.1.6.

$$\sigma_{1,2} = \frac{\sigma_x + \sigma_y}{2} \pm \sqrt{(\frac{\sigma_x - \sigma_y}{2})^2 + \tau_{xy}^2} \qquad \textbf{(2.1.3)}$$

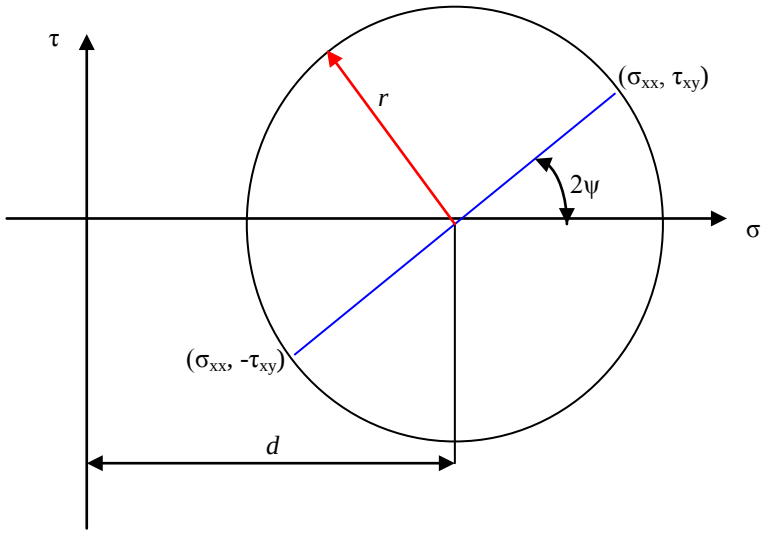

Figure 2.1.6, Möhr circle diagram

$$r = \sqrt{(\frac{\sigma_{xx} - \sigma_{yy}}{2})^2 + \tau_{xy}^2} \quad \textbf{(2.1.4)}$$

$$d = \frac{\sigma_{xx} - \sigma_{yy}}{2} \quad \textbf{(2.1.5)}$$

$$\tan 2\varphi = \frac{\tau_{xy}}{0.5(\sigma_{xx} - \sigma_{yy})} \quad \textbf{(2.1.6)}$$

Consider the force on the sides of rectangle ABCD in Figure 2.1.7,

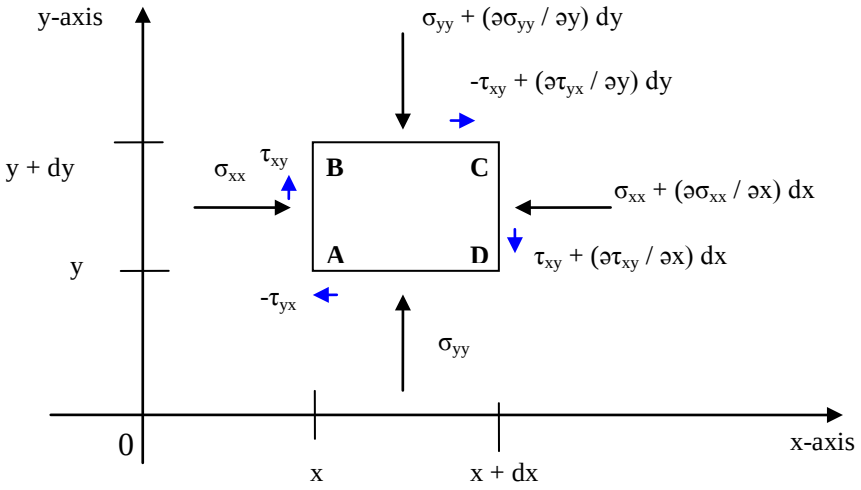

Figure 2.1.7, Stress on a rectangular prism of powder (Source: Brown, R. L., Richards, J. C., [32])

By multiplying the length of the side to the stresses, the forces can then be obtained. Thus the force balance in the x-direction

$$dy\sigma_{xx} - dy(\sigma_{xx} + \frac{\partial \sigma_{xx}}{\partial x} dx) + dx\tau_{yx} - dx(\tau_{yx} + \frac{\partial \tau_{yx}}{\partial y} dy) = 0 \quad \textbf{(2.1.7)}$$

and in the y-direction,

$$dy\tau_{xy} - dy(\tau_{xy} + \frac{\partial \tau_{xy}}{\partial x} dx) + dx\sigma_{yy} - dx(\sigma_{yy} + \frac{\partial \sigma_{yy}}{\partial y} dy) = dxdy\rho_b \quad \textbf{(2.1.8)}$$

For $\tau_{xy} = \tau_{yx}$, the above terms can be simplified to

$$\frac{\partial \sigma_x}{\partial x} + \frac{\partial \tau_{xy}}{\partial y} = 0 \qquad \textbf{(2.1.9)}$$

$$\frac{\partial \tau_{xy}}{\partial x} + \frac{\partial \sigma_y}{\partial y} + \rho_b = 0 \qquad \textbf{(2.1.10)}$$

For an element of solid contained within a discharge bin, the particle flows along the path of the channel, assuming the particles of the element are deposited on the top of the neighbouring particles without out impact. As the element flowing down, the element flows down from this surface is then covered by new layers of the solid **[31]**. Pressures acting on the element increase to a maximum and then decrease as it moves towards the vertex of the channel. The shape of the element changes simultaneously causing the particles of the element to slide on one another, as the pressure increases, the particles are brought closer together then separated apart as the pressure decreases. These pressures cause a change in the bulk density and they are called ***consolidation pressures***. The major pressure on the element is denoted by σ_1 and the minor pressure by σ_2, and the ratio σ_1 / σ_2 varies slightly for a given constant moisture and temperature. This property of bulk solids is usefully expressed by

$$\frac{\sigma_1}{\sigma_2} = \frac{1+\sin\delta}{1-\sin\delta} \qquad \textbf{(2.1.11)}$$

and is referred to as the effective yield function. Angle δ is called the "*effect angle of friction*" and for a given solid has been found to vary only within a few degrees for the range of pressure which occurs in gravity channels. In general, fine and dry solids have low values of δ while coarse and wet solids have large values **[31]**. Figure 2.1.8, shows the construction of the effective yield locus on the Möhr circle.

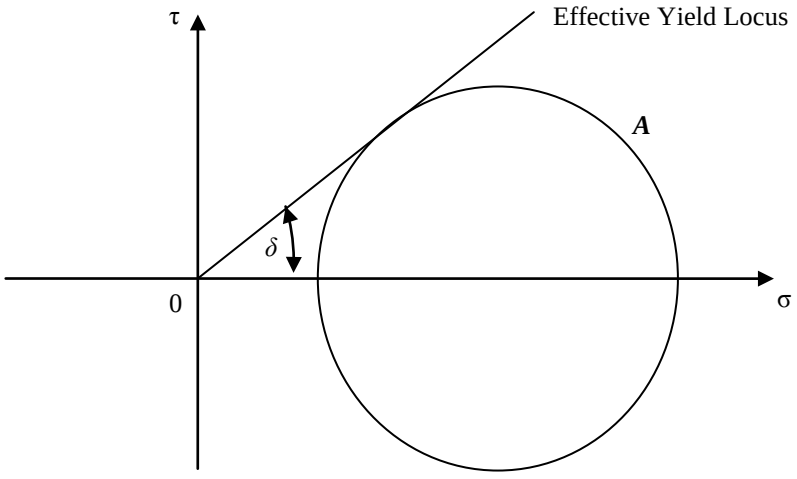

Figure 2.1.8, Formation of effective yield locus (Source: Jenike, A. W., [31])

In discussing the flow – no flow criteria of a powder, consideration regarding the yield strength, which a solid develops as it flows in a channel, is essential. For a cohesive powder, under unconsolidate condition, it has no yield strength, hence the higher the pressure, the greater the consolidation and strength can be obtained for a particular powder **[27]**. Experiment s regarding a particular powder were carried out with the use of a shear cell. When a slip occurs after applying the normal force and shear force, this is sufficient to overcome the angle of internal friction φ, and the result can be expressed with the use of a Möhr circle, which is in terms of yield locus, as shown in Figure 2.1.9.

Sliding occurs when the applied shear force is equal to the shear strength of powder and these materials are called plastic. If the materials are also inelastic, the yield locus is therefore linear; in such a case they are called rigid plastics or Coulomb powders **[31]**. The yield locus for most powders is linear or nearly so for compression stress. From the yield locus, a limiting shear strength under any normal stress is therefore used to define the characteristic of powders and bulk solids.

The yield locus is defined by its slope tan φ and its intercept $-\sigma_a$ on the σ-axis. This intercept can be regarded as an "apparent" tensile strength, then the shear strength τ_f is

$$\tau_f = (\sigma + \sigma_a)\tan\varphi \qquad \textbf{(2.1.12)}$$

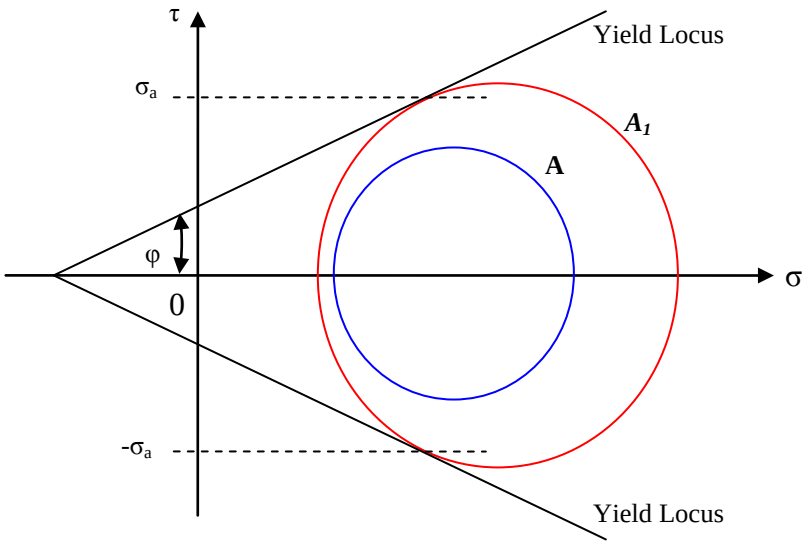

Figure 2.1.9, Mobilization of friction in a Coulomb powder (Source: Brown, R. L., Richards, J. C., [32])

In Figure 2.1.9, the Möhr circle represents the state of stress at point *P* in powder. Any intercepts with yield locus between the circle indicates the frictional forces are fully

mobilised, therefore once sliding takes place, it will continue indefinitely until changes occur on the stress state. The Möhr circle ***A*** is not fully mobilised, since the circle does not intersect with the yield locus, therefore no failure occurs. However, Möhr circle ***A1*** is in tangent with the yield locus, where the frictional forces are fully mobilised and it is said to be in a state of plastic equilibrium. Once the sliding starts, it will continue indefinitely until a change of stress state similar to Möhr circle ***A*** takes place.

In practice, the material is pre-consolidated by placing free weights directly above the powder inside the container. After removal of the free weights, a normal force is gently applied on to the top of the powder, as shown in Figure 2.1.10.

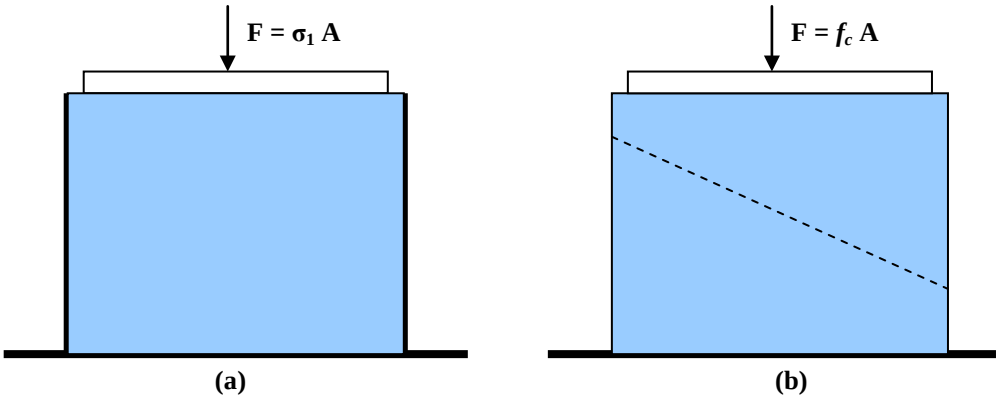

Figure 2.1.10, Set up for measuring the unconfined crushing strength, (a) pre-consolidation, confined in a cylinder, and (b) Normal stress applied to unconfined, pre-consolidated material at failure *f* = *fc*. (Source: Kearney, T., [27])

The stress in the moment of the material's failure gives the *unconfined crushing strength* f_c, which means the applied force causes yield. For the arching problem in a hopper, arching occurs when f_c > F, and the unconfined crushing strength is bigger than the applied strength, therefore when f_c < F, no obstruction will occur **[27]**. For different consolidation pressures applied on the powder result from the shear cell testing, a powder function can be determined from the Möhr circle diagram, as shown in Figure 2.1.11.

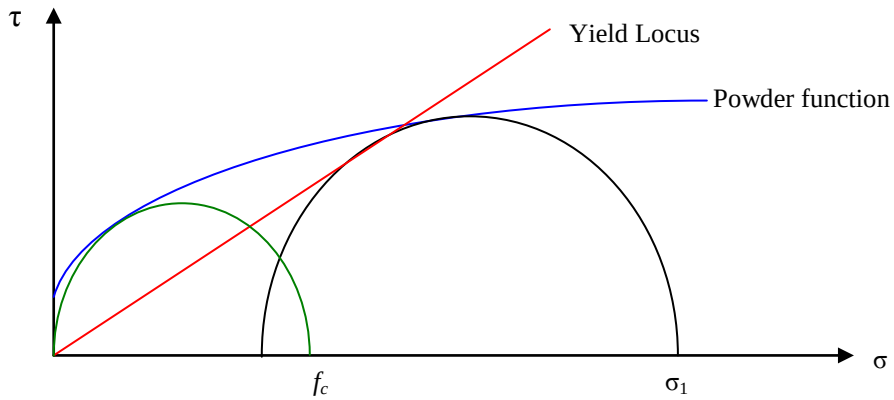

Figure 2.1.11, Application of powder function in Möhr circle

2.1.2 Self-Supporting Dome Over A Circular Aperture

From **Browns, R. L., Richards, J. C. [32],** as the powder flows towards the aperture, even though the wall angle allows the powder to flow continuously, however the size of aperture determines the possible formation of a dome which eventually terminates the flow. Figure 2.1.12 illustrates a slice of the dome contained between the planes θ and $\theta + d\theta$ on the horizontal planes between the radii r and dr with inclined angle ζ to horizontal.

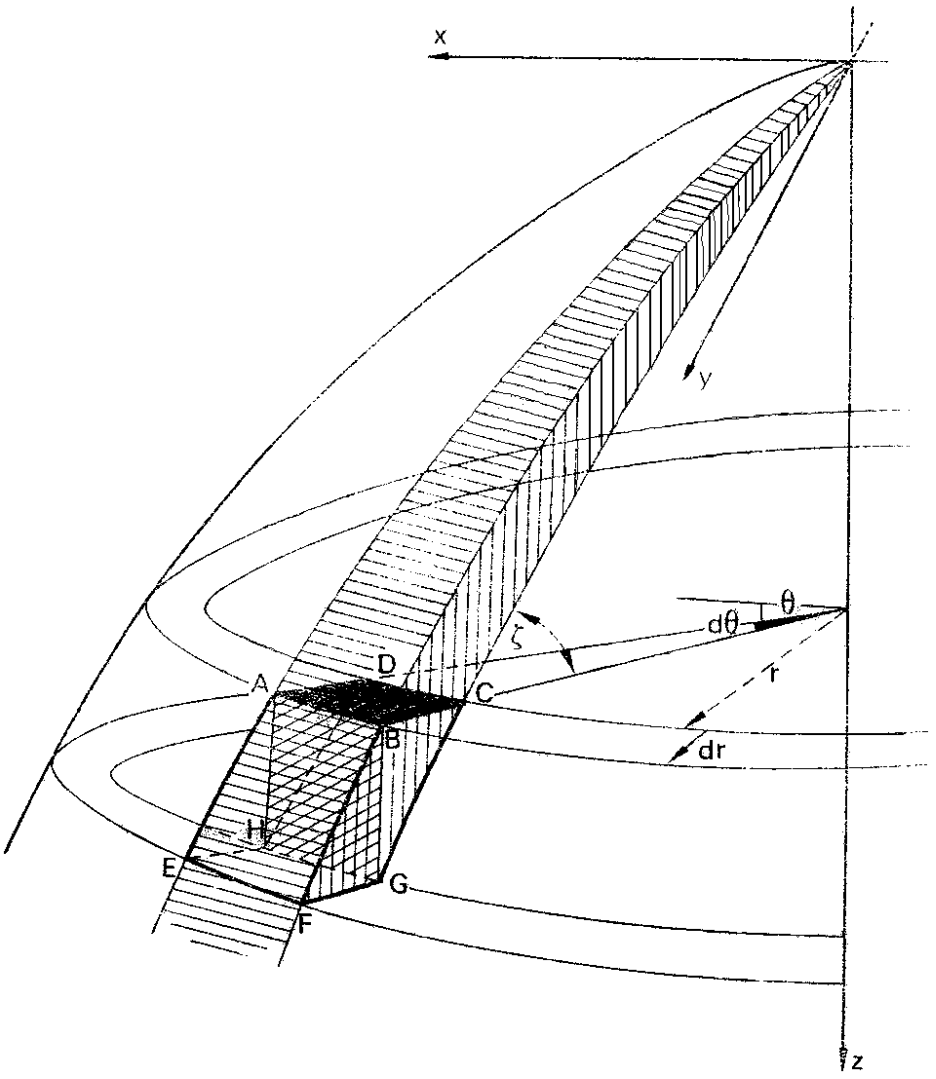

Figure 2.1.12, Portion of cohesive dome over circular aperture (Source: Brown, R. L., Richards, J. C. [32])

Assuming the dome is symmetric about z-axis with uniform thickness; the principle stress σ_2 normal to the dome is zero; the hoop stress σ_0 is constant acting circumferentially; σ_0 the horizontal component of principle stress σ_1 is zero which assumes no shear stress along the circle and their radii. The projection of the slice is shown in Figure 2.1.13.

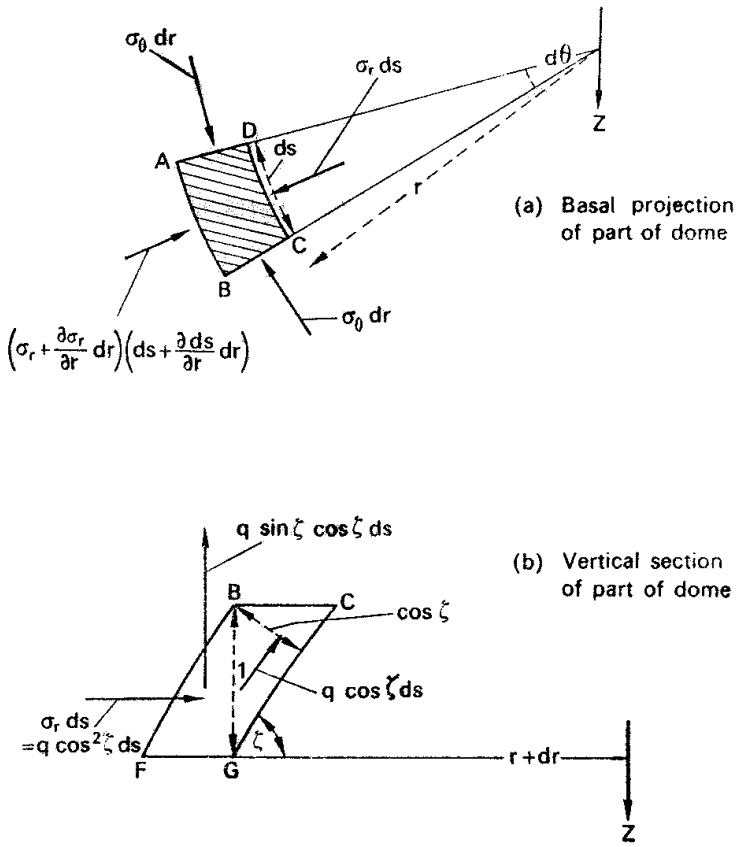

Figure 2.1.13, Sections through the dome (Source: Brown, R. L., Richards, J. C. [32])

As there is no shear along the boundaries of the strip and σ_θ acts normally to the strip, the vertically component of σ_1 equals the self-weight of the portion considered. For bulk density of the powder is ρ_b, and $dS = rd\theta$,

$$\sigma_1 \sin\zeta \cos\zeta dS = \int_0^r \rho_b dS dr$$

$$\sigma_1 \sin\zeta \cos\zeta dS = \upsilon_b d\theta \int_0^r r dr$$

$$\sigma_1 = \frac{\rho_b r}{\sin 2\zeta} \qquad \textbf{(2.1.13)}$$

At the boundary of the dome in the x, y plane where $r = R$, $\sigma_1 = \Sigma_1$, $\zeta = \zeta_1$, then

$$R = \frac{\Sigma_1 \sin 2\zeta_1}{\rho_b} \qquad \textbf{(2.1.14)}$$

This indicates that the larger the stress Σ_1 the larger the dome a material can form, and hence from the assumption made earlier, for a free surface the Möhr circle in Figure 2.1.9 will now

pass through origin as shown in Figure 2.1.14. For the failure in shear, the Möhr circle also touches the yield locus; the maximum shear stress is therefore $0.5f_c$.

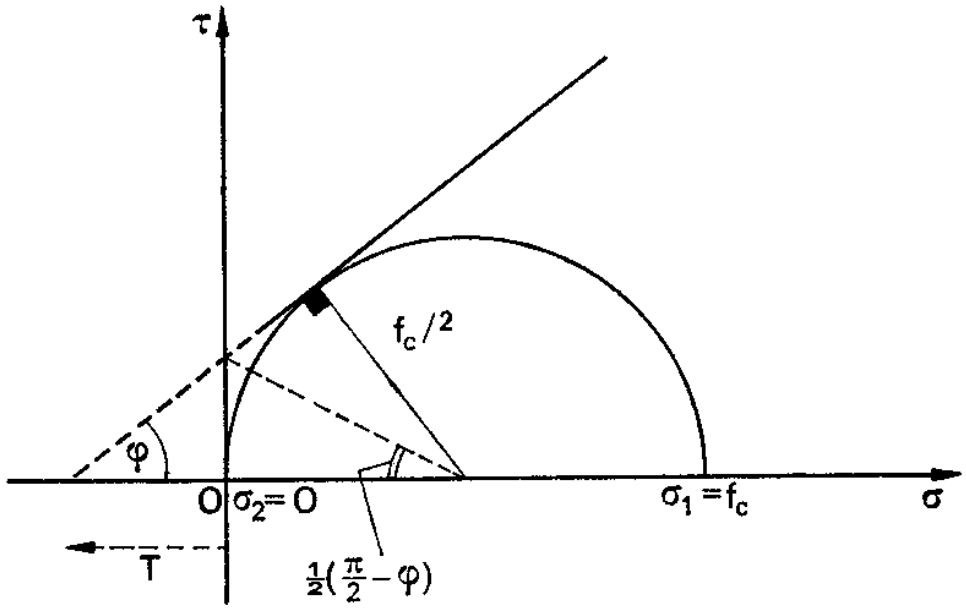

Figure 2.1.14, Möhr circle for free surface (Source: Browns, R. L., Richards, J. C. [32])

If φ is the angle of internal friction of the powder and T is its tensile strength, from the geometry of Figure 2.1.14,

$$\Sigma_1 = f_c = 2T \tan\left(\frac{\pi}{4} + \frac{\varphi}{2}\right)\tan\varphi \qquad \textbf{(2.1.15)}$$

Since angle ζ_1 is the inclination of the surface of the dome to the horizontal at the boundary, thus the radius of the largest dome in the x, y plane is

$$R = \frac{f_c \sin 2\zeta_1}{\rho_b} \qquad \textbf{(2.1.16)}$$

Suggested by **Jenkie, A. W. [31]** for hoppers with walls sloping at angles α_1 less than 70º, ζ_1 can be assumed to be about 45º, therefore equation (2.1.9) is then reduced to

$$R = \frac{f_c}{\rho_b} \qquad \textbf{(2.1.17)}$$

2.1.3 Kinematics of Powder

Similar to all the continuous systems with different phases of materials, for a given unit space, the amount of input into the system will be equal to the amount of output from the system. In Figure 2.1.15, let *N* be the number of granules per square metre per second flowing through an elementary area *dS* m^2 and the subscripts refer to two neighbouring areas enclosing a volume *dV*. For the conservation of number of granules

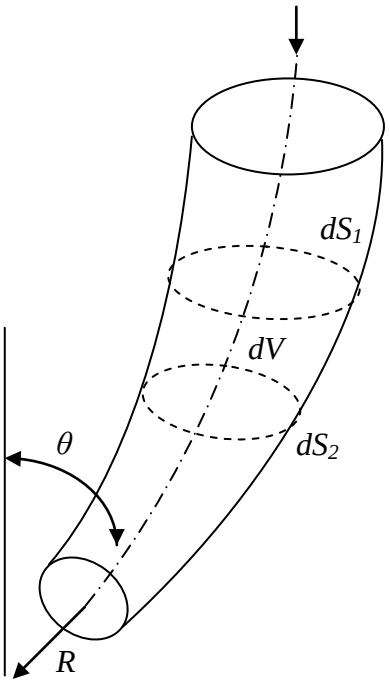

Figure 2.1.15, Stream tube in continuum.

$$N_1 dS_1 = N_2 dS_2 \quad \textbf{(2.1.18)}$$

If *m* is the mass of a granule and *v* m/sec the velocity of the continuum normal to *dS*, and ρ_b is the local bulk density near area *dS*. Assume all the granules have the same weight, then the mass flow rate normal to *dS* will be

$$\rho_b \upsilon = mN \quad \textbf{(2.1.19)}$$

$$q = mN \quad \textbf{(2.1.20)}$$

$$\upsilon = \frac{q}{\rho_b} \quad \textbf{(2.1.21)}$$

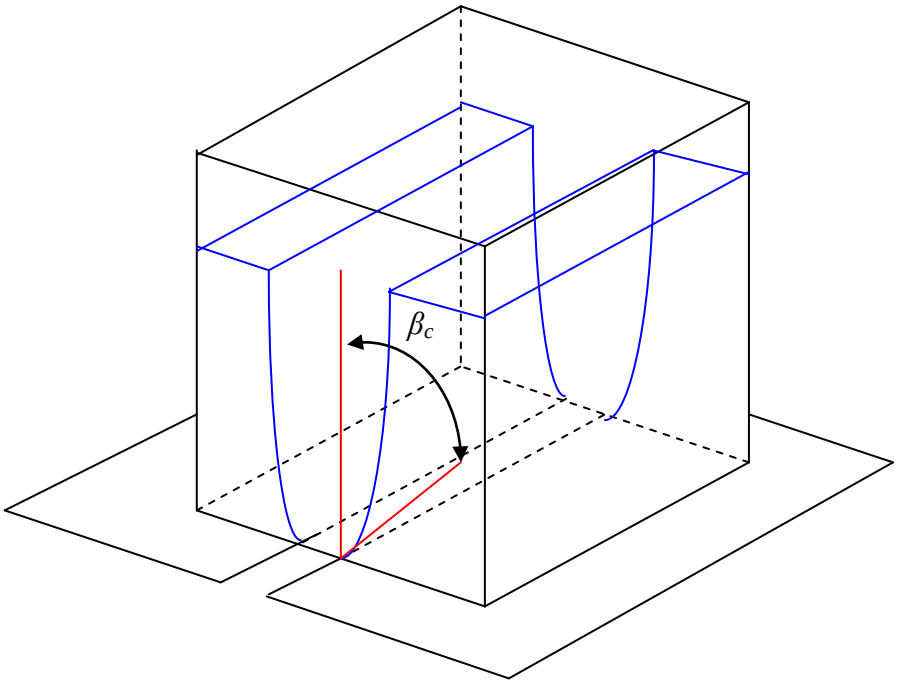

Figure 2.1.16, Angles of approach in central flow (Source: Brown, R. L., Richards, J. C., [32])

From **Brown, R. L., Richards, J. C. [32],** as a powder moves down a wedge, it changes direction as it approaches the aperture, and moves radially towards an apex below the aperture. In a flat-bottom vessel, formation of funnel through the mainstream movement occurs; the slope to the horizontal of the walls of the funnel is steeper than the angle of repose. The angle of approach is defined as the angle to the vertical of the sliding surface at the aperture. For the powder being constrained by the walls of the vessel, if these have a sufficiently large slope, or by the formation of sliding surface within a powder, the flow pattern of a powder approaching an aperture is therefore convergent.

As the slope of the walls decreases, the sliding surface will eventually be detached from the wall, and become horizontal. The mass flow rate will decrease with the wall slope, once a critical angle is reached, and then it will remain constant afterward. Therefore, the angle of approach depends on the material, and geometry of both the vessel and the aperture.

An experiment designed to determine the transition from constrained to unconstrained flow was carried out by **Brown, R. L., Richards, J. C. [32]** with the use of ball bearings for ease of observation. The bearings were observed visually to move in contact with their neighbours, converging in a wedge and apex below the aperture. It was found that the ball-bearings can fall freely until the packing is once again closed up, hence the voids were high above the aperture, which constrains the flow, and there was no constraint on the bearings below the aperture. By carefully constructing an arc with material strips close to the aperture

without disturbing the flow rate, the existence of a free-fall arch was then confirmed near the aperture. Since any point beyond the free-fall arch was unconstrained, without consideration of possible collision within the flow path, therefore the ball-bearing was assumed to be able to fall from stationary with gravity.

Now, considering an elementary volume dV cm^3 illustrated in Fig 2.1.15, work is done on this material by the stresses on the surface of this volume. Since the expected work done on the surface dS_1, dS_2 is insignificant; energy is mainly dissipated on the curved surface of dV by collisions, rotation, and frictional forces within dV. As the flow moves through the stream tube, the volume energy T decreases in the flow direction. The sum of kinetic and potential energy $T\,dV$ can be obtained by taking the polar coordinates R, θ, mass of powder $\rho_b\,dV$, velocity v ms^{-1}, and the vertical height above origin $R\cos\theta$, hence

$$2TdV = \rho_b dV(v^2 + 2gR\cos\theta)$$
$$2T = \rho_b(v^2 + 2gR\cos\theta) \qquad \textbf{(2.1.22)}$$

If dS is the orthogonal to a radius vector R at angle θ, and dS decreases towards the apex, then dS is proportional to R for two-dimensional flow in a wedge, and proportional to R^2 for three-dimensional flow in a cone. From equation of continuity (2.1.18) convert the number flow rate N to velocity v with (2.1.19), hence the discharge velocity is

$$v = \frac{\lambda(\theta)}{R^n} \qquad \textbf{(2.1.23)}$$

Where n = 1 or 2, and λ only depends on θ. Assuming that ρ_b is constant, except the possible discontinuity at $\theta = \beta$, and from equation (2.1.22) into (2.1.23), hence

$$2T = \rho_b\left(\frac{\lambda^2}{R^{2n}} + 2gR\cos\theta\right) \qquad \textbf{(2.1.24)}$$

Since T has a stationary value at radius R_m, where

$$R_m^{2n+1} = \frac{n\lambda^2}{g\cos\theta} \qquad \textbf{(2.1.25)}$$

and this stationary value is minimum at which the energy T_m is therefore

$$R_m^{2n} = \frac{n\lambda^2}{R_m g \cos\theta}$$
$$2T = \rho_b \left(\frac{\lambda^2 R_m g \cos\theta}{n\lambda^2} + 2gR_m \cos\theta\right)$$
$$2T_m = \left(2 + \frac{1}{n}\right)\rho_b g R_m \cos\theta \qquad \textbf{(2.1.26)}$$

From the postulate of T decreasing along a stream tube, the surface R_m, θ may be called the surface of minimum energy, and it must be below and coincide with, the free-fall arch.

Let f be the downwards radial acceleration. Then

$$f = -v\frac{dv}{dR}$$
$$f = \frac{n\lambda^2(\theta)}{R^{2n+1}} \qquad \textbf{(2.1.27)}$$

and hence f increases as R decreases.

At the surface of minimum energy, the radial acceleration of free-fall under gravity at coordinates R_m, θ is therefore

$$f_m = \frac{n\lambda^2(\theta) g \cos\theta}{n\lambda^2(\theta)}$$
$$f_m = g\cos\theta \qquad \textbf{(2.1.28)}$$

It follows that T decreases to a minimum T_m at the free-fall arch; hence the above calculations may also prove the existence of the free-fall arch.

Similar to the orifice plate in fluid mechanics, the existence of *vena contracta* was observed. In the analysis of mass flow rates, it was found that the aperture size has been greatly reduced by a quantity k, where ½ k is the width of the empty annulus. From **Brown, R. L., Richards, J. C. [32],** it was found k is independent of the size of the aperture and of the flow rate; however it varies with the grain size, powder properties and the slope of the vessel walls. Also k is the same for flow through slots of width S as for circular aperture of diameter D.

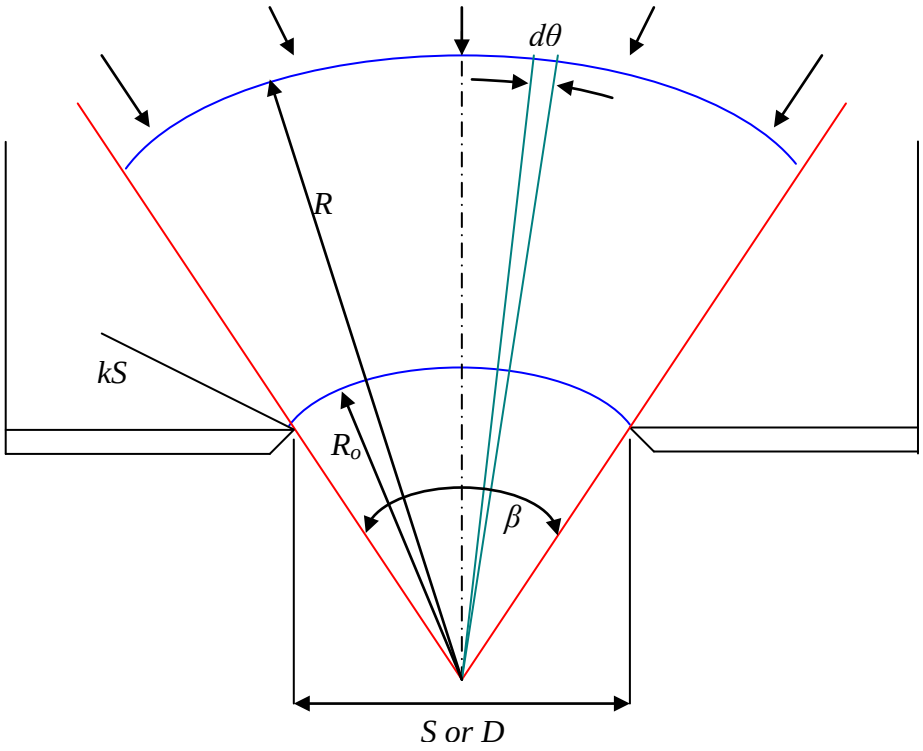

Figure 2.1.17, Location of free-fall arch.

Figure 2.1.17 shows the annulus was taken into account by locating the apex of the wedge or cone at a radial distance R_0 cm, where

$$2R_0 \sin\beta = (S-k) = (D-k) \qquad \textbf{(2.1.29)}$$

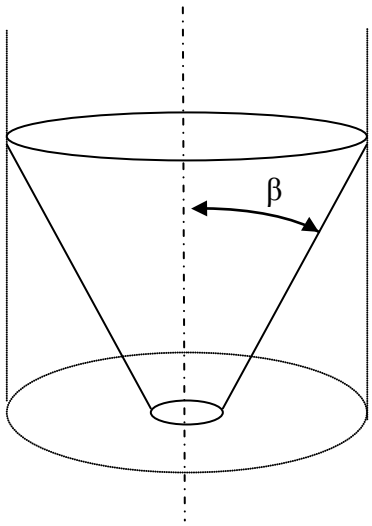

Figure 2.1.18, Discharge of powder through a cone.

The powder flows through a circular aperture of a vertical cone with half-angle β towards the apex as shown in Fig 2.1.17. For $n = 2$ in equation. (2.1.25)

$$R_m^5 = \frac{2\lambda^2}{g\cos\theta} \qquad \textbf{(2.1.30)}$$

From Figure 2.1.16, consider the spherical cap of radius R, the number of grains flowing radially towards the apex between angle θ and $\theta+d\theta$ to the vertical is ($N\ 2\ \pi R\sin\ \theta\ Rd\theta$), where, from equation (2.1.19) and (2.1.20) with $n = 2$

$$N = \frac{\rho_b \lambda}{mR^2}$$
$$Q = \int_0^\beta mN 2\pi R^2 \sin\theta d\theta$$
$$Q = 2\pi\rho_b \int_0^\beta \lambda \sin\theta d\theta \qquad \textbf{(2.1.31)}$$

Assuming that ρ_b is constant, then from equations (2.1.28) and (2.1.29) it follows that

$$\frac{4Q}{\pi\rho_b g^{1/2}(D-k)^{5/2}} = \frac{\int_0^\beta (\frac{R_m}{R_0})^{5/2} \cos^{1/2}\theta \sin\theta d\theta}{\sin^{5/2}\beta} \qquad \textbf{(2.1.32)}$$

Assuming that the free-fall arch coincides with the arc of radius R_0, where $R_m = R_0$, hence,

$$\frac{4Q}{\pi\rho_b g^{1/2}(D-k)^{5/2}} = \frac{2(1-\cos^{3/2}\beta)}{3\sin^{5/2}\beta} = \gamma(\beta) \qquad \textbf{(2.1.33)}$$

The alternative solution is to average the velocity over the spherical cap and treat this powder as having an average height $^1/_2\ R(1 + cos\beta)$. Then from (2.1.22)

$$v_{AV} = \frac{Q}{\rho_b 2\pi R^2(1-\cos\beta)} \qquad \textbf{(2.1.34)}$$

$$2T_{av} = \rho_b[\frac{Q^2}{4\rho^2\pi^2 R^4(1-\cos\beta)^2} + 2g\frac{R}{2}(1+\cos\beta)] \qquad \textbf{(2.1.35)}$$

and the minimum is at

$$R_m^5 = \frac{Q^2}{{\rho_b}^2 \pi^2 (1-\cos\beta)^2 g(1+\cos\beta)} \qquad \textbf{(2.1.36)}$$

Now let $R_m = R_0$, then

$$\frac{4Q}{\pi\rho_b g^{1/2}(D-k)^{5/2}} = \frac{(1-\cos\beta)^{1/2}}{2^{1/2}\sin^{3/2}\beta} = \gamma_{av}(\beta) \qquad \textbf{(2.1.37)}$$

Since $\gamma_{av}(\beta)$ differs from $\gamma(\beta)$ by less than 1 per cent for range of $0^\circ < \beta < 70^\circ$, hence that Q is most likely to be insensitive to the shape of the velocity profile. Therefore, the important rate-determining factor is the extent to which R_m / R_0 differs on this average from unity.

The fundamental theory predicts that flow through a circular aperture of diameter D varies with $(D - K)^{5/2}$, the bulk density of the flowing material and the range of approach β, and the discharge rate is independent from the head of material contained within the vessel, except when nearly empty.

2.1.4 Summary of Powder Mechanics

Powder mechanics is the work based on soil mechanics theory, further evolved in order to cope with the differences such as the cohesive behaviour; therefore powders were regarded as free flowing in soil mechanics.

A shear cell is the most widely used instrument designated to measure the bulk material properties. For a cohesive powder, under unconsolidate condition, it has no yield strength, hence the higher the pressure, the greater the consolidation and strength can be obtained for a particular powder. When a slip occurs after applying the normal force and shear force, this is sufficient to overcome the angle of internal friction φ, and the result can be expressed which is in terms of yield locus in a Möhr circle.

In practice, the powder is pre-consolidated by placing free weights directly above the powder inside the container. After removal of the free weights, a normal force is gently applied on to the top of the powder, however, this may be limited to sieved powder only, since powder lumps may collapse or be deformed during preparation and testing. The stress in the moment

of the material's failure gives the *unconfined crushing strength* f_c, which means the applied force causes yield. When f_c > F, and the unconfined crushing strength is bigger than the applied strength, arching occurs. For different consolidation pressures applied on the powder result from the shear cell testing, a powder function can be determined from the Möhr circle diagram. Hence, the flow – no flow criteria can be determined.

2.2 Cyclone Separation Method

Due to the requirement of high operational efficiency, simple construction, and low maintenance and operating costs, the cyclone separation system has been the most extensively used type of collector for relatively coarse dusts. A cyclone is eventually a settling chamber in which gravitational acceleration is replaced by centrifugal acceleration. The most common form is the return-flow cyclone; its construction features are shown in Figure 2.2.1.

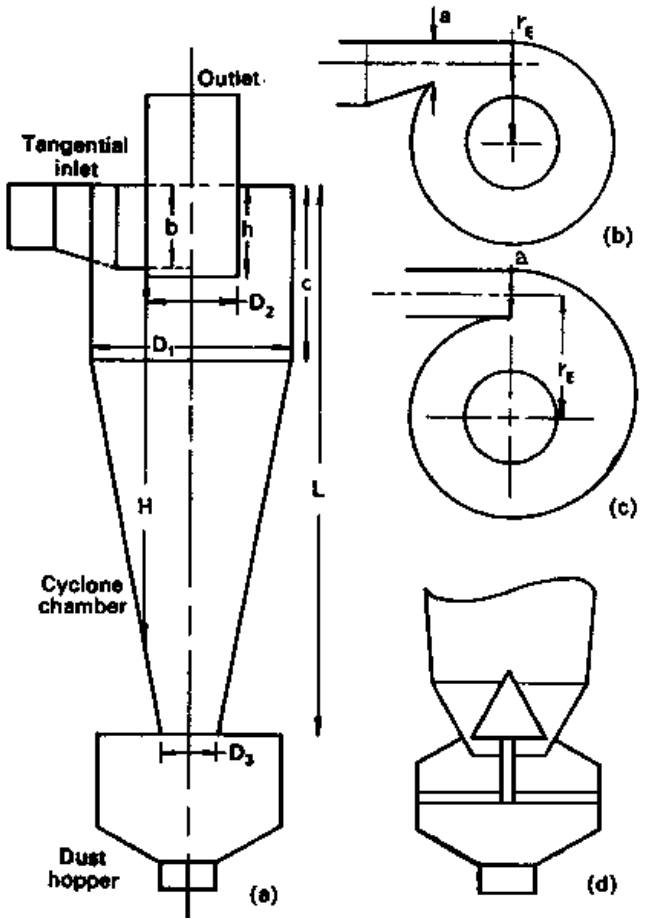

Figure 2.2.1, Schematic diagram of cyclone showing leading dimensions and alternative design features. (a)Vertical section. (b)Tangential inlet. (c)Scroll inlet (180°). (d)Annular discharge to dust hopper (Source: Dorman, R. G. [50])

In Figure 2.2.1, r_E is the radial distance between the centre line of the entrance aperture and the cyclone axis. H is the length of the imaginary cylinder formed by extending the outlet duct downwards to meet the conical chamber wall.

From **Dorman, R. G [50]**, cyclones are made with diameters D_1 ranging from about 10mm to 5m, and for gas throughputs from about $3x10^{-5}$ m^3/s, operating temperatures up to 1000ºC and pressures to $5x10^4$ kN/m^2. For commonly employed operating conditions, the centrifugal

separating force or acceleration may range from 5 times gravity in very large diameter, low-resistance cyclones, and up to 2500 times gravity in a very small, high-resistance unit, hence high abrasion on the chamber wall **[61]**. The pressure drop is usually in the range 0.1-0.2 kN/m^2 and the inlet gas velocity is typically between 10-30 m/s. Although cyclones may be used to collect particles larger than 200 μm, alternative solutions such as gravity settling chambers or inertial separators like a gas-reversal chamber may usually comply well and are less subject to abrasion. Complete removal of particles larger than 20 μm diameter under normal conditions is readily achieved, however, depending on the size of the cyclone and operating system, a dramatic drop of efficiency lower than 50% may occur as the particle size decreases to 5 μm. The sharpness of the cut is variable, but typically there is a four – to eightfold range in diameter between particles collected at 20% and 80% efficiency **[50]**. For high efficiency requirement with small particles, multiple small cyclones mounted parallel give the requisite total flow rate, with a common dust collection chamber.

2.2.1 Air Flow in Cyclone

Although the geometrical shape of the cyclone is simple, the pattern of airflow in the vortex is extremely complex, and indeed no complete theory has yet been given or likely to be forthcoming **[50]**, hence the theoretical calculations of the pressure drop or dust separation efficiency are correspondingly difficult. However, based on experimental observation, simplified theoretical models can be constructed and calculations are permitted to obtain useful indicators of the performance.

At the tangential inlet duct, as the dust-laden air enters the upper cylindrical portion of the cyclone chamber it is pressed to the wall by centrifugal force and descends the chamber in an outer spiral flow path adjacent to the wall, typically 2-7 turns in the height of the cyclone. With the increasing spin velocity as the flow spirals downwards into a lower conical section and inwards towards the axis, the suspended dust particles are thrown outwards by centrifugal force arising from the rotation. In the zone between the outer descending spiral and the inner ascending spiral the vertical component of the velocity is small. The spinning velocity is approximately the same at a given distance from the axis at all heights, as also is the inwards radial component of the flow. The airtight dust collection chamber located at the lower end of the cone collects the separated dust; the air flows inwards towards a central return spiral moving upwards and is discharged through the axial outlet duct located in the centre of the cyclone chamber.

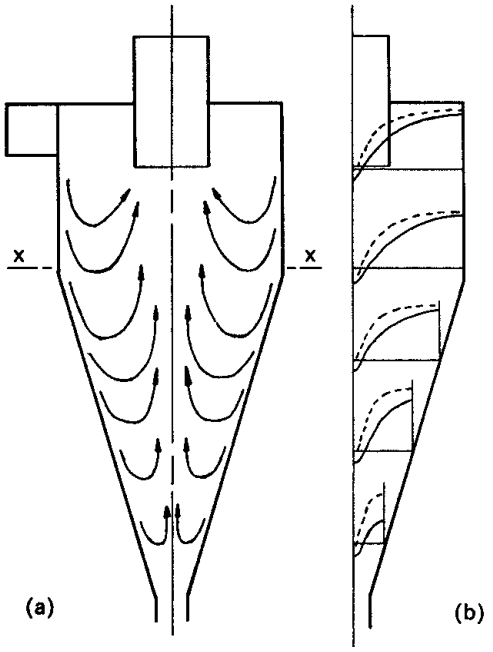

Figure 2.2.2, (a)Flow pattern. (b)Pressure distribution in cyclone (Source: Dorman, R. G. [50])

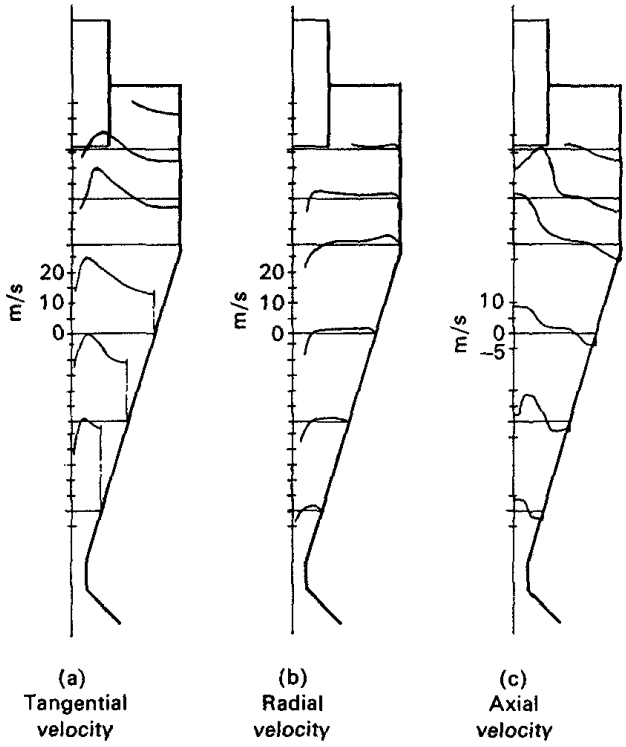

Figure 2.2.3, Velocity components of gas flow in cyclone (Source: Dorman, R. G. [50])

As indicated in Figure 2.2.3(a), due to friction below the main vortex, the spinning speed adjacent to the wall is reduced. The consequence is that the radial pressure gradient due to centrifugal force is reduced in the surface layer as shown in Figure 2.2.2. An inwards circulation, adjacent to the upper wall of the chamber and the outer surface of the outlet duct, appears at the top of the separation chamber.

However, similar to the motion of tea leaves spinning at the bottom of a cup, without attaining the high separation force from the main vortex, this flow carries the particles to the outlet duct entry. Therefore, suggested by **Dorman, R. G. [50]**, certain proprietary design considerations may be required to incorporate a special duct which skims off this flow from the upper edge of the cyclone chamber to the base of the cylindrical section. The swirling of the air extends into the dust-collection hopper from the lower end of the cone, a secondary circulation with a return flow into the core ascending spiral leading to the outlet tube is suspected, as shown in Figure 2.2.4.

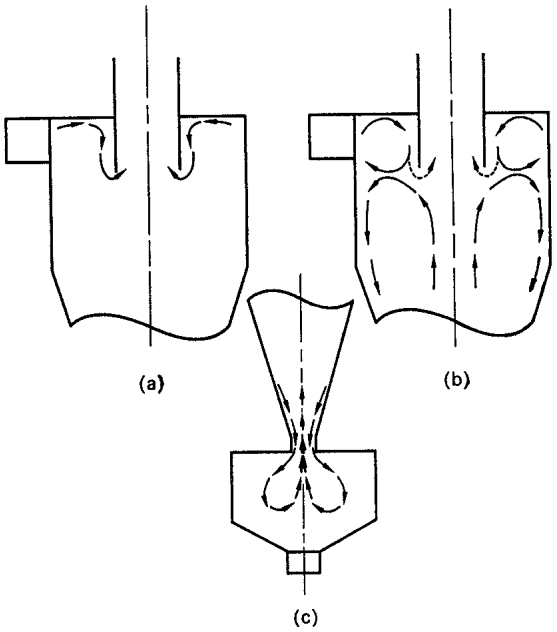

Figure 2.2.4, Secondary circulation in the cyclone (Source: Dorman, R. G. [50])

It is expected a turbulent flow with Reynolds number greater than 10^5 occurs in the cyclone, particularly near the centre of the inner spiral and the boundary layers adjacent to the internal surface **[50]**. In the cyclone chamber, the turbulent component throughout the flow gives a transfer of momentum between the vortex layers and modifies the flow pattern from an ideal fluid. Average gas velocities can be obtained from the cyclone, however turbulent mixing may take place against the predominant flow direction. A dramatic increase in the tangential velocity in comparison with the inlet velocity can be explained by the conservation of energy from Bernoulli's theorem, as expressed below, with the assumption of the working fluid behaving ideally in streamline motion.

$$P_{sr} + \rho u_r^2 / 2 = constant \qquad \textbf{(2.2.1)}$$

Hence, as the fluid is circling in the vortex, then

$$\frac{dp_{sr}}{dr} = -\rho u_r \frac{du_r}{dr} \qquad \textbf{(2.2.2)}$$

Since the radial component of the velocity is relatively small in comparison with the tangential velocity, therefore it is discarded to simplify the result. The increase of the radial pressure gradient is due to the centrifugal forces of the circular motion, therefore

$$\frac{dp_{sr}}{dr} = \frac{\rho u_r^2}{r} \qquad \textbf{(2.2.3)}$$

$$\frac{du_r}{dr} = -\frac{u}{r} \qquad \textbf{(2.2.4)}$$

$$u_r r = const \qquad \textbf{(2.2.5)}$$

When an ideal fluid enters the cyclone in stream-line irrotational flow, it will remain irrotational since the necessary condition has been fulfilled with the above relationship, hence

$$\oint v ds = 0 \qquad \textbf{(2.2.6)}$$

where *ds* is an element of length of a closed path in the fluid. Figure 2.2.5 shows the irrotational flow in the vortex; hence equation (2.2.7) can then be formed from equation (2.2.6) when the second-order terms are discarded.

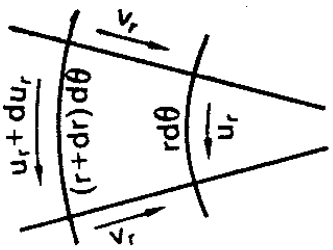

Figure 2.2.5, Illustration of irrotational flow in vortex (Source: Dorman, R. G. [50])

$$\oint v ds = u_r r d\theta - v_r dr - (u_r + du_r)(r + dr)d\theta + v_r dr = -(u_r dr + r du_r)d\theta = 0 \qquad \textbf{(2.2.7)}$$

For an ideal fluid in a vortex, the tangential velocity increases inversely with the radius, and approaches infinity near the axis. The angular velocity increases inversely as the radius squared. Hence the centrifugal force acting on the particles in the fluid flow path would increase as the inverse cube of its distance from the axis. Therefore, the potential of cyclone separation with the action of centrifugal force is viable **[50]**.

In practice, the tangential shear force due to viscosity or turbulent transfer of momentum opposes the increase of angular velocity as the flow moves towards the centre. The consequences are that the spinning velocity slows down below the theoretical expectation (2.2.5), and an empirical equation can be formulated from the experimental observations.

$$u_r = \frac{k}{r^{\beta}} \tag{2.2.8}$$

The overall static pressure drop between radii r_1 and r_2 can be expressed as

$$\Delta P_s = \int_{r_2}^{r_1} \frac{dp_{sr}}{dr} = \int (\frac{\rho u_r^2}{r}) dr \tag{2.2.9}$$

substituting equation (2.2.8) into (2.2.9) and integrate,

$$\Delta p_s = \frac{1}{\beta}(\frac{\rho u_2^2}{2} - \frac{\rho u_1^2}{2}) \tag{2.2.10}$$

For an ideal flow, with the conservation of energy, the static pressure difference is equal to the change in the velocity head, and hence $\beta = 1$. However in practice, if the static pressure difference is twice the change of velocity head, then $\beta = 0.5$, and there is an energy loss of one velocity head difference.

2.2.2 Theory of Similarity Applied to Cyclones

From **Dorman, R. G. [50]**, in a cyclone with given geometrical shape and diameter D_1, the factors affecting the performance include pressure drop Δp, gas density ρ, viscosity η, and mean velocity v_E at the entry orifice. Hence, from the dimensional analysis, dimensionless constants can be constructed from these variables, and Reynolds number *Re* can be recognized on the right-hand side of the equation, and thus the first dimensionless constant

$$\frac{\Delta p}{\rho v_E^2} = f(\frac{v_E \rho D_1}{\eta}) = const \tag{2.2.11}$$

The *Re* is expected to be large (greater than 10^5 in practice) which indicates the inertial force predominant over the viscous forces. It is convenient to express this in the form where Z_E is a dimensionless constant for a particular type of cyclone at the entrance orifice.

$$pv_E = \frac{\rho v_E^2}{2} \quad \textbf{(2.2.12)}$$

$$\frac{\Delta p}{0.5\rho v_E^2} = \frac{\Delta p}{pv_E} = Z_E \quad \textbf{(2.2.13)}$$

Referring to Figure 2.2.1, the volume flow rate of air Q flow through the cyclone is $v_E ab$, and is proportional to $v_E D_1^2$, hence the second dimensionless constant

$$\Delta p D_1^4 / \rho Q^2 = constant \quad \textbf{(2.2.14)}$$

For a given cyclone, the pressure drop is independent of the size if equal gas velocity applies, as indicated in equation (2.2.11), and pressure drop increases as the gas velocity increases. However, it is greatly affected by the dimension when the gas quantity remains unchanged, as indicated in equation (2.2.14). In practice, structural effects such as surface roughness and joint features can also alter the theoretical figures; therefore this relationship is expected only to hold accurately for a single cyclone **[50]**.

Assuming the Strokes' law is obeyed, the ratio of particle mass to the drag force arising from the velocity difference between particle and gas is used to determine the motion of a suspended particle relative to the carrying medium in a cyclone; hence the drag is proportional to the velocity difference. The aerodynamic properties of the particles are characterized by the parameter shown below,

$$\tau = mass / drag\ force\ at\ unit\ velocity\ difference \quad \textbf{(2.2.15)}$$

Hence, for a perfect spherical particle, the parameter is

$$\tau = \frac{m}{2\pi\eta d_p} = \frac{\rho_p d_p^2}{18\eta} \quad \textbf{(2.2.16)}$$

From **Dorman, R. G. [50]**, the parameter τ is the time-constant in which the particle responds to a change in the gas velocity, and it is related to other particles parameter such as the terminal velocity, the range or stop-distance S_v, and the particle acceleration. In comparison with the dimension and the gas flow in a cyclone, the particle size is discarded due to its insignificance, except with the occurrence in τ, and the gravitational effects are also neglected when comparing with the acceleration of the gas stream in the cyclone.

With the inclusion of τ into the dimensional analysis of the gas-particle system, the third dimensionless constant can be obtained. The ratio between the particle stop distances to the characteristic dimension of the system $v\tau/D$ is also known as the Strokes number (*Stk*). The dust movement pattern and particle separation efficiency E is therefore a function of Stroke number (*Stk*) and Z_E for different cyclones as shown below

$$E = f(\frac{v_E \tau}{D_1}, Z_E) \qquad \textbf{(2.2.17)}$$

For determining the limiting value of cyclone collection efficiency, the suffix of L is implied; this will correspond to a definite value of Stk_L of the Strokes number, hence the third dimensionless constant

$$\frac{v_E \tau_L}{D_1} = const = Stk_L \qquad \textbf{(2.2.18)}$$

2.2.3 Limiting Particle Size Theories

To determine the size of particles separated, construction of a theoretical process model is essential. From **Dorman, R. G. [50]**, two different approaches on cyclone separation theories were found; they are the ***Wall Deposition Model*** and the ***Central Vortex Model***, and are listed below:

Wall deposition Model

This theory concerns particles being thrown to the chamber wall by centrifugal force produced by the carrier medium which undergoes circular motion. Factors governing the separation efficiency are such as the magnitude of the centrifugal force, particle mobility, the particle distance from the wall and action time of the force **[50]**. However, the radial component of the gas velocity is very low near the chamber wall, therefore it is ignored.

Assuming a particle has a circumferential gas velocity, a radial velocity relative to the gas in circular motion propels the particle outwards and increases the radial force, and therefore a balance between the centrifugal force and the drag force from this radial motion is maintained. Hence

$$\frac{\tau u_r^2}{r} = \frac{dr}{dt} \qquad \textbf{(2.2.19)}$$

where u_r is assumed to remain constant and equal to the entry velocity v_E. Integrating equation (2.2.20) and replacing u_r with v_E gives

$$r_t^2 - r_{t=0}^2 = 2\tau v_E^2 t \qquad \textbf{(2.2.20)}$$

Starting from the least favourable position at the greatest distance from the wall, the limiting particle trajectory will just arrive at the chamber wall in time for the passage of gas. Assuming the initial distance from the chamber wall is *a*, and the entrance orifice width is

$$r_{t=0} = \frac{D_1}{2} - a \qquad \textbf{(2.2.21)}$$

where $r_t = 0.5\ D_1$, and assuming the gas spirals and makes n_t turns in the cyclone chamber, hence

$$t = \frac{n_t \pi D_1}{v_E} \qquad \textbf{(2.2.22)}$$

Since, particles are assumed to be a complete removal, therefore $E = 1$, and here τ_L or v_{cL} are characterized as the smallest particles that are being removed by the cyclone. By substituting equation (2.2.22),

$$\tau_L = \frac{v_{cL}}{g} = \frac{a(1 - a/D_1)}{2\pi v_E n_t} \qquad \textbf{(2.2.23)}$$

By assuming the descending gas spiral to make n_t turns, of thickness a_s and height b_s, with velocity u_s; the concern regarding the gas spiral thickness, which represents the radial distance that the limiting particles must travel to reach the wall and is equivalent to the width of the orifice entrance, can be avoided. Hence,

$$Q = a_s b_s u_s \tag{2.2.24}$$

$$n_t = \frac{L}{b_s} \tag{2.2.25}$$

$$\frac{a_s}{n_t} = \frac{Q}{L u_s} \tag{2.2.26}$$

and L is the height of the cyclone. Substituting these new assumptions into equation (2.2.23)

$$\tau_L = \frac{v_{cL}}{g} = \frac{Q(1 - a_s / D_1)}{2\pi u_s^2 L} \tag{2.2.27}$$

If a_s is small in comparison with D_1, this becomes

$$\tau_L = \frac{v_{cL}}{g} = \frac{Q}{2\pi u_s^2 L} \tag{2.2.28}$$

which is independent of a_s and n_t.

The outer casing in the real cyclones is conical, instead of cylindrical; as the gas descends the cone, the flow quantity in the outer spiral diminishes. The thickness of the spiral a_s tends to remain constant with compensation from these factors. Despite the diminishing perimeter, the deposition of particles per turn tends to rise with increase of v_r which is caused by the increase of the velocity and centrifugal force as the radius contracts. Suggested by **Dorman, R. G. [50],** the application of this model can perform exceptionally well in the real cyclone.

Central Vortex Model

The balance between the centrifugal force acting on the particle and the inwards drag of the radial component of the gas flow conceives as the critical factor in this cyclone model **[50]**. Due to the centrifugal force, the outwards radial velocity of a particle relative to the gas is $\tau u_r^2 / r$. As the gas velocity v_r is greater than the outwards radial velocity, as a consequence, the particle will have a net inwards velocity. At radius r over the cyclone height H, the mean value of v_r below the outlet duct is $Q/2\pi rH$. Hence, for a particle to be carried inwards, either $\tau u_r^2 / r < Q / 2\pi rH$ or $\tau < Q / 2\pi u_r^2 H$ has to be satisfied.

For the value of τ decreasing with the increase of u_r, the further inwards the particle will be carried before equilibrium of the two velocities is reached. The particle of a given τ will rotate in a stable orbit of fixed radius under the equilibrium position. At $r > r_2$, for small

particles which do not reach the equilibrium at this stage, they will be swept upwards by the ascending inner spiral and discharged into the outlet duct. Hence the limiting particle is therefore given by

$$\tau_L = \frac{v_{cL}}{g} = \frac{Q}{2\pi u_2^2 H} = \frac{Qr_2}{2\pi k^2 H} \qquad \textbf{(2.2.29)}$$

if the empirical relationship $u_r = k / r^{0.5}$ is implied.

The radial velocity will not be maintained constant at all heights in practice, however, it will be distributed by mean, hence for the escaping particles, the value of τ_L will also be taken as the central value corresponding to 50% efficiency if $E = 0.5$.

From both modeling, the maximum particle size tends to be limited by the condition at the centre rather than at the outer wall of the cyclone. The assumption regarding the wall condition (2.2.28) gives the maximum particle size, and (2.2.29) the centre equation gives the mean (E = 50%) size, which will tend to offset the difference in the calculated values of τ_L or v_{cL}.

From equation (2.2.29), if the smaller particles reach the inner spiral and escape completely, then $E = 0$, apart from the spread of τ_L caused by the unequal distribution of v_r. However, due to the aggregation or collision with coarser particles, the particles smaller than the theoretical limit are removed, hence the grade efficiency for smaller particles will depend both on their concentration and the proportion of presence of large particles. With the assumption on the wall deposition model, small particles of all sizes are removed in proportion to their settlement velocity v_c, and the part of the observed efficiency will be accounted for from simultaneous operation of this mechanism. Hence, when determining the shape of the grade-efficiency curve for a particular cyclone design, the relative values of limiting particle size separated at the wall and at the centre respectively may be one of the main factors.

From **Dorman, R. G. [50]**, a concern about the outcome of particles left to accumulate in a stable orbit is still not clear at this stage. The vicinity of the outer tube may have an "escape zone" where the ascending dust stream reaches the area and maintains its high tangential velocity but reduces its radial component. A further proportion of the particles in the dust stream will be removed when the flow moves towards the wall and causes re-circulation with the outer spiral. The concentration of the particles contained in the dust stream will be higher

than in the inlet. The dust descends and enters while still airborne if orbiting at greater radii, and most will ultimately settle here, aided by coagulation at high concentration. However, some may still be retained up the axial core of the inner vortex and escape from the outlet tube.

For the distinction observed from the equations obtained between the models, the wall deposition model indicates that the diameter of the outlet duct is insignificant when determining the efficiency apart from any indirect effect on u_1. As for the central vortex model, as the limiting size diminishes, the overall efficiency increases as D_2 is reduced with D_1.

2.2.4 Summary of Cyclone Separation

A cyclone is eventually a settling chamber in which gravitational acceleration is replaced by centrifugal acceleration. The cyclone separation system has been the most extensively used type of collector for relatively coarse dusts mainly due to its high operational efficiency, simple construction, and low maintenance and operating costs. Due to the high centrifugal separating force, in a cyclone separation, the chamber wall is subject to high abrasion. For particle size greater than 200 μm, alternative separation method may usually comply well and are less subject to abrasion. Complete removal of particles larger than 20 μm diameter under normal conditions is readily achieved, however, depending on the size of the cyclone and operating system, a dramatic drop of efficiency lower than 50% may occur as the particle size decreases to 5 μm.

Since the flow pattern in the vortex is extremely complex, and no complete theory has yes been found, hence the theoretical calculations of the pressure drop or dust separation efficiency are correspondingly difficult. Based on experimental observation, simplified theoretical models can be constructed and calculations are permitted to obtain useful indicators of the performance.

3. DESIGN SPECIFICATION

Understanding the properties of the powder is a pre-requirement in order to foresee the feasibility of further developing the possible processes that may be involved for the system. The selections of the final processes will be based on the practical application of the theories and possible maintenance in the long term; therefore a successful process will then be further improved and implemented into the system development.

Properties which were required to be determined are listed below:

- ***Particle Size*** **–** this finding provides a numerical figure for the application of background theory to determine the feasibility of a particular process.

- ***Bulk Density Measurement*** **–** the bulk density determines the maximum volume of powder that can be loaded into a standard 200 gallon barrel, and the criteria of arch formation in the discharge bin.

- ***Flow Characteristic*** **–** a study based on the theory of powder mechanics determines the required dimensions for the mass flow to occur on the discharge bin.

The goal of the findings is to filter out surplus information and obtain a feasible transportation method and then further develop it. At the end of this section, the base outline of the design requirement for the final transportation process will be obtained from both the understanding of the swarf properties and the outline requirement.

3.1 Particle Size Determination

As mentioned earlier, the particle size is a critical design factor for a successful design of a cyclone separation system. The maximum particle size determines the operating condition of a fluidised bed and the power requirement to drive the fan unit; the minimum particle size determines the separation chamber dimension, efficiency of the separation process, and filter selection for exhaust air. The aim of this process therefore, is to obtain the measurement of maximum and minimum size of particles within the sample, and also size of the unexpected large objects e.g. helical strips formed from the drilling process.

Without additional magnification, the largest size of the strips that were found in the sample was approximately 20.8 mm long, although there hardly any strips measuring longer than 2mm within the given sample. This measurement however, does not include the lumps of powder which were formed after the cleaning process.

Figure 3.1.1, Nikon Shadowgraph

Figure 3.1.2, Clean swarf

Several methods were found for determining the maximum and minimum particle size. The most common method of optical microscopy could not provide a clear image, and the scanning electron microscopy (SEM) does present problems associated with the preparation of the conductivity of the moulding material. Moreover, it was not possible to employ the method associated with the use of a particle size analyser in the Chemical & Process

Engineering Department at the University of Canterbury; the instrument was out of service for a long period of time. The shadowgraph method was therefore selected, mainly due to the time limitation for obtaining a close approximation measurement. A shadowgraph, as shown in Figure 3.1.1, is a project image of the sample area on an enlarged display screen. Figure 3.1.2 shows the samples used to make the slides. The slides, as shown in Figure 3.1.3, have to be transparent which allows the light to pass through and leave the shadow of the particle to be projected.

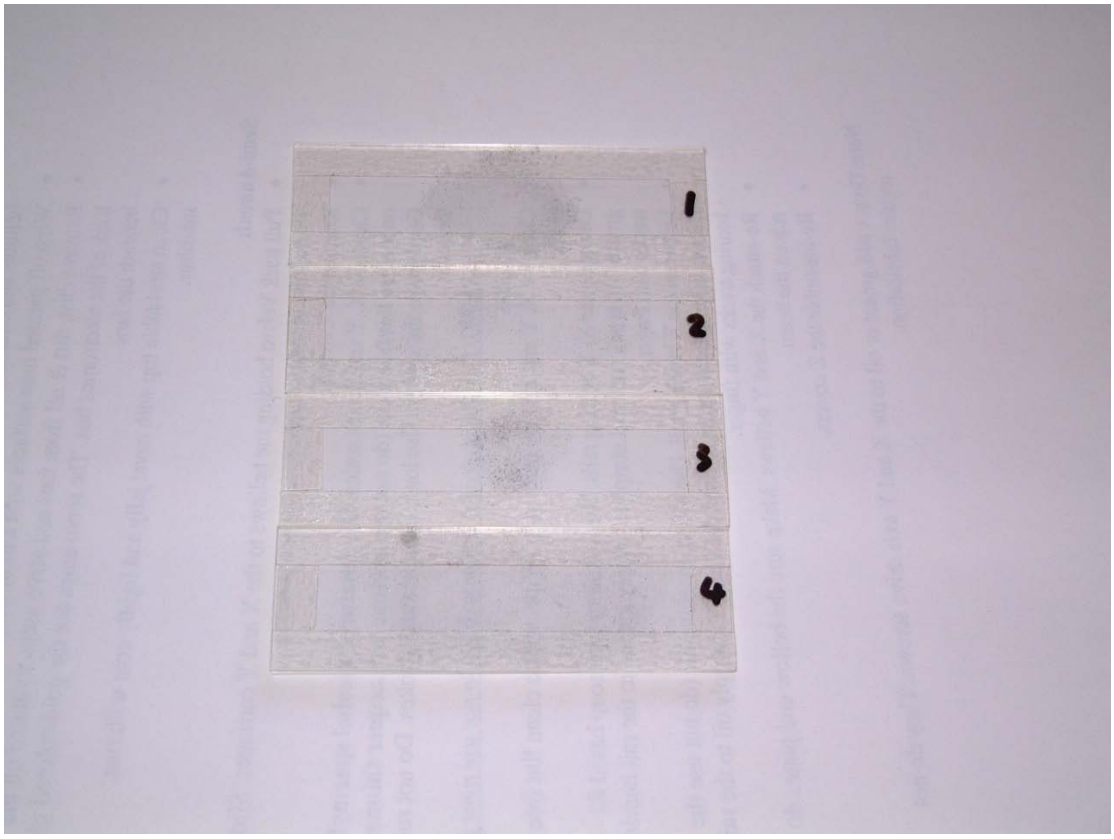

Figure 3.1.3, Sample slides.

The size of the particle measured was Feret's diameter (d_f), and 80 particles were measured from the 4 sample slides. However the Feret's diameter (d_f) was not recommended as the best method to due to its overestimation of particle size **[28]**. Also there was a possibility of identification of a lump instead of an individual particle, therefore, even though the average maximum particle size was 30.4μm and the average minimum was 8.8 μm, a factor of 15% reduction was applied which brought the final result down to 25.84 and 7.48 μm respectively.

3.2 Powder Properties & the Flow Characteristic Determination

Most of the powder properties measurements were conducted within the Department of Chemical & Process Engineering. From Appendix B, the basic properties of the powder were determined from the shear cell experiment; Table 3.2.1 shows the experiment result.

Table 3.2.1, Summary of shear cell experiment result

Bulk Density (kg/m^3)	$F_{critical}$ (MPa)	σ_1 (MPa)	Angle of Repose α	Kinematic angle of wall friction Φ_w
1046.98	705.09	866.5	40	16.44

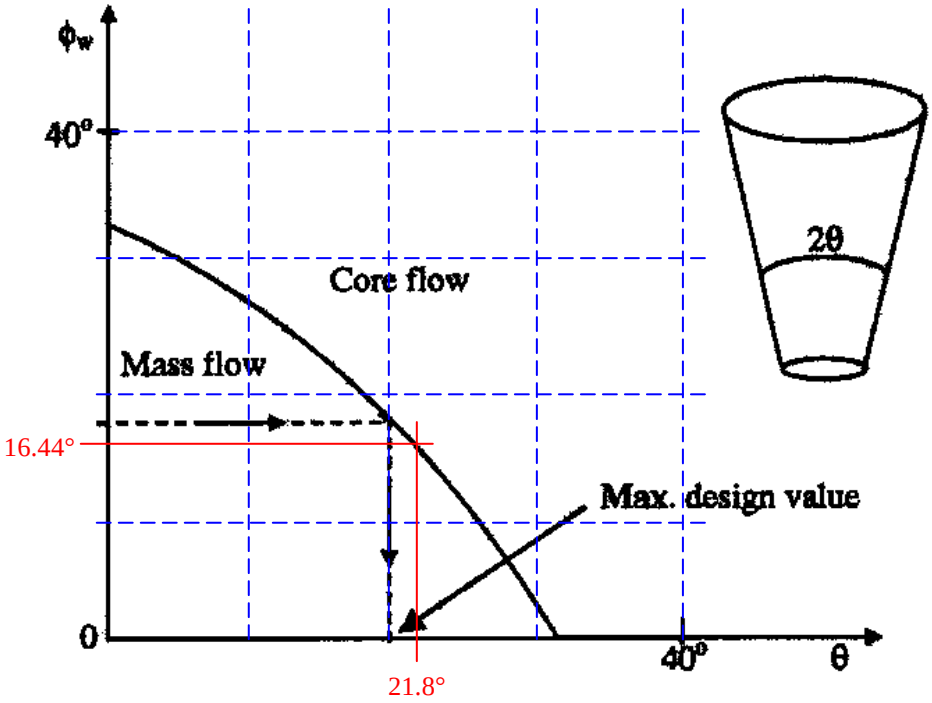

Figure 3.2.1, Kinematic angle of wall friction Φ_w VS half angle θ (Source: Kearney, T. [27])

Figure 3.2.1 shows the relative flow property to the wall slope of the discharge opening, since Φ_w was found to be 16.44°, for a mass flow condition, θ has to be less than 21.8° otherwise core flows will occur.

$$B = 2L_{critical} = \frac{F_{critical} H(\theta)}{\rho_b g} \qquad \textbf{(3.2.1)}$$

where B is the length of the discharge orifice, $L_{critical}$ is the critical half-length of the discharge orifice, $H(\theta)$ is the geometric constant depending on the shape of the orifice and the hopper angle, for conical shape, H(θ) = 2.2. The dimension of the discharge opening was obtained from the equation (3.2.1), and B was found to be Ø151.04mm.

3.3 Conceptual Process Selection

The objective of this section is to provide a broad perspective view on a variety of processes required to construct a complete method which meets the outline requirements. The method for the transportation will be sought by applying a systematic approach adopted from **Pahl, G.** *et al* **[87] and Hales, C. [88]**. A very general design requirement has been listed under the headings *functional, safety, quality, manufacturing, timing, economic, ergonomic, and life cycle* **[88]**, in Table 3.3.1, to provide basic guideline for the process and method selections.

Table 3.3.1, Basic swarf transportation design requirements (Source: Gooch, S. D. [90])

Demand Wish	**Swarf transportation system design basic requirement specification (Requirements under each heading are in order of importance)**
	Functional requirement
D	The mechanism must be able to cope with the existing environment and instruments within the company, e.g. the hopper and trolley. However, minor modifications will be considered.
D	Low or zero dust leakage during discharge process.
W	A fully automatic system.
	Safety requirements
D	Interlock system to prevent operation start without proper engagement of the hopper.
D	Rubber cushion on contact surfaces to prevent spark.
	Quality requirements
D	Design life for mechanism components > 15 years.
D	Compliance with international standards.
	Manufacturing requirements
D	Mechanism to be bolted to a heavy foundation.
D	Exclusive use of manufacturing methods that allows all components to be manufactured in the Mechanical Workshop at University of Canterbury.
D	Minimisation of the machining requirement for all components.
W	Assurance that all major components can be assembled and disassembled using simple hand tools.

	Ergonomic requirements
D	Ease of maintenance
D	Ease of operation, with sufficient indication of the system status.
	Timing requirements
D	Coordination of manufacture with planning schedule at the Mechanical Workshop.
	Economic requirements
D	High efficiency, with minimum labour involvement during the operation.
D	Low maintenance cost, and low consumable components cost.
W	Low production cost and operation cost.
	Ecological requirements
D	Provision of adequate protection of the mechanism and electrical equipment from the outside environment (dust, swarf, and water).
	Life-cycle requirements
D	A service every half year (checks for leakage, replacement of grease, and possible cracks on the surface) and non-destructive inspections of the system structure.

Many methods were found to be feasible for transporting the clean swarf from the hopper and loading it to the barrels, and they fall into three major categories: the electromagnetic, mechanical, and pneumatic transportation methods. In the electromagnetic transportation system, an electromagnet was energised to generate a magnetic field in order to attract ferric base material, then de-magnetised to let the material fall freely. The pneumatic transportation method uses air as the carrier medium to transport the particles to the barrels and the mechanical transportation method requires the use of a mechanical component such as a flat belt, or a screw conveyor to move the particles, e.g. the screw conveying system. The possible processes involved in each method are summarised below in Tables 3.3.2, 3.3.3 and 3.3.4.

Table 3.3.2, Possible processes involve in electromagnetic transportation method

Requirement	Possible Process	Description
Lifting particle up from hopper	Energise the electromagnet. **(P1)**	A powerful electromagnet is attached to a hoist, and energised in order to hold the swarf and lift it out of the hopper at once.
Separation	De-energise the electromagnet. **(P2)**	The electromagnet is de-energised and let the material freely fall into an empty space.
Particle collection and discharge	Mass flow bin **(P3)**	An intermediate space which collects the particles and discharges them when required. All particles within the bin move all the time when discharge takes place.
	Core flow bin **(P4)**	A similar design to the mass flow bin, however due to the wall angle difference, the flow of particles only occurs at the core when discharge take place.
Discharged air	Barrel Filter **(P5)**	A detachable filter unit that attaches to the outlet hole at on the barrel and filters the outlet airflow and discharge into environment.

Table 3.3.3, Possible processes involve in mechanical transportation method

Requirement	Possible Process	Description
Lifting	Hoist **(P6)**	Vertically lifts up the hopper out of the trolley in a frame structure with a hoist.
	Lever arm **(P7)**	Uses the hydraulic actuator to drive the lever arm and lift the hopper up in the air in a circular motion.
	Multi-bar linkage **(P8)**	Combine with hydraulic actuators, and to move the hopper in a circular action while rotation of the hopper also takes place.
Rotating	Hydraulic actuator **(P9)**	Rotation of the hopper is driven by the hydraulic actuator.
	Gear system **(P10)**	Rotation of the hopper is driven by a gear system.

Particle collection and discharge	Mass flow bin Core flow bin	Same as above. Same as above.
Discharged air	Barrel Filter	Same as above.

Table 3.3.4, Possible processes involve in pneumatic transportation method

Requirement	**Possible Process**	**Description**
Lifting particle up from hopper	Vacuum suction **(P11)**	Similar to vacuum cleaner, this sucks the powder from the surface.
	Vortex Generation **(P12)**	Introduces multiple streams of jets in a ring formation, which generate a vortex on the surface of the powder, and lifts it up. This process may require additional use of a fluidised bed.
	Venturi ejector **(P13)**	A partially fluidised bed combines with a high-speed jet which draws the powder from the bottom opening.
Separation	Gravity Settlement **(P14)**	Uses a large empty space for the entrapped particles to settle down by gravity on their own after a period of time.
	Cyclone Separation **(P15)**	Draws the inlet air into the cyclone separation chamber with increasing velocity. As the flow spirals down, this increases the centrifugal force and throws the particles on to the chamber wall and the particles collect at the end of the conical bottom opening.
	Wet Scrub **(P16)**	This introduces the moisture which attaches to the particles and makes them increase in weight and sticks them to the process chamber and collects them at the bottom opening.
Particle collection and discharge	Mass flow bin Core flow bin	Same as above. Same as above.
Discharged	Filter **(P17)**	The filter system for the flow duct collects the remaining

air		particles suspended in the air, and then discharges the clean air into the environment.
	Barrel Filter	The detachable filter is the same as above.

However, not all methods are perfectly suitable for the required task. Each method does have its unique speciality which makes it superior to the others, and therefore after careful consideration and detailed investigation of the background theories, the advantages and disadvantages of each method are tabulated below.

Table 3.3.5, Summary of comparison between different transportation methods

Transportation Method	**Advantage**	**Disadvantage**
Electromagnetic	• Fewer components. • Less process involvement. • Easy to operate. • Ease of maintenance.	• This magnetises the ferric material during lifting, which cause the particles to stick together hence blocking the powder flow. • This magnetises other system components in long-term operations which may greatly affect the discharge process.
Mechanical	• Less process involvement. • Easy to operate. • Ease of maintenance.	• More components may be required. • Noisy to operate.
Pneumatic	• Easy to operate. • Simple to construct. • Ease of maintenance.	• Continuous operating partially fluidised bed and generating vortex may require a large air reservoir to maintain a steady pressure, which heavily loads the air compressor, and it is not economical. • Moving the suction tube to cover a large

		distribution area of material may require an additional complex system design. • Insufficient knowledge of the vortex, therefore this is not practical for implementation in the current situation. • There is low cyclone separation efficiency when the particles are less than 20 μm. • Gravity settlement requires a longer time. • A wet scrub is not permitted due to rusting problems and this requires excessive energy to dry up the swarf. • An additional filter is required for preventing the dust from getting into the fan. • Abrasive particles contact the cyclone separation chamber at high velocity which wears out the chamber wall fast. • This is noisy and may require a longer process time.

The process and method selection are summarised by the process and method selection chart in Figures E1 and E2, where the requirement categories (*functional, safety, quality, manufacturing, timing, economic, ergonomic, ecological, and life-cycle* **[88]**) were scored in terms of meeting the design requirement specification. Two additional categories were included from **Gooch, S. D. [90]**, in this selection: "feasibility" (the level of confidence in making it works) and "information" (meaning the relevant expertise and experience available). By totalling the score of all the successful processes within a particular method, the result will indicate an overall comparison between these three transportation methods as shown in Table E1, hence the conceptual developments will then be conducted on the method with the highest overall score.

This project is aimed at providing a simple, economical, and easy maintenance solution for the company, therefore from selection processes, the implementation of the mechanical transportation method was chosen at this stage as a primary solution and a basis for further development into a final solution.

3.4 Design Requirement

From the experimental result, the repose angle of the swarf indicates that the required hopper rotation is 135° from the initial position in the trolley as shown in Figure 3.4.1.

Figure 3.4.1, Initial position of the hopper.

Since the height of the barrel is 900mm, the minimum distance required between the suspended hopper and the ground level is 1.2m. The swarf contained within the hopper is estimated to be between 350 – 500kg. There are sufficient power supply and compress air connects are ready for use.

As mentioned above, the understanding of swarf property indicates, that in order for the flow to discharge without possible formation of arch, the dimension of the circular opening is required to be greater than Ø151.04mm. However, from the dimensions of the barrel provided, the inlet diameter was restricted to Ø56mm, hence blockage is most likely to occur, and therefore the design of a mass flow bin/core flow bin will not be effective in this situation.

4. CONCEPTUAL DESIGN

The objective of this chapter is to obtain a new improved concept for the mechanical transportation method to cope with the existing hopper and trolley in the company. The solution for the mechanism concept will be sought by applying a systematic approach adopted from **Phal, G.** *et al,* **[87]**, and **Hales, C., [88]**. The processes involved in a complete mechanical transportation method, shown in Table 3.3.3 were reviewed, which regard to the previous process selection; further developments of each the process were carried out and re-weighted. The physical limitations of the basic system requirement were listed in Chapter 3. However, other requirements for the work may be considered under the headings *functional, safety, quality, manufacturing, timing, economic, ergonomic, and life cycle* **[88]**. The full design requirement specification, for the proposed solution to be evaluated, comprises Table 4.1.

Table 4.1, Lifting mechanism requirement specification (Source: Gooch, S. D. [90])

Demand Wish	**Swarf transportation system design requirement specification (Requirement under each heading are in order of importance)**
	Functional requirement
D	The mechanism must be able to cope with the existing environment and instruments within the company, e.g. the hopper and trolley. However, minor modification will be considered.
D	Low or zero dust leakage during discharge process.
D	The hopper has to be able to rotate 135° from its initial position in the trolley, with solid grasp of control mechanism.
D	The discharge opening must be larger than the minimum requirement of Ø151.04mm, and the outer diameter of the discharge pipe connecting to the barrel is less than 56mm
D	Clearance between the rotated hopper suspended and the ground level greater than 1.2m.
W	Fully automatic system.
	Safety requirements
D	Include an emergency stop bottom to isolate power supply in the even of an emergency.
D	Interlock system to prevent operation starting without proper engagement of hopper.
D	Maintain minimum safe spectator distance of 0.25m, and safety gate to prevent objects being caught during operation.

	Quality requirements
D	Design life for mechanism components > 15 years.
D	Wiring for electric machines to comply with NZAS 3000.
D	All manufactured components to be inspected to comply with tolerances specified on manufacturing drawings.
	Manufacturing requirements
D	Mechanism to be bolted to heavy foundation.
D	Only use manufacturing methods that allow all components to be manufactured in Mechanical Workshop at University of Canterbury.
D	Minimise the machining requirement for all components.
W	Ensure that all components can be assembled / disassembled using simple hand tools.
	Ergonomic requirements
D	All independent on-site fine adjustments.
D	User interface to clearly identify key performance control function.
W	Full LCD display to show the operator the current status of the system.
	Timing requirements
D	Coordinate manufacture with planning schedule at Mechanical Workshop.
	Economic requirements
W	Total project material cost as low as possible.
	Ecological requirements
D	Provide adequate protection to mechanism and electrical equipment from the outside environment (dust, swarf, and water).
D	Include fuse-able links and/or circuit breakers to protect control system from power surges.
	Life-cycle requirements
D	Service every half year (checks for leakage, replacement of grease, and possible cracks on the surface) and non-destructive inspection of the system structure.

From the design requirement specifications listed above, a swarf transportation system may be considered under the 5 sub-systems given in the organisation chart, Figure 4.1.

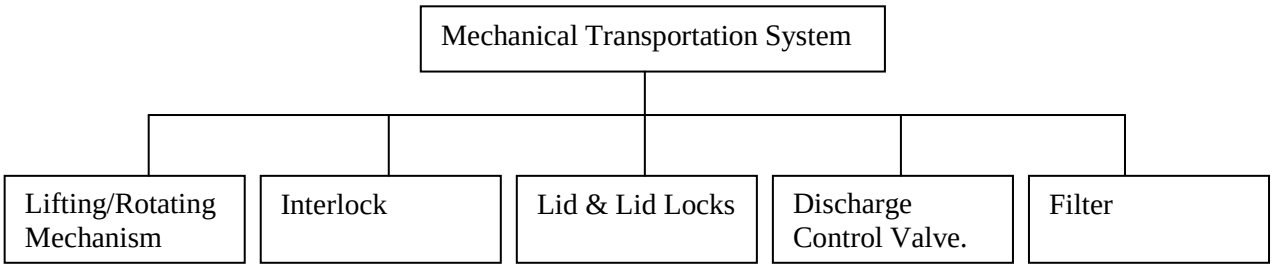

Figure 4.1, Sub-system for the swarf transportation system design.

This chapter will introduce the concept selections for each mechanism in the following order:

1) ***Lifting/Rotation Mechanism Design Concepts*** – the main driving mechanism and support structure for the transportation system.

2) ***Interlock Design Concepts*** – locking mechanism that secures the hopper during operation.

3) ***Lid & Lid Lock Design Concepts*** – the main covering device for the hopper with a discharge port which provides the tube connection for the control valve. The lid lock provides a quick and easy operation to secure the lid to the hopper.

4) ***Discharge Control Valve Design Concepts*** – the open/close powder flow control valve which is employed to connect between the lid and the barrel.

5) ***Filter Design Concepts*** – the filter for removing the particles from exit air on the barrel.

The approach taken is to divide each of the five sub-systems into sub-functions. With the schematic diagrams of the solution principles considered, a morphological matrix can is then constructed **[90]**. From the concept selection chart adopted from **Phal, G.** *et al* **[87]**, the solution principles for each sub-function in the morphological matrix are selected.

Finally, a brief description of the systematic approach method which is employed for reviewing concept selection process.

4.1 Lifting/Rotating Mechanism Design Concepts

The purpose of this section is to establish a new concept for the lifting/rotating mechanism that can cope with the existing company hoppers and trolleys. After considering the sub-system in Figure 4.1, the lifting/rotating mechanism is the critical sub-system for which a concept will be further sought. This sub-system aims to satisfy the design requirement set earlier of a simple method and low cost. This mechanism will be constructed from standard steel sections from Steel & Tube Ltd and painted over to prevent rusting.

The approach taken is to divide each sub-system into possible solutions and to build a morphological matrix using schematic diagrams of the solution principles considered. The selected solution is then highlighted.

Morphological Matrix: Lifting/Rotating Mechanism

From \ Solution	1	2	3
Hoist (A)	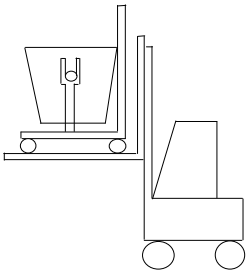	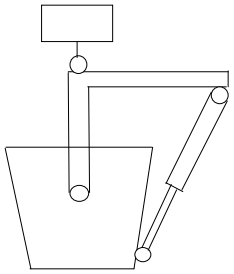	
Lever (B)	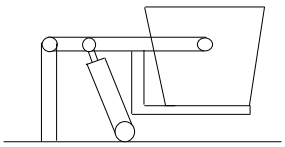	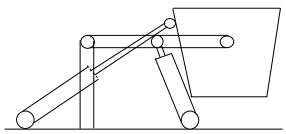	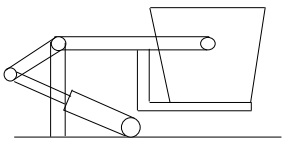
Multi-Link (C)	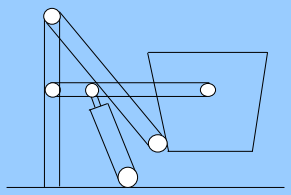	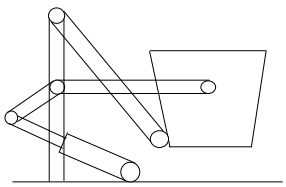	

Figure 4.2, Solution forms considered for the lifting / rotating mechanism.

The original solution (A1) was using a forklift to suspend the trolley and hopper above the waste collection bin, and then the operator manually rotates the hopper with a lever arm and discharges the swarf into the bin. This method was quite a simple and economical solution when dealing with dirty swarf (containing more than 20% of grinding fluids); however, since the property of the swarf changes dramatically after leaching, it is now dried and can be air lifted easily. The conventional method may violate the health and safety issue, therefore a covering lid is required.

As for the discharge flow rate issue, the collection bin originally used is a standard waste management bin, with an opening area approximately 8 m^2. As the entrance is a lot greater than the opening of the hopper, an arch can not during discharge. With the new requirement, due to the limitation of the inlet hole, the hopper is required to be held in a discharge position far much longer than before, therefore the continued use of a forklift in this application is not permitted. Hence, the use of a hoist in a monorail is introduced to replace the forklift (A2).

In the lever and multi-link system, the hydraulic actuators provide the main control mechanism for positioning the hopper. A lever system requires a fix holder to keep the hopper parallel to the lever arm, and a longer stroke. As the actuators extend / retract, the load gradually changes its direction. When the lever arm rotation is greater than 90°, the acceleration of the hopper starts to increase due to gravity, hence the extension of the actuator will be faster than the volume flow rate of the pump, which is uncontrollable; therefore an off-centre valve is required to be added into the hydraulic circuit to maintain good control of the system.

The multi-link system involves complex mathematical calculation; however, the desired position can easily be achieved. Due to safety concerns, the hopper position during the suspension period will not be directly above the area which the operators may need require to attend, e.g. during switching the barrels.

4.2 Interlock Design Concepts

When the hopper is aboard the trolley, it is supported by the two Ø50mm steel rods extended out from the hopper wall and sits in the yokes located on the trolley as shown in Figure 4.3. The interlock mechanism is designated to be part of the lifting/rotating system; it is attached to the tip of the lever arms to contact and secure the hopper support rods and use them as a pivot point to rotate the hopper as the lever arm rotates.

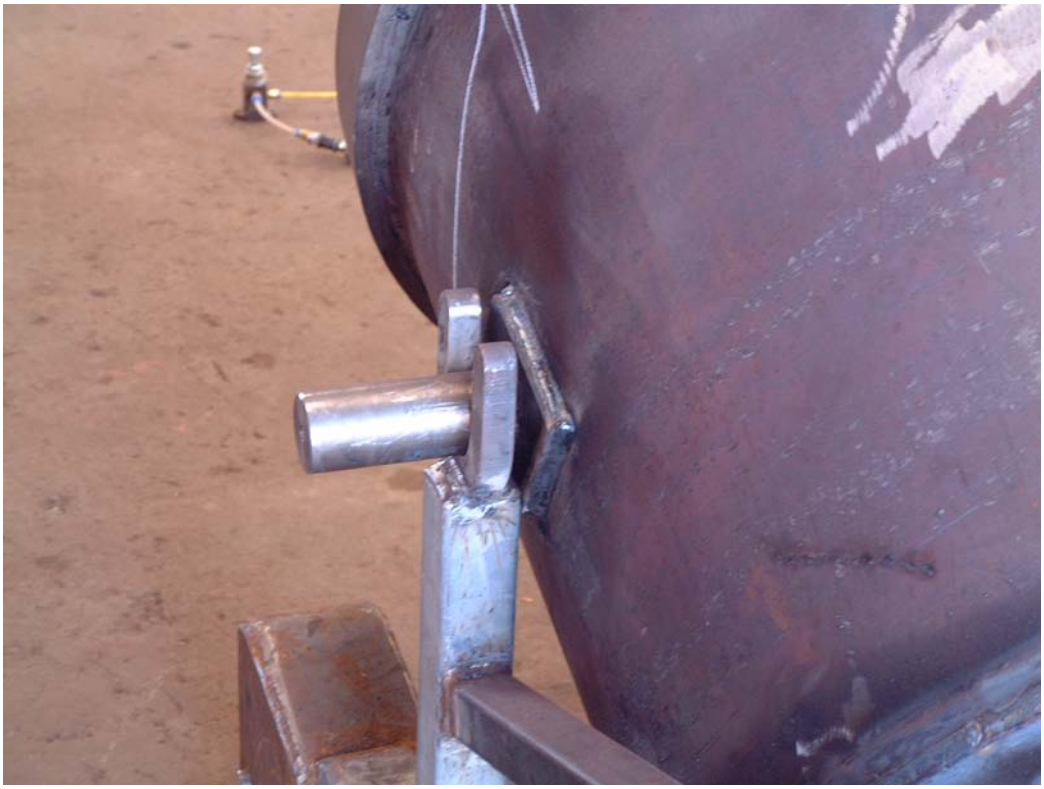

Figure 4.3, Hopper support mechanism on trolley.

The interlock system functions to provide a safe launch signal for the operator to start/stop the process and maintain the hopper's attachment to the lever arm during an emergency or failure in the system. The interlock system consists of two main parts, the interlock body, and sensor platform. The function of the interlock body controls the open/close of the safety lock; the sensor platform functions to detect the contact between the lever arm and the support member in order to correct the position of the tilt sensor. A preliminary investigation has revealed that when multiple sensors are employed, the control system can be implemented for a reasonable cost using a programmable logic controller (PLC). The working principles considered in the development of the shuttle mechanism concept are illustrated in the morphological matrix in Figure 4.3.

Morphological Matrix: Interlock Mechanism			
Solution / Form	**1**	**2**	**3**
Interlock Body (D)	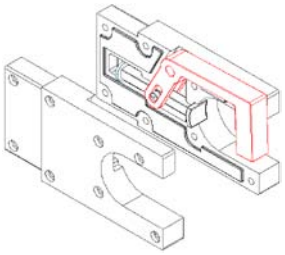	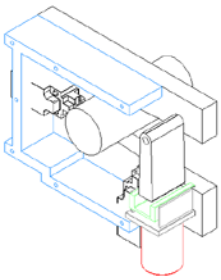	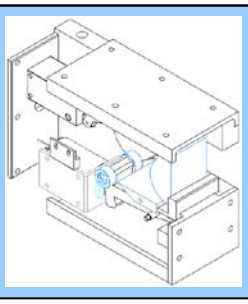
Sensor Platform (E)	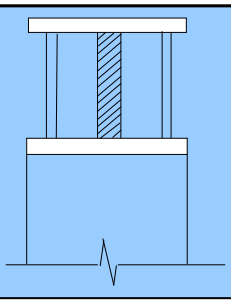		

Figure 4.4, Solution forms considered for the interlock mechanism.

The interlock body in (D1) purely relays the mechanical system, the gate open/close depends on the location of the support rods, hence when the position of the lever arm is greater than 0°, the self weight of the hopper will keep the locking mechanism closed tightly; however, if it is below horizontal, then the hopper will be able to fall out without control. The swing gate with lever blocking mechanism (D2) is driven by a solenoid actuator which gives a better control during emergency; however, there is insufficient feedback to indicate the position of the lever arm and automatically close the gate when supports are in the correct position. With the combination of both mechanical and electrical systems (D3), the support rod gradually moves into the groove when the lever arm stars to rotate which secures the hopper in position. The support rod can only be brought back to the original position when the trolley is present in the correct position. The limit switches and solenoid actuator operate together to provide feedback and assist the lock opening/closing operations to the PLC, therefore to a large extent meeting concerns about the operation of the mechanism.

The sensor platform is located on the support arm, and a limit switch is attached to this device to indicate contact made by the lever arm and provides an additional feedback to decision making on opening/closing of the lock.

4.3 Lid & Lid lock Design Concepts

From the health and safety perspective, since the size of a clean swarf particle is very small, it can be lifted by air easily; hence it is essential to keep the abrasive particle within a close environment during the process. A set of quick release locking mechanisms is required to firmly hold the lid throughout the process. The working principles considered in the development of the lid & lid lock mechanism concepts are illustrated in the morphological matrix in Figure 4.5.

Morphological Matrix: Lid & Lid Lock Mechanism

Solution / Form	1	2	3
Lid (F)	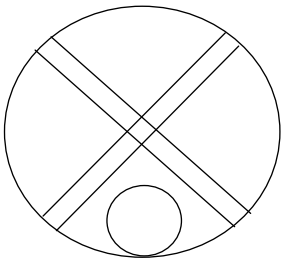	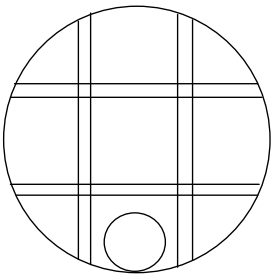	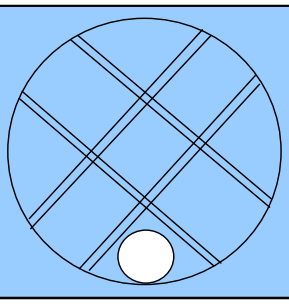
Lid Lock (G)	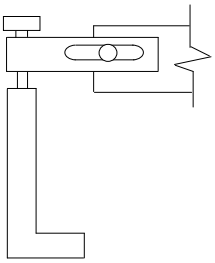	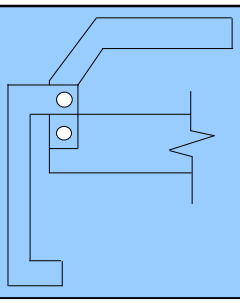	

Figure 4.5, Solution forms considered for the lid and lid lock mechanism.

Since the lid has to take a maximum of 500 kg over a 1.0 m diameter circular area, girders are attached to provide additional support, and the lid locks are attached on both ends of the girders. In order to reduce the overall thickness and weight of the lid, and maintain low deflection, multiple girders (F2 & F3) made by RHS members are used. The location of the lid locks may come in contact with the hopper and lifting/rotating mechanism during the discharge process; hence the selected solution has sufficient clear space for lid lock installation (F3). Both the screw type lid lock (G1) and over-centre lock (G2) have the advantage of easy operation; however, the screw type lock does require additional tools to tighten/loosen during engaging/disengaging the lock and more time to complete the locking/unlocking operation. Therefore the over-centre lock was selected.

4.4 Discharge Control Valve Design Concepts

The function of the control valve is to control the open/close operation and directed the flow of the clean swarf into a barrel with minimum leakage of powder into environment. As mentioned earlier in chapter 3, the minimum requirement of the tube size for mass flow is Ø150.04 mm; however, the inlet size on the barrel in limited to Ø56 mm, therefore blockage is most likely to occur at this section of the discharging process. A pneumatic vibrator was considered necessary to break the arch and maintain a more steady flow.

The working principles considered in the development of the lid & lid lock mechanism concepts are illustrated in the morphological matrix in Figure 4.6.

Morphological Matrix: Control Valve Mechanism			
Solution / Form	**1**	**2**	**3**
Control Valve (H)	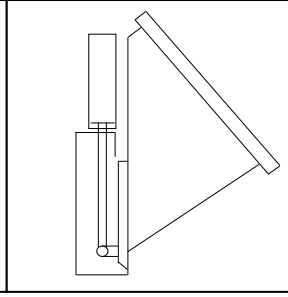	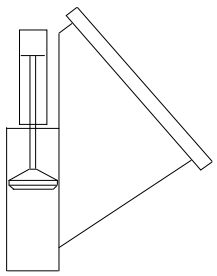	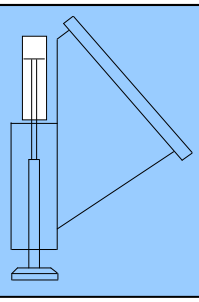

Figure 4.6, Solution forms considered for the control valve mechanism.

All the mechanisms are operated with the use of a double acting pneumatic actuator; however, the sliding gate mechanism (H1) may most likely generate a bending moment on the actuator and damage it. The internal valve (H2) provide good protection for the actuator, and the extension stroke can assist the operation by breaking the arch that forms in the flow duct and stops an efficient flow. However, when the powder builds up in the duct, the retraction stroke may not be able to complete due to this obstruction. The external valve (H3) resolves the possible problems that occur during the extension/retraction of the actuator; the possible damage due to bending moment may be resolved with a guiding rail installed in the duct to direct the actuator path.

4.5 Filter Design Concepts

When the discharge of powder takes place, the air within the barrel will be pushed out through the outlet hole on the barrel; however, a small amount of the particles will be transported from this stream of flow. The function of the filter is to stop the suspended particles in the discharge air from coming out of the outlet hole on the barrel.

The working principles considered in the development of the lid & lid lock mechanism concepts are illustrated in the morphological matrix in Figure 4.6.

Morphological Matrix: Filter Mechanism			
Solution / Form	**1**	**2**	**3**
Filter (I)	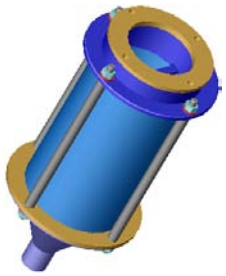	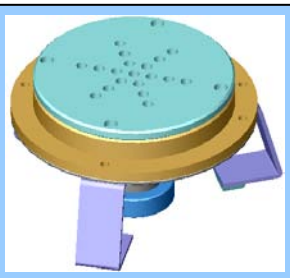	

Figure 4.7, Solution forms considered for the filter mechanism.

The filter is designed to fit directly to the outlet hole of the barrel and allow the exit air to flow through the filtering medium. The filtered particles then fall back into the barrel as soon as the exit air flow is stopped e.g. the discharge process is stopped. Both solutions (I1 & I2) use filter paper to entrap the suspended particles on the exit air flow. Since the exit flow velocity from the barrel is estimated to be slow, standard filter paper from BIOLAB was selected. As the filter is required to be portable, light weight, and has to fit well on the barrel, compact size filter was selected (I2).

4.6 The Final Concept Selected for the Transportation System

The aspects of each of the principle solutions considered for the sub-systems shown schematically in Figures 4.2, 4.4, 4.5, 4.6 and 4.7 were assessed in terms of the design requirement specification in Table 4.1.

The concept selection process is summarised by the concept selection charts in Figures F1, and F2 where the requirement categories (*Functional, Safety, Quality, Manufacturing, Timing, Economic, Ergonomic, Ecological, and Life-cycle* **[88]**) were scored in terms of meeting the design requirement specification. Two additional categories from **Gooch, S. D. [90]**, were included in the concept selection process: "feasibility" (the level of confidence in making it works) and "information" (meaning the relevant expertise and experience available).

The selected concepts for each sub-system were reviewed using a conceptual design work sheet adopted from **Hales, C. [88]** in Figures F3. The conceptual design work sheet reflects a good level of confidence for the chosen mechanism function; therefore it was decided to proceed to improve the arrangement in terms of meeting the manufacturing, safety and economic requirements.

5. EMOBDIMENT DESIGN

The transportation system is designed to lift the hopper out from the trolley and rotate 135° in order to discharge the swarf out from hopper into the barrels.

The purpose of this section is to present the proposed solution developed for the swarf transportation system and the required driving mechanisms, e.g. hydraulic actuator, pneumatic actuator, further in depth. This chapter will break down the transportation system into six sections listed as follows:

1) ***Lifting/Rotating Mechanism Design*** – this section includes the description of the multi-link lifting/rotating mechanism along with interlock attachments, the lid lifting mechanism, and the required modification on the existing hopper.

2) ***Interlock Equipment Specification*** – this section details the logical control for the interlock system which has been designed to maintain the supporting rod in the holding position if a state of emergency occurs.

3) ***Lid & Lid Lock Design*** – this section includes the design of the lid, lid lock, flange and rubber tube connection.

4) ***Prototype Valve Design*** – the main focus for the discharge from hopper to barrel mainly relays on the design of the control valve, therefore, a description of this component will be included in this section. This includes the design of the pneumatic system and associated circuit.

5) ***Filter Design & Specification*** – this section provides the detail specification for the design of the filter unit and how it is fitted on the barrel.

6) ***Hydraulic System Design*** – since the multi-link lifting/rotating mechanism and lid lifting mechanism are powered by hydraulic actuators, therefore a hydraulic circuit is required to be designed.

7) ***Detail Design***: the overall detail design of the system will be described in this section.

With the announcement regarding to the withdrawal of the industrial sponsorship half way through the project, the construction of the full scale system was forced to stop. However, the development of the transportation system was continued right to an initial stage. A preparatory hydraulic circuit and the pneumatic circuit were designed, however, validation from the supplier is essential before any construction can be carried forwards, therefore detail parts specification and costing were not included at this stage.

5.1 Lifting/Rotating Mechanism Design

Even though the lifting/rotating mechanism included the interlocks and lid lifting mechanism attached on the structure; however the detail of the interlock will be described in a later section. This mechanism consists of 8 major components: base post, lid lifting mechanism, primary arm, secondary arm, 8" & 14" hydraulic actuator unit, linkage arm, and the modification joint on the hopper as shown in the diagrams below:

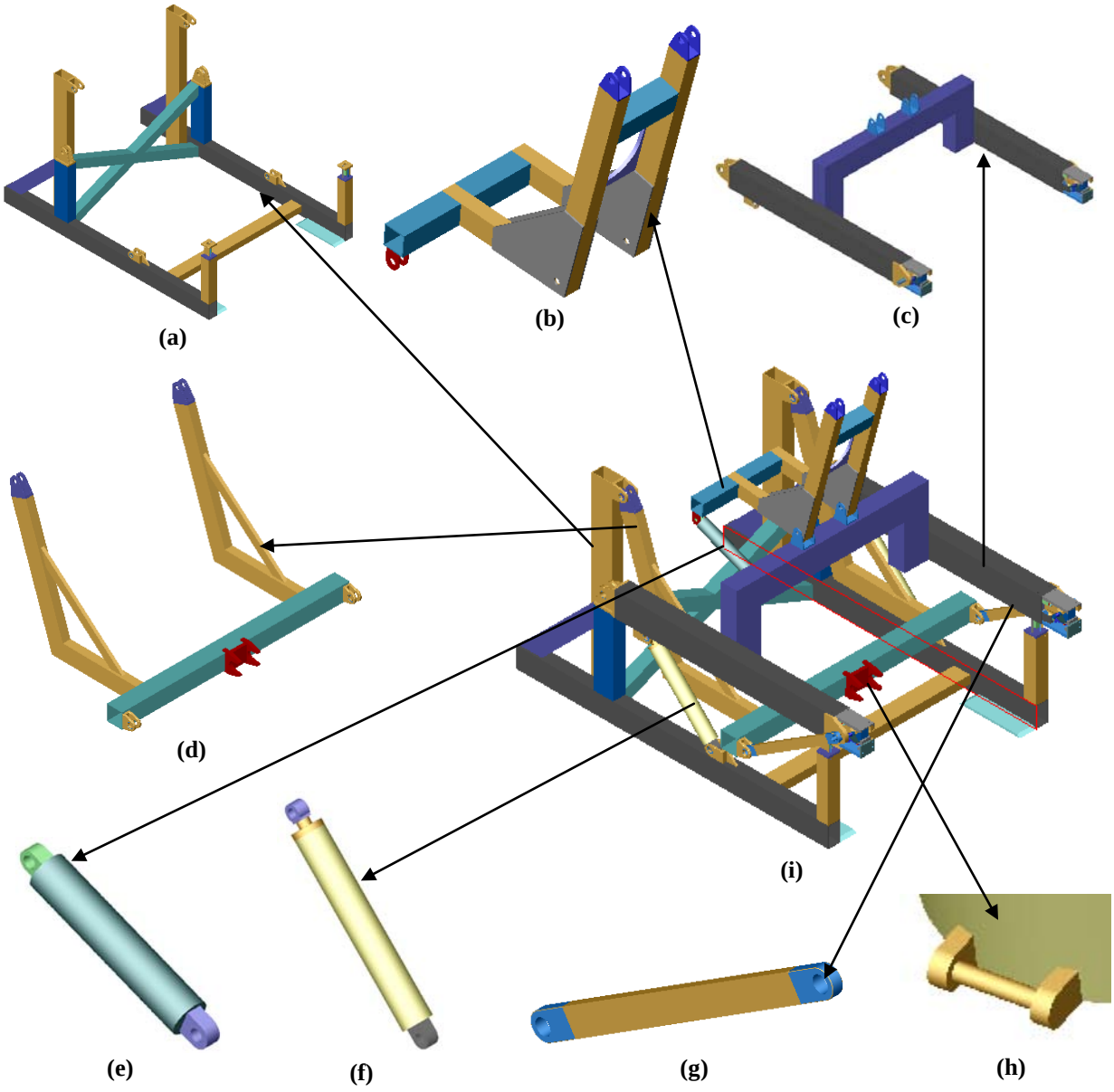

Figure 5.1, Embodiment for the lifting / rotating mechanism with 8 major components (a) base post, (b) lid lifting mechanism, (c) primary arm, (d) secondary arm, (e) 8" Hydraulic actuator unit , (f) 14" hydraulic actuator unit, (g) linkage arm, (h) modified joint on the hopper, which combined and formed the lifting/rotation mechanism in (i).

Objectives of this development of the mechanism, as shown above, were to maximise the structure stability and be certain no structural interference will occurred under operation between the rotating members.

The primary arm and secondary arm were connected to the lower and upper joint respectively on the base post with bush bearing and shoulder bolts kept it in location, and the linkage arms were then connected at the free joints between the primary and the secondary arm from both sides to avoid interference while keeping the structure from falling apart. Cross members were applied to provide lateral support for all the structures.

Two standard 2" bore, 1.25" piston rod with 14" stroke length Victor hydraulic actuators is determined in order to provide a maximum primary arm rotation of 80° while the hopper undergoes 135° rotation. The selected actuators from the catalogue provide sufficient force to drive the entire mechanism with 60% of the specified pressure rating. The connection locations on the primary arm and base post were also determined form the spreadsheet; bush bearing with shoulder bolt fixture were applied to secure the devices.

The lid lifting mechanism was an additional adapted feature in the lifting/rotating mechanism. It was welded onto the cross-member on the primary arm and driven by a 2" bore, 1.0" rod with 8" stroke length Victor hydraulic actuator. The lid lifting mechanism was designed to provide 75° rotation and sufficient force at 60% of the rated operating condition to lift the lid up with a chain linked between the two objects. The hydraulic actuator connection locations on the primary arm were also determined from the spreadsheet; bush bearings with shoulder bolt fixture were applied to secure the devices.

All the hydraulic tube/pipe connections were required to be kept away from the rotating joints to avoid being caught during operation. Additional installation of clamps on the transportation system to secure the piping/tubing may be considered.

The interlocks were installed on the tips of the primary arm with four M5 x 25mm screws and washers to tightly secure the position of the units on each side. The electrical wirings were kept within the RHS sections of the primary arm and re-exposed at the other ends of the section for further connections.

The primary arm supports which are part of the interlock system were welded on at the far ends of the base post. Electrical wiring of these components was to be kept within the SHS section and then re-exposed near the ground level for further connection.

An additional joint was constructed and welded onto the hopper which modified it to work with the designed system. Since there are more than 2 hoppers within the company, both of the hoppers will be required to undergo the modification. Both the support rods and the new additional joint on the hopper will need to be lightly greased before operation. This minimises the wear between the contact surfaces on both the hopper and the transportation unit.

5.2 Interlock Equipments Specification

The solvent used in the leaching process is the highly flammable hexane; therefore it is required to prevent any possible sparks produced during an emergency situation (e.g. if the hopper falls down and produces sparks). With the high risk issue, systematic development on the interlock system is required. Objectives in the development of the interlock system were to determine the logic control requirement in order to firmly secure the supporting rod in place during emergency and then specify the electronic components required in the system.

A large variety of sensors, proximity switches, and limit switches is available for detecting the position of the primary arm in the lifting/rotating mechanism and position of the support rod on the hopper. These electronic components considered most likely to be suitable for this application are categorised into 5 types: optical, induction, magnetic, title, and limit switch.

After thorough investigation, it was noticed that the optical, magnetic, and induction type sensors were not suitable for this application. Regular cleaning will be required for the use of the optical sensor in the dusty environment (even though the transportation is designed to be leakage free, however, dust build up is still possible from other surrounding devices). The induction and magnetic sensor are very sensitive to ferric materials, and since most of the surrounding components are made of steel, signals from the sensors is therefore not accurate.

The proposed design as shown in Figure 5.2.1 the interlock body and Figure 5.2.2 the sensor platform includes only the limit switches and tilt sensors to determine the operating status for the solenoid actuator.

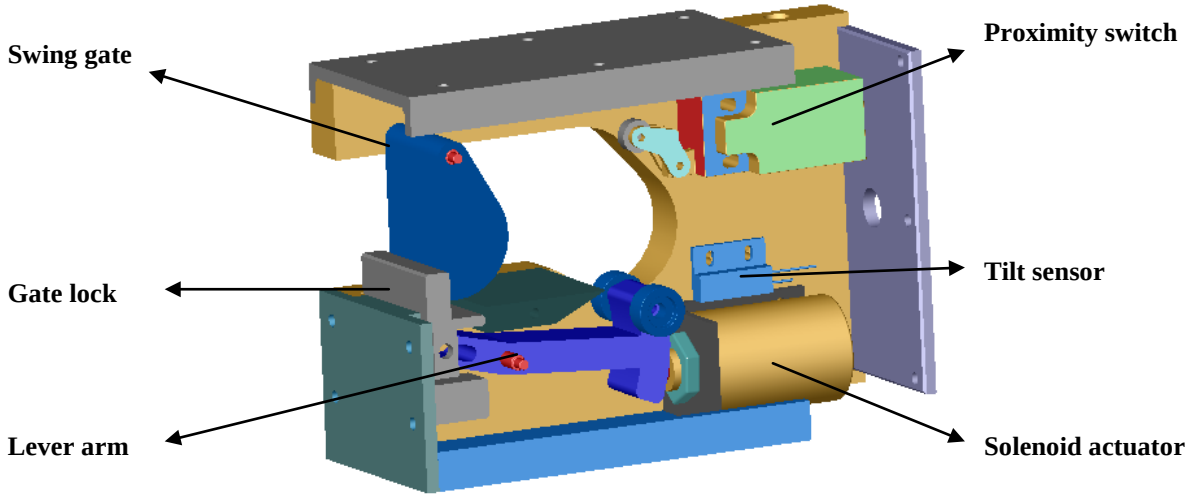

Figure 5.2.1, Embodiment for the interlock

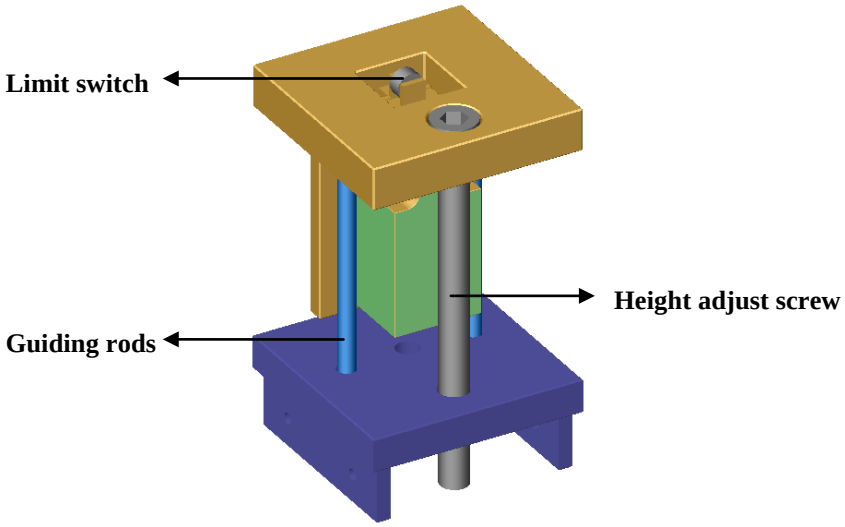

Figure 5.2.2, Embodiment for the sensor platform.

On the interlock body, a limit switch was installed with the screws specified by the manufacture on the base plate, and located at the position where the support rod makes contact with the tip. Two tilt sensors were positioned in the interlock system in order to provide sufficient comparison in decision making; one is placed horizontally (T_{S1}), and the other is 2° below horizontal (T_2).

The solenoid actuator was located on a mounting plate with a M16 nut provided by the manufacture. It was then located to provide interference for the mechanical lever system while energised, which secures the gate lock to stop the swing gate while reducing the exit dimension to stop the support rod falling out.

All the electronic components were fastened onto one of the base plate. Together with the top and bottom cover plate, it was then assembled with M5 screws. A front cover plate and joint plate were placed to secure the locking mechanisms from other sources of interference.

The sensor platform was designed to attach onto the primary support arm on the base post with four M4 screws and washers. The primary arm is meant to make contact with the limit switch while in the horizontal position, which provides an additional signal to determine the operating status for the interlock system. An M10 threaded rod was attached between the two plates to provide fine adjustment.

5.2.1 Logic Control of Interlock System

Figure 5.2.3 shows the interlock mechanism located on the right hand side of the primary arm.

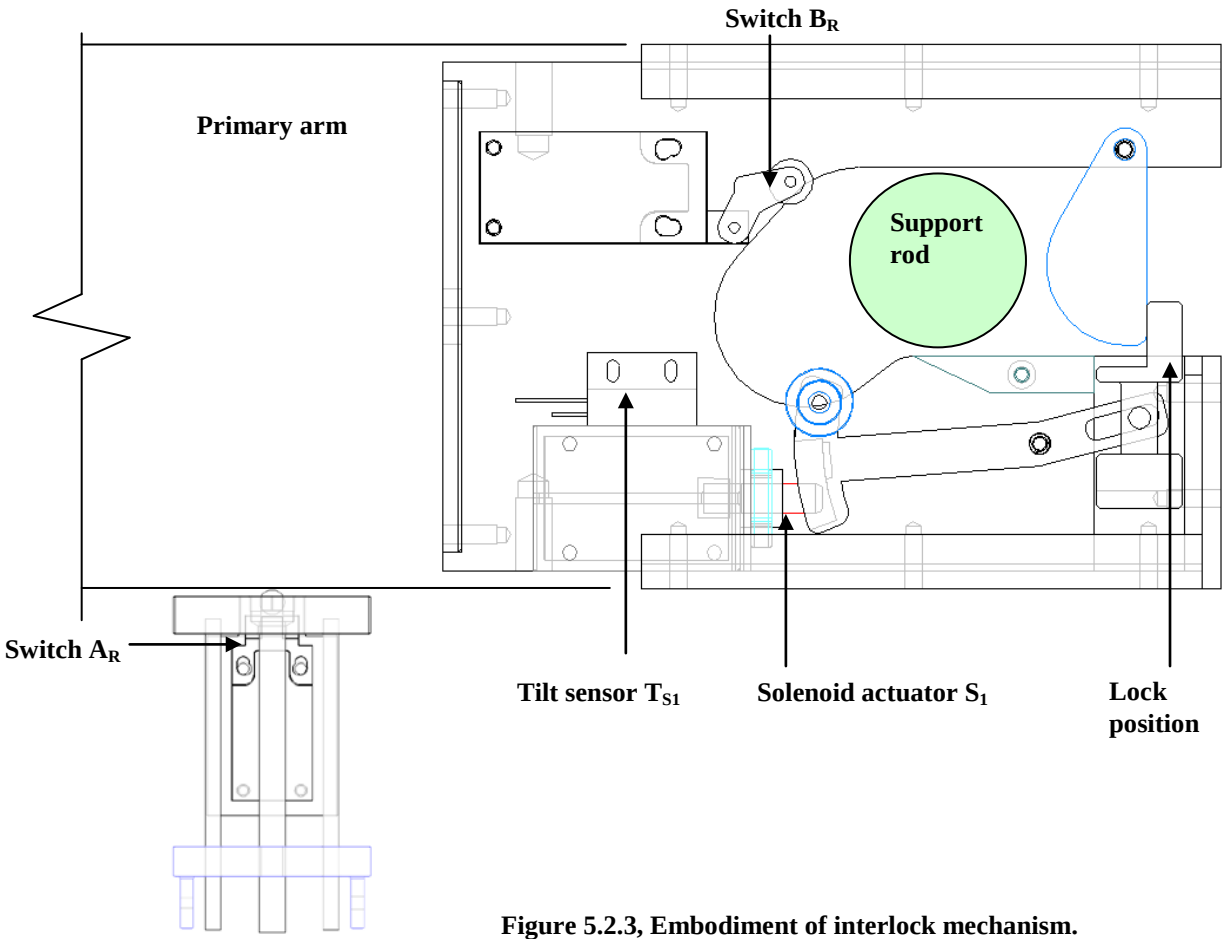

Figure 5.2.3, Embodiment of interlock mechanism.

The trolley with hopper aboard is required to be manually pushed to the transportation system. The interlock system was designed to stay in the locking position while no power is supplied; hence it is necessary to turn the transportation system power on before the trolley makes any contact with the system. The ascending and descending operating sequences of the interlock system are as shown in Figure 5.2.4, and 5.2.5 respectively.

Manually push the trolley towards the transportation system. Support rods on the hopper make first contact with the swing gate.	**Support rods contact with the switch B_R and B_L.**	**Support rods descended to the designed yokes due to self-weight. The support rods no longer contacts switch B_R and B_L.**
Hydraulic status: Fully Close **Primary arm status: Horizontal** **Interlock status: Unlock** **System status: Not Ready**	**Hydraulic status: Fully Close** **Primary arm status: Horizontal** **Interlock status: Lock** **System status: Go Ready**	**Hydraulic status: Extending** **Primary arm status: + Tilt** **Interlock status: Lock** **System status: Go Ready**

Figure 5.2.4, Ascending operating sequences.

Hopper holds in discharge position, and ready for boarding to trolley. Support rods still secured in the yokes. **Hydraulic status: Fully Open** **Primary arm status: + Tilt** **Interlock status: Lock** **System status: Go Ready**	→	**Hopper gradually descends until the support rods contact with the yokes on the trolley, then support rods are lifted and make contact with switch B_R and B_L.** **Hydraulic status: Retracting** **Primary arm status: + Tilt** **Interlock status: Lock** **System status: Go Ready**

→	**The hopper is back on the trolley, which requires to be manually disengaged and makes no contact with switch B_R and B_L,** **Hydraulic status: Fully Close** **Primary arm status: Horizontal** **Interlock status: Unlock** **System status: Not Ready**

Figure 5.2.5, Descending operating sequences.

The operating behaviour of the tilt sensor in Figure 5.2.6 is described in Table 5.2.1. It was found a single tilt sensor is insufficient to correctly determine whether the primary arm has been tilted or not.

Table 5.2.1, Sensor behaviour

Angle (deg)	Sensor Status
-4 > θ	OFF
-2 = θ	OFF
-2 < θ < 2	ON/OFF
2 = θ	ON
4 > θ	ON

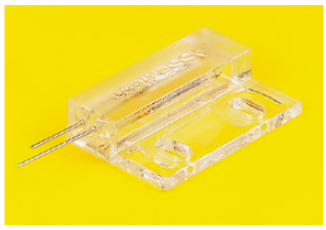

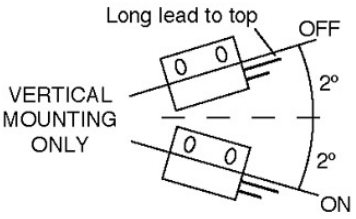

Figure 5.2.6, Tilt sensor (Source: Farnell Website)

By combining two tilt sensors together, as described earlier, T_{S1} horizontally installed and T_{S2} installed with -2° tilt, the combined signals can then be compared, as shown in Table 5.2.2.

Table 5.2.2, Combine status of tilt sensors on ascending and descending operation

Primary Arm (deg)		T_{S1} (deg)	T_{S1} Status	T_{S2} (deg)	T_{S2} Status	Tilt (Yes/No)
-4 > θ	**Up**	-4 > θ_{Ts1}	OFF	-6 > θ_{Ts2}	OFF	**NO**
-2 = θ		-2 = θ_{Ts1}	OFF	-4 = θ_{Ts2}	OFF	**NO**
-2 < θ < 2		-2 < θ_{Ts1} < 2	OFF	-4 < θ_{Ts2} < 0	OFF	**NO**
2 = θ		2 = θ_{Ts1}	ON	0 = θ_{Ts2}	OFF	**NO**
4 < θ	**UP/Down**	4 < θ_{Ts1}	ON	2 < θ_{Ts2}	ON	**YES**
2 = θ	**Down**	2 = θ_{Ts1}	ON	0 = θ_{Ts2}	ON	**YES**
-2 < θ < 2		-2 < θ_{Ts1} < 2	ON	-4 < θ_{Ts2} < 0	OFF	**NO**
-2 = θ		-2 = θ_{Ts1}	OFF	-4 = θ_{Ts2}	OFF	**NO**
-4 > θ		-4 > θ_{Ts1}	OFF	-6 > θ_{Ts2}	OFF	**NO**

An overall logic flow diagram for the interlock system is shown in Figure 5.2.7.

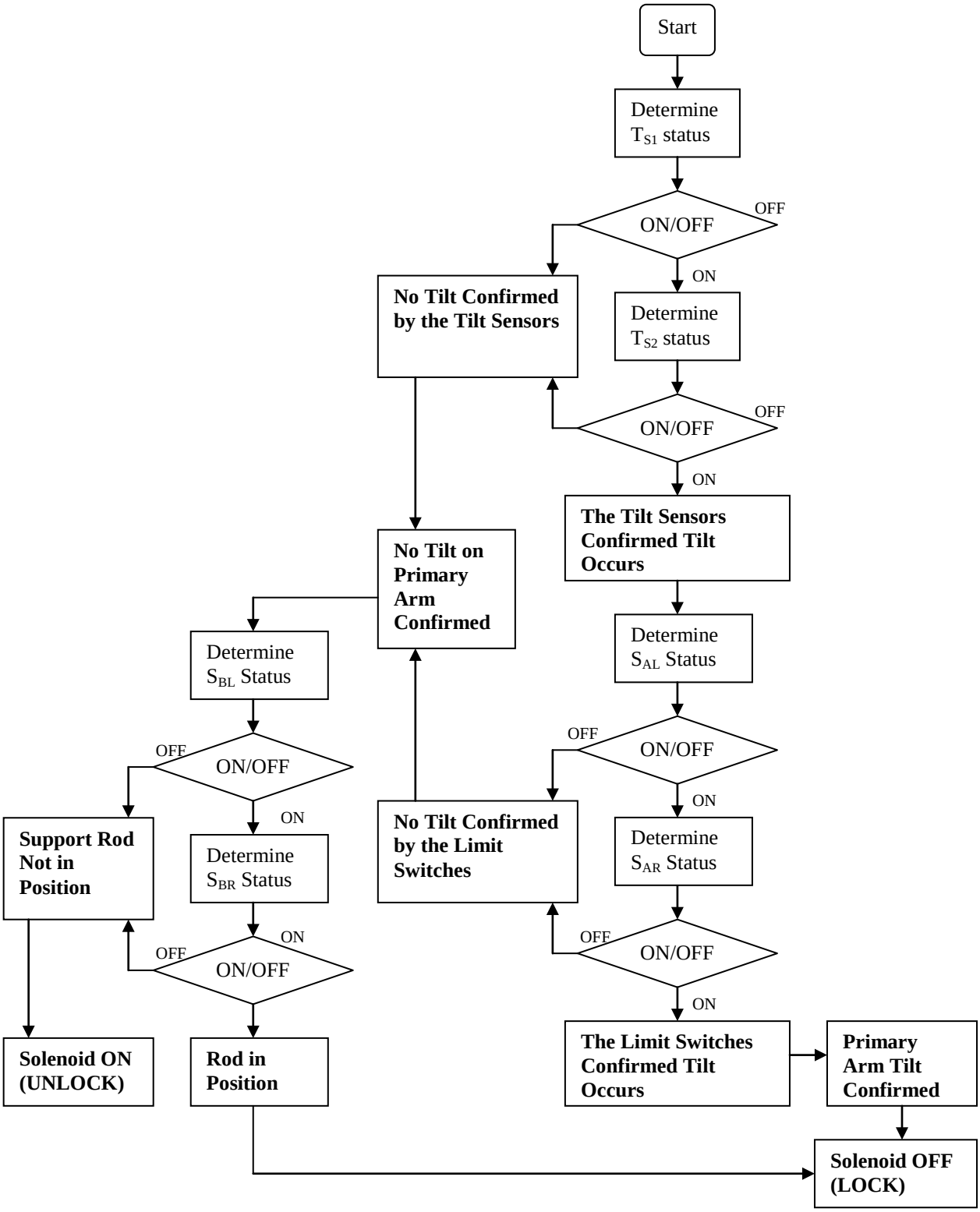

Figure 5.2.7, Logic flow diagram for the interlock system.

Note: Subscript L & R indicated the location of the limit switch on left and right

5.2.2 Interlock Parts Selection & Specification

Table 5.3 listed the electronics selected for the design of the interlock system; however, this does not include the relative connection mediums between sensors/switches to the PLC unit.

Table 5.3, Electronic components list in interlock system

Parts	**Type**	**Code**	**Manufacture**	**Quantity**
T_{S1}, T_{S2}	Mercury tilt sensor	TSM4/240	ASSEMTech	2
S_B	Limit switch	D4D132N	Omron	2
S_A	Limit switch	D4D162N	Omron	2
Actuator	Solenoid actuator	GHUZ040M20D01 24V100%	Emessem	2
Controller	PLC Controller	PLC Starter Kit	IMO	1

5.3 Lid & Lid Lock Design

After operating lifting/rotating mechanism, the hopper is in the designed position to let the powder flow freely. A lid is designed to keep the powder in the hopper while discharging takes place and a set of lid locks is there for securing the lid. This mechanism consists of 8 major components: lip A, lip B, lid base plate, locking ring, girder, tube flange, lid joint, and lid lock as shown in the diagrams below:

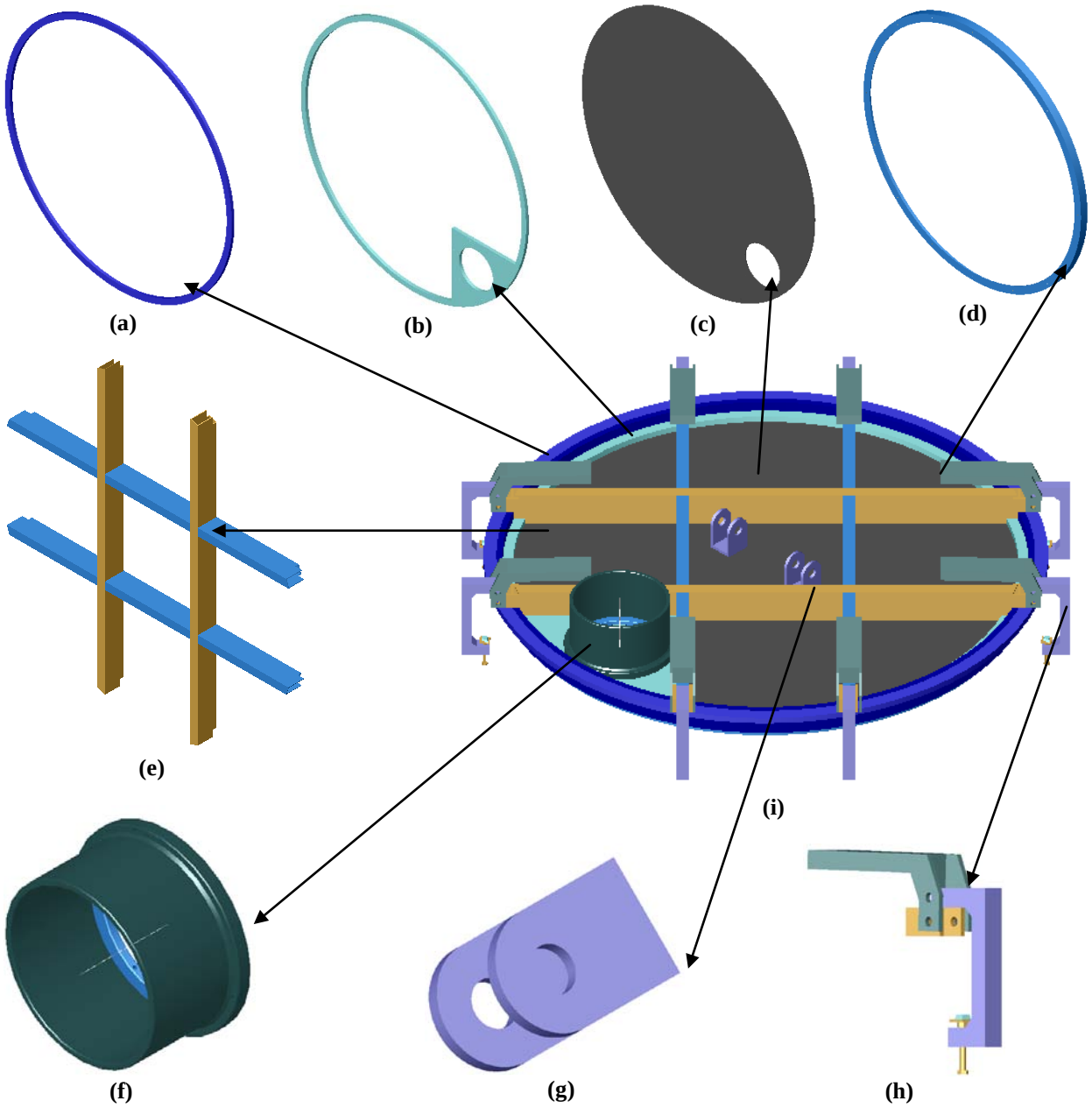

Figure 5.3, Embodiment for the lid and lid lock mechanism with 8 major components (a) lip B, (b) lip A, (c) lid base plate, (d) locking ring, (e) girder, (f) tube flange, (g) lid joint, (h) lid lock, which combines and forms the lid and lid lock mechanism in (i).

Objectives of this development on the mechanism shown above were to maximise the structure stiffness with minimum weight increase. The lid lock is aimed to operate with minimum effort and be able to adjust with simple tools. Any parts coming in continuous contact with the discharging powder are subjected to heavy wear; therefore ease of replacement is required. Moreover, interference between the lid and any structure during operation is not permitted.

The lip B provides the guide to the hopper, the girder is welded on to it to provide the extra support and lip A is then welded on to provide connections for the flange. The lid base plate is known as a wearing part; therefore it was secured by the locking ring and fastened with sixteen M5 screws. A flange with a tube locking device was attached onto the lip A with M5 bolts; this is designed for the use of 6" Goodyear Artrec material handling tube, and sealant is required to be applied into the gap between the tube and the flange. Eight over-centre locks were welded on to the ends of the girder to provide even support. Fine adjustment can be made from the bolt attached on the lid lock. Two lid joints were welded onto the lid base plate to provide the linkage between the lid lifting mechanism and the lid via a chain.

5.4 Prototype Valve Design

As the powder travels through the rubber tube connected from the hopper to the other end, the powder is stacks up due to the physical limitation of the inlet hole on the barrel, which limits the discharge port terminal dimension. The volume of clean swarf contained within a hopper is sufficient to fill approximately 2½ of 200 gallon barrels; therefore a control valve is required to obstruct the flow when demanded. The objective of this section is to develop a valve mechanism which can control the flow of powder without jamming up by the particles, and also fit precisely to the inlet hole on the barrel. Figure 5.1 displayed the proposed design.

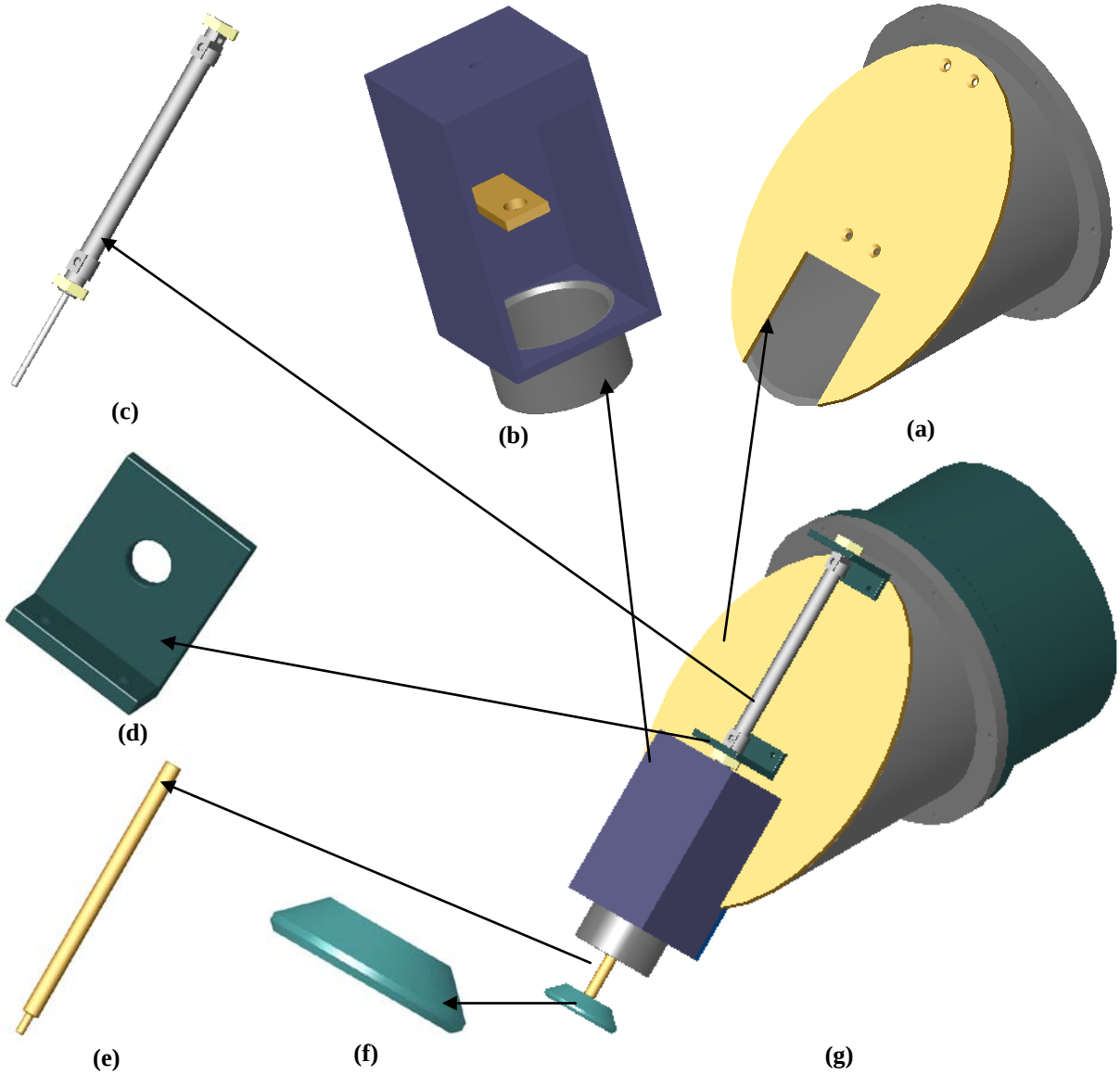

Figure 5.4.1, Embodiment for the valve mechanism with 6 major components (a) Perspex discharge port, (b) valve body, (c) pneumatic actuator, (d) actuator mounting, (e) extend rod, (f) valve, which combines and forms the valve mechanism in (g).

The prototype valve is made of perspex in order to observe the movement of the powder contained inside; the pneumatic circuit designed for driving the valve is detailed in the following section.

A valve body is constructed to be slightly larger than the inlet hole, with the discharge port of Ø50mm, machined down from a Ø60 x 5 perspex tube. All perspex joints were glued with proper perspex adhesive; however, additional M2 screws were used to further strengthen the valve body in order to withstand a heavier load if required.

The valve is powered by a FESTO 10mm bore 100mm stroke pneumatic actuator fitted on the actuator mountings and secured with an M12 nut provided from the manufacturer. Actuator mountings were fastened with countersink screws onto the perspex discharge port from inside. An additional o-ring was placed into the small groove made on the valve body where the actuator rod entered, and the actuator was positioned against the o-ring to keep it in place after assembly was completed.

The extend rod was fitted onto the actuator rod and goes through the guide hole in the valve body; the valve was then fastened onto the other end of the extend rod and secured with an M4 nut and washer.

5.4.1 Pneumatic Circuit Design

The pneumatic system is designed to drive the control valve with the compressed air supplied in the factory. A 100mm stroke, 10mm bore pneumatic actuator was selected for this application with a pneumatic ball vibrator chosen to loosen up the arch and encourage the powder flow. This section covers the design of the pneumatic circuit which is required by the system, and logic control for the system.

This is a preliminary design for the pneumatic circuit and is used as a base structure for further development and part selection; therefore further information may be required from Whites Pneumatic Equipment Ltd for detail parts specification and their expertise before carrying out the pneumatic circuit construction.

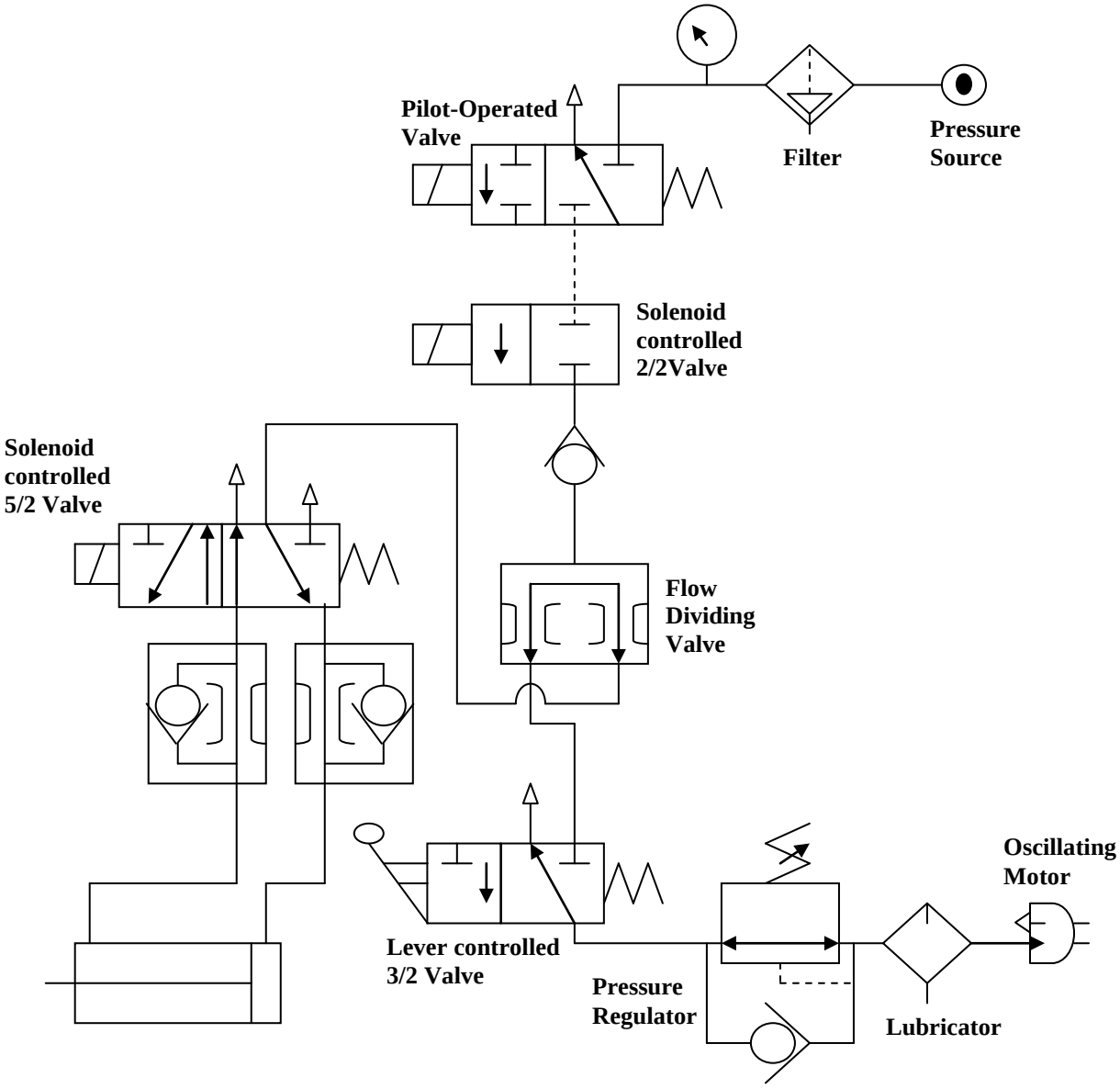

Figure 5.4.2, Pneumatic circuit for the transportation system.

Figure 5.4.3 shows the basic pneumatic circuit for the system. The compressed air line located on the wall was connected to power the pneumatic system. The compressed air withdrawn from the pipe, flows through the filter unit to remove the moisture then enters the 2/2 electronically controlled solenoid valve. This valve is controlled by the PLC unit with the operating action determined based on the interlock status. The exit flow into a 4/3 pilot operating valve to check the delivered pressure meets with the system requirement. The air was then directed to a flow dividing valve; one exit directs the flow to a 5/2 solenoid control valve which handles the control of the actuator, and the other to a 3/2 lever control valve and powers the vibrator. After the air enters the 5/2 valve, each of the 2 exit ports is connected with a flow control valve to keep the rate of flow unaffected by the variations in inlet pressure. A non-return valve is connected parallel to the flow control valve and provides a return flow route for the discharge air. At the 3/2 valve, the exit terminal is connected to the pressure regulator, which controls the flow entering the K-13 pneumatic vibrator from VIBTECH. A lubricator is installed between the exit from the pressure regulator and the vibrator inlet; as air flows through the lubricator, a mist of oil is carried out along with the flow, to lubricate the rotating ball spinning in the vibrator.

The exit air from the vibrator at this stage is discharged into the environment, however, this flow of air is feasible to be re-used as an external jet stream to assist the discharge process after it flow through a filter.

5.4.2 Control of Pneumatic System

All the operation associated with the pneumatic system is controlled by PLC only the 3/2 valve and the pressure regulator are controlled manually. Proper visual signals are displayed to indicate the system status before proper operation can be carried forward. The control flow sequence is detailed in Figure 5.4.4.

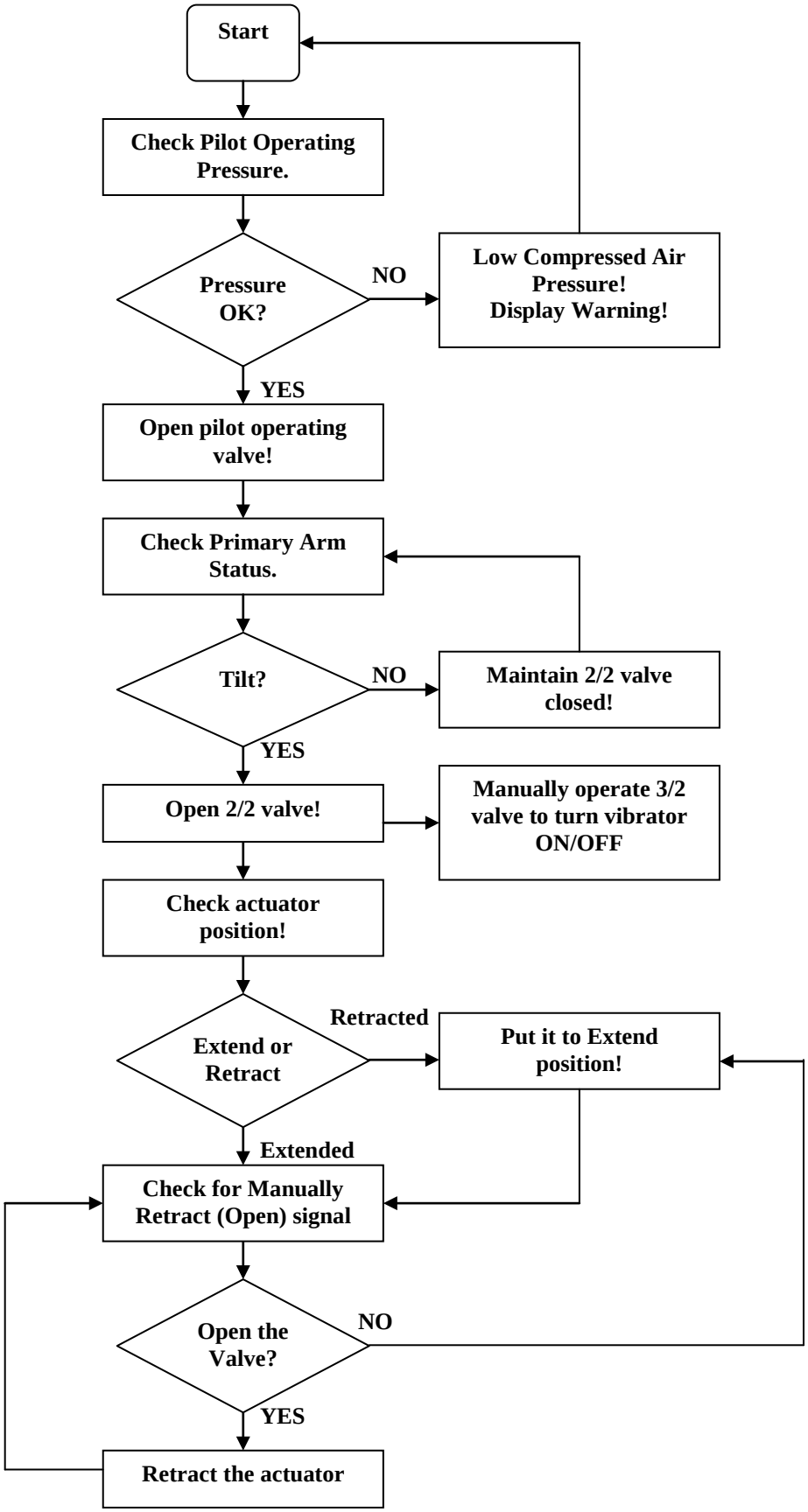

Figure 5.4.3, Flow diagram for the hydraulic control system.

5.5 Filter Design & Specification

As the powder discharged out from valve fall into the barrel, air inside the barrel was being pushed out from the outlet hole along with some suspended particles. This stream of air is then discharged into the surrounding workplace; due to the health and safety issue, further treatment on the air stream is essential. The objective of this section is to develop a filter unit which removes the particles from the air stream in a compact, portable, and detachable shape and can to be adapted straight onto the outlet hole of the hopper with minimum effort.

The filter unit proposed in Figure 5.5 consists of 5 major components: funnel, filter holder, filter cover, support legs, and funnel end cap.

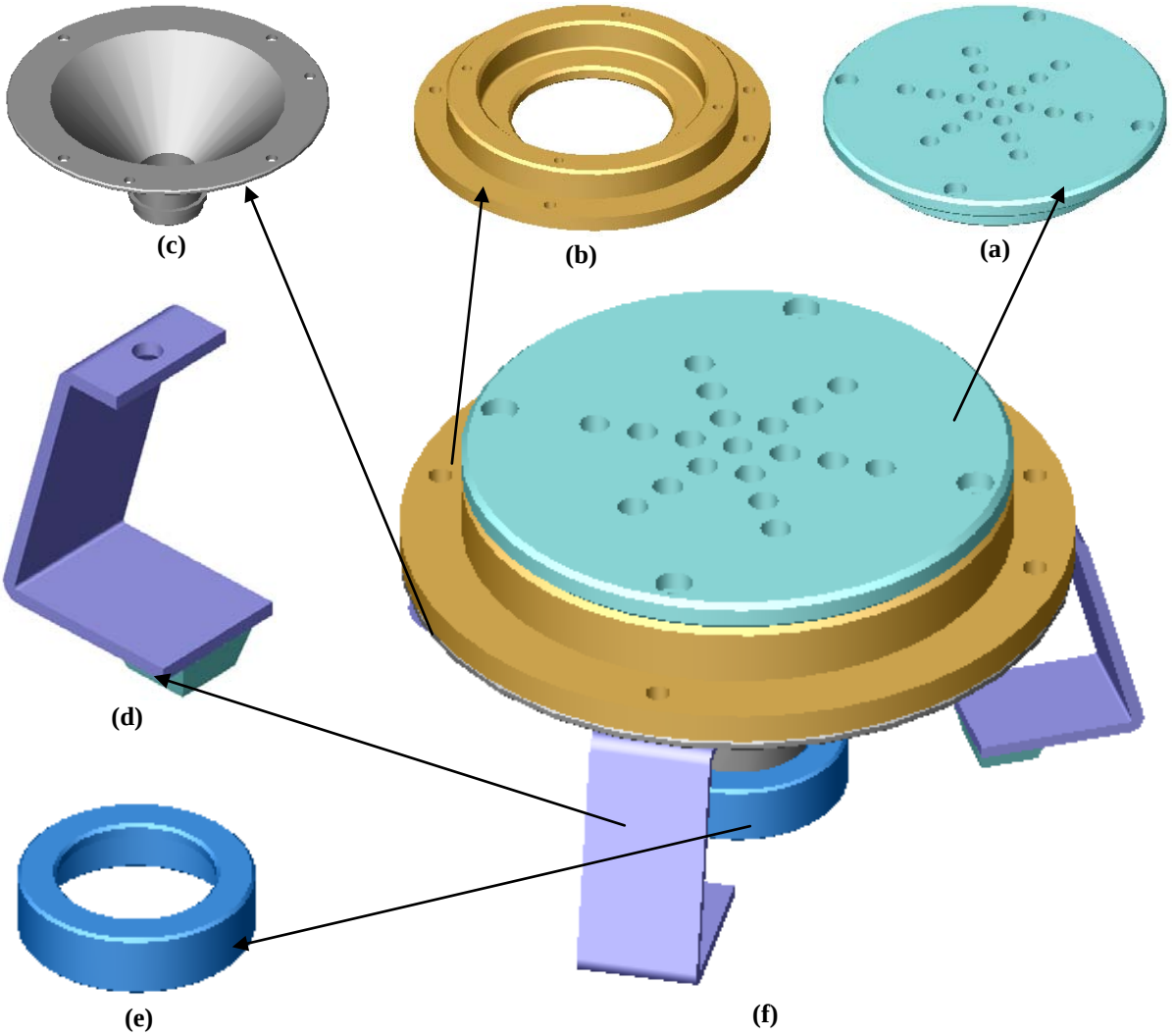

Figure 5.5, Embodiment for the filter mechanism with 5 major components (a) filter cover, (b) filter holder, (c) funnel, (d) support leg, (e) funnel end cap, which combines and forms the filter unit in (f).

From the powder properties determination, and the amount of particles that will be built up from the outlet hole, it was found that due to the physical limitation of the outlet hole, the change of wall angle cannot significantly change the flow property. Therefore, the funnel is designed with a 45° incline wall angle, which is slightly greater than the angle of repose for the powder, to ensure the powder flow occurs.

The filter holder was designed to fit standard Ø70mm BioLab filter paper into the slot located at the centre, and held down with the edge of the filter cover. Multiple layers of filter paper can be loaded into the filter holder; however, three layers were recommended and it can provide sufficient strength to avoid particle penetration which damages the filter paper and result as dust leaking occurs; therefore weekly regular checks are required to be performed. The particle flow with the discharged air into the funnel and is removed from the stream by the filter paper as the air passes through. Multiple Ø5.0mm holes were made in the filter to provide a discharge route for the exit air. Three support legs were made to hold the filter unit from tipping over and 3M feet bumptons were fitted on the leg to provide extra grip. The filter holder and filter cover were held by 4 counter bore M3 bolts. A funnel end cap made of soft rubber is used to seal the gap between the funnel and outlet hole on the barrel by interference fit on the outlet hole.

5.6 Hydraulic System Design

The hydraulic system is designed to provide more than sufficient force to drive the transportation system with 60% of the actuator's rating. As mentioned earlier in section 5.1, two 14" hydraulic actuators were selected for this application and an 8" actuator was selected for lid lifting application. The objective of this section is to design a hydraulic circuit which is required by the system, and logic control for the system.

5.6.1 Hydraulic Circuit Design

This is a preliminary design for the hydraulic circuit and used as a base structure for further development and part selection; therefore further information may be required to be obtained from Mr Aaron Witbrock at MARTIN HYDRAULIC Ltd for detail parts specification and their expertise before carrying out the hydraulic circuit construction.

Figure 5.6.1 shows the basic hydraulic circuit required by the system. The hydraulic fluid is first pumped out from the 5litre reservoir and flows through the filter then enters the DC pump unit, rating 4.5litre/min. The hydraulic fluid then enters the pilot operating valve to check for the required pressure and moves to the 4/3 solenoid control valve which was implemented to direct the flow to power either the lid lifting mechanism or the lifting/rotating mechanism, with logic control based on the interlock system status. Moreover, this is designed to operate only one mechanism at a time, mainly due to the safety requirement, therefore flow can only be direct to either one of the mechanisms or maintain neutral. The fluid comes out from either exit port and enters a 4/3 lever control valve which controls the position of the actuator movement with a control lever. A flow dividing valve is connected directly at the exit port and divides the flow into a fixed ratio substantially independent of pressure variations and delivers to the two 14" stroke actuators. A similar arrangement is applied for the flow path to the actuator attached on the lid lifting mechanism; however, no flow dividing valve is connected. None return valves are applied in the hydraulic circuit close to the junction points. Since the pilot operating valves have electrical signal outputs, therefore wirings to the PLC unit are essential.

All the hose connection is required to be attached on to the base post and also avoid any possible interference with the lifting/rotating mechanism operation. Proper installation of attachment clamps on the base post is encouraged to keep the hoses tidy and well organised with appropriate labels.

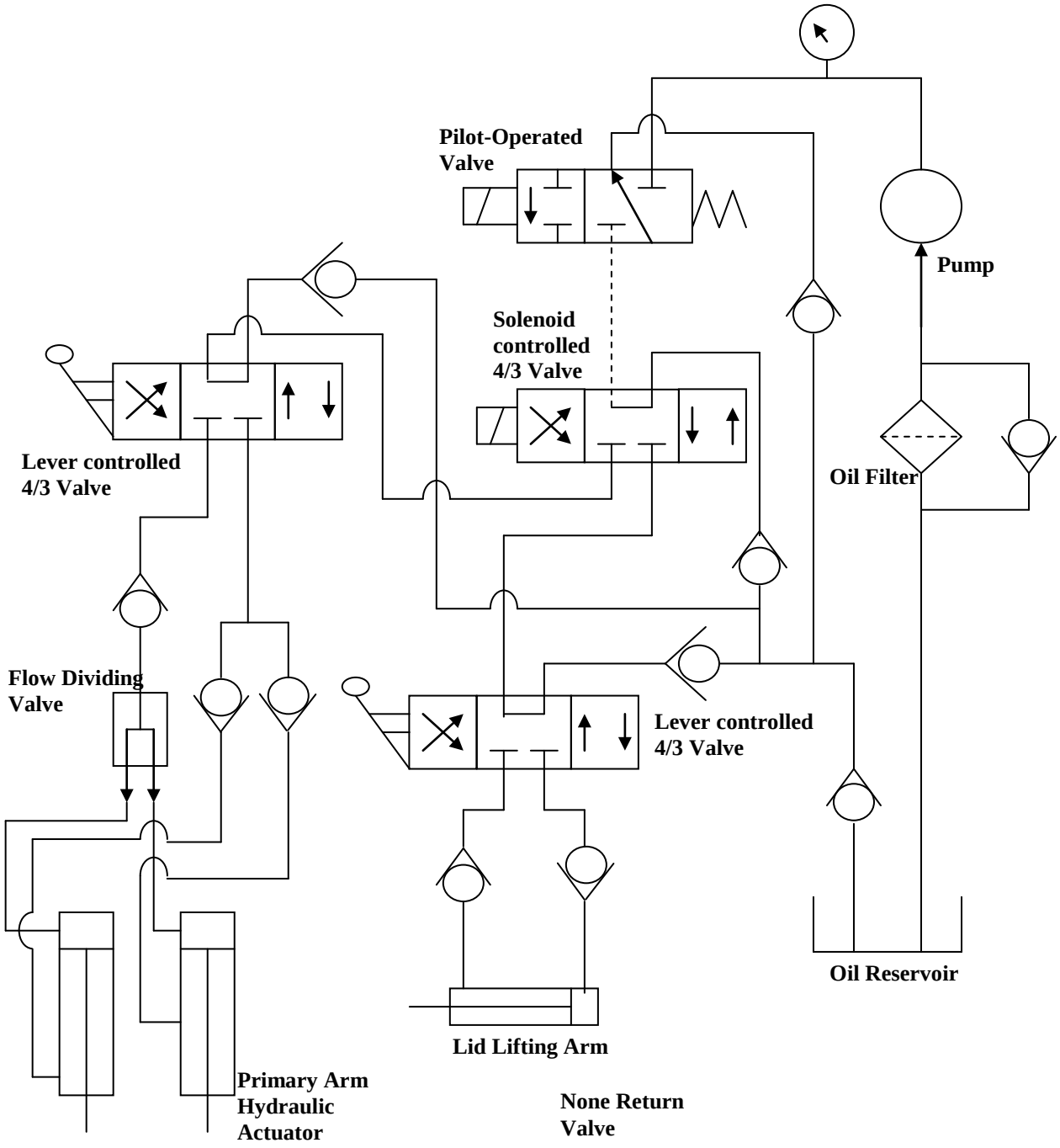

Figure 5.6.1, Hydraulic circuit for the transportation system.

5.6.2 Control of Hydraulic System

Most of the operation associated with the hydraulic system is required to be manually carried out, however, the pilot operating valve and 4/3 solenoid valve is controlled by PLC and the proper visual signals are displayed to indicate the system status before proper operation can be carried forward. The control flow sequence is detailed in Figure 5.6.2.

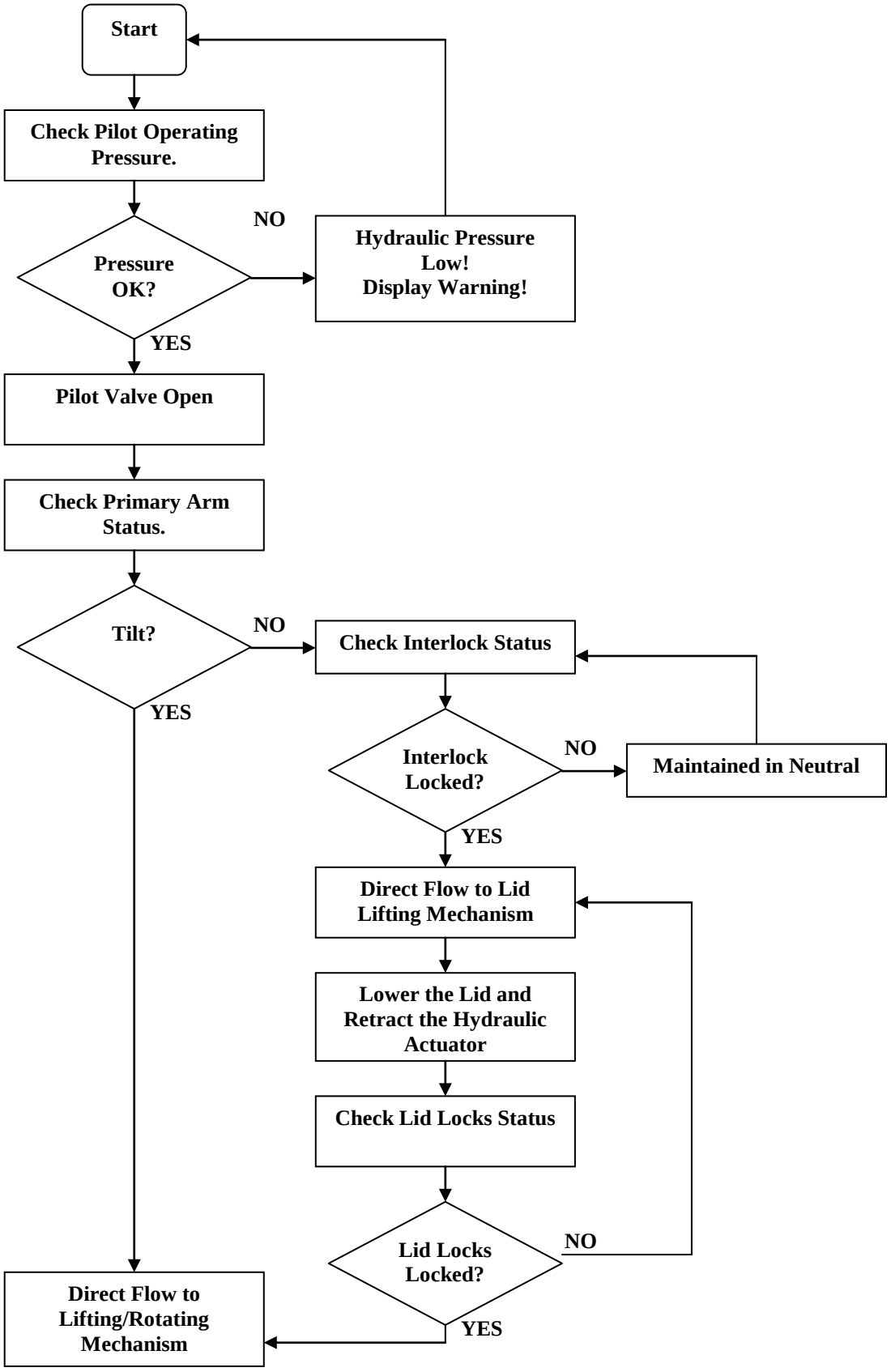

Figure 5.6.2, Flow diagram for the hydraulic control system.

5.7 Detail Design

The embodiment design for each sub-systems were reviewed using an embodiment design work sheet adopted form **Hales, C. [88]** in Figure F4. As mentioned at the start of this chapter, the transportation system was only developed to a preliminary stage, due to the withdrawal of the industrial sponsorship; therefore, the major mechanical components regarding to the function of the transportation system have been designed and prepared in the drawing files. An overall assembly view is shown below in the Figure 5.7.

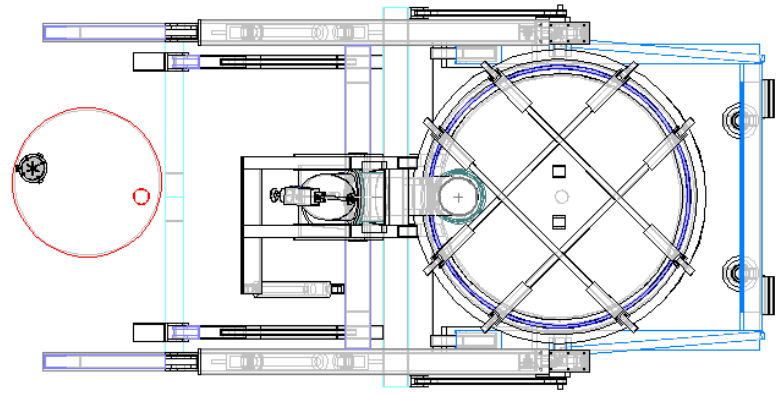

(a) Top view

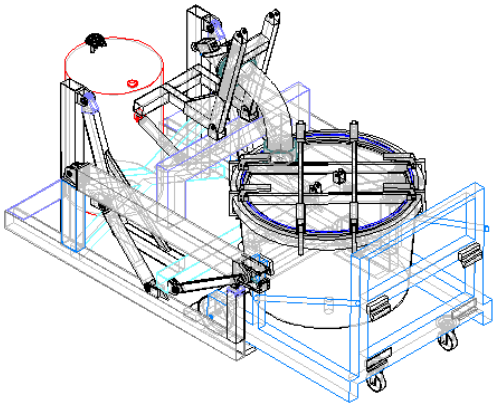

(b) Isometric view

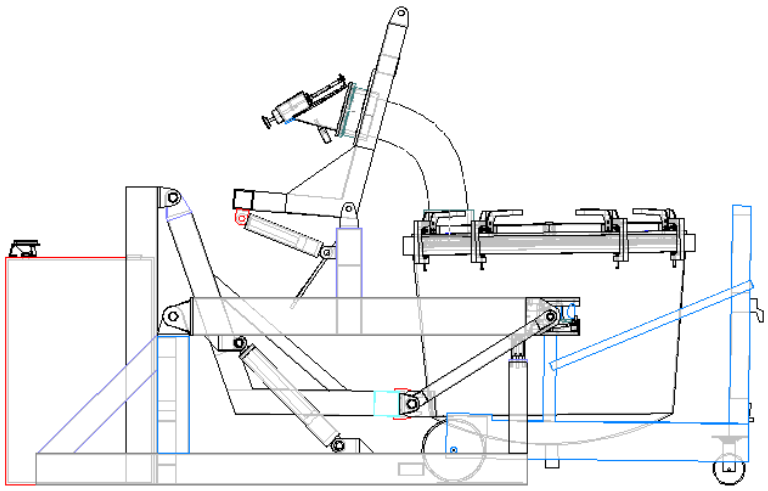

(c) Front view

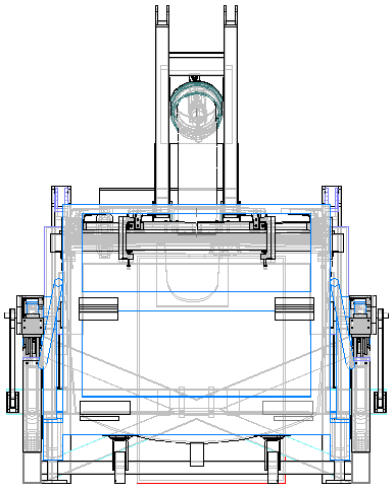

(d) Side view

Figure 5.7, General assembly view of the transportation system.

For detail information on the operation sequence of the transportation, please refer to Appendix G.

All the structural components were designed based on the Steel & Tube Ltd catalogue, and the hinge joints were designed to be manufactured from MS steel plate.

Mainly due to the financial difficulty, the hydraulic, pneumatic, and electrical system were designed to a preliminary stage as demonstrated in the previous sections, and the logical controls strategy is regard to the those systems were developed in Figure H-1. The hydraulic pump, and PLC unit did not appear in the diagram above, and it was aimed to be placed close to the control terminal where the operators may be standing.

Some concerns were that there may not be sufficient proof of the performance of the transportation system, therefore a test rig designed to simulate the flow path from the hopper to the barrel was built and will be discussed in chapter 6.

It was unfortunate that the development of the transportation system had to be placed on hold; the detail design stage was assessed using the detail design checklist in Figure F-5. However, the major focus of the design at this stage was mainly focused on the mechanical components therefore, other additional developments which may be required to be refined in the future; it was not considered critical at this stage.

6. DESIGN VALIDATION

This chapter introduces the importance of design validation before a full scale construction can be commenced. From the experiments conducted earlier on the powder; it was known that a tube size larger than Ø150.04 mm can avoid the formation of any arch which obstructs the discharge. However, the physical limitation of the barrel outlined the maximum permissible inlet size of Ø56 mm. Therefore it is vital to design and construct a full scale size of the flow path through the powder may be flowing under actual operating conditions. Moreover, the performance of implementing a pneumatic vibrator into the discharge system may still be required for verification of actual test result.

An experiment is conducted through the use of the test rig to verify the achievements of the design. Minor modification on the control valve design will be recommended based on the experimental result. This chapter will be divided into five sections as listed below:

1) ***Full Scale Channel Design –*** this section starts from the outline requirements of a full scale channel design, having all dimensions associated with the actual design employed, and construction of the test rig completed at the end.

2) ***Discharge Experiment*** – this section introduces the experiment designed to test the flow properties of the powder. This experiment is conducted with the test rig and the result is used to validate the actual design.

3) ***Effect of the Pneumatic Vibrator on Discharge –*** the implementation of the pneumatic vibrator and its effectiveness on resolving the flow obstruction is observed from the discharge experiment and described in this section.

4) ***Valve Modification –*** a minor modification which can be carried out when the effect of the pneumatic vibrator does not match the requirement is introduced in this section.

5) ***Discussion*** – this section arranges the experimental finding and relates those findings back to the theoretical understanding.

6) ***Conclusion and Recommendation –*** finally, recommendations on modifying the control valve will take place with comments on the overall transportation system development.

6.1 Full Scale Channel Design

Since flow obstruction is expected to occur when the discharge dimension decreases below Ø150.04mm, the arch formation is likely to occur within the valve unit, and the mechanism proposed to resolve the situation is a pneumatic vibrator. However, this assumption was based on dried and sieved powder; therefore a full scale channel was designed and constructed based on detailed transportation system design. Hence, for any changes in the powder properties such as humidity, obstruction may occur.

An angle greater than 40° is required to enable the particle sliding to occur, and from the design of the transportation system, an angle of 45° was used. However, this does not include the angle on the hopper (pot) wall. Due to the high production cost on complex surface machining with steel, the hopper wall dimensions are unable to be duplicated. Despite the circular curvature and the minor incline angle along the hopper height, a rectangular container was built to contain a fixed amount of powder which simulates the discharge opening of the hopper lid. The material selected here is perspex, which ease the manufacturing and at the same time provides a transparent view window for observation.

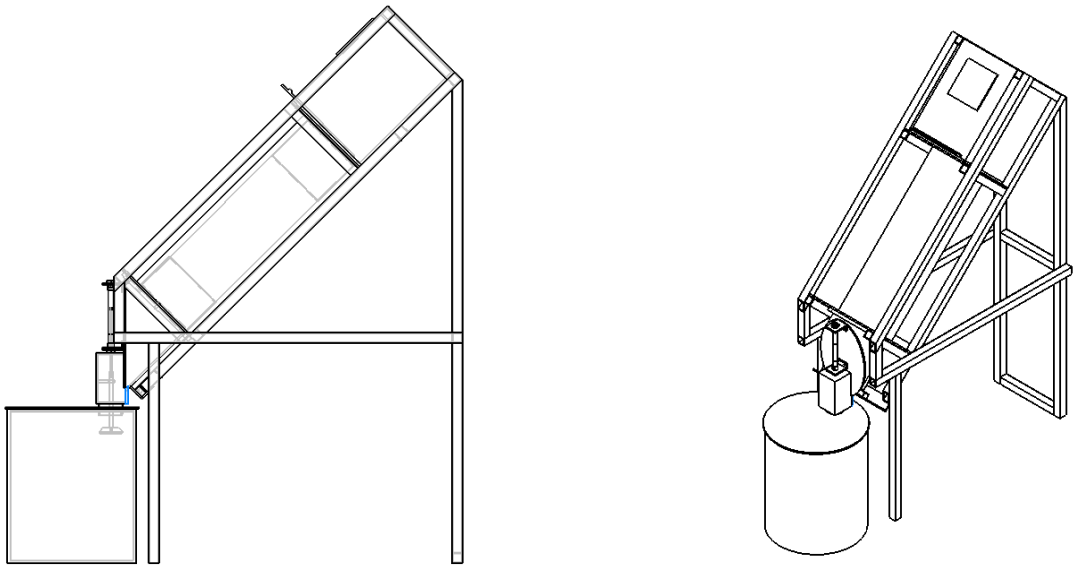

(a) **(b)**

Figure 6.1, Test rig model, (a) front view, (b) isometric view.

The perspex container is positioned at the same designated angle as the transportation system. A 500mm length of Ø152.40mm Goodyear Artrec material handling tube is connected to the flanges and secured with clamps. The prototype valve has been constructed with perspex in

order to visualise the flow of the powder. Figure 6.1, shows the model of the test rig, and Figure 6.2 shows the actual test rig with pneumatic system attached.

Figure 6.2, Actual test rig with pneumatics circuit on board.

6.2 Discharge Experiment & Initial Result

Two types of powder were collected from **C.A. Nichol [10]** from the Department of Chemical & Process Engineering at the University of Canterbury. In the white plastic container is the dried and sieved powder which was used in the Peschl Shear Cell experiment, and the large steel bucket contains clean powder after the leaching process, without sieving. Figure 6.3 shows the powders stored in the containers.

(a) **(b)**

Figure 6.3, Powders in containers, (a) DS-Powder in plastic container, (b), DU-Powder in steel bucket.

Experiments have been conducted on both types of powders, and experimental observations have been recorded. Here, the dried and sieved powder is denoted as ***DS-Powder***; and the dried and un-sieved powder is ***DU-Powder***.

Since DS-Powder is used in the shear cell experiment, therefore the result from this experiment can be used to validate the data from shear cell testing. However, after the swarf was washed and dried under a vacuum environment, the powder tended to form agglomerates and aggregates. The condition of the powder is not suitable for testing with shear cell. Hence, the DU-Powder can represent the actual flow condition more directly than the shear cell experiment.

6.2.1 DS-Powder Initial Test Results

A simple experiment using the designed test rig was conducted to validate the design. A fixed amount of DS-Powder stored in closed plastic containers was loaded into the perspex container which provides consistent consolidation pressure. The sliding gate was then opened to allow the powder to discharge, which simulates the powder discharge from the hopper through the flange. Through the perspex container, no arch formation was observed, however not all powders have been discharged. Most of the powder was discharged through the circular opening except for the bottom corners of the container (due to the zero curvature of the sliding surface which was employed; after discharge had taken place, some powders remained in the container and collected at the an angle of repose), and small amounts sticking to the container wall due to electrostatics. The flange dimension can thus be validated at this stage.

The powder was kept within the valve and the rubber tube after it has been discharged from the container since the valve is initially closed. Once the valve opened up, only a small amount of powder has fell into the bucket, and it was observed that an arch formed within the valve discharge port as expected. This part of the experiment was conducted five times to verify the result obtained from the Peschl Shear Cell experiment, and a satisfactory result was obtained.

6.2.2 DU-Powder Initial Test Results

The DU-Powder was tested in a similar method to the DS-Powder. However, lumps of powder which had formed during the recycling process, which could be broken during multiple testing, hence it is impossible to restore the same flow condition. Therefore, only the first result is considered as critical.

The DU-Powder was loaded into the container and the sliding gate was opened, however, a dome was observed and the discharge was obstructed. With minor impact shocks from the perspex container wall, the dome was broken and the actual flow continued. Similar obstruction was observed at the expected location within the valve when closed. As the break down of the powder lumps is an irreversible process, by keeping the valve closed, several tests regarding the initial flow path from hopper through the flange can be conducted. A total of three tests associated with the initial flow path were conducted, however, formation of a dome was observed in all the trials, hence, the dimension of the discharge opening on the hopper and the flange is insufficient. Figure 6.4, shows the blockage occurs within the valve when DU-Powder is introduced into the flow path.

(a) **(b)**

Figure 6.4, Blockage within the valve when DU-Powder was introduced into the flow path, (a) close shot of DU-Powder first transferred into perspex container, (b) blockage occur in the valve body.

After the initial testing, the discharge channel filled up with DU-Powder, and the full load condition can be simulated. Since the initial flow path was obstructed and the blockage within the valve was expected to occur, multiple arches were assumed to take place within the path. Therefore by resolving the blockage within the valve, possible formation of an arch within the rubber tube can then be determined, and this will be conducted in the later sections.

6.3 Effect of the Pneumatic Vibrator on Powder Flow rate

The K-13 pneumatic vibrator from VIBTECH was activated in order to break the arches which obstruct the powder discharge within the valve. The pressure regulator controls the vibration frequency and from the technical data provided by the manufacturer, the operating pressure range is 2-6 bar. Table 6.1 shows the technical operating data of the pneumatic vibrator.

Table 6.1, Technical operating data of VIBTECH K-13 pneumatic vibrator

Type: K-13	2 Bar	4 Bar	6 Bar
Frequency (Hz)	16,000	20,800	23,600

Regarding the positioning of the vibrator, from the literature research, **Wassgren, C. R.** *et al* **[38]** and **Weathers, R. C.** *et al* **[39]** have suggested that the vertical vibration does not have any effect on the flow of the powder, however, horizontal vibration does improve the flow significantly by loosening up the arch.

Since the pneumatic vibrator is designed to be attached onto the valve, three common positions were tested before any installation is taken place, as shown in Figure 6.5.

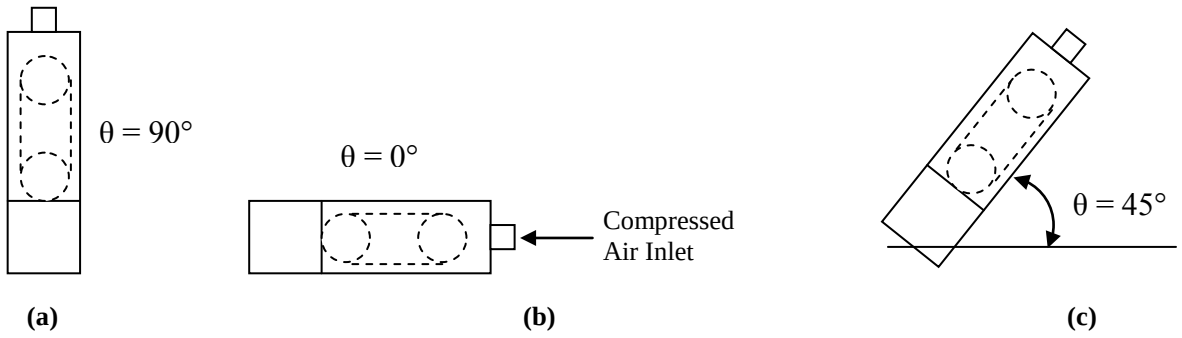

Figure 6.5, Position of the pneumatic vibrator, (a) vertical θ = 90°, (b) horizontal θ = 0°, and (c) θ = 45°

By hand holding the vibrating unit running at 5 bar, at which the actual valve will be operating, any minor movement can dramatically affect the vibrating frequency. The accelerating of the metallic ball within the vibrator is directly proportional to the operating pressure and the incline angle. Any change of the angle will have significant effect on the response time of the vibrator; hence the actual implementation in the valve unit may be unable to provide a satisfactory effect.

Since all the pneumatic components are rated at 6 bar, testing regarding the vibrating unit was conducted within the operating range and the results are as shown below in Table 6.2.

Table 6.2, Strength (amplitude) of the pneumatic vibrator in different operating conditions

Angle θ (°)	**Operating Pressure (bar)**								
	2.0	**2.5**	**3.0**	**3.5**	**4.0**	**4.5**	**5.0**	**5.5**	**6.0**
0	4	4	5	6	7	8	8	9	9
45	0	0	0	0	1	1	1	2	2
90	0	0	0	0	0	0	0	1	1

Note: the strength of the vibration is expressed from 0-9, where 0 means no vibration and 9 as very strong vibration.

Hence, the pneumatic vibrator can only be efficient when placed horizontally. The implementation of the pneumatic vibrator on both DS-Powder and DU-Powder does not show a strong effect on the flow since the powder is densely packed. The flow obstructing arch was unable to be resolved instantly with the pneumatic vibrator unit, along with the slow response time for the pneumatic vibrator to reach its operating frequency after a change of incline angle occurred. Therefore it is concluded that the implementation of pneumatic vibrator is no longer considered.

A more orientation independent mechanism is required to break the arch, and from the current system development, the use of compressed air on soothing the flow may be feasible. The pneumatic vibrator consumes large quantities of compressed air, therefore by withdrawing this source of air and directing it through a nozzle, the effect will be more direct.

6.4 Valve Modification

Since the employment of the pneumatic vibrator was unable to resolve the flow obstruction effectively, an alternative method involving inserting a compressed air nozzle through the valve body, and directly aiming it at the dome successfully destroyed it. Figure 6.6 shows the layout of this modification.

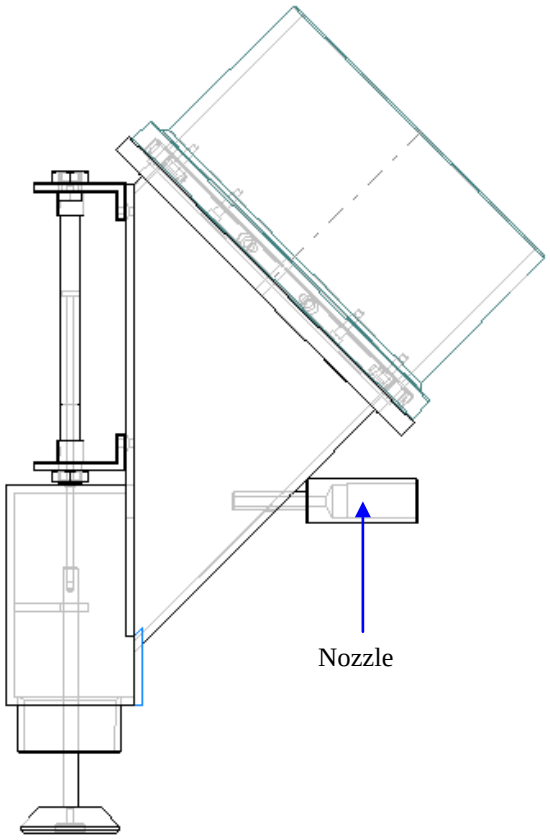

Figure 6.6, Nozzle modification on the valve

Both the DS-Powder and DU-Powder have been tested with the modified valve. Significant flow improvement was observed on the DS-Powder, and most the powders were able to be collected at the end, hence this arrangement was able to cope with the ideal experimental environment. However, the system does require to be sealed tightly since the additional pressure added into the flow system also encourages the particles to be airborne. Any minor leakage can pollute the surrounding environment, and also breaches the health and safety requirement. The employment of compressed air to break the dome was found to be very effective. Once the dome is broken, the flow can be started again, however, after a short period of time, approximately 5 seconds, obstruction will occur again if the compressed air stops flowing from the nozzle. A timer which controls the supply of compressed air to the nozzle can be applied to reduce the amount of air usage, and also improve the efficiency.

As for the DU-Powder, the compressed air was able to break the dome and encourage the flow of powders which are in front of the nozzle; nevertheless obstructions were still experienced at the valve entrance, as shown in Figure 6.7.

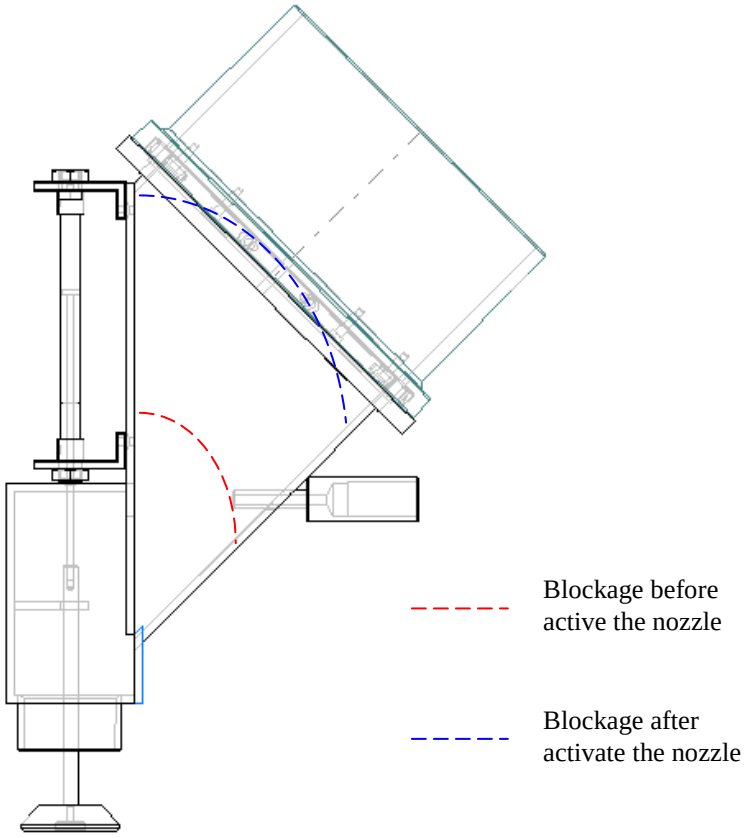

Figure 6.7, Location of blockage before and after the nozzle activates

After all the powder within the valve has been removed, blockage was still experienced within the rubber tube, hence with the current design; multiple formations of arches along the flow path have significantly obstructed it. With multiple variables, such as moisture and lump formation, which can significantly affects the discharging process, at this stage, no further testing can be continued. It is concluded that the current dimension of the discharge path is undersized.

6.5 Discussion

After the first stage oil recovery process, the powder was in the form of densely packed cake. The formation of powder lumps was originally due to the combination of both the pressurised environment and residual oil entrapped within the swarf. The secondary recovery system starts from sprinkling the hexane from the top of the extraction chamber to percolate through the swarf by gravity. In both the first wash and second wash, the hexanes were collected from the bottom of the hopper, and the residual hexane was required to be collected from the drying process.

At this stage, the powder lumps can easily be deformed or collapse when sufficient force is applied directly from above. However, during the discharging process, multiple forces acting on a lump of powder from surrounding areas, it tends to rotate the lump while sliding down, and slide. as shown in Figure 6.8.

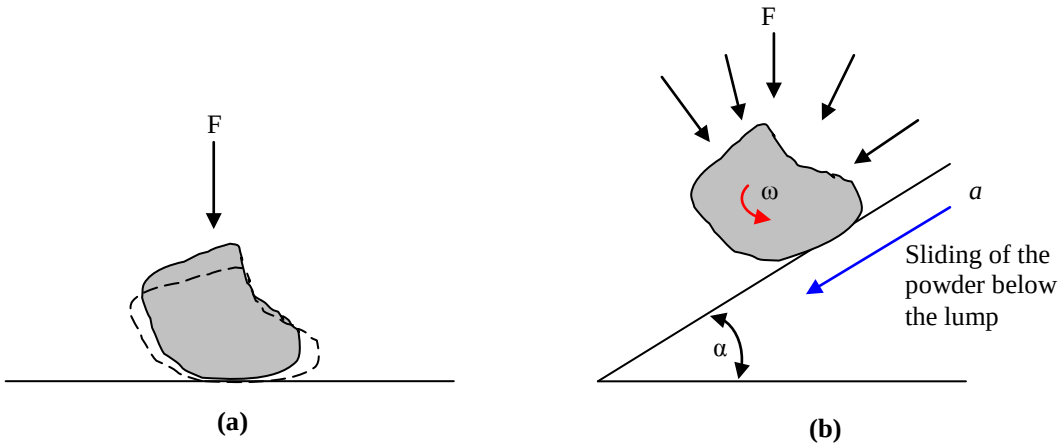

Figure 6.8, Free body diagram of a lump of powder (a) with direct force applied, (b) when the lump is flowing.

However, with the current shear cell testing method, the powder lumps will collapse or be deformed when consolidated during sample preparation. Hence the flow property of the powder lumps could not be determined.

In the drying process, compressed air was introduced into the extraction chamber. As air passed through the bed of swarf, a decrease of surrounding temperature due to the evaporation of hexane which consumes energy was noticed. The surrounding temperature will increase once hexane is fully vaporised, and hence the completion of the drying process was achieved. However, according to the laboratory trials conducted by **C. A. Nichol [10],** the moisture in the surrounding air was condensed since the evaporation process decreases the surrounding temperature. The water came from air not only condensed on the surface of the swarf, but

also within the swarf. A minimum of -10°C was recorded during the laboratory trials; therefore frost can be formed both on the surface and within the swarf. Although the surrounding temperature may increase after all the hexane has been removed, and the total removal of the condensed water could not be justified at this stage.

Both the extraction of hexane and removal of condensed water within the swarf rely on factors such as time, air temperature, air velocity, and contact area and also the amount of swarf contained within the hopper. The flow property of the powder depends on the bulk solid properties, and the properties of the contact medium, (such as air, oil, water, or hexane) which in this case is water and its weight percentage in a given volume. Since the contact medium content within the swarf can significantly alter the flow property of the powder, a successful powder transfer process will be rely heavily on the design of the drying process.

In the flow testing experiment, the amount of surrounding moisture entrapped into DU-Powder was in doubt. Since the storage facility of the DU-Powder was simply a thin layer of plastic cover, and with the location where the testings were conducted, this additional humidity may also greatly affect the experimental result.

6.6 Conclusion and Recommendation

From the above testing with the swarf, it was noticed that the formation of a lump during oil recovery process can significantly the flow properties of the powder. With the current shear cell testing method, it was not possible to test the actual flow properties of the powder lumps, however a base line requirement of the powder could be obtained.

Together with findings on the literature search, it was found that with the drying process employed by **C. A. Nichol [10],** a large quantity of air was introduced into the extraction chamber and passed through the swarf bed. Removal of hexane was successfully conducted in the laboratory; however, due to the evaporation of hexane, the temperature of the swarf bed was significantly decreased. Due to the low temperature environment, moisture content within the extraction chamber was condensed and entrapped in the metal matrix. The amount of moisture contained within the swarf will significantly affect the flow property; hence the success of the discharge process heavily depends on the design of the drying process.

The discharge experiment has revealed that the implementation of a pneumatic vibrator was ineffective in resolving the flow obstruction caused by formation or arching. Modification on the valve was carried out with an additional nozzle positioned at the location where the dome was formed. The nozzle aimed at the dome, and by directing the inlet air from the pneumatic vibrator to a nozzle, the compressed air was found to be effectively destroying the obstruction with minimum effort. A timer which controls the compressed air inlet to the nozzle may be introduced into the pneumatic system to reduce the air usage and also improve the efficiency.

With regard to the dimension of the valve, at this stage, the prototype valve was found only applicable to DS-Powder. Increase of the dimension of the prototype valve was found to be essential to implemented the design into the actual construction of the transportation, however, the enlargement of the valve design will be scaled up based on the available rubber tube size. Currently an inner diameter of 6” Goodyear Artrec material handling tube was employed and attached to the prototype valve. The size available from the manufacturer increases at 2” interval; hence the next size up is 8”. However, since the moisture contained within the swarf may vary with the condition of the drying process operation, and the dimension of the rectangular perspex container employed on the test rig is 220mm, then the equivalent diameter is approximately 9.8”. Therefore a 10” tube size is recommended to be tested in the future.

Regarding the direction on future development of the transportation system, the shear cell testing and other testing methods maybe required to be employed to determine the flow properties of the powder under different humidity. Since currently the project is no longer sponsored by the industry, further development on a pneumatic transportation may also be considered, especially with the vortex lifting method for educational and research purposes. However, the feasibility of a cyclone separation method that will be employed in conjunction with the vortex lifting method is still not recommended, since other alternative solutions such a as gravity settling chamber may offer less wear and more efficient separation efficiency.

Overall, the prototype valve design works relatively well to maintain the powder within the valve body while experiencing minor vibration and impacts. One minor improvement other than the scale up requirement is recommended on the valve design. With the current design, the pneumatic actuator is directly connected to the valve body and controls the valve open/close operation. The actuator push rod moves in and out of the valve, and also has direct contact with the powder. Since the size of the actuator push rod is relatively small, a suitable seal for this application could not be obtained. An o-ring was in the end selected and placed into the actuator path, and the actuator body was therefore positioned to push the o-ring against and the valve body to achieve a good sealing quality. Since the powder is fine and abrasive, therefore, the o-ring is expected to be a consumable part, hence the possibility of this powder going into the actuator is high. By further extending the extension rod, the actuator can then be rotated and placed parallel to the current location and connected to the extension rod via a new linkage. However, minor modification on the pneumatic circuit is required in order to have the actuator operating in the right direction. This arrangement can avoid the direct exposure of the actuator rod into a dusty environment; thus, a more reliable valve system can be achieved.

REFERENCE

A. Extraction Process

1. **Grigor J. E.**, *Solvent Extraction From Steel Swarf Using Hexane*, University of Canterbury, Department of Chemical & Process Engineering, Final Year Project Report 2000.
2. **Fu H., Mathews M. A.**., *Separation Processes for Recovering Alloy Steel From Grinding Sludge: Supercritical Carbon dioxide Extraction and Aqueous Cleaning*, Separation Science and Technology, **V34** n6-7, Apr-May 1999, pp.1411~1427.
3. **Brady, Basil O., Kao, Chien-Ping C., Dooleym, Kerry M., Knopf, Carl F., Gambrell, Robert P.**, *Supercritical Extraction of Toxic Organic From Soils*, Industrial & Engineering Chemistry Research, **V26**, n2, Feb 1987, pp261~268.
4. **Beudoin, Stephen P., Grant, Christine S., Garbonell, Robert G.**, *Removal of Organic Film From Solid Surface Using Aqueous Solution of Nonionic Surfactant I: Experiments*, Industrial & Engineering Chemistry Research, **V34**, n10, Oct 1995, pp3307~3317.
5. **Beudoin, Stephen P., Grant, Christine S., Garbonell, Robert G.**, *Removal of Organic Film From Solid Surface Using Aqueous Solution of Nonionic Surfactant II: Theory*, Industrial & Engineering Chemistry Research, **V34**, n10, Oct, 1995, pp3318~3325.
6. **Gannon, Keith O., Bibring, Peter, Raney Kelvin., Ward, Anthony J., Wilson, David J., Underwood, Julie L., Debelak, Kenneth A.**, *Soil Clean Up by In-situ Surfactant Flushing III – Laboratory Results*, Separation Science and Technology, **V24**, n14, Nov 1989, pp1073~1094.
7. **Underwood, Julie L., Debelak, Kenneth A., Wilson, David J.**, *Soil Clean Up by In-situ Surfactant Flushing VI – Reclamation of Surfactant Recycle*, Separation Science and Technology, **V28**, n9, Jul 1993, pp1647~1669.
8. **Underwood, Julie L., Debelak, Kenneth A., Wilson, David J.**, *Soil Clean Up by In-situ Surfactant Flushing VIII – Reclamation of Multi-component Contaminated Sodium Dodecylsulfate Solution in Surfactant Flushing*, Separation Science and Technology, **V30**, n11, Jun 1995, pp2277~2299.
9. **Clarke, Ann N., Plumb, Patrick D., Subramanyan, T. K., Wilson, David J.**, *Soil Clean Up by Surfactant Washing I – Laboratory Result and Mathematical Modelling*, Separation Science and Technology, **V26**, n3, Mar 1991, pp301~344.

10. **Nichol, C. A.,** *Development of a Prototype Unit for Oil Recovery From Grinding Sludge: a thesis submitted for the degree of Master of Engineering at the Department of Chemical & Process Engineering,* 2003, University of Canterbury.

B. Lubrication, Drill Bits Material, & Manufacturing Process

11. **Moller, U. J., Boor, U.,** *Lubricants in Operation,* , English translation edited by **Landsdown, A. R.**, VDI Verlag, Mechanical Engineering Publications Limited.
12. **Springborn, R. K.**, Cutting and Grinding Fluid: Selection and Application, ASTME (American Society of Tool and Manufacturing Engineers)
13. **Kalpakjian, Serope.,** *Manufacturing Engineering and Technology,* 3rd edition, 1995, Addison-Wesley Publishing Company
14. **Drozda, Tom., Wick, Charles., Benedict, John T., Veilleux, Raymond F., Bakerjian, Ramon., Society of Manufacturing Engineers,** *Tool and Manufacturing Engineers Handbook,* 4th edition, **V1,** 1983, Society of Manufacturing Engineers.
15. **Shaw, Milton Clayton.,** *Principles of Abrasive Processing,* Oxford Series on Advanced manufacturing, **V13,** 1996, Oxford Science Publication.
16. **Benedict, Gary F.,** *Nontraditional Manufacturing Processes,* Manufacturing Engineering and Materials Processing, **V19,** 1987, Dekker
17. **Kalpakjian, Serope., Schmid, Steven R.,** *Manufacturing Engineering and Technology,* 4th edition, 2001, Prentice Hall.
18. **ASM International Handbook Committee,** *ASTM Metal Handbook,* 10th edition, **V1,** 1990, American Society for Metals.

C. Environmental Issues & Waste Management

19. **Neal, A. W.**, *Industrial Waste: its handling, disposal and re-use* 1971, London: Business Books.
20. **Bahu, Richard., Crittenden, Barry., O'Hara, John.**, *Management of Process Industry Waste: an introduction*, 1997, Institution of Chemical Engineers.
21. **Nemerow, Nelson L., Agardy, Frank J.**, *Strategies of Industrial and Hazardous Waste Management,* 1998, Van Nostrand Reinhold, A Divisionof International Thomson Publishing Inc.
22. **Guyer, Howard H.,** *Industrial Processes and Waste Stream Management,* 1998, John Willey & Sons, Inc.
23. **Ministry for the Environment.**, *The 1995 National Landfill Census*, 1997, Ministry for the Environment, New Zealand.

24. **Ministry for the Environment.**, *The 1998/1999 National Landfill Census Report*, 2000, Ministry for the Environment, New Zealand.
25. **Ministry for the Environment.**, *Solid Waste Analysis Protocol*, 2002, Ministry of Environment, New Zealand.
26. **Clancey, D., Canterbury Regional Council (Christichurch, N. Z.). Environmental Management Group,** *Used Oil in Canterbury: Production, Recovery, and Environment Impacts*, 1999, Canterbury Regional Council.

D. Particle Technology & Powder Mechanics

27. **Kearney, T.,** *Solid Flow Experiment Handout,* 2002, Chemical & Process Engineering, University of Canterbury
28. **Allen, Terence.,** *Particle Size Measurement,* **V1,** 1997, Chapmand & Hall.
29. **Allen, Terence.,** *Particle Size Measurement,* **V2,** 1997, Chapmand & Hall.
30. **Cambou, Bernard, and International Centre for Mechanical Sciences**, *Behaviour of Granular Materials*, 1998, Springer Wien New York.
31. **Jenike, Andrew W.,** *Storage and Flow of Solids***,** Bulletin of the University of Utah, **V53**, n26, Nov 1964.
32. **Brown, R. L., Richards, J. C.**, *Principles of Powder Mechanics: essays on packing and flow of powder and bulk solids*, 1970, Pergamon Press.
33. **Arnold, P. C., McLean, A. G., Roberts, A. W.**, *Bulk Solids: Storage, Flow & Handling*, 1978, TUNRA Ltd, the University of Newcastle.
34. **Orr, Clyde, JR**, *Particulate Technology*, 1966, Macmillian New York.
35. **Reisner, W., Eisenhart, Rothe M v.,** *Bins and Bunkers for Handling Bulk Materials: Practical Design and Techniques*, 1971, Trans Tech Publications.
36. **Stepanoff, Alexey J.,** *Gravity Flow of Bulk Solid and Transportation of Solids in Suspension*, 1969, John Wiley & Sons, Inc.
37. **IEA Coal Research.,** *Fundamentals of Bulk Solids Flow***,** 1986, IEA Coal Research, London.
38. **Wassgren, Carl R., Hunt, Melany L., Brennen, Christopher E.,** *Effects of Vertical Vibration on Hopper Flows of Granular Material*, Mechanics of Deformation and Flow of Particulate materials, American Society of Civil Engineers (ASCE), 1997, pp335-348
39. **Weathers, R. C., Hunt, M. L., Brennen, C. E., Lee, A. T., Wassgren, C. R.,** *Effects of Horizontal Vibration on Hopper Flows of Granular Materials*, Mechanics

of Deformation and Flow of Particulate materials, American Society of Civil Engineers (ASCE), 1997, pp349-360

40. **Peschl, I.,** *Principals of Soil Mechanics for the Characterisation of Industrial Powders*, Powder Handling & Processing, **V13**, n1, Jan-Mar, 2001, pp11-18.
41. **Arnold, P. C.,** *Some Observations on the Importance of Particle Size in Bulk Solids Handling*, Powder Handling & Processing, **V13,** n1, Jan-Mar, 2001, pp35-40.
42. **Tejchman, J.,** *Scale Effects in Bulk Solids During Silo Flow***,** Powder Handling & Processing, **V13**, n2, Apr-Jun, 2001, pp165-171.
43. **Peschl, I.,** *Arching and Ratholing in Silos*, Powder Handling & Processing, **V13**, n4, Oct-Dec, 2001, pp357-363.
44. **Jenike, A. W.,** *Quantitative Design of Mass-Flow Bins*, Powder Technology, **V1,** Sep, 1967, pp237-244
45. **Moore, B. A., Arnold, P. C.,** *An Alternative Presentation of the Design Parameters for Mass Flow Hoppers*, Powder Technology, **V42,** 1985, pp79-89
46. **Ducker, J. R., Ducker, M. E., Nedderman, R. M.,** *The Discharge of Granular Materials form Unventilated Hopper*, Powder Technology, **V42,** 1985, pp3-14.
47. **Bradley, M. S., Farnish, R. J., Pittman, A. N., Leaper, M. C.,** *Caking by Moistrue Migration of Bulk Solids – An Investigation of Causes*, IMECHE Conference Transactions: From Bulk Powder to Bulk: International Conference on Powder and Bulk Solids Handling, 2000, Professional Engineering for the Institution of Mechanical Engineers, pp39-44.
48. **Matchett, A. J., Armstrong, B., Peace, J., A Reliable,** *Vibrationally Activated, Mass Flow Hopper System*, IMECHE Conference Transactions: From Bulk Powder to Bulk: International Conference on Powder and Bulk Solids Handling, 2000, Professional Engineering for the Institution of Mechanical Engineers, pp537-544.
49. **Arnold P. C.,** *Some Observations on the Relevance of Flow Properties in the Selection of Bin Dischargers*, IMECHE Conference Transactions: From Bulk Powder to Bulk: International Conference on Powder and Bulk Solids Handling, 2000, Professional Engineering for the Institution of Mechanical Engineers, pp557-566.

E. Separation & Pneumatic Conveying System

50. **Dorman, Richard George.,** *Dust Control and Air Cleaning*, 1974, Pergamon Press.
51. **Batel, Wilhelm.,** *Dust Extraction Technology: Principles, Methods, Measurement Technique*, English translation from the German by **Hardbottle, R.,** 1976, Stonehouse, Glos: Technicopy Ltd.

52. **Sittig, Marshall.,** *Particulates and Fine Dust Removal: Processes and Equipment,* Pollution Technology Review, n34, 1977, Park Ridge.
53. **Storch, Otakar.,** *Industrial separators for Gas Cleaning,* Chemical Engineering Monographs, V6, 1979, Amsterdam: Elsevier.
54. **Ogawa, Akira.,** *Separation of Particles From Air and Gases,* Uniscience Series on Fine Particle Science and Technology, **V1**, 1984, CRC Press
55. **Ogawa, Akira.,** *Separation of Particles From Air and Gases,* Uniscience Series on Fine Particle Science and Technology, **V2,** 1984, CRC Press
56. **Engineering Equipment User Association.,** *Separation of Dust From Gases,* Handbook (Engineering Equipment Users Association) E.E.U.A., n19, 1968, Constable and Company Ltd
57. **Johnes, H. R.,** Find *Dust and Particulates Removal,* Pollution Control Review, n11, 1972, Noyes Data Corp.
58. **Mody, Vinit., Jakjete, Raj.,** *Dust Control Handbook,* Pollution Technology review, n161, 1988, Noyes Data Corp.
59. **Wöhlbier, Reinhard, H.,** *Pneumatic Conveying of Bulk & Powder,* The Best of Bulk Handling 1981-1985, **V D/86,** 1986, Trans Tech publication
60. **Rhodes, M. J.,** *Introduction to Particle Technology,* 1998, John Wiley.
61. **Pery, Robert H., Green, Don W., Mloney, James O.,** *Perry's Chemical Engineers' Handbook,* 7th edition, 1997, McGraw-Hill
62. **Abrahamson, John.,** *Course Handout,* 2002, Chemical & Process Engineering, University of Canterbury.

F. Hydraulic & Pneumatic System Design

63. **Barber, Antony.,** *Pneumatic Handbook,* 8th edition, 1997, Elsvier Science.
64. **Parr, E. A.,** *Hydraulic and Pneumatics: A Technician's and Engineer's Guide,* 2nd edition, 1998, Butterworth-Heinemann.
65. **Kay, Francis Xavier.,** *Pneumatic Circuit Design,* 1966, Machinery Publishing Co.,
66. **Pinches, Michael J., Callear, Brian J.,** *Powder Pneumatics,* 1997, Prentice Hall.

G. Vortex Technology

67. **Saffman, P. G.,** *Vortex Dynamics,* Cambridge Monographs on Mechanics and Applied Mathematics, 1992, Cambridge University Press.

68. **Cottet, Georges-Henri., Koumoutsakos, Petros D.,** Vortex *Methods: Theory and Practice*, 2000, Cambridge University Press.
69. **Lugt, Hans J.,** *Vortex Flow in Nature and Technology*, 1983, Wiley.
70. **Glenny, D. E., Pyestock, N. G. T. E,** *Ingestion of Debris into Intakes by Vortex Action*, Aeronautical Research Council, n1114, 1970, H. M. Stationery Office.
71. **Wakelin, W.,** *The Vortex Cleaner*, University of Canterbury, Department of Mechanical Engineering, Final Year Project 1999.
72. **Patel, R.,** *A Vortex Cleaner*, University of Canterbury, Department of Mechanical Engineering, Final Year Project 1997.
73. **Lee, C. R. A.,** *A Vortex Cleaner*, University of Canterbury, Department of Mechanical Engineering, Final Year Project 1987.
74. **Post, D.,** *Vortex Cleaner*, University of Canterbury, Department of Mechanical Engineering, Final Year Project 1981.

H. Mechanism Design & Mechanics of Materials

75. **Erdman, Arthur G., Sandor, George, N.,** *Mechanism Design: Analysis and Synthesis*, **V1,** 1984, Prentice-Hall.
76. **Erdman, Arthur G., Sandor, George, N.,** *Mechanism Design: Analysis and Synthesis*, **V2,** 1984, Prentice-Hall.
77. **Molian, S.,** *Mechanism Design: The Practical Kinematics and Dynamics of Machinery*, 1997, Elsevier.
78. **Wöhlbier, Reinhard H.,** *Mechanical Conveying, Transporting & Feeding*, The Best of Bulk Solids Handling 1981-1985, **V D/86,** 1987, Trans Tech Publication.
79. **Sclater, Neil, Chironis, Nicholas P.,** *Mechanisms and Mechanical Devices Source Book*, 3rd edition, 2001, McGraw-Hall.
80. **Brockenbrough, Roger L., Merritt, Frederick S.,** Structural *Designer's Handbook*, 3rd edition, 1999, McGrew-Hill.
81. **Hamrock, Bernard J., Jacobson, Bo O., Schmid, Steven R.,** *Fundamentals of Machine Elements*, 1999, WCB/McGrew-Hill.
82. **Shigley, Joseph Edward.,** *Mechanical Engineering Design*, 1st Metric Edition, Mc-Grew-Hill Series in Mechanical Engineering, 1986, McGrew-Hill.
83. **Megson, T. H. G.,** *Structural and Stress Analysis*, 1996, Arnold.
84. **Wysack, Roy.,** *Designing Parts with SolidWorks*, 1998, CAD/CAM Publishing.
85. **Simmons, Colin H., Maguire, Dennis E.,** *Manual of Engineering Drawing*, 1995, Eward Arnold.

86. **Hibbeler, R. C.,** *Mechanics of Materials*, 3rd edition, 1997, Prentice Hall International, Inc.
87. **Pahl, G., Beitz, Wolfgong.,** *Engineering Design: a Systematic Approach*, 1996, Springer.
88. **Hales, Crispin.,** *Manaing Engineering Design*, 1993, Longman Science & Technical.

I. Thesis & Scientific Report Writing

89. **Paradise, James G., Zimmeman, Muriel.,** *The MIT Guide to Science and Engineering Communication*, 1997, MIT Pres.
90. **Gooch, S. D.,** *Design and Mathematical Modelling of the Kinetic Sculpture Blade: a thesis submitted for the degree of Doctor of Philosophy at the Department of Mechanical Engineering, University of Canterbury*, 2001, University of Canterbury.

APPENDIX A – Particle Size Determination with Shadowgraph

A-1 Preparation of Sample

Great care has to be taken in slide preparation since the measurement sample is so small that it is difficult to make it representative of the bulk. Many particulate systems retain their agglomerates and aggregates, if it is necessary to retain their integrity; the dispersing procedure needs to be very gentle **[28]**. A small portion of dust was sieved to break up the large lump of powders, the powder was lightly dusted on the top of the glass slides, and then enclosed with a cover piece in order to maintain its orientation during the project period, and four sample slides were made.

A-2 Feret's Diameter (d_f) Measurement

Optical microscopy is most often used for the examination of particles from 3 μm to 150 μm. The theoretical lower limit is approximately 0.2 μm but the diffraction halo around the particle gives a gross overestimation of particle size **[28]**. Its most severe limitation is the small depth of field so that, as a slide has a wide range of sizes, only a few particles are in focus at any one time. Similar to optical microscopy, the shadowgraph comes with the advantage of eliminating the depth of field problem and can obtain measurements down to 0.2 μm, however the surface detail of the particle are unable to revealed. A simple magnifying glass is suitable for particles above 150 μm.

The images seen in a shadowgraph are projected area whose dimensions depend on the particles' orientation on the slide. Particles in stable orientation tends to present their maximum area to the user, hence the size measured by shadowgraph tend to be greater than those measured by other methods. Any one particle has an infinite number of linear dimensions, therefore if the chord length is measured at a random, the length will depend upon the particle orientation on the slide. These orientation dependent measurements are known as statistical diameters, and are only useful when a large number of measurements are made. They are measured parallel to some fixed direction and are acceptable only when orientation is random; i.e. the distribution of diameters measured parallel to some other direction must give the same size distribution. Since they are representative of the two largest particles' dimensions – the smallest is perpendicular to the viewing plane if the particles are in a stable orientation – the diameters will generally be larger than the Strokes diameters in

the gravity sedimentation methods. With Strokes law relating particle size to settling velocity in equation

$$d_{st} = \sqrt{\frac{18\eta u}{(\rho_s - \rho_f)g}} \qquad \textbf{(A1)}$$

Where d_{st} is the Stroke diameter, η is viscosity, u is particle settling velocity under gravity g, ρ_s is the particle density, and ρ_f is the fluid density. From **Perry, R. H.** *et al* **[61]**, the Stroke diameter is defined as the diameter of a sphere having the same density and the same velocity as the particle in a fluid of the same density and viscosity setting under laminar flow conditions.

The Feret's Diameter (d_f) is the distance between two tangents on opposite sides of the particle parallel to some fixed direction **[28]**, however, since the shape of the particles were not perfectly round, a horizontal and a vertical measurement on each particle was obtained and the average value was then recorded for each particle measurement. Particles which were targeted here were the both the smallest and largest appeared on the shadowgraph, and 40 samples were made on both sizes.

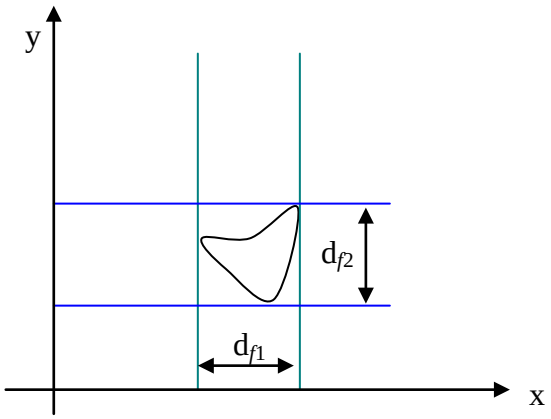

Figure A-1, Feret's diameter (d_f) measurement

APPENDIX B – Powder Properties Determination with Shear Cell

Most of the powder properties' measurements were conducted in the Particle Technology Laboratory within the Department of Chemical & Process Engineering at the University of Canterbury.

B-1 Calibration of the Peschl Shear Cell

From **Kearney, T. [27]**, the Peschl Shear Cell was connected with a compressed air supply, and the inlet pressure was set to 4 bar, without any powder in the cell, and the air bearing in the shear cell head was cleaned and checked for sensitivity. The friction of the vertical movement of the cell was balanced out by altering the small weight from the counter-balance weight until the shaft of the head began to fall with slight push downwards.

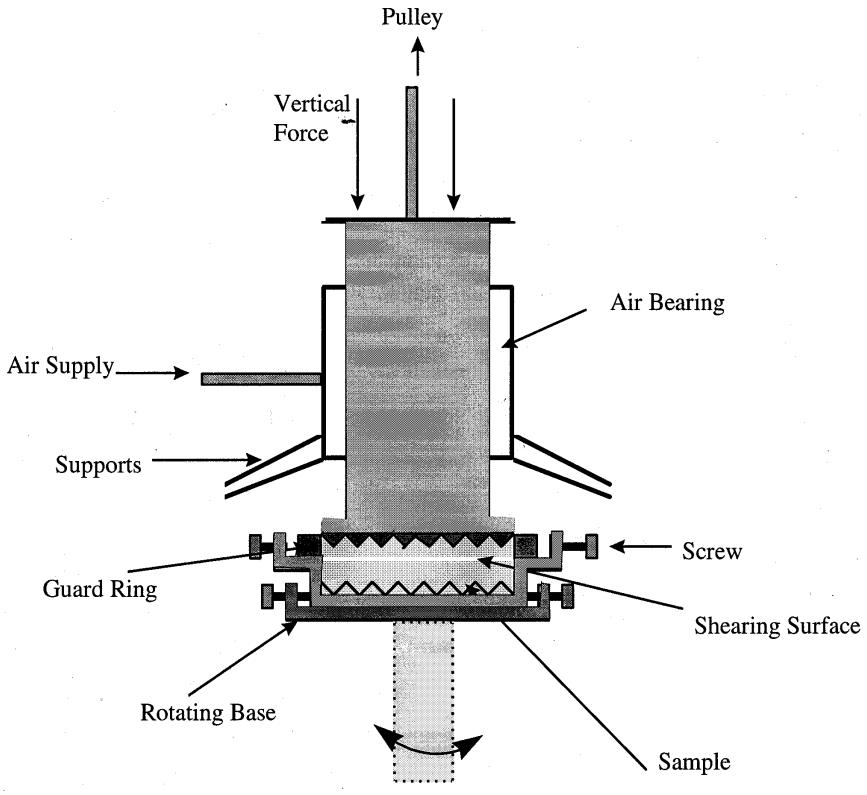

Figure B-1, Peschl shear cell (Source: Kearney, T. [27])

The detachable arm was assembled onto the top of the shear head by removing the calibration pulley. Two hundred grams of weights were loaded on the bob and the cell and/or recorder setting were adjusted to give a chart displacement of about 90% of the width of the chart

paper. The weight placed on the bob was gradually increased, and the change of corresponding displacement recorded. The effective average shear stress across the annulus τ was assume to be constant across the whole shearing surface, and can then be determined by equation

$$T = WR_1 = \tau(\frac{2}{3}\pi R_2^3) \quad \textbf{(B1)}$$

where T is the torque, W is the loading weight, R_1 (radius)= 0.102m, and R_2 (radius of the shear cell head) = 0.031m. The calibration result is listed below in Table B-1.

Table B-1, Shear cell calibration result

Displacement	Mass (g)	$T = WR_1$ (Nm)	τ (Nm^{-2})
0	0	0	0
1.3	30	0.03	481.1
3.3	80	0.08	1283.0
5.3	130	0.1301	2048.8
7.25	180	0.1801	2886.7
9.225	230	0.2301	3688.5

All settings on the shear cell at this stage were maintained constant until all the property measurements regarding to the powder were completed

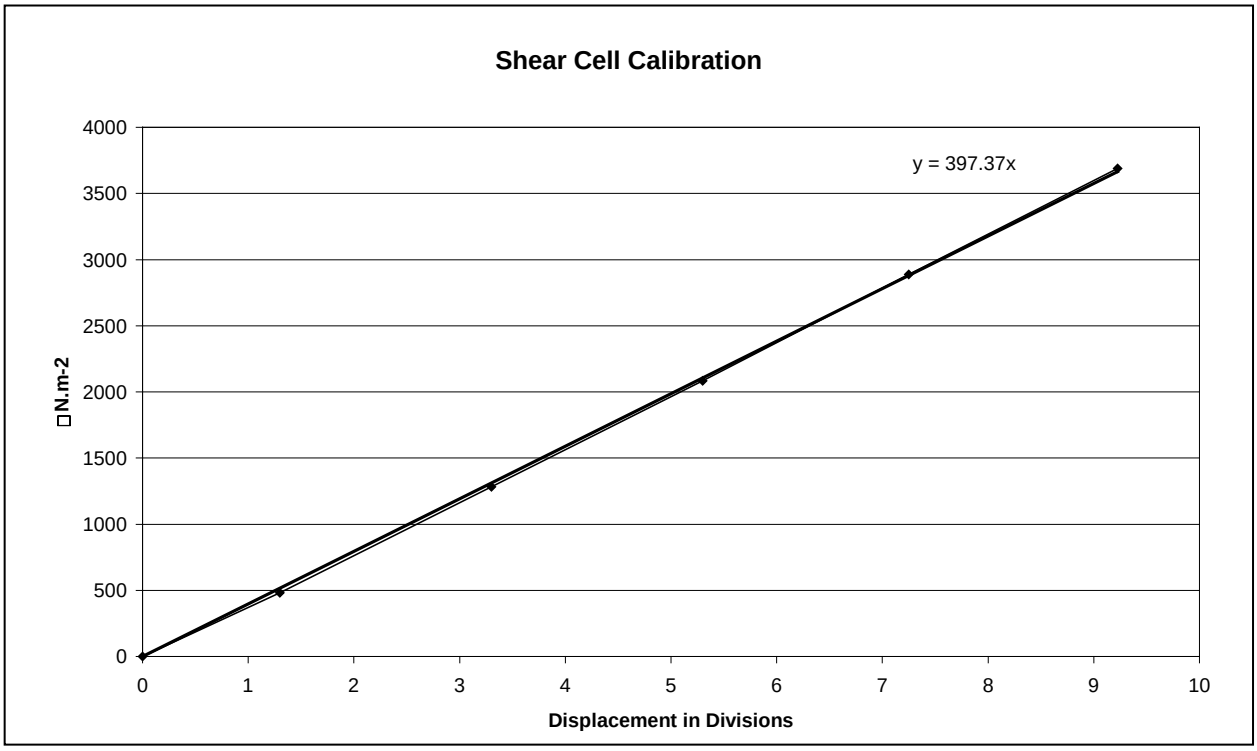

Figure B-2, Shear cell calibration.

B-2 Yield Loci for Powder/Powder & Powder/Wall Shearing

At least four different consolidation weights between 0.25 to 1 kg must be used to ensure that the powder function may be generated with reasonable certainty **[27]**.

B-2.1 Sample Preparation

The guard-ring was clamped to the trough of the shear cell with three screws. The covering was placed on the guard-ring; the powder was sieved and levelled off with metal straightedge. The chosen consolidation weight was loaded on the perspex cylinder and placed directly on top of the powder for one minute. The weight, perspex cylinder and plastic cover-ring were all removed. The filled-trough was gently placed on the turntable of the shear cell and firmly secured, the fill was checked to ensure that it was levelled, and the guard-ring was then loosened.

The shear head was mounted on to the turntable. The retractable arm of the load cell was lowered down to the shear head until contact was made, then the counter-balance yoke was connected. The chosen consolidation weight was loaded and the shear head gently lowered on to the turntable. The powder was sheared in both clock wise and anti-clockwise direction until a steady maximum value is obtained, then the consolidated sample was then ready for testing. It was necessary to make new samples for each different consolidation weight.

B-2.2 Powder/Powder Shear Test

The powder was sheared once until a maximum displacement was seen and reverse sheared until zero displacement was obtained. Some of the original consolidation weight was removed and the shearing/reverse cycle was repeated with five different weights within each consolidation, this had to include the consolidation weight. Results are listed in Tables B-2, B-3, B-4 and B-5, and the angle of internal friction δ of steel powder under different consolidations was determined from Möhr circle diagrams and summarised in Table B-6.

Table B-2, 150g consolidation powder/powder shear result

Displacement	Mass (g)	τ (Nm^{-2})	σ (MPa)
0.4	0	158.9	0
0.75	50	298.0	162.5
1.05	100	417.2	324.9
1.3	150	516.6	487.4

Table B-3, 250g consolidation powder/powder shear result

Displacement	Mass (g)	τ (Nm^{-2})	σ (MPa)
0.35	0	139.1	0
0.75	50	298.0	162.5
1.15	100	417.0	324.9
1.55	150	516.9	487.4
1.9	200	755.0	649.9
2.2	250	874.2	812.3

Table B-4, 400g consolidation powder/powder shear result

Displacement	Mass (g)	τ (Nm^{-2})	σ (MPa)
0.4	0	158.9	0
1.1	100	437.1	324.9
1.85	200	735.1	649.9
2.5	300	993.4	974.8
3.1	400	1231.8	1299.7

Table B-5, 600g consolidation powder/powder shear result

Displacement	Mass (g)	τ (Nm^{-2})	σ (MPa)
0.35	0	139.1	0
1.2	100	476.8	324.9
1.9	200	755.0	649.9
2.65	300	1053.0	974.8
3.35	400	1331.2	1299.7
3.9	500	1549.7	1624.7
4.5	600	1788.2	1949.6

Figures B-3, B-4, B-5, and B-6 show the yield loci for powder/powder shearing under different consolidation loads.

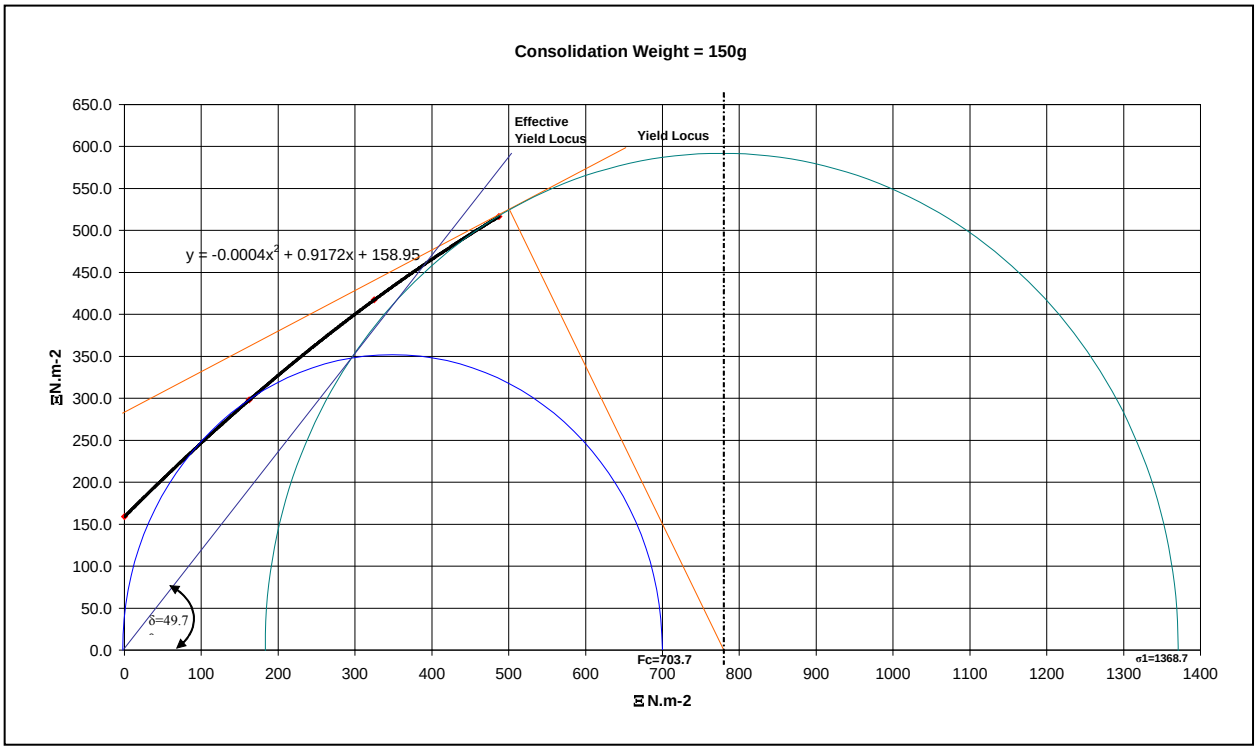

Figure B-3, Möhr circle diagram of steel powder at 150g consolidation.

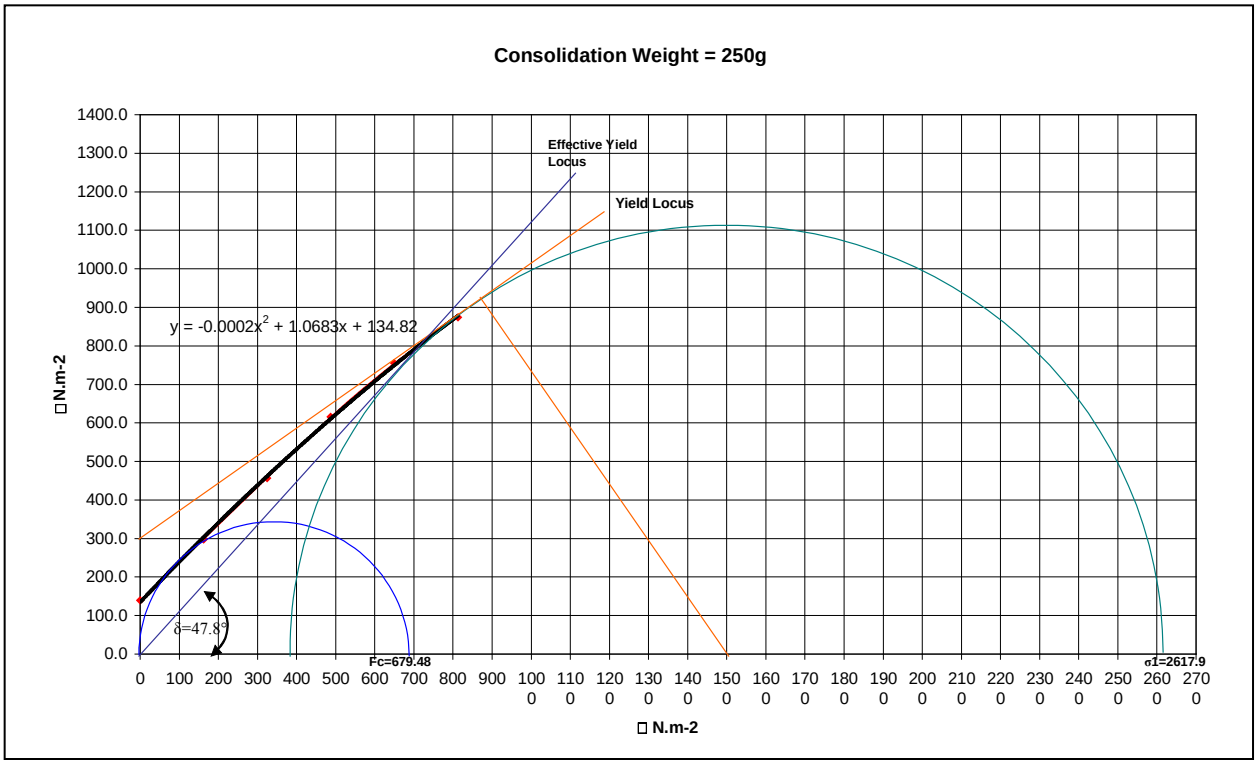

Figure B-4, Möhr circle diagram of steel powder at 250g consolidation.

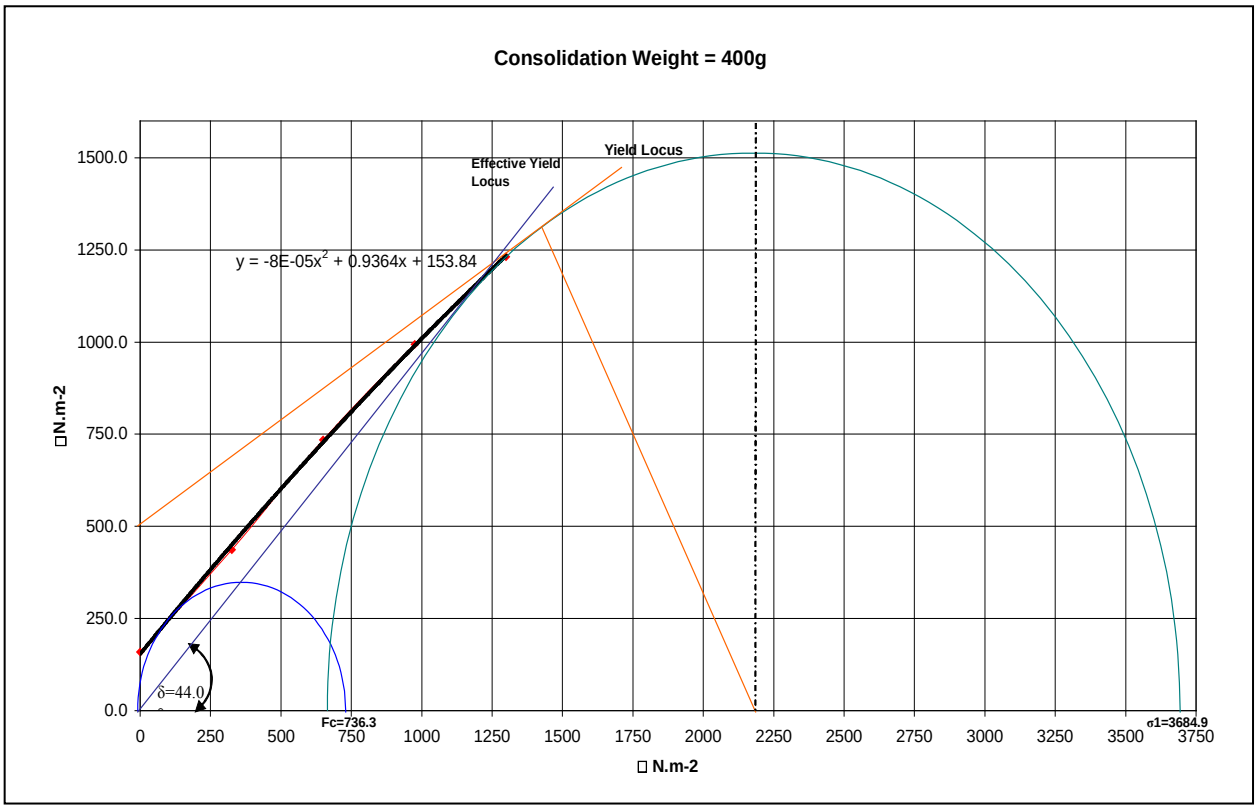

Figure B-5, Möhr circle diagram of steel powder at 400g consolidation.

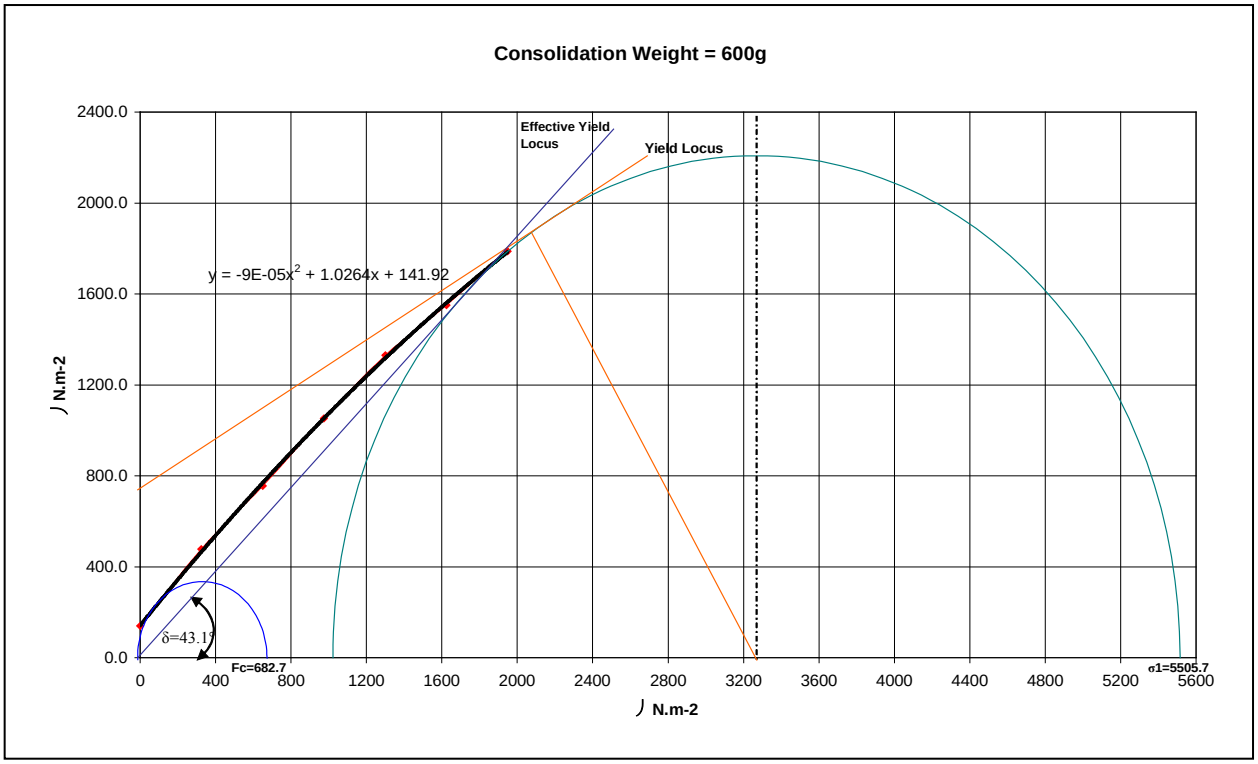

Figure B-6, Möhr circle diagram of steel powder at 600g consolidation.

Table B-6, Summary of angle of internal friction obtained from powder/powder shear test

Consolidation Load (g)	Angle of internal friction δ
150	49.67
250	47.84
400	44.01
600	43.11

B-2-.3 Powder/Wall Shear Test

Similar procedures were used to test the shear between the powder and the wall. By inserting the material disk into the trough before filling it with powder and performing the shear test, the angle of friction with the wall was then be obtained. Table B-6 shows the powder/wall shear test result.

Table B-7, 400g consolidation powder/wall shear result.

Displacement	Mass (g)	τ (Nm^{-2})	σ (MPa)
0.35	0	139.1	0
0.55	50	218.6	162.5
0.7	100	278.2	324.9
0.775	150	308.0	487.4
0.9	200	357.6	649.9
1	250	397.4	812.3
1.1	300	437.1	974.8
1.2	350	476.8	1137.3
1.4	400	556.3	1299.7

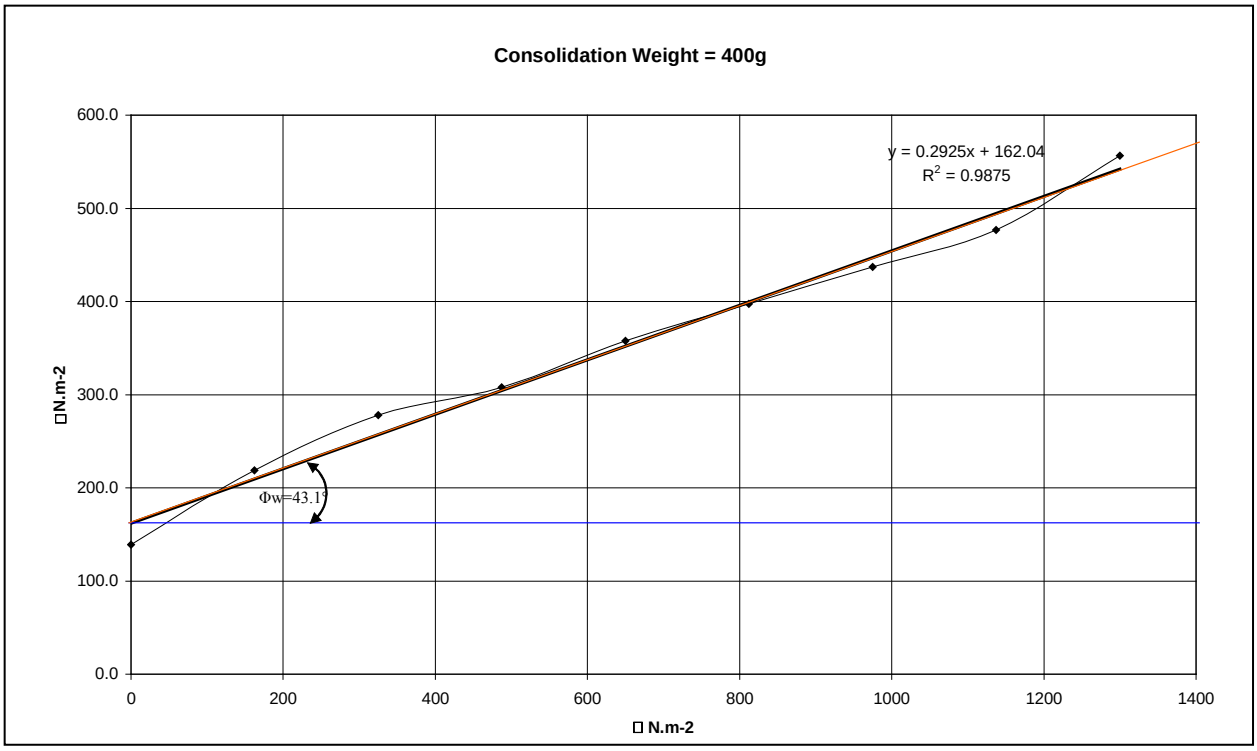

Figure B-7, Kinematic angle of wall friction.

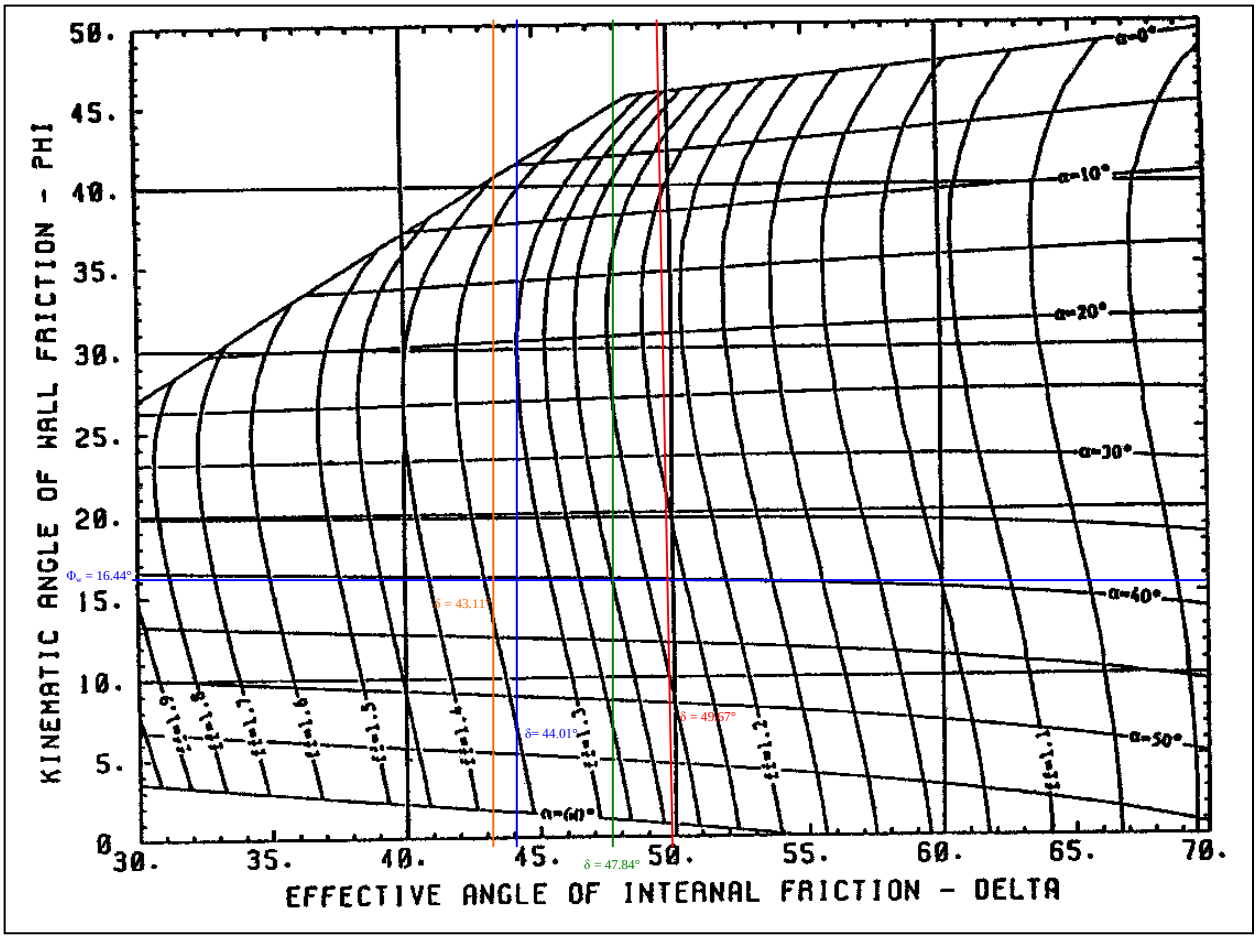

Figure B-8, Plan flow hopper design parameter (Source: Kearney, T. [27])

The kinematic angle of wall friction Φ_w was found to be 16.44°, hence the flow factor ff and angle of repose α for each test can be determined from Figure B-8, and then recorded in Table B-9.

Table B-9, Flow factor

Consolidation Load (g)	Angel of Repose α (°)	Flow Factor ff	Fc (N)	σ_1 (MPa)	F = σ_1 / ff (N)
150	39.0	1.129	703.71	1368.69	1113.66
250	39.0	1.258	679.48	2671.87	2130.08
400	39.5	1.312	736.33	3684.91	2998.30
600	40.0	1.318	682.72	5505.69	4479.81

The powder function was obtained and plotted in Figure B-9, the intersection between two lines was $F_{critical}$ and it was found to be 866.5 MPa, and the equivalent force applied on the powder within the perspex container was 26510.5N.

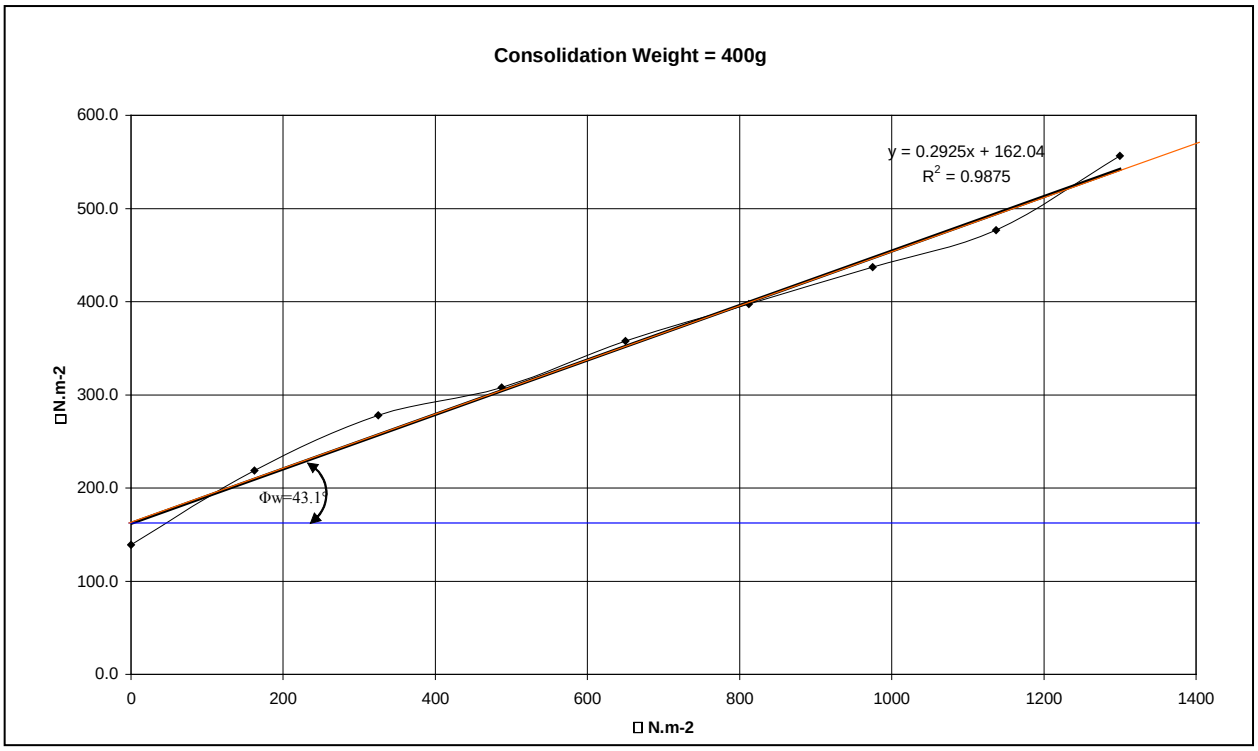

Figure B-9, Graph of Fc VS σ_1

B-3 Bulk Density

Bulk density of the powder can be varied with different consolidation pressures. In this experiment the consolidation pressure was simulated by applying static axial loading over a known size of container. When different static weights are placed, the powder in the container can be assessed to find a function with regards to the density and this can be determined from Figure B-10.

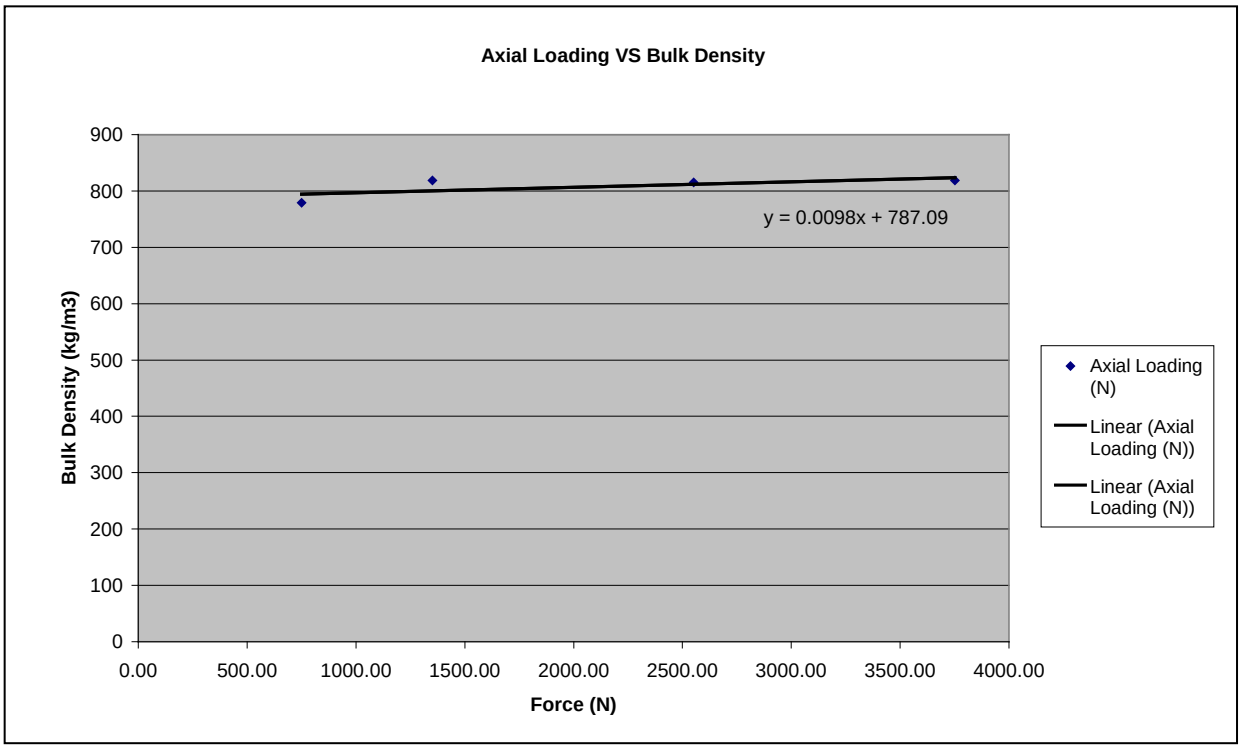

Figure B-10, Axial loading VS bulk density graph of clean steel powder.

By applying the equivalent force of $F_{critical}$ obtained from Figure B-9 into the bulk density equation, the bulk density was found to be 1046.89 kg/m^3.

APPENDIX C – Cyclone Separation Requirement

Research regarding the practical implications of understanding cyclone separation has been conducted by both the industries and research centres. However, a universal mathematical expression for the vortex has yet to come, since the expression developed by each party has a unique superiority. This is due to the various hypothetical assumptions made regarding the data obtained from experimental data.

Two approaches were taken in this section to determine the general requirements for a cyclone system to separate the given particle size which was determined earlier. A course handout from Chemical & Process Engineering (CAPE) at University of Canterbury, written by **Prof. Abrahamsom J. [62]** on the cyclone separation system was used as one of the calculation methods, and the other from **Perry, R. H.** *et al* **[61],** which is denoted as CAPE 's method and Perry's method respectively.

C-1 CAPE's Method

A practical method taught in the undergraduate Chemical & Process Engineering course at the University of Canterbury is described below, with three different design dimensions relative to outlet duct diameter as listed in Table C-1, and detailed diagram descriptions in Figure C-1,

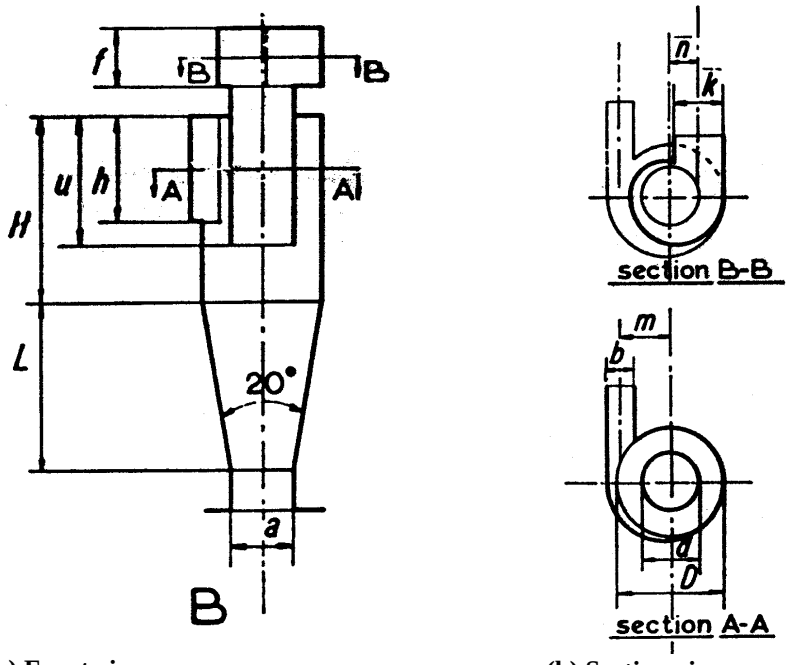

(a) Front view **(b) Section views**

Figure C-1, Detailed description of cyclone separator (a) front view, (b) section views. (Source: Abrahamson, J. [62])

Table C-1, Cyclone separator dimensions in proportional to *d* (Source: Abrahamson, J. [62])

Parameter / Dimension Relationship	A	B	C
d	1.0	1.0	1.0
D	2.5	1.9	3.3
a	≤ 1.0	≤ 1.0	≤ 1.0
b	0.66	0.5	0.89
f	0.89	0.89	0.89
h	1.2	1.6	0.89
H	1.6	2.9	1.67
k	0.89	0.89	0.89
m	0.92	1.0	1.23
n	1.25	0.5	0.5
u	1.4	2.0	1.3

This method uses the Strokes number with an assumption regarding the concentration of the particles at the inlet to justify the efficiency of the separation process.

$$Stk = \frac{x^2 v_{in} \rho_p}{\mu D} \quad \textbf{(C-1)}$$

$$Y = \frac{x}{x_{50}} = \frac{\sqrt{Stk}}{\sqrt{Stk_{50}}} \quad \textbf{(C-2)}$$

$$\eta = \frac{1}{m + \frac{k}{Y^n}} \quad \textbf{(C-3)}$$

where x is the particle size, v_{in} the inlet velocity, ρ_p the particle density, μ the gas viscosity, and D the diameter of the cyclone.

For a dilute system, such as 10 g/m^3, as shown in Figure C-2, together with the calculated result, it was found that a very large entry velocity (1600 m/s) and a relatively small cyclone outlet duct dimension (Ø5mm) is required to achieve 50% efficiency. All of the three given dimension relationships were applied, and similar efficiency was observed from the results; hence it is impossible to use a cyclone achieve an efficient separation in this case. As the inlet particle concentration increases, the efficiency curve will shift upward; this is mainly due to the aggregation or collision of particle with each other in the flow. However, since the

requirement of the inlet velocity is far beyond realistic practicability, it is concluded to be as unfeasible.

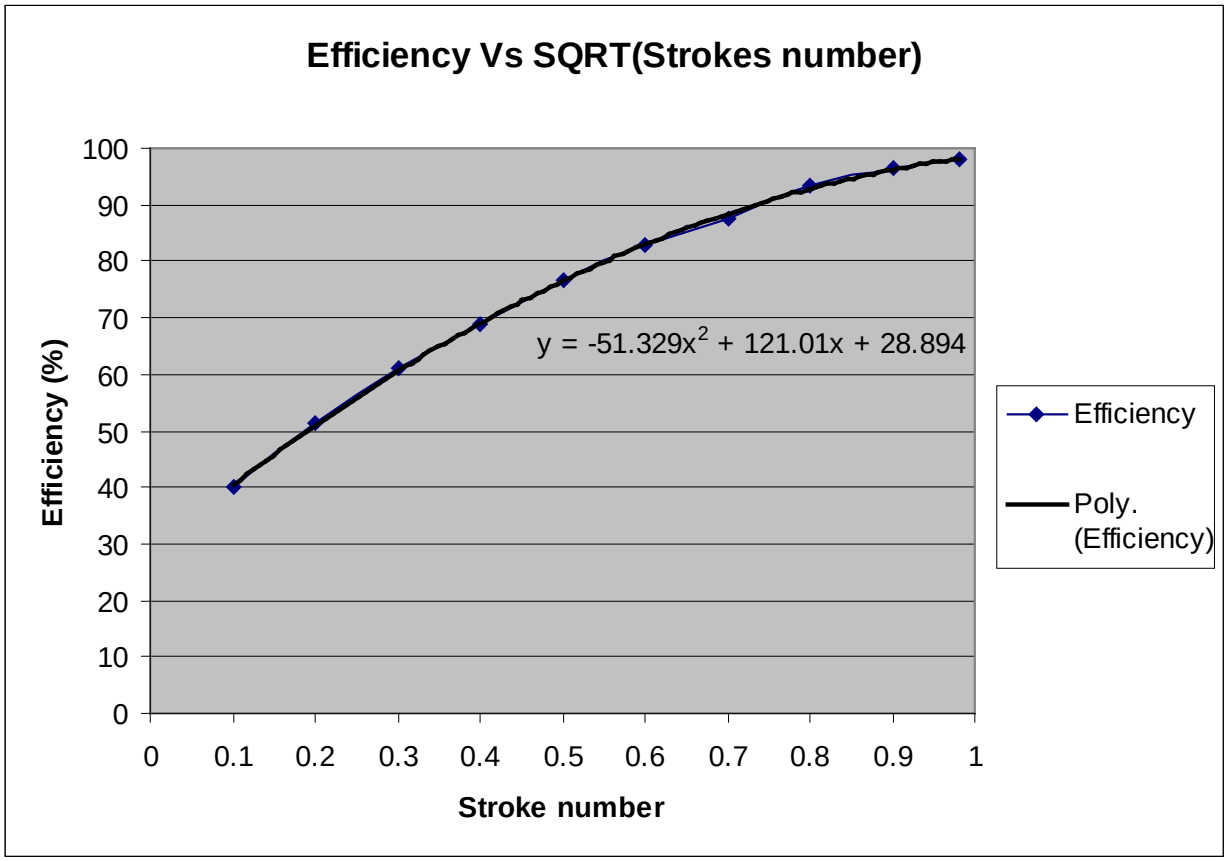

Figure C-2, Cyclone separation efficiency with inlet particle concentration of 10 g/m^3.

A comparison with the alternative analytical method will be conducted and reviewed in the next section, and a final conclusion will then be drawn.

C-2 Perry's Method

This method was found in one of the most highly recommended text books in the chemical engineering field, and here it is used to verify the previous analysis in order to justify the feasibility of the cyclone separation process in the implementation of the transportation system development.

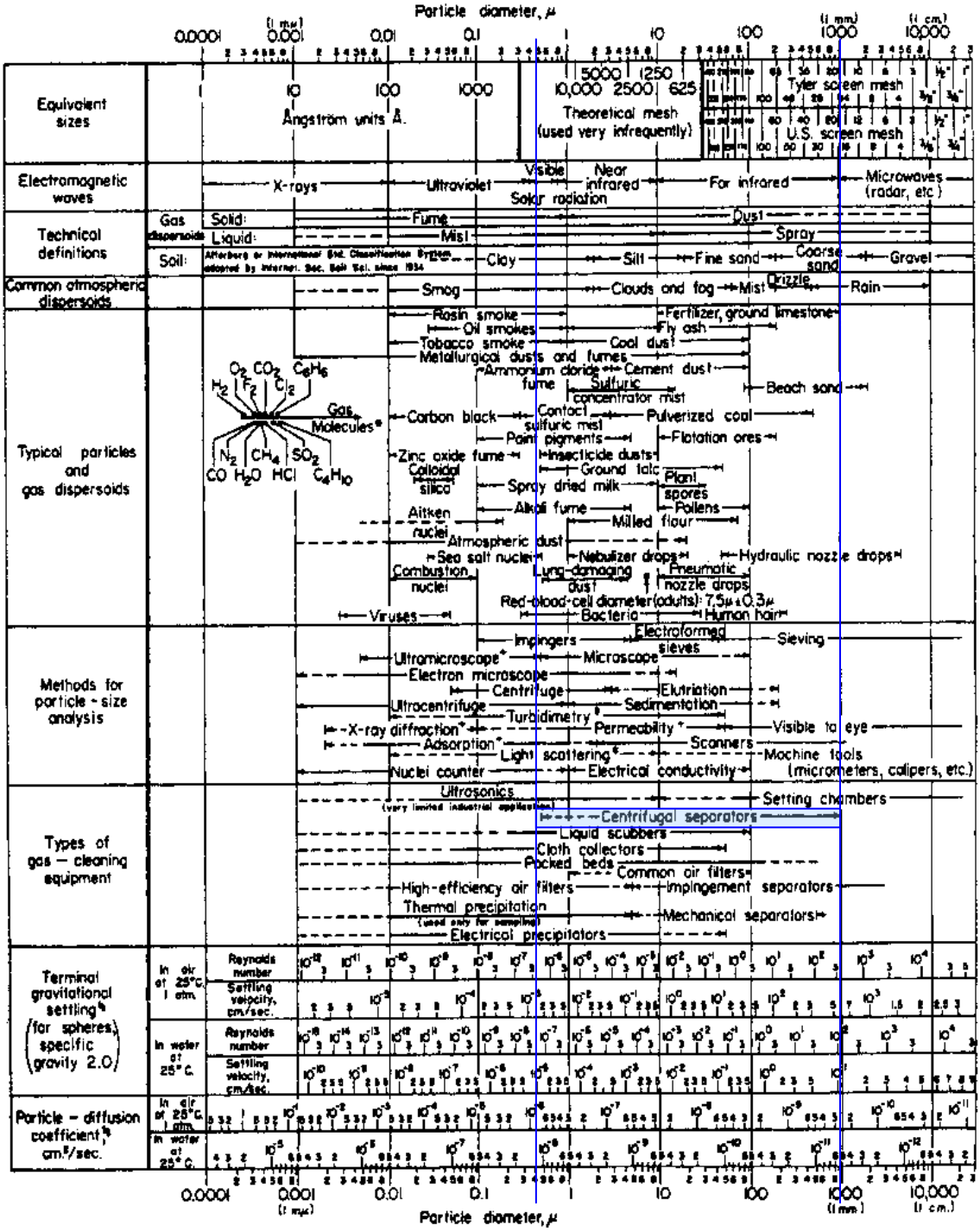

Figure C-3, Characteristics of particles and particle dispersoids (Source: Perry, R. H., Green, D. W., Maloney, J. O. [61])

Using a broad overview of the separation technologies as shown in Figure C-2, it was found that the cyclone separation process can cover a wide range of particle size from 0.5 – 1000 μm. However the efficiency dropped sharply when particles are smaller than 20 μm.

The detailed description of the dimension relationship is shown in Figure C-4. The number of effective spiral paths of the gas flowing in the cyclone has been taken into account and related to the inlet velocity. However, this is for a very dilute system, since the inlet particle concentration is difficult to predict at this stage.

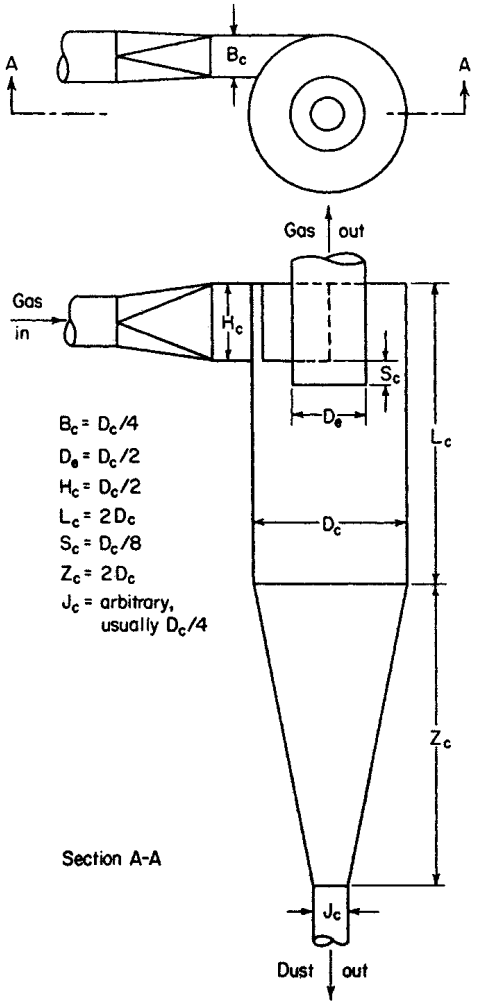

Figure C-4, Cyclone separator proportions (Source: Perry, R. H., Green D. W., Maloney, J. O. [62])

This analytical method is concerned with the theoretical particle size that can be removed by the cyclone as expressed as below,

$$D_{pth} = \sqrt{\frac{9\mu_g B_c}{\pi N_s v_{in}(\rho_p - \rho_g)}} \qquad \textbf{(C-4)}$$

where D_{pth} is the theoretical particle size, μ_g the gas viscosity, B_c the dimension of the cyclone, N_s the effective number of spital, v_{in} the gas inlet velocity, and ρ_p, ρ_g is the density of gas and particle respectively.

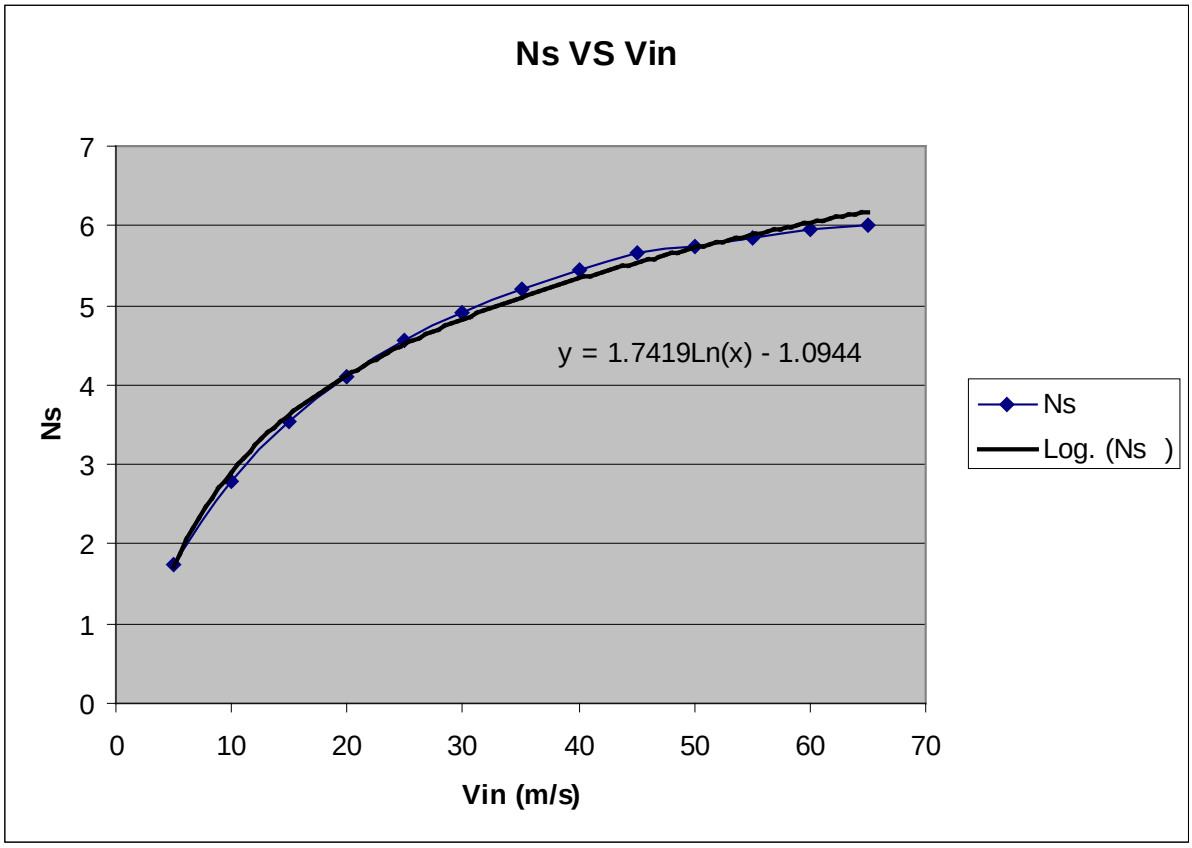

Figure C-5, N_s versus velocity – where the larger of either the inlet or outlet velocity is used

Figure C-5 is used to determine the value N_s when an assumed inlet velocity is used. It was found that for a practical inlet velocity of 30 m/s, and an outlet duct of Ø5mm, only particles larger than 109.3 μm can be separated. By rearranging the equation to determine the inlet velocity required, with the particle size set to 8.8 μm, the inlet velocity was also found to be impossible to be achieved in reality. Therefore the implementation of a cyclone separation unit into the transportation system will no longer be considered.

APPENDIX D – Vortex Study

Much research regarding the application of a vortex in the design of the vacuum cleaners has been conducted under the Department of Mechanical Engineering at the University of Canterbury in the last 40 years. Most of the experimental data regarding the vortex were gathered through undergraduate final year projects, and a significant amount of understanding has been achieved and used to compare the data with the theoretical estimation. Although none of those prototypes are able to offer an efficient performance at this stage, the theoretical estimation still holds and encourages further research in this area.

The centripetal force due to the circular motion of the fluid causes a significant pressure drop in the core of the vortex, providing a lifting capability similar to that of tornados and cyclones. The presence of the vortex can be observed in everyday action such as the motion of leaves moving in a swirling wind, or sink draining.

The project was originally conceived of to solve an existing problem by researching a more efficient method. Therefore, given the limited amount understanding on the vortex both theoretically and practically, the vortex lifting method has been discarded. However, investigation has been carried out to verify its importance and possible implementation for further development in the future.

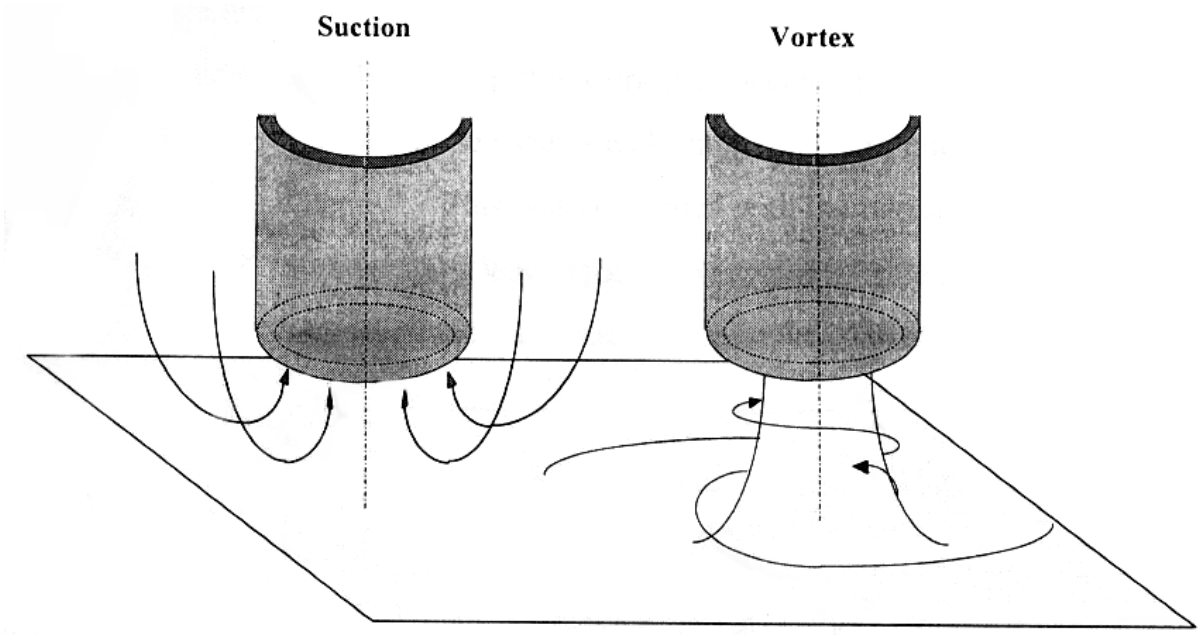

Figure D-1, Motion of the local fluid affected by suction and vortex (Source: Wakelin, W. [71])

In the conventional vacuum cleaner, as shown in Figure D-1, in which the disturbance of localised air is withdrawn by the suction into the hose, many operational limitations still exist. Theoretically, a vortex in an inviscid fluid cannot be terminated within the medium; rather it results in the formation of a ring which extends to infinity or to the physical boundary **[74]**. Hence, the influence of a vortex can extend further into the fluid than the conventional plain suction provide by vacuum cleaner. A greater effective range is provided by the vortex which is suitable for application on lifting particles from an irregular geometry; and hence it has high potential in the industry for further development of a highly efficiency transportation.

A mathematical model concerned with the velocity profile and pressure distribution about the fluid axis of rotation was found, and through using the simplified mathematical modelling, the lifting capability of the vortex can be determined; however, these were assumed to be under 2-D conditions. This fluid is modelled as two separate regions. The inner region is called the *Forced/Rotational Vortex*, which is assumed to rotate as a rigid body and has the same angular velocity about some fixed axis **[72]**. Beyond this rotating core is the outer region, commonly known as the *Free/Irrotational Vortex*, and is assumed that the streamlines of the fluid run in concentric circles with each other, and also that the fluid particles moving on these streamlines do not rotate about their own axis. This chapter covers the basic fundamental theories on the fluid dynamics of the vortex.

D-1 Mathematical Modelling

The Eulerian approach was taken with the properties of a fluid considered with respect to the spatial and time coordinates, which is opposed to the Lagrangian approach where individual particles of fluid were studied **[74]**.

D-1.1 Conservation of Mass & Momentum

For an elemental cube, the governing differential equation for the conservation of mass is,

$$\frac{\partial \rho}{\partial t} + \frac{\partial (\rho u)}{\partial x} + \frac{\partial (\rho v)}{\partial y} + \frac{\partial (\rho w)}{\partial z} = 0 \qquad \textbf{(D-1)}$$

where the flow velocity is

$$\underset{\leftarrow}{q} = u\underset{\cdot}{i} + v\underset{\leftarrow}{j} + w\underset{\leftarrow}{k} \qquad \textbf{(D-2)}$$

Hence, for steady incompressible flow, equation (D-1) is reduced to

$$\frac{\partial u}{\partial x} + \frac{\partial v}{\partial y} + \frac{\partial w}{\partial z} = 0 \qquad \textbf{(D-3)}$$

For a stressed element of fluid which equates to Newton's second law, then

$$\frac{\partial (\rho u_i)}{\partial t} + u_j \frac{\partial (\rho u_i)}{\partial x_j} = \frac{\partial \sigma_{i_j}}{\partial x_j} + B_i \qquad \textbf{(D-4)}$$

Hence, for a steady, incompressible flow, from (D-3) and (D-4) can reduces to,

$$u\frac{\partial u}{\partial x} + v\frac{\partial u}{\partial y} + w\frac{\partial u}{\partial z} = \frac{\partial \sigma_{xx}}{\partial x} + \frac{\partial \tau_{xy}}{\partial y} + \frac{\partial \tau_{xz}}{\partial z} + B_x \qquad \textbf{(D-5)}$$

D-1.2 Navier-Strokes equations

From **Post, D. [74]**, these equations were derived from the conservation of momentum, and may be applied with high accuracy to problems involving viscosity variations when the velocity gradient is not too large. In most situations, this assumption can be held and the Navier-Strokes equations can be apply in the incompressible flow problems. The Navier-Strokes equations for incompressible flow rate,

$$\rho\left[\frac{\partial u_i}{\partial t}+u_j\frac{\partial u_i}{\partial x_j}\right]=-\frac{\partial P}{\partial x_i}+B_i+\mu\frac{\partial^2 u_i}{\partial x_j^2} \qquad \textbf{(D-6)}$$

in Cartesian tensor notation, or in vector notation as shown below:

$$\rho\frac{D\underset{\leftarrow}{v}}{Dt}=-\nabla P+\underset{\leftarrow}{B}+\mu\nabla^2\underset{\leftarrow}{v} \qquad \textbf{(D-7)}$$

D-1.3 Element Rotation, Circulation and Vorticity

From **Post, D. [74],** consider an element of fluid undergoing a rotation in two-dimensional flow, as shown in Figure D-2.

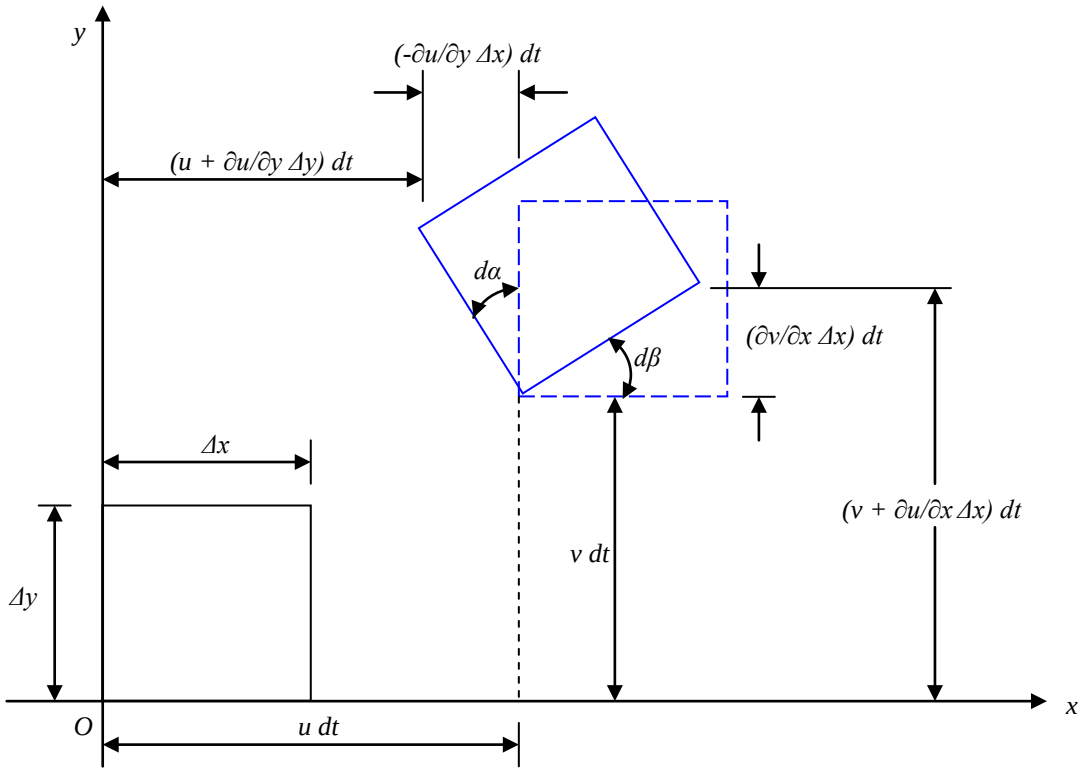

Figure D-2, Element of fluid undergoing rotation in 2-D flow (Source: Post, D. [74])

The rate of rotation of the two perpendicular faces of the element in the (x,y) coordinate is used to define the rate of the rotation of the element. In the 2-D flow, the rate of rotation can be expressed as

$$\omega_z = \frac{1}{2}\frac{(d\alpha + d\beta)}{dt} = \frac{1}{2}\left[\frac{\partial v}{\partial x} - \frac{\partial u}{\partial y}\right] \quad \textbf{(D-8)}$$

Hence, similar in 3-D flow

$$\omega_x = \frac{1}{2}\left[\frac{\partial w}{\partial y} - \frac{\partial v}{\partial z}\right] \quad \textbf{(D-9)}$$

$$\omega_y = \frac{1}{2}\left[\frac{\partial u}{\partial z} - \frac{\partial w}{\partial x}\right] \quad \textbf{(D-10)}$$

This may be expressed mathematically as

$$\underleftarrow{\omega} = \frac{1}{2} curl \underleftarrow{v} = \frac{1}{2}\nabla x \underleftarrow{v} \quad \textbf{(D-11)}$$

$$\underleftarrow{v} = u\underleftarrow{i} + v\underleftarrow{j} + w\underleftarrow{k} \quad \textbf{(D-12)}$$

where the $\underleftarrow{v}$ is the velocity vector at x, y. For the rotation vector $\underleftarrow{\omega}$ equal zero, then the flow is said to be irrotational and hence,

$$\frac{\partial w}{\partial y} = \frac{\partial v}{\partial z} \quad \textbf{(D-13)}$$

$$\frac{\partial u}{\partial z} = \frac{\partial w}{\partial x} \quad \textbf{(D-14)}$$

$$\frac{\partial v}{\partial x} = \frac{\partial u}{\partial y} \quad \textbf{(D-15)}$$

The line integral of the velocity vector around an enclosed contour is used to define the circulation region of the fluid.

$$\Gamma = \oint \underleftarrow{v} \cdot \underleftarrow{dl} \quad \textbf{(D-16)}$$

Using Strokes' theorem, this is also

$$\Gamma = \iint_A \nabla x \underset{\leftarrow}{v} \cdot \underset{\leftarrow}{ds} \quad \textbf{(D-17)}$$

$$\underset{\leftarrow}{ds} = \underset{\leftarrow}{n} \cdot ds \quad \textbf{(D-18)}$$

where $\underset{\leftarrow}{ds}$ is a vector normal to the enclosed region with a magnitude, *ds*, of the elemental area, as show in Figure D-3.

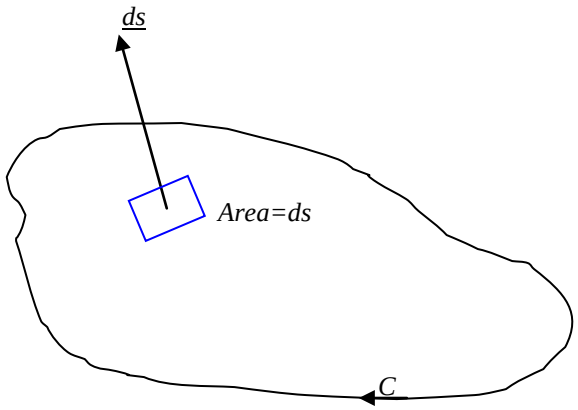

Figure D-3, Circulation of fluid in an enclosed area (Source: Post, D. [74])

Substituting equation (D-12) into (D-17), and with equation (D-13), (D-14) and (D-15)

$$\oint \underset{\leftarrow}{v} \cdot dl = \oint u dx + v dy + w dz \quad \textbf{(D-19)}$$

$$\oint \underset{\leftarrow}{v} \cdot dl = \iint \left[\frac{\partial v}{\partial x} - \frac{\partial u}{\partial y}\right] dxdy + \iint \left[\frac{\partial w}{\partial y} - \frac{\partial v}{\partial z}\right] dydz + \iint \left[\frac{\partial u}{\partial z} - \frac{\partial w}{\partial x}\right] dxdz \quad \textbf{(D-20)}$$

$$\oint \underset{\leftarrow}{v} \cdot dl = \iint 2w_z dxdy + \iint 2w_x dydz + \iint 2w_y dzdx \quad \textbf{(D-21)}$$

The vorticity vector is defined as

$$\underset{\leftarrow}{G} = 2\underset{\leftarrow}{\omega} \quad \textbf{(D-22)}$$

$$\Delta\Gamma = G_n \Delta s \quad \textbf{(D-23)}$$

where G_n is the vorticity vector component normal to the surface element *ds* as shown in Figure D-3. Since the flux of vorticity through the given surface of interest is equal to the circulation along the core enclosing the surface. From equations (D-13), (D-14) and (D-15),

$$G_x = \frac{\partial w}{\partial y} - \frac{\partial v}{\partial z} \quad \textbf{(D-24)}$$

$$G_y = \frac{\partial u}{\partial z} - \frac{\partial w}{\partial x} \quad \textbf{(D-25)}$$

$$G_z = \frac{\partial v}{\partial x} - \frac{\partial u}{\partial y} \quad \textbf{(D-26)}$$

Hence,

$$\frac{\partial G_x}{\partial x} + \frac{\partial G_y}{\partial y} + \frac{\partial G_z}{\partial z} = 0 \quad \textbf{(D-27)}$$

$$\nabla \cdot \underleftarrow{G} = 0 \quad \textbf{(D-28)}$$

Therefore, by the divergence theorem, this is often referred to as the principle of the conservation of vorticity.

$$\iiint_V \nabla \cdot \underleftarrow{G} dv = \iint_s \underleftarrow{G} \cdot \underleftarrow{ds} = 0 \quad \textbf{(D-29)}$$

Assuming the tangential line to the local vorticity vector is a vortex line, and a vortex tube is a surface made up of the vortex lines, the component of the vorticity vector normal to the vortex tube G_z, is zero **[74]**. Therefore, there is no vorticity flux through the surface of a vortex tube. Hence for any cross-section of an elementary vortex tube with uniformly distributed vorticity,

$$\Gamma = G_n s = const \quad \textbf{(D-30)}$$

Since no vorticity can leave the vortex tube, the product of the angular velocity and the area of the vortex tube remain constant along the vortex tube. By substituting equation (D-22), hence

$$\omega_n \cdot s = const \quad \textbf{(D-31)}$$

In a rotational fluid, if the vorticity is due to potential vortex motion, only a single line may exist along the centre of the potential vortices within an infinite set of vortex lines. The vortex tube cannot begin or end inside a fluid which is shown by equation (D-30); therefore a

vortex filament must start and end at the boundaries of the fluid, or close into a ring, or extend to infinity **[74]**.

D-1.4 The Generalised Bernoulli Equation

Assuming the flow is irrotational, Bernoulli's equation can be applied between any two points in the flow that are not necessarily along the same streamline. Furthermore, assuming the fluid is inviscid, there will be no shear stress acting and only the surface stress will be due to pressure. Therefore, for an incompressible fluid, the Navier-Strokes equation (D-6) can then reduced to

$$\frac{\partial u}{\partial t} + u\frac{\partial u}{\partial x} + v\frac{\partial u}{\partial y} + w\frac{\partial u}{\partial z} = B_x - \frac{1}{\rho}\frac{\partial P}{\partial z} \qquad \textbf{(D-32)}$$

Assuming the flow is irrotational, then with equation (D-13), (D-14), and (D-15) substituted into (D-32), hence, for steady flow,

$$\frac{\partial}{\partial x}(\frac{1}{2}u^2 + \frac{1}{2}v^2 + \frac{1}{2}w^2) = B - \frac{1}{\rho}\frac{\partial P}{\partial x} \qquad \textbf{(D-33)}$$

Let $B_x = gh$, then

$$\frac{\partial}{\partial x}(\frac{1}{2}|\underset{\leftarrow}{v}|^2 + \frac{P}{\rho} + gh) = 0 \qquad \textbf{(D-34)}$$

$$\frac{1}{2}|\underset{\leftarrow}{v}|^2 + \frac{P}{\rho} + gh = const \qquad \textbf{(D-35)}$$

D-1.5 Incompressible Potential Flow, Stream Function & Complex Potential

For irrotational flow, a sufficient and necessary condition which will be explained later on, are required to represent the velocity vector field as a scalar potential function φ. Mathematically, if

$$\nabla x \underset{\leftarrow}{v} = 0 \qquad \textbf{(D-36)}$$

$$\underset{\leftarrow}{v} = \nabla\varphi \qquad \textbf{(D-37)}$$

and for

$$\underset{\leftarrow}{G} = \underset{\leftarrow}{w} = 0 \quad \textbf{(D-38)}$$

$$u = \frac{\partial \varphi}{\partial x} \quad \textbf{(D-39)}$$

$$v = \frac{\partial \varphi}{\partial y} \quad \textbf{(D-40)}$$

$$w = \frac{\partial \varphi}{\partial z} \quad \textbf{(D-41)}$$

only in the absence of shear stress, is potential or irrotational flow possible. Hence if the above condition holds, $d\varphi$ is an exact differential and hence the integral

$$\int_1^2 \underset{\leftarrow}{v} dl = \int_1^{22} u dx + v dy + w dz = \int_1^2 d\varphi = \varphi_2 - \varphi_1 \quad \textbf{(D-42)}$$

Equation (D-42) can be seen to be independent of the path joining the two points. Assuming continuity as equation (D-3), φ is a solution to Laplace's equation,

$$\nabla \cdot \underset{\leftarrow}{v} = 0 \quad \textbf{(D-43)}$$

$$\frac{\partial^2 \varphi}{\partial x^2} + \frac{\partial^2 \varphi}{\partial y^2} + \frac{\partial^2 \varphi}{\partial z^2} = \nabla^2 \varphi = 0 \quad \textbf{(D-44)}$$

The contour C surrounds must be a singularity, hence equation (D-16) become

$$\oint_C \underset{\leftarrow}{v} \cdot dl = 0 \quad \textbf{(D-45)}$$

and the scalar potential, $\underline{v}$ can be described in the spherical polar coordinates as follow,

$$v_r = \frac{\partial \varphi}{\partial r} \quad \textbf{(D-46)}$$

$$v_\theta = \frac{\partial \varphi}{\partial \theta} \quad \textbf{(D-47)}$$

$$v_\psi = \frac{\partial \varphi}{r \sin \psi} \frac{\partial \varphi}{\partial \psi} \quad \textbf{(D-48)}$$

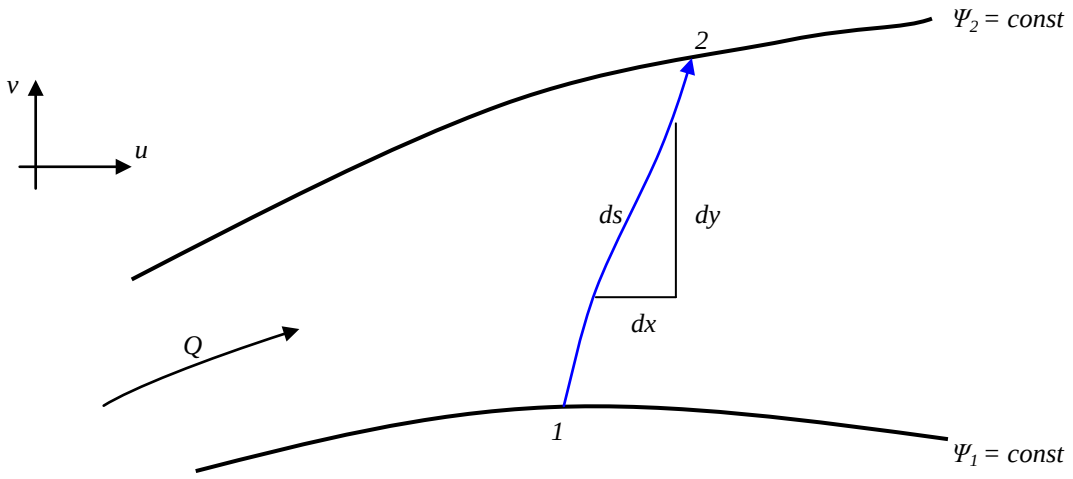

Figure D-4, 2-D Flow across streamlines (Source: Post, D. [74])

For any 2-D flow regardless of the flow condition, a stream function ψ can be used to define it. Hence, the flowrate between the streamlines is equal to the numerical difference between two streamlines. Since the flow can cross a streamline, as shown in Figure D-4, the total flow is therefore

$$dQ = \underset{\leftarrow}{v} \cdot \underset{\leftarrow}{n} ds = udy - vdx \quad \textbf{(D-49)}$$

$$Q_{12} = \int_C udy - vdx \quad \textbf{(D-50)}$$

Substitute (D-38) and (D-39) into (D-48), with minor corrections on the sign convention, then

$$Q_{12} = \int_1^2 d\psi = \psi_2 - \psi_1 \quad \textbf{(D-51)}$$

which is independent of the flow path C, hence expressed in the polar coordinates,

$$v_r = \frac{1}{r}\frac{\partial \psi}{\partial \theta} \quad \textbf{(D-52)}$$

$$v_\theta = -\frac{\partial \psi}{\partial r} \quad \textbf{(D-53)}$$

Equations (D-37), (D-39) and (D-40) are the Cauchy-Riemann conditions, and are sufficient and necessary for a complex function to be analytic (i.e., differentiable over the domain except perhaps at a few singular points) and thus they can represent the real and imaginary

parts of a complex variable [xx]. Hence, for two real valued functions $\varphi(x,y)$ and $\psi(x,y)$ of two real variables x and y have continuous first derivatives that satisfy the Cauchy-Riemann equations in the domain D, then the complex function is,

$$F(z) = \varphi(x, y) + i\psi(x, y) \quad \textbf{(D-54)}$$

where $z = x + iy$. Moreover, the real and imaginary part of a complex function that is analytic in D is the solutions of Laplace's equation, which can be easily proved as follows:

$$\frac{\partial u}{\partial x} = \frac{\partial^2 \varphi}{\partial x^2} = \frac{\partial^2 \psi}{\partial x \partial y} \quad \textbf{(D-55)}$$

$$\frac{\partial v}{\partial y} = \frac{\partial^2 \varphi}{\partial y^2} = -\frac{\partial^2 \psi}{\partial x \partial y} \quad \textbf{(D-56)}$$

From equations (D-55) and (D-56), then

$$\frac{\partial^2 \varphi}{\partial x^2} + \frac{\partial^2 \varphi}{\partial y^2} = \frac{\partial^2 \psi}{\partial x^2} - \frac{\partial^2 \psi}{\partial y^2} = 0 \quad \textbf{(D-57)}$$

Two important Cauchy's theorems used in Complex analysis are listed below,

(1) $\oint_C f(z)dz = 0$, Cauchy's Integral Theory. **(D-58)**

(2) $\oint_C \frac{f(z)}{z - z_0} dz = 2\pi i f(z_o)$, Cauchy's Integral Formula. **(D-59)**

The complex velocity is derived from

$$\frac{dF}{dz} = \frac{\partial \varphi}{\partial x} + i\frac{\partial \psi}{\partial x} = u - iv \quad \textbf{(D-60)}$$

for the limit $\Delta y \rightarrow 0$ and then $\Delta x \rightarrow 0$, and

$$\frac{dF}{dz} = \frac{\partial \psi}{\partial y} - i\frac{\partial \varphi}{\partial y} = u - iv \quad \textbf{(D-61)}$$

for the limit $\Delta x \rightarrow 0$.

Since both (D-60) and (D-61) satisfy the Cauchy-Riemann equations, and let the complex velocity be,

$$\frac{d\overline{F}}{dz} = u + iv \qquad \textbf{(D-62)}$$

Hence,

$$\frac{dF}{dz} \cdot \frac{d\overline{F}}{dz} = (u - iv)(u + iv) = u^2 + v^2 \qquad \textbf{(D-63)}$$

$$|v|^2 = \left|\frac{dF}{dz}\right|^2 \qquad \textbf{(D-64)}$$

With $|v|^2$ determined, the generalised Bernoulli equation can then be used to obtain the pressure in the flow.

D-1.6 Variation of Velocity in Vortex Flow

The Free Vortex region is considered in the variation of velocity in vortex motion. As shown in Figure D-5, consider a thin shell of air distance *r* away from the centre of rotation.

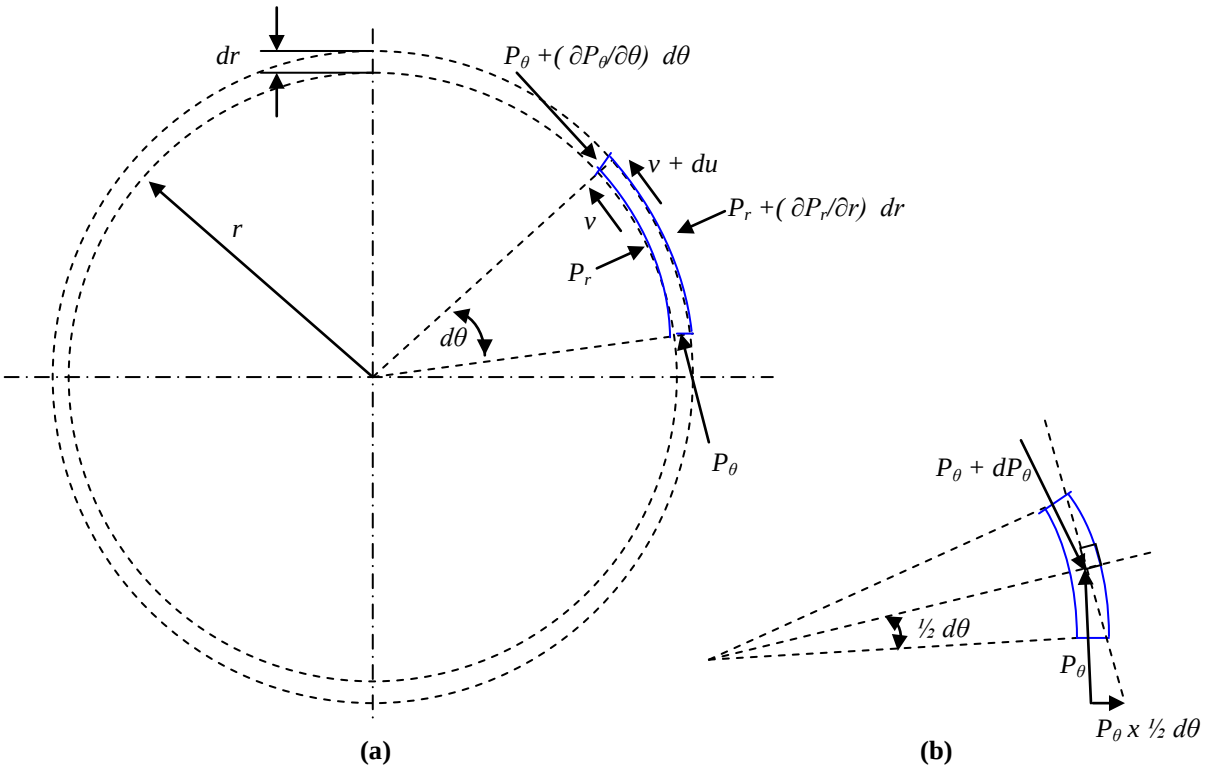

Figure D-5, Pressure in a free vortex, (a) at the distance *r* away from centre, (b) very small θ (Source: Post, D. [74])

Assuming that the flow condition depends only on *r*, then

$$\frac{\partial P_\theta}{\partial \theta} = 0 \qquad \textbf{(D-65)}$$

and assuming the average of the radial pressure P_r and $P_r + dP_r$ as the tangential pressure acting over the width *dr*, then

$$P_\theta = P_r + \frac{1}{2} dP_r \qquad \textbf{(D-66)}$$

Hence, for steady circulation, the radial forces balance is,

$$\sum F = P \cdot r d\theta - (P + dP)(r + dr)d\theta + 2(P + \frac{1}{2} dP) Sin \frac{d\theta}{2} dr = ma \qquad \textbf{(D-67)}$$

For small θ, sin θ = θ, hence

$$r dP d\theta - \frac{1}{2} dP dr d\theta = ma \qquad \textbf{(D-68)}$$

The centripetal acceleration of the fluid at steady circulation is

$$a = \frac{v^2}{r} \qquad \textbf{(D-69)}$$

The mass of the fluid element is

$$m = \rho\, r\, dr\, d\theta \qquad \textbf{(D-70)}$$

hence (D-65) can then be reduced to

$$dP(r - \frac{1}{2} dr)d\theta = (\rho r dr d\theta) \frac{v^2}{r} \qquad \textbf{(D-71)}$$

Assume ½ *dr* is negligible, then (D-71) is reduced to

$$r\,dP = \rho\, v^2\, dr \qquad \textbf{(D-72)}$$

From Bernoulli's equation, for an incompressible flow

$$P + \frac{1}{2}\rho v^2 = P + dP + \frac{1}{2}\rho(v + dv)^2 = P + dP + \frac{1}{2}\rho(v^2 + 2v\,dv + dv^2) \qquad \textbf{(D-73)}$$

which gives

$$dP = -\rho\, v\, dv \qquad \textbf{(D-74)}$$

and hence,

$$r\,dP = \rho\, v^2\, dr = -r\,\rho\, v\, dv$$
$$v\, dr + r\, dv = 0 \qquad \textbf{(D-75)}$$

Therefore, for a free vortex,

$$vr = const = C$$
$$v = \frac{C}{r} \qquad \textbf{(D-76)}$$

Since there is a singularity at the origin, therefore it is assumed that the air within the core rotates as a solid cylinder rotating at a uniform angular velocity. Hence the velocity profile of the simplified vortex can be seen as in Figure D-6.

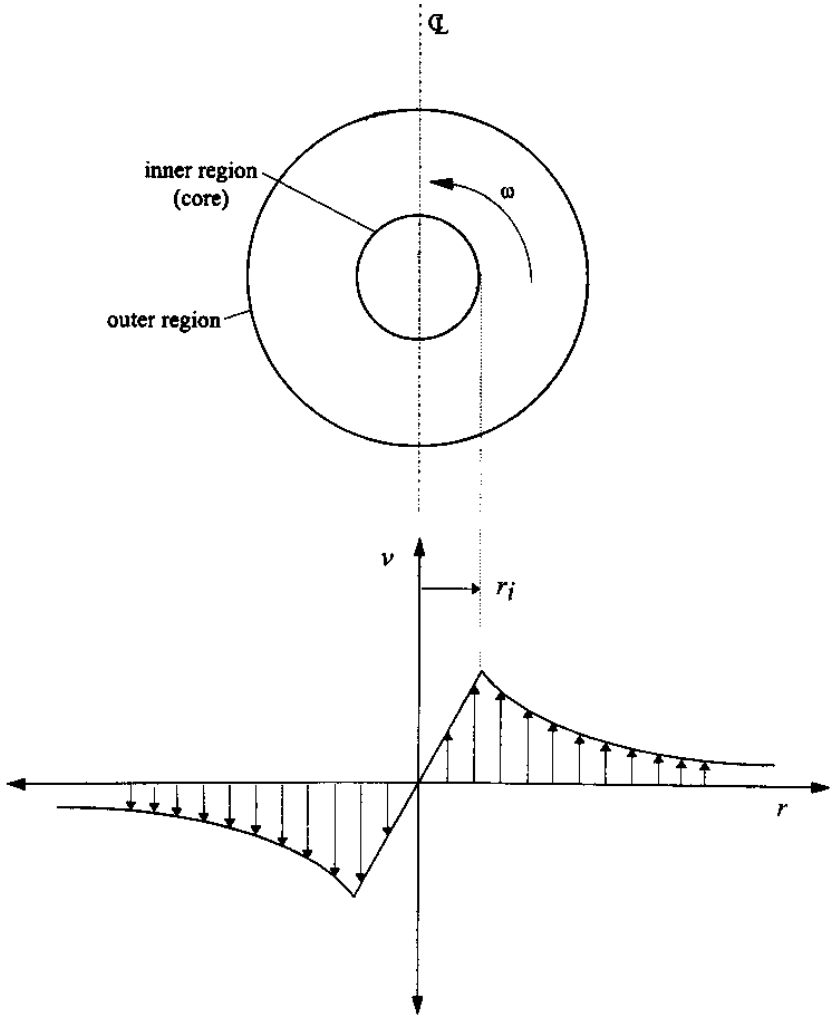

Figure D-6, Typical velocity distribution in a simplified vortex (Source: Patel, R. [72])

D-2 Vortex Motion

D-2.1 Free Vortex

From **Post, D. [74]**, in a free vortex, from equation (D-76),

$$v_r = 0 \tag{D-77}$$

$$v_\theta \propto \frac{1}{r} = \frac{1}{r}\frac{\partial \varphi}{\partial \theta} = \frac{C}{r} \tag{D-78}$$

From **Post, D. [74]**, for Cauchy's Integral Theorem and equation (D-45) considering the complex velocity, the circulation about any contours which do not enclose the origin is

$$\Gamma = \oint_{C_1} \underset{\leftarrow}{v} \cdot dl$$

$$\Gamma = \sum \oint_{C_i} v_\theta dl = \sum \oint_{C_i} v_\theta dl$$

$$\Gamma = \sum \oint_{C_i} v_{\theta_2} r_2 d\theta - v_{\theta_1} r_1 d\theta = \sum \oint_{C_i} \left(\frac{C}{r_2} r_2 - \frac{C}{r_1} r_1\right) = 0 \tag{D-79}$$

Hence, for a contour that encloses the origin (where there is a singularity)

$$\Gamma = \oint_C v_\theta dl = \int_0^{2\pi} v_\theta r d\theta = \int_0^{2\pi} C d\theta$$

$$\Gamma = 2\pi C \tag{D-80}$$

However,

$$\oint \underset{\leftarrow}{v} \cdot \underset{\leftarrow\leftarrow}{ds} = \iint \underset{\leftarrow}{G} \cdot \underset{\leftarrow\leftarrow}{dA} \tag{D-81}$$

therefore, the vorticity is zero everywhere except at $r = 0$, where it is indeterminate. As from equation (D-78),

$$\varphi = C\theta = \frac{\Gamma}{2\pi}\theta \tag{D-82}$$

where $C = \Gamma / 2\pi$ is called the strength of the vortex.

The complex potential of a free vortex is

$$F = \frac{i\Gamma}{2\pi}\ln z = \frac{i\Gamma}{2\pi}\ln r l^{i\theta}$$

$$F = \frac{i\Gamma}{2\pi}\left[\ln r + i\theta\right] = -\frac{\Gamma\theta}{2\pi} + \frac{i\Gamma}{2\pi}\ln r \qquad \textbf{(D-83)}$$

Hence,

$$\varphi = -\frac{\Gamma\theta}{2\pi} \qquad \textbf{(D-84)}$$

$$\psi = \frac{\Gamma}{2\pi}\ln r \qquad \textbf{(D-85)}$$

$$\left|\underset{\leftarrow}{v}\right|^2 = \left|\frac{dF}{dz}\right|^2 = \left|\frac{i\Gamma}{2\pi z}\right|^2 = \left\{\left|\frac{i\Gamma}{2\pi}\right|\left|\frac{1}{z}\right|\right\}^2 = \left(\frac{\Gamma}{2\pi r}\right)^2 \qquad \textbf{(D-86)}$$

Since the flow is irrotational, therefore the Bernoulli's equation (D-35) can be applied, and hence,

$$P = \frac{1}{2}\rho v^2 = P_o$$

$$P = P_o - \frac{1}{2}\rho\frac{\Gamma^2}{4\pi^2 r^2} = P_o - \frac{\rho\Gamma^2}{8\pi^2 r^2} \qquad \textbf{(D-87)}$$

D-2.2 Forced Vortex

Figure D-7 shows that the fluid within the forced vortex region was considered as a rigid body, i.e. $v_\theta = \omega r$.

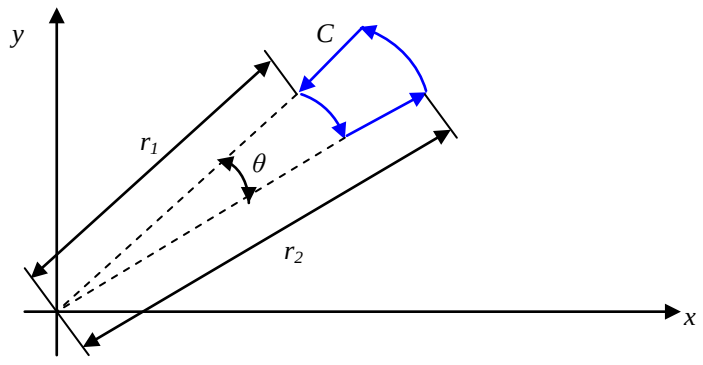

Figure D-7, Element of fluid in forced vortex (Source: Post, D. [74])

and can be expressed as follows,

$$\oint_C \underset{\leftarrow}{v} \cdot \underset{\leftarrow}{ds} = \int (v_{\theta_2} r_2 - v_{\theta_1} r_1) d\theta \quad \textbf{(D-88)}$$

$$\Gamma = \omega\theta(r_2^2 - r_1^2) \quad \textbf{(D-89)}$$

then the area enclosed by the contour is

$$A = \int_{r_1}^{r_2} (\theta r) dr = \frac{\theta}{2}(r_2^2 - r_1^2) \quad \textbf{(D-90)}$$

Substituting equation (D-90) into (D-89), then

$$\Gamma = 2\omega A \quad \textbf{(D-91)}$$

and for

$$\underset{\leftarrow}{G} = G_z \quad \textbf{(D-92)}$$

$$u = -\omega y \quad \textbf{(D-93)}$$

$$v = \omega x \quad \textbf{(D-94)}$$

then from equation (D-22) and (D-26), hence

$$G_z = \frac{\partial v}{\partial x} - \frac{\partial u}{\partial y} = 2\omega \quad \textbf{(D-95)}$$

In a physical vortex such as a tornado, the air circulating in the core in a circular path by due to the effect of the radial pressure gradient in the forced vortex **[73,74]**. Therefore a minimum pressure must be at the centre and increase outward. Hence the velocity must be zero at the centre, which contradicts Bernoulli's equation. For the equilibrium of an element with volume per unit length *V*,

$$V = r\, dr\, d\theta \quad \textbf{(D-96)}$$

The inward force due to the radial pressure gradient on the element is $dP\ (r - \frac{1}{2}\, dr)\, d\theta$, and assuming $\frac{1}{2}\, dr$ is insignificant compared to *r*, then equation (D-68) can be reduced to

$$rdPd\theta = ma \tag{D-97}$$

and for

$$dP = (\frac{\partial P}{\partial r})dr \tag{D-98}$$

$$\omega = \frac{v}{r} \tag{D-99}$$

$$r\omega^2 = \frac{v^2}{r} \tag{D-100}$$

and substitute (D-98) and (D-100)into (D-97)

$$r(\frac{\partial P}{\partial r})drd\theta = \rho rdrd\theta\frac{v^2}{r}$$
$$\frac{dP}{dr} = \rho\omega^2 r$$
$$P = \frac{1}{2}\rho\omega^2 r^2 + C \tag{D-101}$$

With equation (D-87), the pressure on the boundary of the free vortex can determine which is the outer surface of the core, and from this the constant C can then be determined. Let *a* be the distance from the origin to the outer surface of the core, hence from equations (D-101) and (D-87)

$$P_a = P_o - \frac{\Gamma^2\rho}{8\pi^2 a^2} = \frac{1}{2}\rho\omega^2 a^2 + C$$
$$C = P_o - \frac{\rho\Gamma^2}{8\pi^2 a^2} - \frac{1}{2}\rho\omega^2 a^2 \tag{D-102}$$

therefore, inside the core

$$P = P_o - \frac{\rho\Gamma^2}{8\pi^2 a^2} - \frac{1}{2}\rho\omega^2(a^2 - r^2) \tag{D-103}$$

Since $\Gamma = 2\pi rv$ is on or outside of the vortex core, Γ can be evaluated on the core surface from the flow condition within the core, where $r = a$, hence

$$\Gamma = 2\pi a v = 2\pi a(\omega a) = 2\pi\omega a^2 \quad \textbf{(D-104)}$$

$$\omega = \frac{\Gamma}{2\pi a^2} \quad \textbf{(D-105)}$$

Substituted back into (D-103), then

$$P = P_o - \frac{\rho\Gamma^2}{8\pi^2 a^2}\left[2 - (\frac{r}{a})^2\right] \quad \textbf{(D-106)}$$

a minimum occurs at r = 0, i.e.

$$P_{\min} = P_o - \frac{\rho\Gamma^2}{4\pi^2 a^2} \quad \textbf{(D-107)}$$

From Figure D-8, the pressure drop between infinity and the centre of the vortex, half occurs from infinity to the core surface and the other half occurs in the core itself.

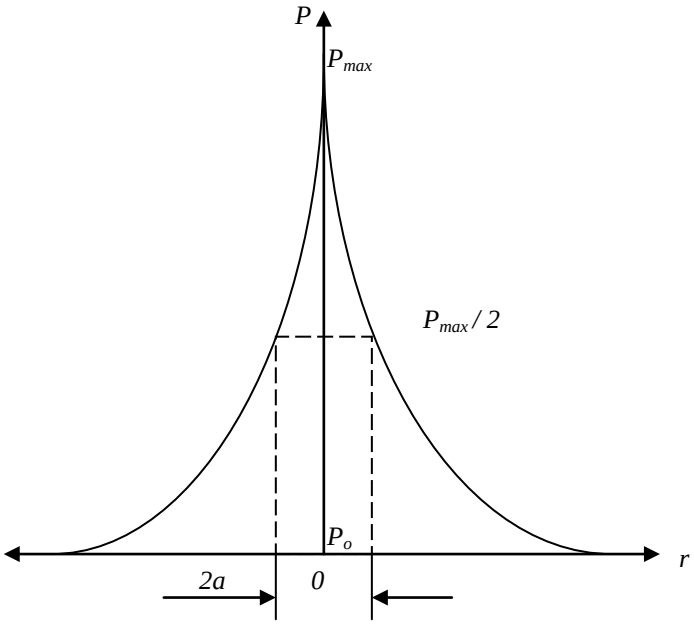

Figure D-8, Pressure distribution across a vortex.

D-3 Lifting Force within a Vortex

From **Lee, C. R. A. [73] and Post, D. [74],** the force acting on a finite particle can be obtained from the findings from pressure distribution in equation (D-106). Consider a particle of radius r_p situated at the foot of the vortex

$$F = \int_0^{r_p} P 2\pi r dr \qquad \textbf{(D-108)}$$

Substituting for *P* from equation (C-106) and

$$F = \int_0^{r_p} (P_o - \frac{\rho\Gamma^2}{4\pi^2 a^2}(2 - (\frac{r}{a})^2))2\pi r dr = P_o \pi r_p^2 - \frac{\rho\Gamma^2 r_p^2}{4\pi a^2} + \frac{\rho\Gamma^2 r_p^4}{16\pi a^4} \qquad \textbf{(D-109)}$$

When the particle is at the point of being lifted by the vortex, from **Post, D. [74]**, the following equality holds.

Force on the lower surface of the particle due to ambient conditions - *Force on upper surface of particle due to vortex* = *Weight of particle.*

Hence,

$$P_o \pi r_p^2 - F = \frac{4}{3}\pi r_p^3 \rho_p g \qquad \textbf{(D-110)}$$

Equating vertical forces on the particle

$$\frac{\rho_p g r_p}{\rho_a \omega_p^2 r_p^2} = \frac{3}{4}(1 - \frac{r_p^2}{4r_i^2})\frac{r_i^2}{r_p^2} \qquad \textbf{(D-111)}$$

APPENDIX E – Process Selection

Process Selection Chart

Swarf Transportation Methods

Sheet 1 of 2

Concept No.	*Functional (geometry, motion, load paths, compatibility, control)*	*Manufacturing, Quality, & Life Cycle (Production, purchase, assembly, waste)*	*Ergonomic, Ecological, & Safety (user, environment, appeal)*	*Feasibility (potential, confidence)*	*Economics & Timing (materials, manufacturing, operational)*	*Information (cooperation, expertise, experience)*	*Comments*	*Score*	*Develop Further*	*Eliminate*	*Get more Information*
P1		+	+		+	+	ADV: simple and easy to use and easy to maintain. DAV: magnetic surrounding ferric base components	**4**	+		
P2		+	+		+	+	ADV: simple and easy to use and easy to maintain. DAV: complete de-magnetise of swarf takes time and may not be successful.	**4**	+		
P3	+	+	+	+	+	+ +	ADV: simple easy construction. DAV: bulky.	**7**	+		
P4	+	+	+	+	+	+ +	ADV: simple easy construction. DAV: bulky.	**7**		+	
P5	+ +	+	+	+	+	+ +	ADV: portable and easy to use. DAV: only allow flow velocity otherwise filter medium may be damaged.	**8**	+		
P6	+ +	+ +		+	+	+ +	ADV: simple and easy to use, and easy to maintain. DAV: hopper swinging when suspended.	**8**		+	
P7	+ +	+ +	+	+	+	+ +	ADV: simple and easy to use, and easy to maintain. DAV: hard to control when rotating over 90°	**9**		+	
P8	+ +	+ +	+ +	+ +	+	+ +	ADV: simple and easy to use, and easy to maintain. DAV: complex analysis.	**11**	+		
P9	+ +	+ +	+ +	+ +	+	+ +	ADV: simple and easy to install. DAV: more complex piping.	**11**	+		
P10	+	-		+	-	+ +	ADV: simple and easy to install. DAV: large torque required high change of gear ratio.	**2**		+	
P11	+ +	+ +	+ +	+ +		+ +	ADV: simple to construct no requirement to lift the hopper. DAV: large area to cover.	**10**	+		

Key: (+) yes + 1, (-) no -1, ( ) neutral 0, (?) insufficient information
ADV: Advantage, DAV: Disadvantage.

Figure E1, Process selection for the various transportation methods.

Process Selection Chart

Swarf Transportation Methods

Sheet 2 of 2

Concept No.	*Functional (geometry, motion, load paths, compatibility, control)*	*Manufacturing, Quality, & Life Cycle (Production, purchase, assembly, waste)*	*Ergonomic, Ecological, & Safety (user, environment, appeal)*	*Feasibility (potential, confidence)*	*Economics & Timing (materials, manufacturing, operational)*	*Information (cooperation, expertise, experience)*	*Comments*	*Score*	*Develop Further*	*Eliminate*	*Get more Information*
P12		+	+	-		-	ADV: deeper penetration of the swarf from the surface. DAV: insufficient knowledge.	**0**		+	
P13	+	-	+	+		+	ADV: simple to construct. DAV: requires large modification on existing equipments.	**3**		+	
P14	+	+ +	+ +	+ +		+	ADV: simple and easy to construct. DAV: bulky and requires long operation time.	**8**	+		
P15	+	+ +	+ +	-	- -	+	ADV: simple to construct. DAV: separation efficiency largely depends on particle size, high wear on equipments.	**3**		+	
P16	+	+ +	+ +		- - -	+	ADV: high separation efficiency can be achieved. DAV: an additional drying process may be required to prevent rusting to occur.	**3**		+	
P17	+	+	+	+		+	ADV: prevent damage on fan unit. DAV: an absolute requirement in pneumatic transportation method.	**5**	+		

Key: (+) yes + 1, (-) no -1, ( ) neutral 0, (?) insufficient information
ADV: Advantage, DAV: Disadvantage.

Figure E2, Concept selection for various transportation methods.

Since for a complete transportation method requires 4 essential steps: lifting (hopper and / or particles), separating, discharging, and filtering, therefore the weighting for the most feasible transportation method will grades base on the summation of best process scored in each steps, as shown in Table E1. However, since for the pneumatic transportation method, there is an additional filtering process required to prevent damage on fan unit, therefore the score for the additional process will not be considered in the weighting.

Table E1, Overall weighting of various transportation methods.

Steps	**Transportation Method**		
	Electromagnetic	Mechanical	Pneumatic
Lifting	4	11	10
Separating	4	11	8
Discharging	7	7	7
Filtering	8	8	8
Total Score	23	37	33

APPENDIX F – Concept Selection

Concept Selection Chart

Sub-System 1&2: Lifting / Rotating & Interlock Mechanism

Sheet 1 of 1

Concept No.	*Functional (geometry, motion, load paths, compatibility, control)*	*Manufacturing, Quality, & Life Cycle (Production, purchase, assembly, waste)*	*Ergonomic, Ecological, & Safety (user, environment, appeal)*	*Feasibility (potential, confidence)*	*Economics & Timing (materials, manufacturing, operational)*	*Information (cooperation, expertise, experience)*	*Comments*	*Score*	*Develop Further*	*Eliminate*	*Get more Information*
A1	+	-	-	+	+	+	ADV: very low manufacturing cost. DAV: poor utilisation of factory facility, and man power. Note: this was the original process within the company.	**2**		+	
A2	+	+ +	-	+	+	+	ADV: low manufacturing cost and easy to use. DAV: swinging motion occur when suspended in air.	**5**		+	
B1	+	+		+ +	+	+ +	ADV: easy to manufacture and operate. DAV: safety concern associate with the access area.	**7**		+	
B2	+		+	+	+	+ +	ADV: kept the load away from the possible access area. DAV: complex hydraulic control, and manufacturing difficulty.	**6**			+
B3	+	+		+ +		+ +	ADV: easy to manufacture and operate. DAV: safety concern associate with the access area.	**6**		+	
C1	+	+ +	+ +	+ +	+	+ +	ADV: kept the load away from the possible access area. DAV: additional load on structure due to deflection.	**10**	+		
C2	+	+ +	+ +	+ +		+ +	ADV: kept the load away from the possible access area. DAV: additional load on structure due to deflection.	**9**		+	
D1			+	+		+	ADV: simple spring control mechanism. DAV: poor control and feedback, high machining cost involves	**3**		+	
D2		+ +	+	+	+ +	+	ADV: simple solenoid control mechanism, easy construction. DAV: insufficient feedback to indicates the status.	**7**		+	
D3	+ +	+ +	+ +	+	+	+	ADV: multi-stage feed and control ensure high safety requirement has reached. DAV: high material cost.	**9**	+		
E1	+	+ +	+ +	+ +	+ +	+	ADV: simple construction and easy adjustment. DAV: damage may occur due to heavy impacts.	**10**	+		

Key: (+) yes + 1, (-) no -1, ( ) neutral 0, (?) insufficient information
ADV: Advantage, DAV: Disadvantage.

Figure F1, Concept selection for the lifting / rotating & interlock mechanism.

Concept Selection Chart

Sub-System 3,4, & 5: Lid, Lid Lock, Discharge Control Valve, & Filter Mechanism

Sheet 1 of 1

Concept No.	*Functional (geometry, motion, load paths, compatibility, control)*	*Manufacturing, Quality, & Life Cycle (Production, purchase, assembly, waste)*	*Ergonomic, Ecological, & Safety (user, environment, appeal)*	*Feasibility (potential, confidence)*	*Economics & Timing (materials, manufacturing, operational)*	*Information (cooperation, expertise, experience)*	*Comments*	*Score*	*Develop Further*	*Eliminate*	*Get more Information*
F1		+	+	+	+	+ +	ADV: simple construction. DAV: bulky, hard to keep the thickness down which might interfere with other structures.	**6**		+	
F2	-	+	+	+	+	+ +	ADV: simple construction, very robust. DAV: structure interferences may occur.	**5**		+	
F3	+	+	+	+	+	+ +	ADV: simple construction, very robust DAV: smaller area available to create an opening tube connection.	**7**	+		
G1	+	+	+	+	+	+ +	ADV: simple and easy to operates DAV: requires additional tools to operate.	**7**		+	
G2	+	+	+ +	+	+	+ +	ADV: simple and easy to operate DAV: bulky.	**8**	+		
H1	+	+	+	+	+	+	ADV: easy to control DAV: possible damage on pneumatic actuator, and leakage.	**6**		+	
H2		+	+		+	+	ADV: good valve mechanism protection DAV: possible blockage in the retraction stroke.	**4**		+	
H3	+ +	+	+	+ +	+	+	ADV: easy to control DAV: possible damage on pneumatic actuator.	**8**	+		
I1	+	+ +	+	+ +	+	+ +	ADV: large settlement space. DAV: bulky.	**9**		+	
I2	+ +	+	+ +	+ +	+	+ +	ADV: small compact size. DAV: more machining requires.	**10**	+		

Key: (+) yes + 1, (-) no -1, ( ) neutral 0, (?) insufficient information
ADV: Advantage, DAV: Disadvantage.

Figure F2, Concept selection for lid, lid lock, control valve and filter mechanism.

Conceptual design work sheet

The transportation mechanism

Requirements	Contributing Factors	Current Status: Good	Current Status: Marginal	Current Status: Poor	Required Action: Proceed	Required Action: Revise	Required Action: N/A
Functional	Overall geometry	■	□	□	■	□	□
	Motion of parts	■	□	□	■	□	□
	Forces involved	■	□	□	■	□	□
	Energy needed	■	□	□	■	□	□
	Materials to be used	□	□	□	□	□	■
	Control system	□	□	□	□	□	■
	Information flow	□	□	□	□	□	■
Safety	Operational	■	□	□	■	□	□
	Human	■	□	□	■	□	□
	Environmental	■	□	□	■	□	□
Quality	Quality assurance	□	■	□	■	□	□
	Quality control	□	■	□	■	□	□
	Reliability	■	□	□	■	□	□
Manufacturing	Production of components	□	■	□	■	□	□
	Purchases of components	■	□	□	■	□	□
	Assembly	□	■	□	■	□	□
	Transport	□	■	□	■	□	□
Timing	Design schedule	□	■	□	■	□	□
	Development schedule	□	■	□	■	□	□
	Production schedule	□	□	■	□	■	□
	Delivery schedule	□	□	■	□	■	□
Economic	Marketing costs	□	□	□	□	□	■
	Design costs	□	□	□	□	□	■
	Development costs	□	■	□	■	□	□
	Manufacturing costs	□	■	□	■	□	□
	Distribution costs	□	□	□	□	□	■
Ergonomic	User needs	□	■	□	■	□	□
	Ergonomic design	□	■	□	■	□	□
	Cybernetic design	□	□	■	□	■	□
Ecological	Material selection	■	□	□	■	□	□
	Working fluid selection	■	□	□	■	□	□
Aesthetic	Customer appeal	□	■	□	■	□	□
	Fashion	□	□	□	□	□	■
	Future expectation	□	□	□	□	□	■
Life cycle	Distribution	□	□	□	□	□	■
	Operation	□	■	□	■	□	□
	Maintenance	■	□	□	■	□	□
	Disposal	□	□	□	□	□	■

Figure F3, Conceptual design worksheet for the transportation system design, (Source: Hales, C. [88])

Embodiment design work sheet

The transportation mechanism

Requirements	Contributing Factors	Current Status					Required Action		
		Good		Marginal		Poor	Proceed	Revise	N/A
Functional	Overall geometry	■	□	□	□	□	■	□	□
	Motion of parts	■	□	□	□	□	■	□	□
	Forces involved	■	□	□	□	□	■	□	□
	Energy needed	■	□	□	□	□	■	□	□
	Materials to be used	■	□	□	□	□	■	□	□
	Control system	□	■	□	□	□	■	□	□
	Information flow	□	■	□	□	□	■	□	□
Safety	Operational	■	□	□	□	□	■	□	□
	Human	■	□	□	□	□	■	□	□
	Environmental	□	□	□	□	□	□	□	■
Quality	Quality assurance	■	□	□	□	□	■	□	□
	Quality control	■	□	□	□	□	■	□	□
	Reliability	■	□	□	□	□	■	□	□
Manufacturing	Production of components	□	■	□	□	□	■	□	□
	Purchases of components	■	□	□	□	□	■	□	□
	Assembly	■	□	□	□	□	■	□	□
	Transport	■	□	□	□	□	■	□	□
Timing	Design schedule	■	□	□	□	□	■	□	□
	Development schedule	■	□	□	□	□	■	□	□
	Production schedule	□	■	□	□	□	■	□	□
	Delivery schedule	□	■	□	□	□	■	□	□
Economic	Marketing costs	□	□	□	□	□	□	□	■
	Design costs	□	□	□	□	□	□	□	■
	Development costs	■	□	□	□	□	■	□	□
	Manufacturing costs	■	□	□	□	□	■	□	□
	Distribution costs	□	□	□	□	□	□	□	■
Ergonomic	User needs	■	□	□	□	□	■	□	□
	Ergonomic design	■	□	□	□	□	■	□	□
	Cybernetic design	□	■	□	□	□	■	□	□
Ecological	Material selection	■	□	□	□	□	■	□	□
	Working fluid selection	■	□	□	□	□	■	□	□
Aesthetic	Customer appeal	■	□	□	□	□	■	□	□
	Fashion	□	□	□	□	□	□	□	■
	Future expectation	□	□	□	□	□	□	□	■
Life cycle	Distribution	□	□	□	□	□	□	□	■
	Operation	■	□	□	□	□	■	□	□
	Maintenance	■	□	□	□	□	■	□	□
	Disposal	■	□	□	□	□	■	□	□

Figure F4, Embodiment design worksheet for the transportation system design, (Source: Hales, C. [88])

Detail design work sheet

The transportation mechanism

Requirements	Contributing Factors	Current Status					Required Action		
		Good		Marginal		Poor	Proceed	Revise	N/A
Functional	Overall geometry	■	□	□	□	□	□	□	■
	Motion of parts	■	□	□	□	□	□	□	■
	Forces involved	■	□	□	□	□	□	□	■
	Energy needed	■	□	□	□	□	□	□	■
	Materials to be used	■	□	□	□	□	□	□	■
	Control system	■	□	□	□	□	□	□	■
	Information flow	■	□	□	□	□	□	□	■
Safety	Operational	■	□	□	□	□	□	□	■
	Human	■	□	□	□	□	□	□	■
	Environmental	□	□	□	□	□	□	□	■
Quality	Quality assurance	■	□	□	□	□	□	□	■
	Quality control	■	□	□	□	□	□	□	■
	Reliability	■	□	□	□	□	□	□	■
Manufacturing	Production of components	■	□	□	□	□	□	□	■
	Purchases of components	■	□	□	□	□	□	□	■
	Assembly	■	□	□	□	□	□	□	■
	Transport	■	□	□	□	□	□	□	■
Timing	Design schedule	■	□	□	□	□	□	□	■
	Development schedule	■	□	□	□	□	□	□	■
	Production schedule	□	□	□	□	□	□	□	■
	Delivery schedule	□	□	□	□	□	□	□	■
Economic	Marketing costs	□	□	□	□	□	□	□	■
	Design costs	■	□	□	□	□	□	□	■
	Development costs	■	□	□	□	□	□	□	■
	Manufacturing costs	□	□	□	□	□	□	□	■
	Distribution costs	□	□	□	□	□	□	□	■
Ergonomic	User needs	■	□	□	□	□	□	□	■
	Ergonomic design	■	□	□	□	□	□	□	■
	Cybernetic design	□	■	□	□	□	□	□	■
Ecological	Material selection	■	□	□	□	□	□	□	■
	Working fluid selection	■	□	□	□	□	□	□	■
Aesthetic	Customer appeal	■	□	□	□	□	□	□	■
	Fashion	□	□	□	□	□	□	□	■
	Future expectation	□	□	□	□	□	□	□	■
Life cycle	Distribution	□	□	□	□	□	□	□	■
	Operation	■	□	□	□	□	□	□	■
	Maintenance	■	□	□	□	□	□	□	■
	Disposal	■	□	□	□	□	□	□	■

Figure F5, Detail design worksheet for the transportation system design, (Source: Hales, C. [88])

APPENDIX G – Operating Procedure

The hopper is aboard on the trolley after the oil recycling process, and it is required to be manually guided to the transportation system, as shown in Figure G-1.

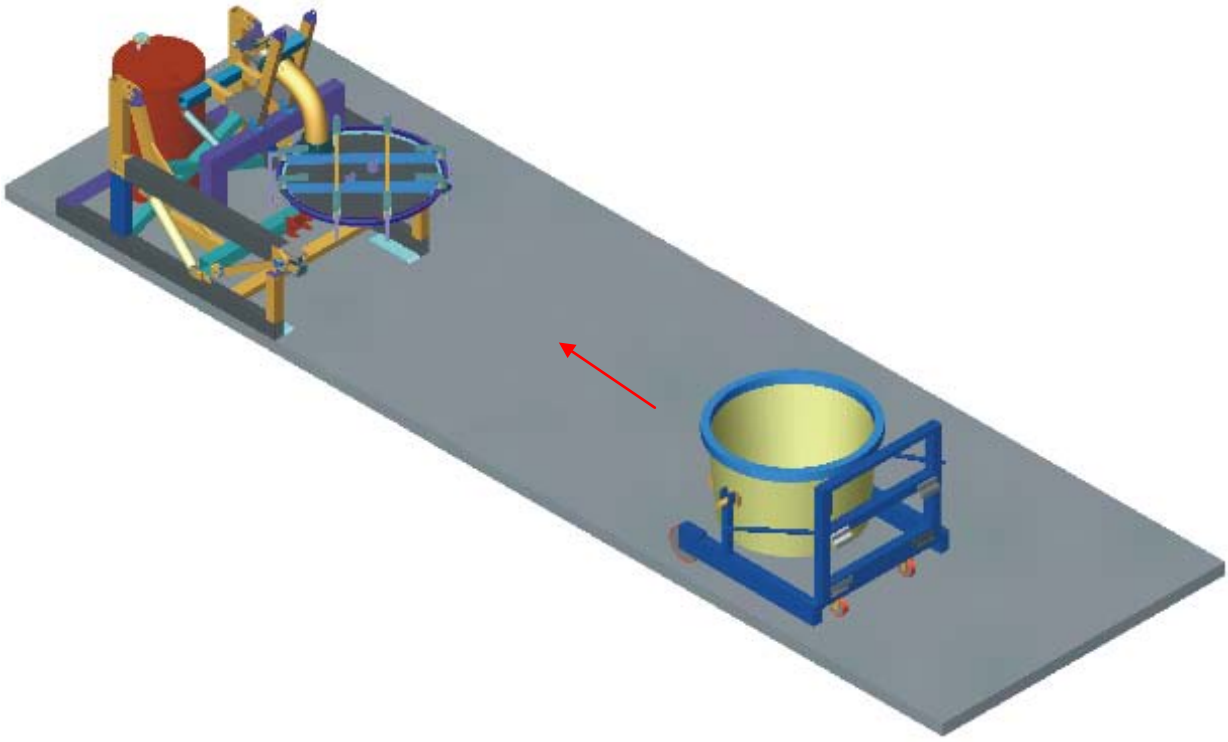

Figure G-1, Hopper aboard on trolley moving towards transportation system

The operating procedures are as follow:

1) Power up the transportation system before the trolley and hopper is engaged. The support rods on the hopper make contacts with the limit switches at different positions as they move through the interlock (Refer to Chapter 5.2).
2) Once the hopper and trolley is in position, the support rods are now well secured by the interlock system, and the hopper lid can then be lowered by operating the 8" hydraulic actuator; however the lid is required to be manually guided to fit onto the hopper.
3) Disengage the chains which is attached on the lid joints, then fully retracts the 8" hydraulic actuator, as shown in Figure G-2.
4) Manually set the lid locks to locking position.
5) Attach the filter onto the outlet hole of the drum, and adjust the support legs to make the filter stand up well.

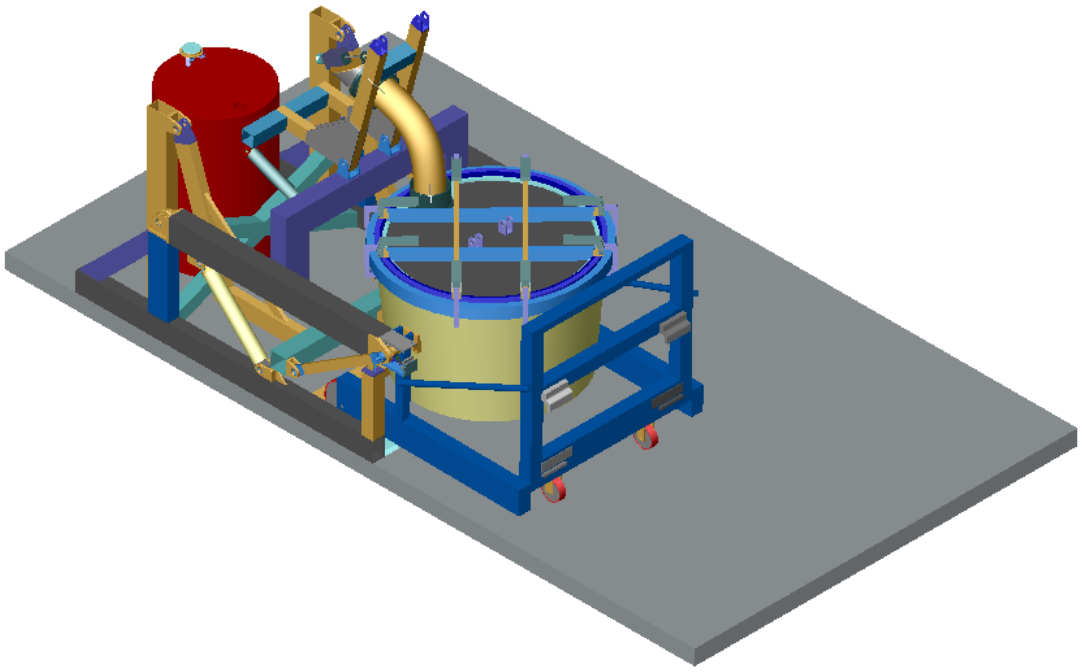

Figure G-2, Hopper engaged into the transportation system with lid attached.

6) Operate the 14” hydraulic actuators to lift the hopper up from the trolley, and the hopper undergoes 135° rotation when the actuator is fully extended, as shown in Figure G-3.

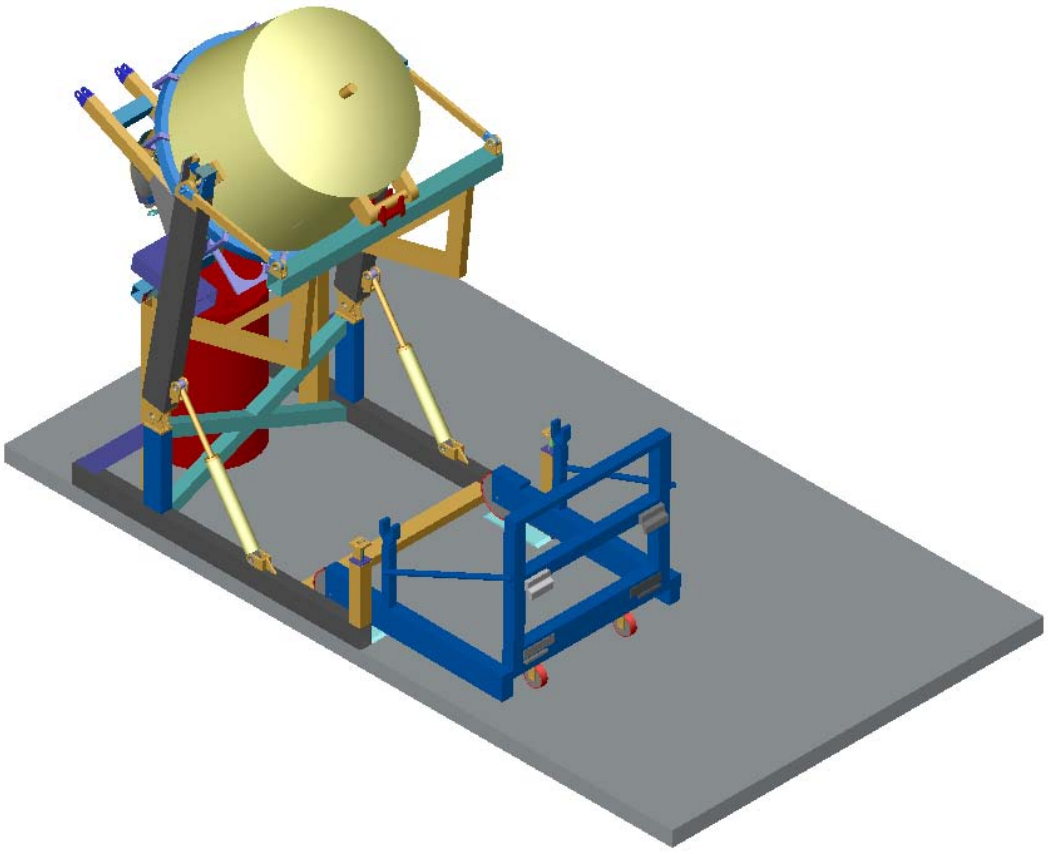

Figure G-3, Hopper rotate 135° when 14” hydraulic actuator is fully extended

6) Manually attach the discharge valve to the inlet port of the barrel, and start the discharging process.
7) Disengage the connection between the valve and inlet port of the barrel when change of barrel takes place. Lower the hopper down slightly and then manually move the barrel out of the loading zone.
8) Reposition the hopper back to discharge position when a new empty barrel is in place.

APPENDIX H – Logic Control System

By combining the flow diagram from Interlock system (Refer to Chapter 5.2), the hydraulic circuit (Refer to Chapter 5.6), and the Pneumatic circuit (Refer to Chapter 5.4), an overall control flow diagram can be formed, as shown in Figure H-1.

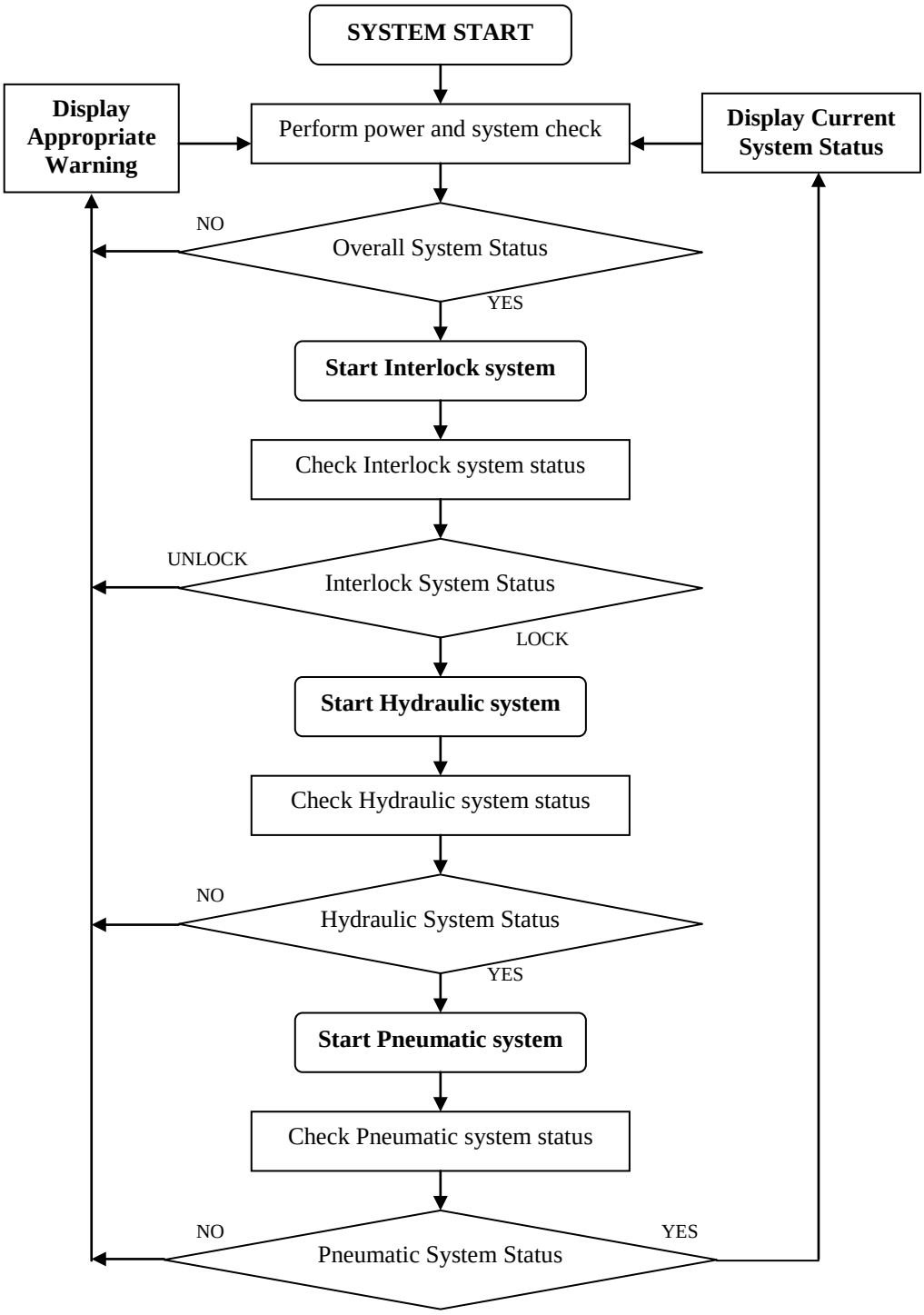

Figure H-1, Logic flow diagram of the overall system

APPENDIX I – Detail Drawing of Test Rig

Appendix I: Detail Drawing of the Test Rig

Appendix I: Detail Drawing of the Test Rig

Appendix I: Detail Drawing of the Test Rig

Appendix I: Detail Drawing of the Test Rig

Appendix I: Detail Drawing of the Test Rig

Appendix I: Detail Drawing of the Test Rig

APPENDIX J – Detail Drawing of Transportation System

ABSTRACT

Patience & Nicholson (NZ) Limited, a Canterbury based drill bits manufacturing company is currently suffering heavy losses of grinding oil from their recycling facility. With the high production rate, approximately 80 tons of waste sludge is produced after the recycling process every year, and 20-30% of the weight of the swarf is the entrapped oil. This waste product from the fluke grinding process is currently discarded. An estimated saving of $40000 can be achieved if this oil can be recovered; then the remaining steel powder can be sold to the material supplier in France. This unnecessary loss of material is why Patience & Nicholson wish to understand the feasibility of the development of a recovery system to recycle the oil and steel from the swarf.

The aim of this work was to develop a transportation system which copes with both the current and new extraction facility. The clean swarf was required to be loaded into 200 gallon barrels. The flow property was determined and the physical limitation from the barrel's entry port was perceived. Several transportation methods were investigated to reduce abrasion during transportation. A transportation method via a multi linkage was selected.

A full scale flow channel was designed and constructed to simulate the discharge from hopper to barrel in the actual system. Formation of lumps and unexpected moisture resulted as flow obstruction from dome formation was experienced in the flow channel. The dried, sieved powder was found to flow well with the currently design. Hence, enlargement of the current design is required to compensate for the unpredictable humidity in the clean swarf after extraction. A direct injection of compressed air can then be implemented for arch destruction at the predicted locations.

ACKNOWLEDGEMENTS

I would like to express my appreciation to a number of people whose support and encouragement made this thesis possible. Firstly, to my supervisor **Dr David R. Aitchison** without whom the opportunity to undertake this project would not have existed. Secondly, to **Dr Shane D. Gooch** AND **Dr S. Ilanko** on the excellent guidance and technical support on my thesis, and **Dr Keith Alexander** for the consultations on the test rig design, while my supervisor is on leave.

Thanks to the workshop staff: **Scott Amies** for the scheduling of the production, **Paul Wells** for the construction and modification of the test rig and manufacturing suggestions, **Ken Brown** for unlimited quick access to all the parts in the storeroom, and **Rodney Elliott** on the purchase of pneumatic components. Thanks to **Kelvin Stobbs** and **Eric Cox** on the suggestion of particle size measurements and the available space for testing. Also, many thanks to **Julian Murphy** and **Julian Phillips** on the expertise and guidance on the selections of sensor and limit switch.

Thanks to the staff in Chemical & Process Engineering (CAPE): **Professor John Abrahamson** for his guidance on the investigation of the cyclone separation, and also Miss **Christine A. Nichol** on both the technical and information support associated with this project.

Thanks to the staff in **Chalston Engineering** for their admirable patience and valuable suggestions when consulted on the details.

Thanks to all the staff in the **Academic Skill Centre: Writing and Study Skills (WASS)**, for their patience and grammatical support.

Thanks to all the friends, **Angelo C. Garcia, Ben Low, Andrew Tsai, Kiki Leung, Eric Hung, Siew King Hung, Angela Chen, Dean Kirk, Hamhum Lin** my room mates **Amanda Batchelor, Allan Saville** for all their support, encouragement and wonderful times during the difficult period.

Finally, to my family, many thanks to my parents both the financial support and encouragement on the research, and also my girl friend, **Biddy O**, for being there for me all the time.

TABLE OF CONTENTS

REFERENCE

A. Extraction Process

1. **Grigor J. E.**, *Solvent Extraction From Steel Swarf Using Hexane*, University of Canterbury, Department of Chemical & Process Engineering, Final Year Project Report 2000.
2. **Fu H., Mathews M. A.**., *Separation Processes for Recovering Alloy Steel From Grinding Sludge: Supercritical Carbon dioxide Extraction and Aqueous Cleaning*, Separation Science and Technology, **V34** n6-7, Apr-May 1999, pp.1411~1427.
3. **Brady, Basil O., Kao, Chien-Ping C., Dooleym, Kerry M., Knopf, Carl F., Gambrell, Robert P.**, *Supercritical Extraction of Toxic Organic From Soils*, Industrial & Engineering Chemistry Research, **V26**, n2, Feb 1987, pp261~268.
4. **Beudoin, Stephen P., Grant, Christine S., Garbonell, Robert G.**, *Removal of Organic Film From Solid Surface Using Aqueous Solution of Nonionic Surfactant I: Experiments*, Industrial & Engineering Chemistry Research, **V34**, n10, Oct 1995, pp3307~3317.
5. **Beudoin, Stephen P., Grant, Christine S., Garbonell, Robert G.**, *Removal of Organic Film From Solid Surface Using Aqueous Solution of Nonionic Surfactant II: Theory*, Industrial & Engineering Chemistry Research, **V34**, n10, Oct, 1995, pp3318~3325.
6. **Gannon, Keith O., Bibring, Peter, Raney Kelvin., Ward, Anthony J., Wilson, David J., Underwood, Julie L., Debelak, Kenneth A.**, *Soil Clean Up by In-situ Surfactant Flushing III – Laboratory Results*, Separation Science and Technology, **V24**, n14, Nov 1989, pp1073~1094.
7. **Underwood, Julie L., Debelak, Kenneth A., Wilson, David J.**, *Soil Clean Up by In-situ Surfactant Flushing VI – Reclamation of Surfactant Recycle*, Separation Science and Technology, **V28**, n9, Jul 1993, pp1647~1669.
8. **Underwood, Julie L., Debelak, Kenneth A., Wilson, David J.**, *Soil Clean Up by In-situ Surfactant Flushing VIII – Reclamation of Multi-component Contaminated Sodium Dodecylsulfate Solution in Surfactant Flushing*, Separation Science and Technology, **V30**, n11, Jun 1995, pp2277~2299.
9. **Clarke, Ann N., Plumb, Patrick D., Subramanyan, T. K., Wilson, David J.**, *Soil Clean Up by Surfactant Washing I – Laboratory Result and Mathematical Modelling*, Separation Science and Technology, **V26**, n3, Mar 1991, pp301~344.

10. **Nichol, C. A.,** *Development of a Prototype Unit for Oil Recovery From Grinding Sludge: a thesis submitted for the degree of Master of Engineering at the Department of Chemical & Process Engineering,* 2003, University of Canterbury.

B. Lubrication, Drill Bits Material, & Manufacturing Process

11. **Moller, U. J., Boor, U.,** *Lubricants in Operation,* , English translation edited by **Landsdown, A. R.**, VDI Verlag, Mechanical Engineering Publications Limited.
12. **Springborn, R. K.**, Cutting and Grinding Fluid: Selection and Application, ASTME (American Society of Tool and Manufacturing Engineers)
13. **Kalpakjian, Serope.,** *Manufacturing Engineering and Technology,* 3rd edition, 1995, Addison-Wesley Publishing Company
14. **Drozda, Tom., Wick, Charles., Benedict, John T., Veilleux, Raymond F., Bakerjian, Ramon., Society of Manufacturing Engineers,** *Tool and Manufacturing Engineers Handbook,* 4th edition, **V1,** 1983, Society of Manufacturing Engineers.
15. **Shaw, Milton Clayton.,** *Principles of Abrasive Processing,* Oxford Series on Advanced manufacturing, **V13,** 1996, Oxford Science Publication.
16. **Benedict, Gary F.,** *Nontraditional Manufacturing Processes,* Manufacturing Engineering and Materials Processing, **V19,** 1987, Dekker
17. **Kalpakjian, Serope., Schmid, Steven R.,** *Manufacturing Engineering and Technology,* 4th edition, 2001, Prentice Hall.
18. **ASM International Handbook Committee,** *ASTM Metal Handbook,* 10th edition, **V1,** 1990, American Society for Metals.

C. Environmental Issues & Waste Management

19. **Neal, A. W.**, *Industrial Waste: its handling, disposal and re-use* 1971, London: Business Books.
20. **Bahu, Richard., Crittenden, Barry., O'Hara, John.**, *Management of Process Industry Waste: an introduction*, 1997, Institution of Chemical Engineers.
21. **Nemerow, Nelson L., Agardy, Frank J.**, *Strategies of Industrial and Hazardous Waste Management*, 1998, Van Nostrand Reinhold, A Divisionof International Thomson Publishing Inc.
22. **Guyer, Howard H.,** *Industrial Processes and Waste Stream Management,* 1998, John Willey & Sons, Inc.
23. **Ministry for the Environment.**, *The 1995 National Landfill Census*, 1997, Ministry for the Environment, New Zealand.

24. **Ministry for the Environment.**, *The 1998/1999 National Landfill Census Report*, 2000, Ministry for the Environment, New Zealand.
25. **Ministry for the Environment.**, *Solid Waste Analysis Protocol*, 2002, Ministry of Environment, New Zealand.
26. **Clancey, D., Canterbury Regional Council (Christichurch, N. Z.). Environmental Management Group,** *Used Oil in Canterbury: Production, Recovery, and Environment Impacts*, 1999, Canterbury Regional Council.

D. Particle Technology & Powder Mechanics

27. **Kearney, T.,** *Solid Flow Experiment Handout,* 2002, Chemical & Process Engineering, University of Canterbury
28. **Allen, Terence.,** *Particle Size Measurement,* **V1,** 1997, Chapmand & Hall.
29. **Allen, Terence.,** *Particle Size Measurement,* **V2,** 1997, Chapmand & Hall.
30. **Cambou, Bernard, and International Centre for Mechanical Sciences**, *Behaviour of Granular Materials*, 1998, Springer Wien New York.
31. **Jenike, Andrew W.,** *Storage and Flow of Solids***,** Bulletin of the University of Utah, **V53**, n26, Nov 1964.
32. **Brown, R. L., Richards, J. C.**, *Principles of Powder Mechanics: essays on packing and flow of powder and bulk solids*, 1970, Pergamon Press.
33. **Arnold, P. C., McLean, A. G., Roberts, A. W.**, *Bulk Solids: Storage, Flow & Handling*, 1978, TUNRA Ltd, the University of Newcastle.
34. **Orr, Clyde, JR**, *Particulate Technology*, 1966, Macmillian New York.
35. **Reisner, W., Eisenhart, Rothe M v.,** *Bins and Bunkers for Handling Bulk Materials: Practical Design and Techniques*, 1971, Trans Tech Publications.
36. **Stepanoff, Alexey J.,** *Gravity Flow of Bulk Solid and Transportation of Solids in Suspension*, 1969, John Wiley & Sons, Inc.
37. **IEA Coal Research.,** *Fundamentals of Bulk Solids Flow***,** 1986, IEA Coal Research, London.
38. **Wassgren, Carl R., Hunt, Melany L., Brennen, Christopher E.,** *Effects of Vertical Vibration on Hopper Flows of Granular Material*, Mechanics of Deformation and Flow of Particulate materials, American Society of Civil Engineers (ASCE), 1997, pp335-348
39. **Weathers, R. C., Hunt, M. L., Brennen, C. E., Lee, A. T., Wassgren, C. R.,** *Effects of Horizontal Vibration on Hopper Flows of Granular Materials*, Mechanics

of Deformation and Flow of Particulate materials, American Society of Civil Engineers (ASCE), 1997, pp349-360

40. **Peschl, I.,** *Principals of Soil Mechanics for the Characterisation of Industrial Powders*, Powder Handling & Processing, **V13**, n1, Jan-Mar, 2001, pp11-18.
41. **Arnold, P. C.,** *Some Observations on the Importance of Particle Size in Bulk Solids Handling*, Powder Handling & Processing, **V13,** n1, Jan-Mar, 2001, pp35-40.
42. **Tejchman, J.,** *Scale Effects in Bulk Solids During Silo Flow***,** Powder Handling & Processing, **V13**, n2, Apr-Jun, 2001, pp165-171.
43. **Peschl, I.,** *Arching and Ratholing in Silos,* Powder Handling & Processing, **V13**, n4, Oct-Dec, 2001, pp357-363.
44. **Jenike, A. W.,** *Quantitative Design of Mass-Flow Bins,* Powder Technology, **V1,** Sep, 1967, pp237-244
45. **Moore, B. A., Arnold, P. C.,** *An Alternative Presentation of the Design Parameters for Mass Flow Hoppers*, Powder Technology, **V42,** 1985, pp79-89
46. **Ducker, J. R., Ducker, M. E., Nedderman, R. M.,** *The Discharge of Granular Materials form Unventilated Hopper,* Powder Technology, **V42,** 1985, pp3-14.
47. **Bradley, M. S., Farnish, R. J., Pittman, A. N., Leaper, M. C.,** *Caking by Moistrue Migration of Bulk Solids – An Investigation of Causes,* IMECHE Conference Transactions: From Bulk Powder to Bulk: International Conference on Powder and Bulk Solids Handling, 2000, Professional Engineering for the Institution of Mechanical Engineers, pp39-44.
48. **Matchett, A. J., Armstrong, B., Peace, J., A Reliable,** *Vibrationally Activated, Mass Flow Hopper System,* IMECHE Conference Transactions: From Bulk Powder to Bulk: International Conference on Powder and Bulk Solids Handling, 2000, Professional Engineering for the Institution of Mechanical Engineers, pp537-544.
49. **Arnold P. C.,** *Some Observations on the Relevance of Flow Properties in the Selection of Bin Dischargers*, IMECHE Conference Transactions: From Bulk Powder to Bulk: International Conference on Powder and Bulk Solids Handling, 2000, Professional Engineering for the Institution of Mechanical Engineers, pp557-566.

E. Separation & Pneumatic Conveying System

50. **Dorman, Richard George.,** *Dust Control and Air Cleaning*, 1974, Pergamon Press.
51. **Batel, Wilhelm.,** *Dust Extraction Technology: Principles, Methods, Measurement Technique,* English translation from the German by **Hardbottle, R.,** 1976, Stonehouse, Glos: Technicopy Ltd.

52. **Sittig, Marshall.,** *Particulates and Fine Dust Removal: Processes and Equipment,* Pollution Technology Review, n34, 1977, Park Ridge.
53. **Storch, Otakar.,** *Industrial separators for Gas Cleaning,* Chemical Engineering Monographs, V6, 1979, Amsterdam: Elsevier.
54. **Ogawa, Akira.,** *Separation of Particles From Air and Gases,* Uniscience Series on Fine Particle Science and Technology, **V1**, 1984, CRC Press
55. **Ogawa, Akira.,** *Separation of Particles From Air and Gases,* Uniscience Series on Fine Particle Science and Technology, **V2,** 1984, CRC Press
56. **Engineering Equipment User Association.,** *Separation of Dust From Gases,* Handbook (Engineering Equipment Users Association) E.E.U.A., n19, 1968, Constable and Company Ltd
57. **Johnes, H. R.,** Find *Dust and Particulates Removal,* Pollution Control Review, n11, 1972, Noyes Data Corp.
58. **Mody, Vinit., Jakjete, Raj.,** *Dust Control Handbook,* Pollution Technology review, n161, 1988, Noyes Data Corp.
59. **Wöhlbier, Reinhard, H.,** *Pneumatic Conveying of Bulk & Powder*, The Best of Bulk Handling 1981-1985, **V D/86,** 1986, Trans Tech publication
60. **Rhodes, M. J.,** *Introduction to Particle Technology,* 1998, John Wiley.
61. **Pery, Robert H., Green, Don W., Mloney, James O.,** *Perry's Chemical Engineers' Handbook,* 7th edition, 1997, McGraw-Hill
62. **Abrahamson, John.,** *Course Handout*, 2002, Chemical & Process Engineering, University of Canterbury.

F. Hydraulic & Pneumatic System Design

63. **Barber, Antony.,** *Pneumatic Handbook,* 8th edition, 1997, Elsvier Science.
64. **Parr, E. A.,** *Hydraulic and Pneumatics: A Technician's and Engineer's Guide,* 2nd edition, 1998, Butterworth-Heinemann.
65. **Kay, Francis Xavier.,** *Pneumatic Circuit Design,* 1966, Machinery Publishing Co.,
66. **Pinches, Michael J., Callear, Brian J.,** *Powder Pneumatics,* 1997, Prentice Hall.

G. Vortex Technology

67. **Saffman, P. G.,** *Vortex Dynamics,* Cambridge Monographs on Mechanics and Applied Mathematics, 1992, Cambridge University Press.

68. **Cottet, Georges-Henri., Koumoutsakos, Petros D.,** Vortex *Methods: Theory and Practice*, 2000, Cambridge University Press.
69. **Lugt, Hans J.,** *Vortex Flow in Nature and Technology*, 1983, Wiley.
70. **Glenny, D. E., Pyestock, N. G. T. E,** *Ingestion of Debris into Intakes by Vortex Action*, Aeronautical Research Council, n1114, 1970, H. M. Stationery Office.
71. **Wakelin, W.,** *The Vortex Cleaner*, University of Canterbury, Department of Mechanical Engineering, Final Year Project 1999.
72. **Patel, R.,** *A Vortex Cleaner*, University of Canterbury, Department of Mechanical Engineering, Final Year Project 1997.
73. **Lee, C. R. A.,** *A Vortex Cleaner*, University of Canterbury, Department of Mechanical Engineering, Final Year Project 1987.
74. **Post, D.,** *Vortex Cleaner*, University of Canterbury, Department of Mechanical Engineering, Final Year Project 1981.

H. Mechanism Design & Mechanics of Materials

75. **Erdman, Arthur G., Sandor, George, N.,** *Mechanism Design: Analysis and Synthesis*, **V1,** 1984, Prentice-Hall.
76. **Erdman, Arthur G., Sandor, George, N.,** *Mechanism Design: Analysis and Synthesis*, **V2,** 1984, Prentice-Hall.
77. **Molian, S.,** *Mechanism Design: The Practical Kinematics and Dynamics of Machinery*, 1997, Elsevier.
78. **Wöhlbier, Reinhard H.,** *Mechanical Conveying, Transporting & Feeding*, The Best of Bulk Solids Handling 1981-1985, **V D/86,** 1987, Trans Tech Publication.
79. **Sclater, Neil, Chironis, Nicholas P.,** *Mechanisms and Mechanical Devices Source Book*, 3rd edition, 2001, McGraw-Hall.
80. **Brockenbrough, Roger L., Merritt, Frederick S.,** Structural *Designer's Handbook*, 3rd edition, 1999, McGrew-Hill.
81. **Hamrock, Bernard J., Jacobson, Bo O., Schmid, Steven R.,** *Fundamentals of Machine Elements*, 1999, WCB/McGrew-Hill.
82. **Shigley, Joseph Edward.,** *Mechanical Engineering Design*, 1st Metric Edition, Mc-Grew-Hill Series in Mechanical Engineering, 1986, McGrew-Hill.
83. **Megson, T. H. G.,** *Structural and Stress Analysis*, 1996, Arnold.
84. **Wysack, Roy.,** *Designing Parts with SolidWorks*, 1998, CAD/CAM Publishing.
85. **Simmons, Colin H., Maguire, Dennis E.,** *Manual of Engineering Drawing*, 1995, Eward Arnold.

86. **Hibbeler, R. C.,** *Mechanics of Materials,* 3rd edition, 1997, Prentice Hall International, Inc.
87. **Pahl, G., Beitz, Wolfgong.,** *Engineering Design: a Systematic Approach,* 1996, Springer.
88. **Hales, Crispin.,** *Manaing Engineering Design,* 1993, Longman Science & Technical.

I. Thesis & Scientific Report Writing

89. **Paradise, James G., Zimmeman, Muriel.,** *The MIT Guide to Science and Engineering Communication,* 1997, MIT Pres.
90. **Gooch, S. D.,** *Design and Mathematical Modelling of the Kinetic Sculpture Blade: a thesis submitted for the degree of Doctor of Philosophy at the Department of Mechanical Engineering, University of Canterbury,* 2001, University of Canterbury.

APPENDIX A – Particle Size Determination with Shadowgraph

A-1 Preparation of Sample

Great care has to be taken in slide preparation since the measurement sample is so small that it is difficult to make it representative of the bulk. Many particulate systems retain their agglomerates and aggregates, if it is necessary to retain their integrity; the dispersing procedure needs to be very gentle **[28]**. A small portion of dust was sieved to break up the large lump of powders, the powder was lightly dusted on the top of the glass slides, and then enclosed with a cover piece in order to maintain its orientation during the project period, and four sample slides were made.

A-2 Feret's Diameter (d_f) Measurement

Optical microscopy is most often used for the examination of particles from 3 μm to 150 μm. The theoretical lower limit is approximately 0.2 μm but the diffraction halo around the particle gives a gross overestimation of particle size **[28]**. Its most severe limitation is the small depth of field so that, as a slide has a wide range of sizes, only a few particles are in focus at any one time. Similar to optical microscopy, the shadowgraph comes with the advantage of eliminating the depth of field problem and can obtain measurements down to 0.2 μm, however the surface detail of the particle are unable to revealed. A simple magnifying glass is suitable for particles above 150 μm.

The images seen in a shadowgraph are projected area whose dimensions depend on the particles' orientation on the slide. Particles in stable orientation tends to present their maximum area to the user, hence the size measured by shadowgraph tend to be greater than those measured by other methods. Any one particle has an infinite number of linear dimensions, therefore if the chord length is measured at a random, the length will depend upon the particle orientation on the slide. These orientation dependent measurements are known as statistical diameters, and are only useful when a large number of measurements are made. They are measured parallel to some fixed direction and are acceptable only when orientation is random; i.e. the distribution of diameters measured parallel to some other direction must give the same size distribution. Since they are representative of the two largest particles' dimensions – the smallest is perpendicular to the viewing plane if the particles are in a stable orientation – the diameters will generally be larger than the Strokes diameters in

the gravity sedimentation methods. With Strokes law relating particle size to settling velocity in equation

$$d_{st} = \sqrt{\frac{18\eta u}{(\rho_s - \rho_f)g}} \qquad \textbf{(A1)}$$

Where d_{st} is the Stroke diameter, η is viscosity, u is particle settling velocity under gravity g, ρ_s is the particle density, and ρ_f is the fluid density. From **Perry, R. H.** *et al* **[61]**, the Stroke diameter is defined as the diameter of a sphere having the same density and the same velocity as the particle in a fluid of the same density and viscosity setting under laminar flow conditions.

The Feret's Diameter (d_f) is the distance between two tangents on opposite sides of the particle parallel to some fixed direction **[28]**, however, since the shape of the particles were not perfectly round, a horizontal and a vertical measurement on each particle was obtained and the average value was then recorded for each particle measurement. Particles which were targeted here were the both the smallest and largest appeared on the shadowgraph, and 40 samples were made on both sizes.

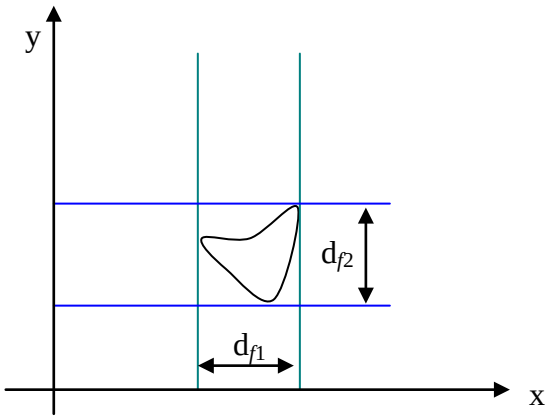

Figure A-1, Feret's diameter (d_f) measurement

APPENDIX B – Powder Properties Determination with Shear Cell

Most of the powder properties' measurements were conducted in the Particle Technology Laboratory within the Department of Chemical & Process Engineering at the University of Canterbury.

B-1 Calibration of the Peschl Shear Cell

From **Kearney, T. [27]**, the Peschl Shear Cell was connected with a compressed air supply, and the inlet pressure was set to 4 bar, without any powder in the cell, and the air bearing in the shear cell head was cleaned and checked for sensitivity. The friction of the vertical movement of the cell was balanced out by altering the small weight from the counter-balance weight until the shaft of the head began to fall with slight push downwards.

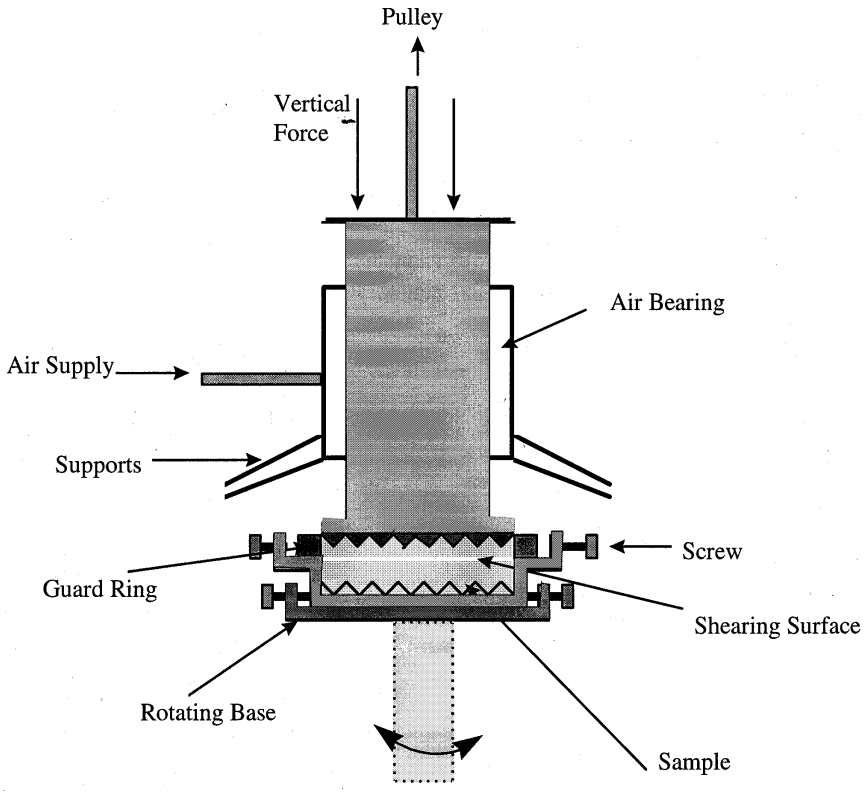

Figure B-1, Peschl shear cell (Source: Kearney, T. [27])

The detachable arm was assembled onto the top of the shear head by removing the calibration pulley. Two hundred grams of weights were loaded on the bob and the cell and/or recorder setting were adjusted to give a chart displacement of about 90% of the width of the chart

paper. The weight placed on the bob was gradually increased, and the change of corresponding displacement recorded. The effective average shear stress across the annulus τ was assume to be constant across the whole shearing surface, and can then be determined by equation

$$T = WR_1 = \tau(\frac{2}{3}\pi R_2^3) \quad \textbf{(B1)}$$

where T is the torque, W is the loading weight, R_1 (radius)= 0.102m, and R_2 (radius of the shear cell head) = 0.031m. The calibration result is listed below in Table B-1.

Table B-1, Shear cell calibration result

Displacement	Mass (g)	$T = WR_1$ (Nm)	τ (Nm^{-2})
0	0	0	0
1.3	30	0.03	481.1
3.3	80	0.08	1283.0
5.3	130	0.1301	2048.8
7.25	180	0.1801	2886.7
9.225	230	0.2301	3688.5

All settings on the shear cell at this stage were maintained constant until all the property measurements regarding to the powder were completed

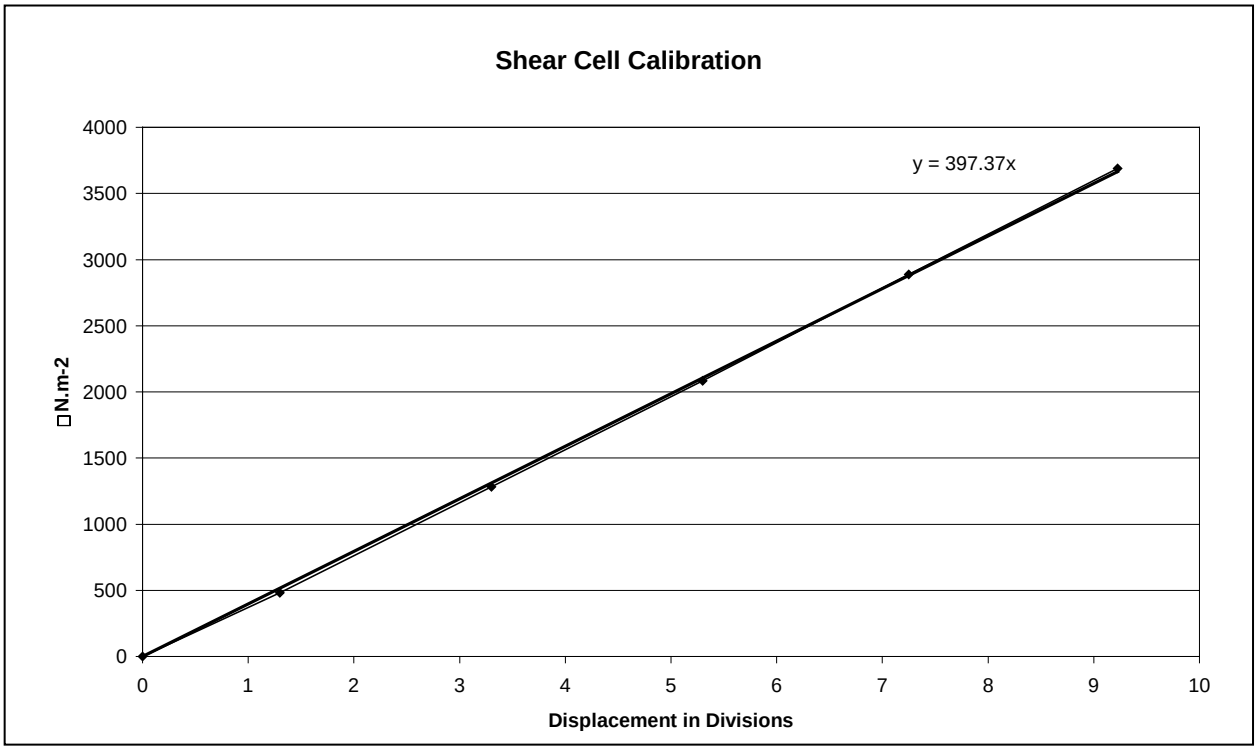

Figure B-2, Shear cell calibration.

B-2 Yield Loci for Powder/Powder & Powder/Wall Shearing

At least four different consolidation weights between 0.25 to 1 kg must be used to ensure that the powder function may be generated with reasonable certainty **[27]**.

B-2.1 Sample Preparation

The guard-ring was clamped to the trough of the shear cell with three screws. The covering was placed on the guard-ring; the powder was sieved and levelled off with metal straightedge. The chosen consolidation weight was loaded on the perspex cylinder and placed directly on top of the powder for one minute. The weight, perspex cylinder and plastic cover-ring were all removed. The filled-trough was gently placed on the turntable of the shear cell and firmly secured, the fill was checked to ensure that it was levelled, and the guard-ring was then loosened.

The shear head was mounted on to the turntable. The retractable arm of the load cell was lowered down to the shear head until contact was made, then the counter-balance yoke was connected. The chosen consolidation weight was loaded and the shear head gently lowered on to the turntable. The powder was sheared in both clock wise and anti-clockwise direction until a steady maximum value is obtained, then the consolidated sample was then ready for testing. It was necessary to make new samples for each different consolidation weight.

B-2.2 Powder/Powder Shear Test

The powder was sheared once until a maximum displacement was seen and reverse sheared until zero displacement was obtained. Some of the original consolidation weight was removed and the shearing/reverse cycle was repeated with five different weights within each consolidation, this had to include the consolidation weight. Results are listed in Tables B-2, B-3, B-4 and B-5, and the angle of internal friction δ of steel powder under different consolidations was determined from Möhr circle diagrams and summarised in Table B-6.

Table B-2, 150g consolidation powder/powder shear result

Displacement	Mass (g)	τ (Nm^{-2})	σ (MPa)
0.4	0	158.9	0
0.75	50	298.0	162.5
1.05	100	417.2	324.9
1.3	150	516.6	487.4

Table B-3, 250g consolidation powder/powder shear result

Displacement	Mass (g)	τ (Nm^{-2})	σ (MPa)
0.35	0	139.1	0
0.75	50	298.0	162.5
1.15	100	417.0	324.9
1.55	150	516.9	487.4
1.9	200	755.0	649.9
2.2	250	874.2	812.3

Table B-4, 400g consolidation powder/powder shear result

Displacement	Mass (g)	τ (Nm^{-2})	σ (MPa)
0.4	0	158.9	0
1.1	100	437.1	324.9
1.85	200	735.1	649.9
2.5	300	993.4	974.8
3.1	400	1231.8	1299.7

Table B-5, 600g consolidation powder/powder shear result

Displacement	Mass (g)	τ (Nm^{-2})	σ (MPa)
0.35	0	139.1	0
1.2	100	476.8	324.9
1.9	200	755.0	649.9
2.65	300	1053.0	974.8
3.35	400	1331.2	1299.7
3.9	500	1549.7	1624.7
4.5	600	1788.2	1949.6

Figures B-3, B-4, B-5, and B-6 show the yield loci for powder/powder shearing under different consolidation loads.

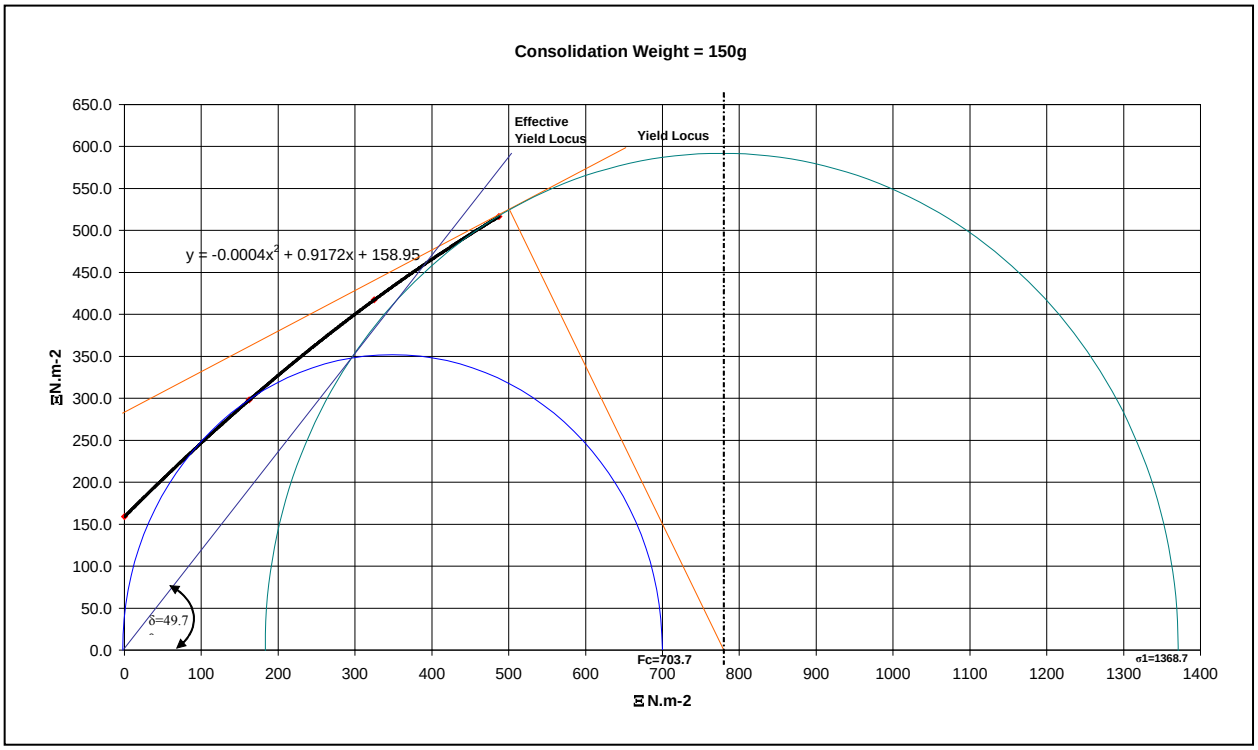

Figure B-3, Möhr circle diagram of steel powder at 150g consolidation.

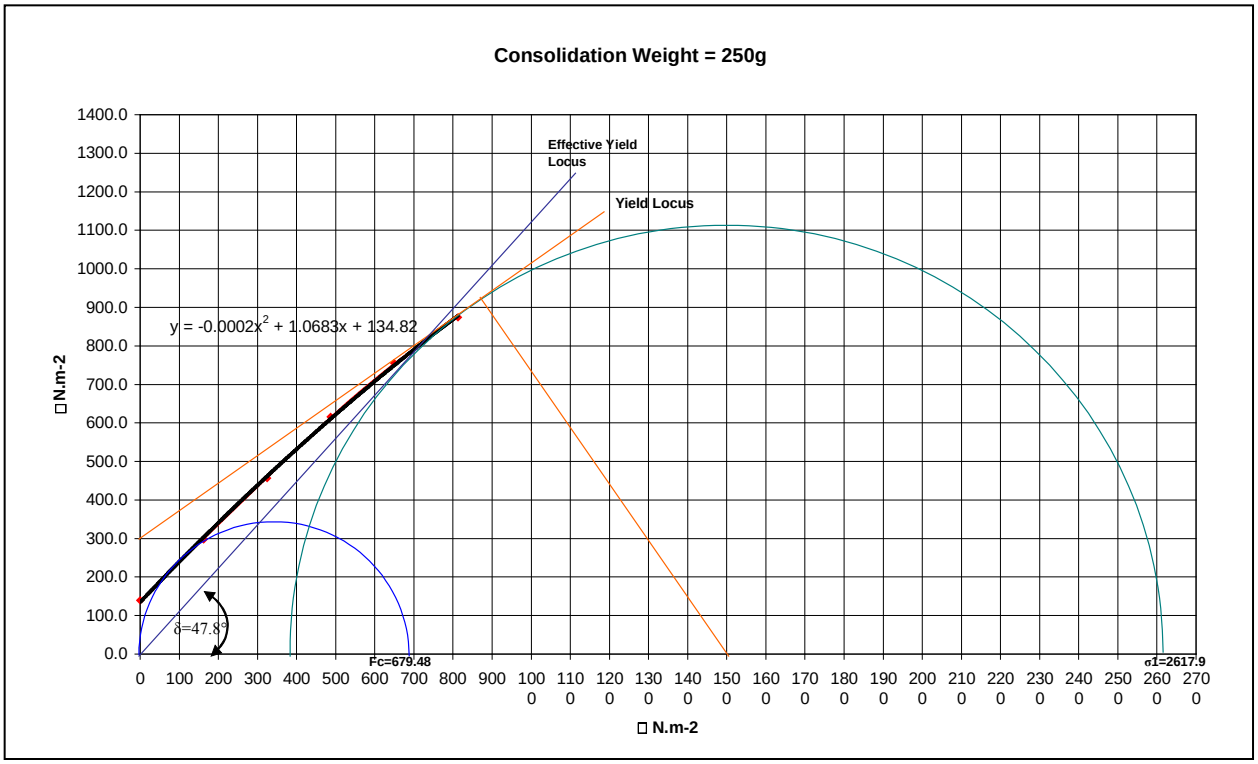

Figure B-4, Möhr circle diagram of steel powder at 250g consolidation.

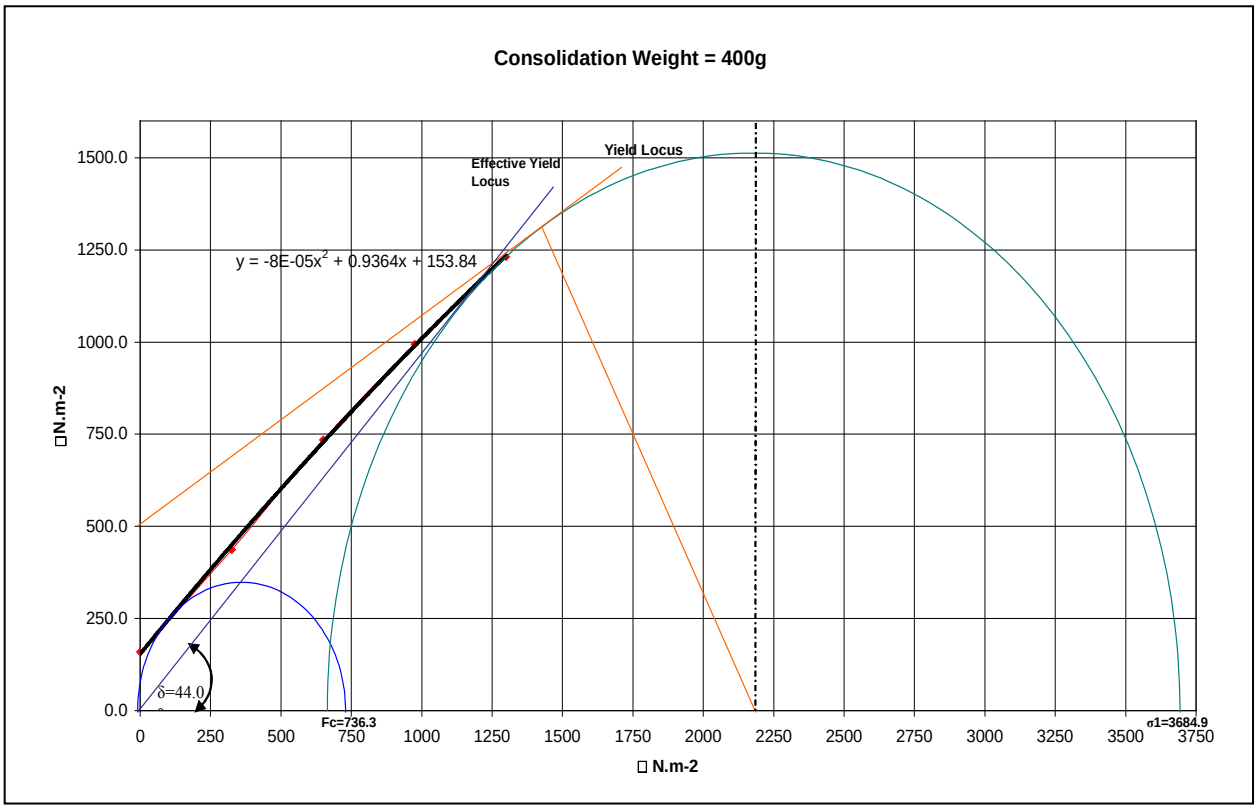

Figure B-5, Möhr circle diagram of steel powder at 400g consolidation.

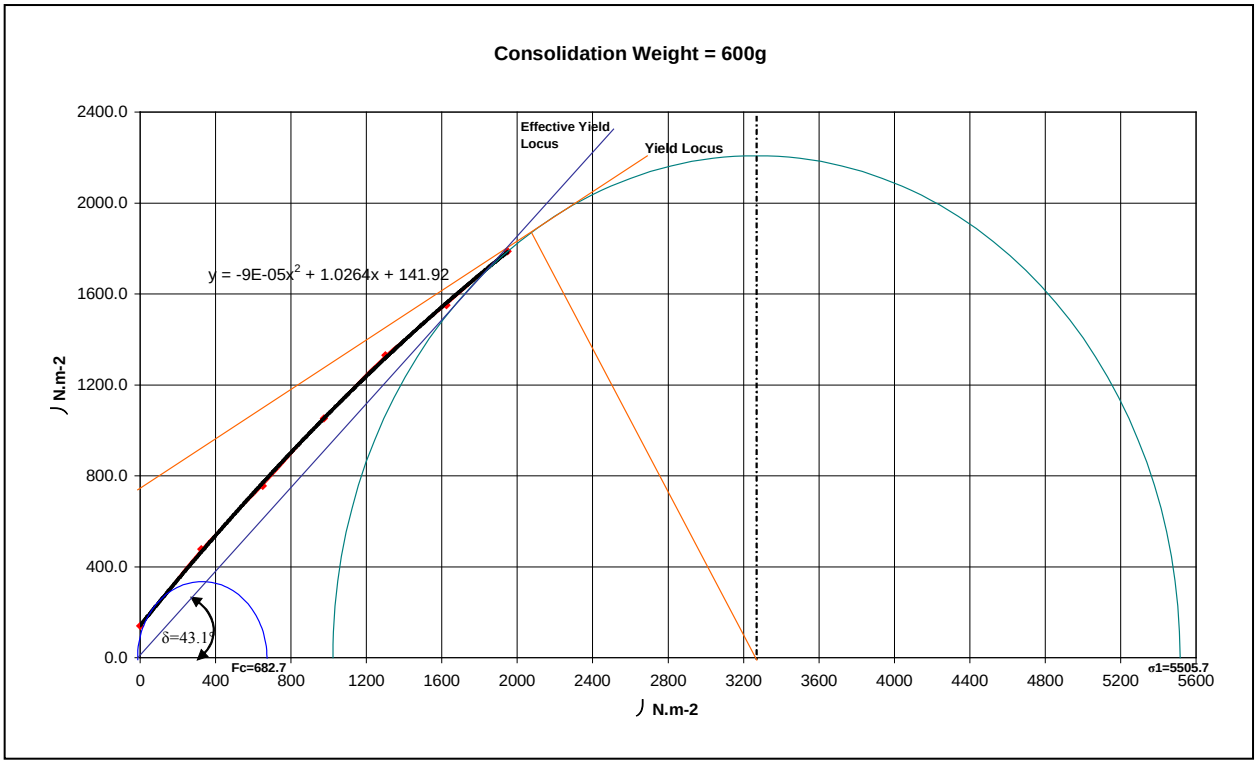

Figure B-6, Möhr circle diagram of steel powder at 600g consolidation.

Table B-6, Summary of angle of internal friction obtained from powder/powder shear test

Consolidation Load (g)	Angle of internal friction δ
150	49.67
250	47.84
400	44.01
600	43.11

B-2-.3 Powder/Wall Shear Test

Similar procedures were used to test the shear between the powder and the wall. By inserting the material disk into the trough before filling it with powder and performing the shear test, the angle of friction with the wall was then be obtained. Table B-6 shows the powder/wall shear test result.

Table B-7, 400g consolidation powder/wall shear result.

Displacement	Mass (g)	τ (Nm^{-2})	σ (MPa)
0.35	0	139.1	0
0.55	50	218.6	162.5
0.7	100	278.2	324.9
0.775	150	308.0	487.4
0.9	200	357.6	649.9
1	250	397.4	812.3
1.1	300	437.1	974.8
1.2	350	476.8	1137.3
1.4	400	556.3	1299.7

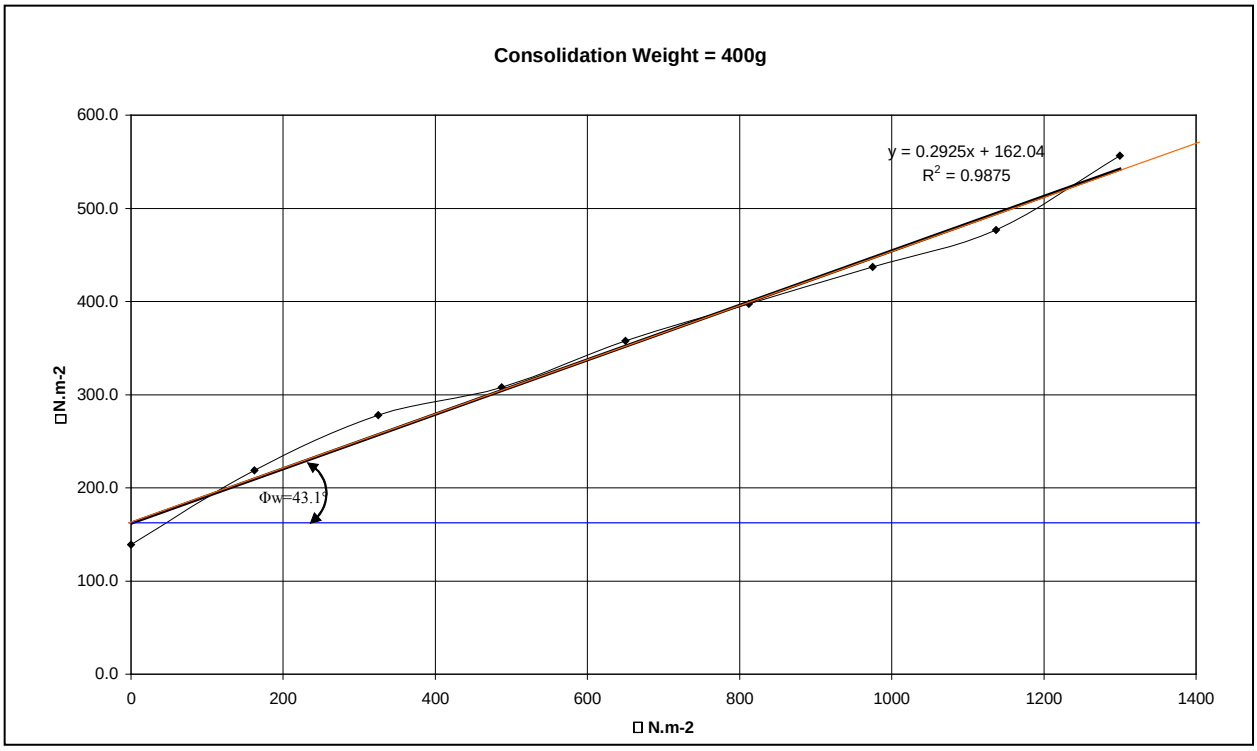

Figure B-7, Kinematic angle of wall friction.

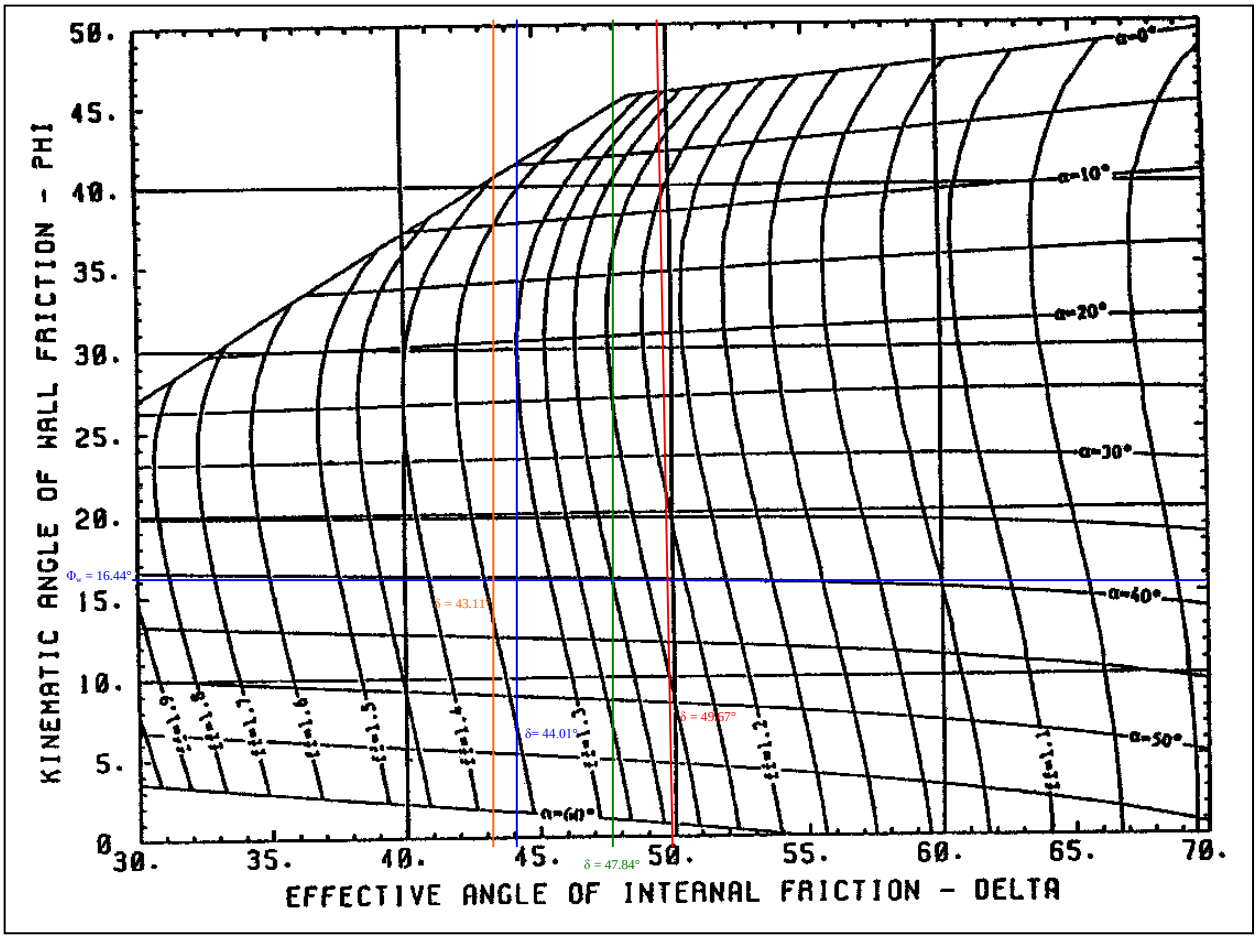

Figure B-8, Plan flow hopper design parameter (Source: Kearney, T. [27])

The kinematic angle of wall friction Φ_w was found to be 16.44°, hence the flow factor ff and angle of repose α for each test can be determined from Figure B-8, and then recorded in Table B-9.

Table B-9, Flow factor

Consolidation Load (g)	Angel of Repose α (°)	Flow Factor ff	Fc (N)	σ_1 (MPa)	F = σ_1 / ff (N)
150	39.0	1.129	703.71	1368.69	1113.66
250	39.0	1.258	679.48	2671.87	2130.08
400	39.5	1.312	736.33	3684.91	2998.30
600	40.0	1.318	682.72	5505.69	4479.81

The powder function was obtained and plotted in Figure B-9, the intersection between two lines was $F_{critical}$ and it was found to be 866.5 MPa, and the equivalent force applied on the powder within the perspex container was 26510.5N.

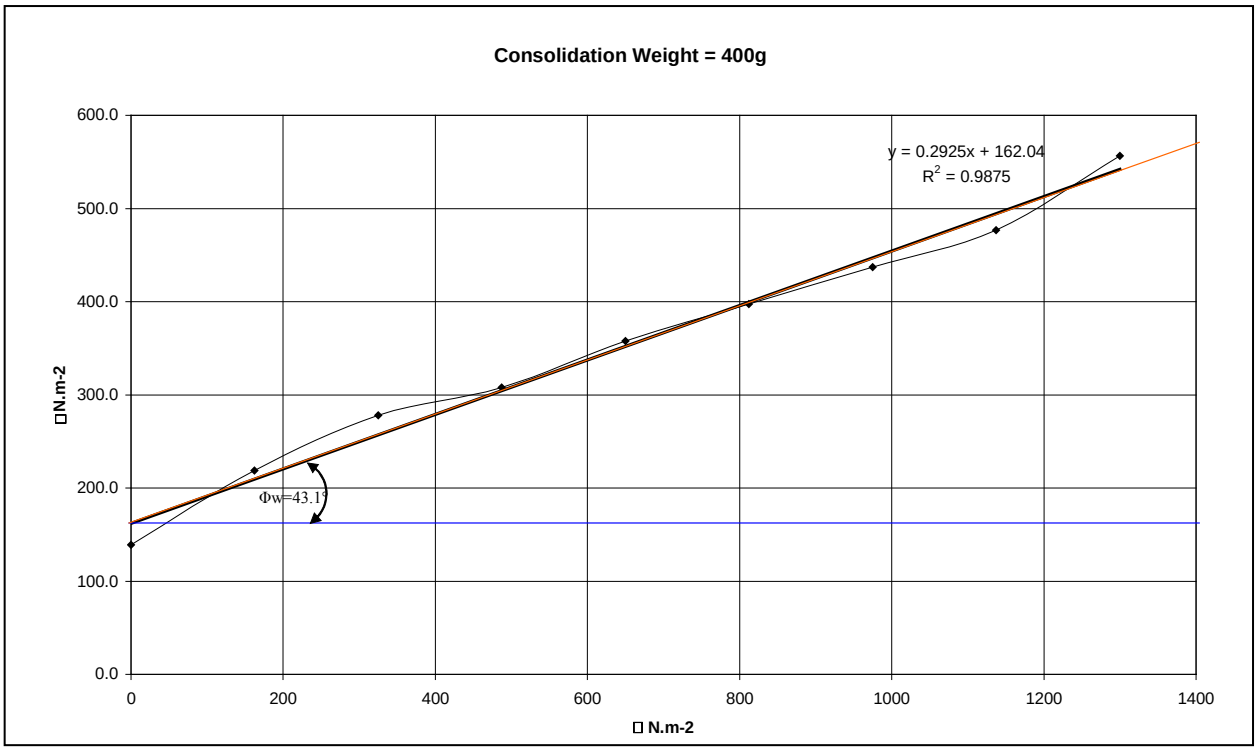

Figure B-9, Graph of Fc VS σ_1

B-3 Bulk Density

Bulk density of the powder can be varied with different consolidation pressures. In this experiment the consolidation pressure was simulated by applying static axial loading over a known size of container. When different static weights are placed, the powder in the container can be assessed to find a function with regards to the density and this can be determined from Figure B-10.

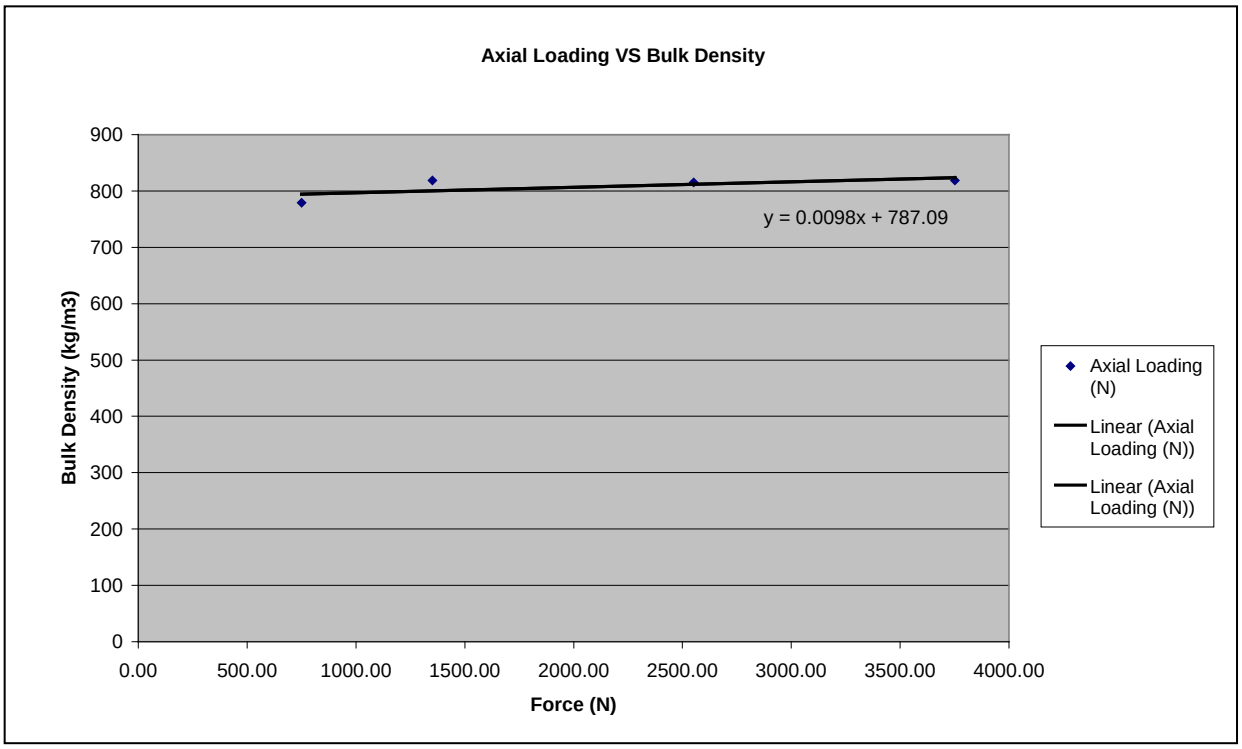

Figure B-10, Axial loading VS bulk density graph of clean steel powder.

By applying the equivalent force of $F_{critical}$ obtained from Figure B-9 into the bulk density equation, the bulk density was found to be 1046.89 kg/m^3.

APPENDIX C – Cyclone Separation Requirement

Research regarding the practical implications of understanding cyclone separation has been conducted by both the industries and research centres. However, a universal mathematical expression for the vortex has yet to come, since the expression developed by each party has a unique superiority. This is due to the various hypothetical assumptions made regarding the data obtained from experimental data.

Two approaches were taken in this section to determine the general requirements for a cyclone system to separate the given particle size which was determined earlier. A course handout from Chemical & Process Engineering (CAPE) at University of Canterbury, written by **Prof. Abrahamsom J. [62]** on the cyclone separation system was used as one of the calculation methods, and the other from **Perry, R. H.** *et al* **[61],** which is denoted as CAPE 's method and Perry's method respectively.

C-1 CAPE's Method

A practical method taught in the undergraduate Chemical & Process Engineering course at the University of Canterbury is described below, with three different design dimensions relative to outlet duct diameter as listed in Table C-1, and detailed diagram descriptions in Figure C-1,

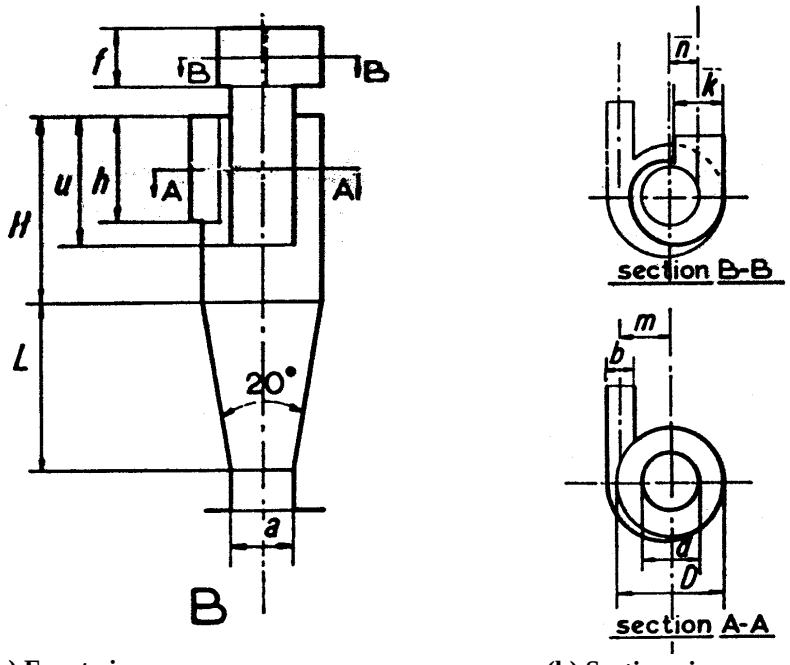

(a) Front view **(b) Section views**

Figure D-1, Detailed description of cyclone separator (a) front view, (b) section views. (Source: Abrahamson, J. [62])

Table C-1, Cyclone separator dimensions in proportional to *d* (Source: Abrahamson, J. [62])

Parameter / Dimension Relationship	A	B	C
d	1.0	1.0	1.0
D	2.5	1.9	3.3
a	≤ 1.0	≤ 1.0	≤ 1.0
b	0.66	0.5	0.89
f	0.89	0.89	0.89
h	1.2	1.6	0.89
H	1.6	2.9	1.67
k	0.89	0.89	0.89
m	0.92	1.0	1.23
n	1.25	0.5	0.5
u	1.4	2.0	1.3

This method uses the Strokes number with an assumption regarding the concentration of the particles at the inlet to justify the efficiency of the separation process.

$$Stk = \frac{x^2 v_{in} \rho_p}{\mu D} \quad \textbf{(C-1)}$$

$$Y = \frac{x}{x_{50}} = \frac{\sqrt{Stk}}{\sqrt{Stk_{50}}} \quad \textbf{(C-2)}$$

$$\eta = \frac{1}{m + \frac{k}{Y^n}} \quad \textbf{(C-3)}$$

where x is the particle size, v_{in} the inlet velocity, ρ_p the particle density, μ the gas viscosity, and D the diameter of the cyclone.

For a dilute system, such as 10 g/m^3, as shown in Figure C-2, together with the calculated result, it was found that a very large entry velocity (1600 m/s) and a relatively small cyclone outlet duct dimension (Ø5mm) is required to achieve 50% efficiency. All of the three given dimension relationships were applied, and similar efficiency was observed from the results; hence it is impossible to use a cyclone achieve an efficient separation in this case. As the inlet particle concentration increases, the efficiency curve will shift upward; this is mainly due to the aggregation or collision of particle with each other in the flow. However, since the

requirement of the inlet velocity is far beyond realistic practicability, it is concluded to be as unfeasible.

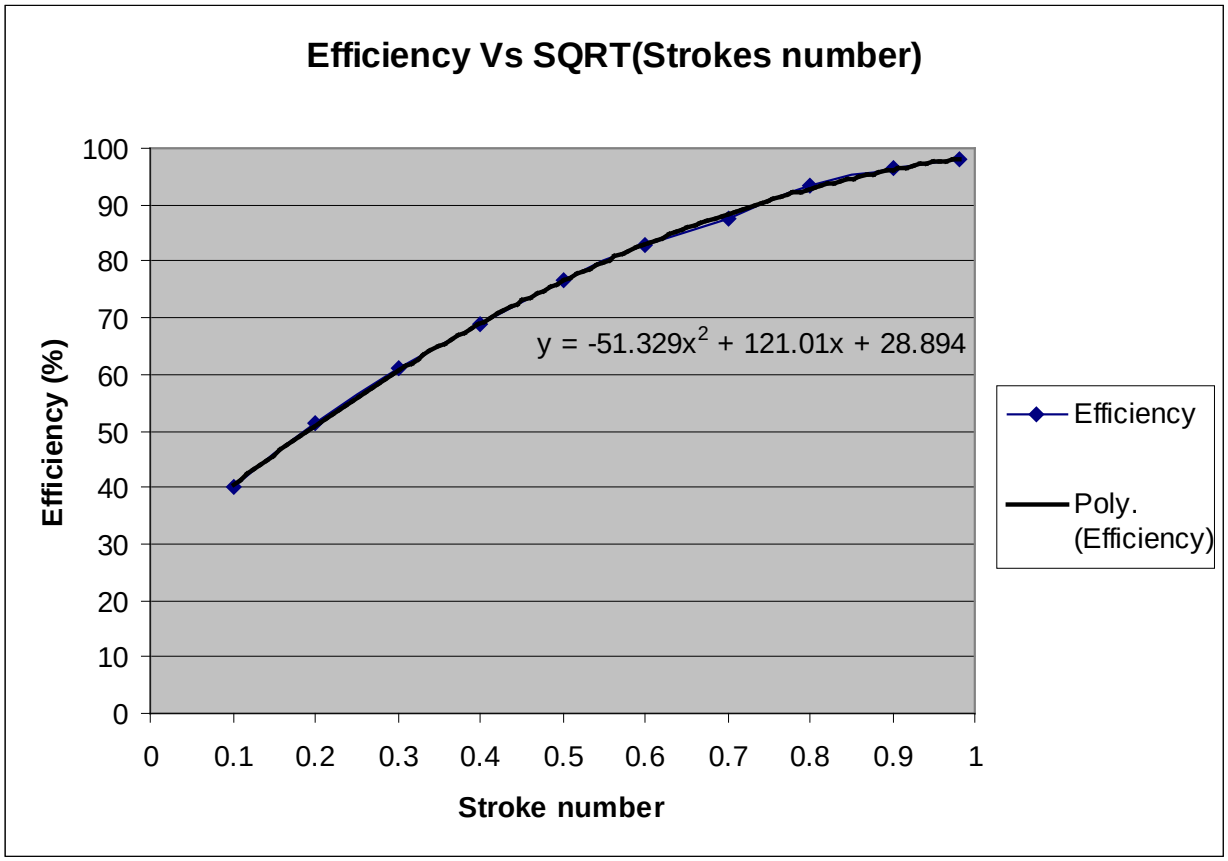

Figure C-2, Cyclone separation efficiency with inlet particle concentration of 10 g/m^3.

A comparison with the alternative analytical method will be conducted and reviewed in the next section, and a final conclusion will then be drawn.

C-2 Perry's Method

This method was found in one of the most highly recommended text books in the chemical engineering field, and here it is used to verify the previous analysis in order to justify the feasibility of the cyclone separation process in the implementation of the transportation system development.

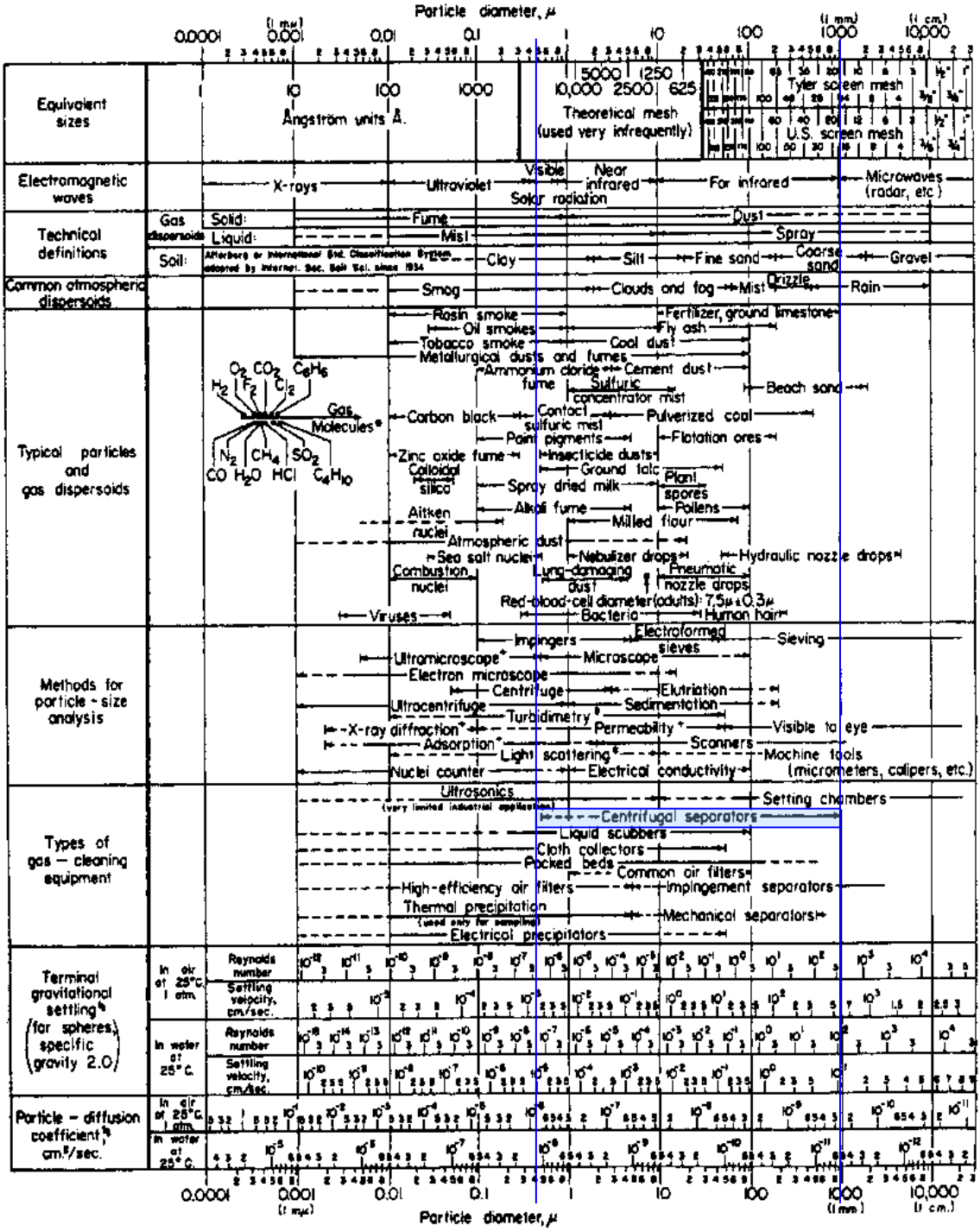

Figure C-3, Characteristics of particles and particle dispersoids (Source: Perry, R. H., Green, D. W., Maloney, J. O. [61])

Using a broad overview of the separation technologies as shown in Figure C-2, it was found that the cyclone separation process can cover a wide range of particle size from 0.5 – 1000 μm. However the efficiency dropped sharply when particles are smaller than 20 μm.

The detailed description of the dimension relationship is shown in Figure C-4. The number of effective spiral paths of the gas flowing in the cyclone has been taken into account and related to the inlet velocity. However, this is for a very dilute system, since the inlet particle concentration is difficult to predict at this stage.

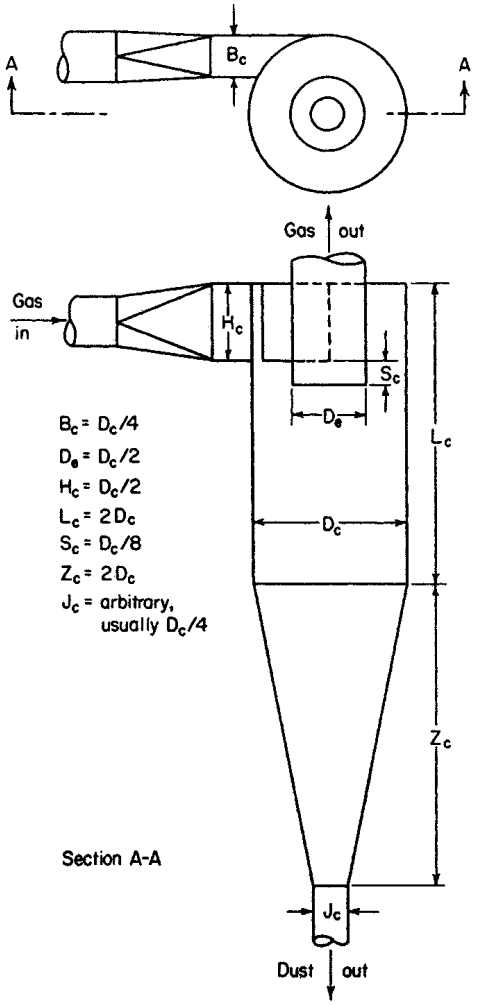

Figure C-4, Cyclone separator proportions (Source: Perry, R. H., Green D. W., Maloney, J. O. [62])

This analytical method is concerned with the theoretical particle size that can be removed by the cyclone as expressed as below,

$$D_{pth} = \sqrt{\frac{9\mu_g B_c}{\pi N_s v_{in}(\rho_p - \rho_g)}} \qquad \textbf{(C-4)}$$

where D_{pth} is the theoretical particle size, μ_g the gas viscosity, B_c the dimension of the cyclone, N_s the effective number of spital, v_{in} the gas inlet velocity, and ρ_p, ρ_g is the density of gas and particle respectively.

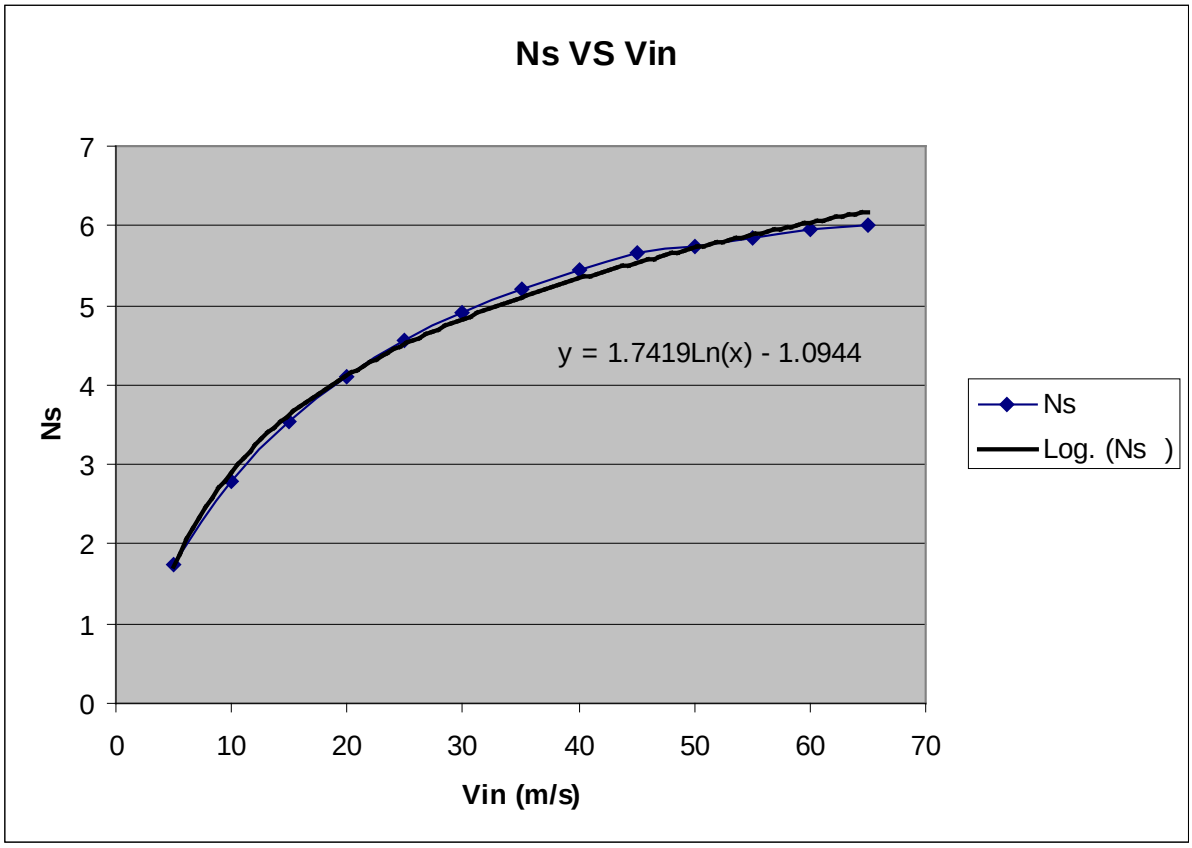

Figure C-5, N_s versus velocity – where the larger of either the inlet or outlet velocity is used

Figure C-5 is used to determine the value N_s when an assumed inlet velocity is used. It was found that for a practical inlet velocity of 30 m/s, and an outlet duct of Ø5mm, only particles larger than 109.3 μm can be separated. By rearranging the equation to determine the inlet velocity required, with the particle size set to 8.8 μm, the inlet velocity was also found to be impossible to be achieved in reality. Therefore the implementation of a cyclone separation unit into the transportation system will no longer be considered.

APPENDIX D – Vortex Study

Much research regarding the application of a vortex in the design of the vacuum cleaners has been conducted under the Department of Mechanical Engineering at the University of Canterbury in the last 40 years. Most of the experimental data regarding the vortex were gathered through undergraduate final year projects, and a significant amount of understanding has been achieved and used to compare the data with the theoretical estimation. Although none of those prototypes are able to offer an efficient performance at this stage, the theoretical estimation still holds and encourages further research in this area.

The centripetal force due to the circular motion of the fluid causes a significant pressure drop in the core of the vortex, providing a lifting capability similar to that of tornados and cyclones. The presence of the vortex can be observed in everyday action such as the motion of leaves moving in a swirling wind, or sink draining.

The project was originally conceived of to solve an existing problem by researching a more efficient method. Therefore, given the limited amount understanding on the vortex both theoretically and practically, the vortex lifting method has been discarded. However, investigation has been carried out to verify its importance and possible implementation for further development in the future.

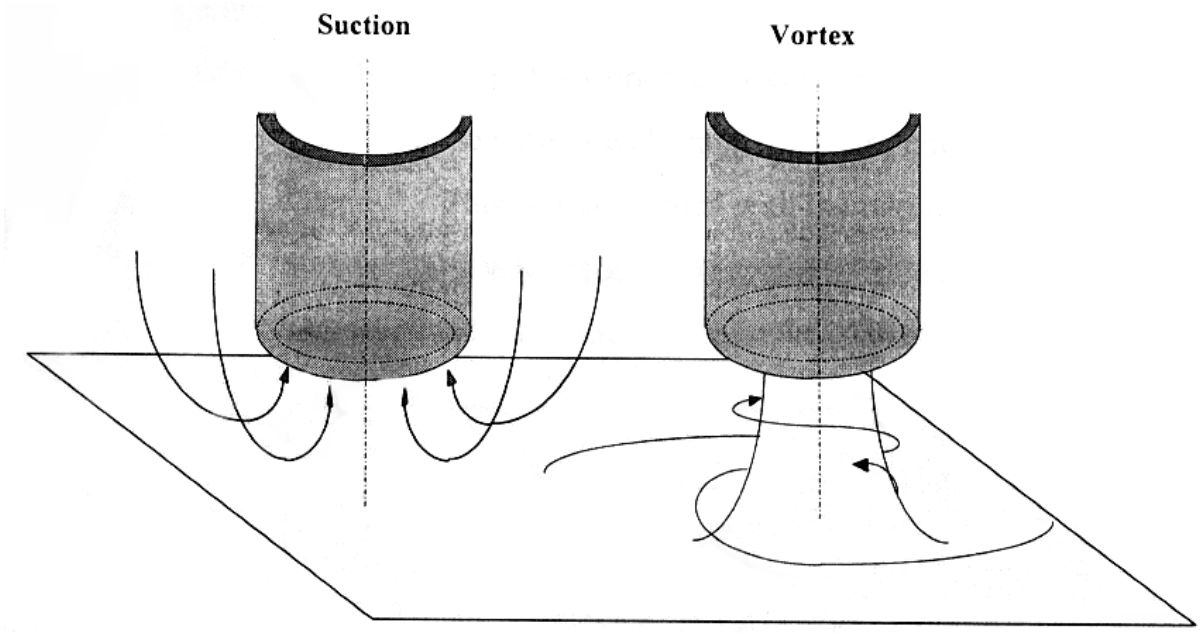

Figure D-1, Motion of the local fluid affected by suction and vortex (Source: Wakelin, W. [71])

In the conventional vacuum cleaner, as shown in Figure D-1, in which the disturbance of localised air is withdrawn by the suction into the hose, many operational limitations still exist. Theoretically, a vortex in an inviscid fluid cannot be terminated within the medium; rather it results in the formation of a ring which extends to infinity or to the physical boundary **[74]**. Hence, the influence of a vortex can extend further into the fluid than the conventional plain suction provide by vacuum cleaner. A greater effective range is provided by the vortex which is suitable for application on lifting particles from an irregular geometry; and hence it has high potential in the industry for further development of a highly efficiency transportation.

A mathematical model concerned with the velocity profile and pressure distribution about the fluid axis of rotation was found, and through using the simplified mathematical modelling, the lifting capability of the vortex can be determined; however, these were assumed to be under 2-D conditions. This fluid is modelled as two separate regions. The inner region is called the *Forced/Rotational Vortex*, which is assumed to rotate as a rigid body and has the same angular velocity about some fixed axis **[72]**. Beyond this rotating core is the outer region, commonly known as the *Free/Irrotational Vortex*, and is assumed that the streamlines of the fluid run in concentric circles with each other, and also that the fluid particles moving on these streamlines do not rotate about their own axis. This chapter covers the basic fundamental theories on the fluid dynamics of the vortex.

D-1 Mathematical Modelling

The Eulerian approach was taken with the properties of a fluid considered with respect to the spatial and time coordinates, which is opposed to the Lagrangian approach where individual particles of fluid were studied **[74]**.

D-1.1 Conservation of Mass & Momentum

For an elemental cube, the governing differential equation for the conservation of mass is,

$$\frac{\partial \rho}{\partial t} + \frac{\partial (\rho u)}{\partial x} + \frac{\partial (\rho v)}{\partial y} + \frac{\partial (\rho w)}{\partial z} = 0 \qquad \textbf{(D-1)}$$

where the flow velocity is

$$\underset{\leftarrow}{q} = u\underset{\cdot}{i} + v\underset{\leftarrow}{j} + w\underset{\leftarrow}{k} \qquad \textbf{(D-2)}$$

Hence, for steady incompressible flow, equation (D-1) is reduced to

$$\frac{\partial u}{\partial x} + \frac{\partial v}{\partial y} + \frac{\partial w}{\partial z} = 0 \qquad \textbf{(D-3)}$$

For a stressed element of fluid which equates to Newton's second law, then

$$\frac{\partial (\rho u_i)}{\partial t} + u_j \frac{\partial (\rho u_i)}{\partial x_j} = \frac{\partial \sigma_{i_j}}{\partial x_j} + B_i \qquad \textbf{(D-4)}$$

Hence, for a steady, incompressible flow, from (D-3) and (D-4) can reduces to,

$$u\frac{\partial u}{\partial x} + v\frac{\partial u}{\partial y} + w\frac{\partial u}{\partial z} = \frac{\partial \sigma_{xx}}{\partial x} + \frac{\partial \tau_{xy}}{\partial y} + \frac{\partial \tau_{xz}}{\partial z} + B_x \qquad \textbf{(D-5)}$$

D-1.2 Navier-Strokes equations

From **Post, D. [74]**, these equations were derived from the conservation of momentum, and may be applied with high accuracy to problems involving viscosity variations when the velocity gradient is not too large. In most situations, this assumption can be held and the Navier-Strokes equations can be apply in the incompressible flow problems. The Navier-Strokes equations for incompressible flow rate,

$$\rho\left[\frac{\partial u_i}{\partial t}+u_j\frac{\partial u_i}{\partial x_j}\right]=-\frac{\partial P}{\partial x_i}+B_i+\mu\frac{\partial^2 u_i}{\partial x_j^2} \qquad \textbf{(D-6)}$$

in Cartesian tensor notation, or in vector notation as shown below:

$$\rho\frac{D\underset{\leftarrow}{v}}{Dt}=-\nabla P+\underset{\leftarrow}{B}+\mu\nabla^2\underset{\leftarrow}{v} \qquad \textbf{(D-7)}$$

D-1.3 Element Rotation, Circulation and Vorticity

From **Post, D. [74],** consider an element of fluid undergoing a rotation in two-dimensional flow, as shown in Figure D-2.

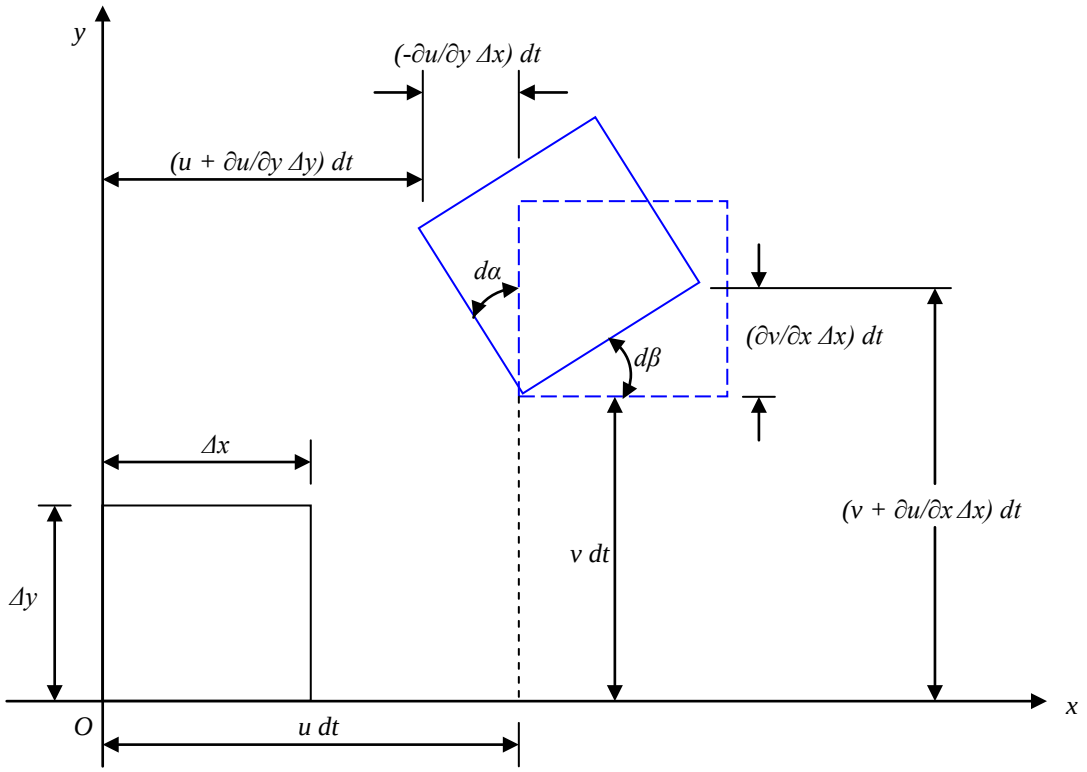

Figure D-2, Element of fluid undergoing rotation in 2-D flow (Source: Post, D. [74])

The rate of rotation of the two perpendicular faces of the element in the (x,y) coordinate is used to define the rate of the rotation of the element. In the 2-D flow, the rate of rotation can be expressed as

$$\omega_z = \frac{1}{2}\frac{(d\alpha + d\beta)}{dt} = \frac{1}{2}\left[\frac{\partial v}{\partial x} - \frac{\partial u}{\partial y}\right] \quad \textbf{(D-8)}$$

Hence, similar in 3-D flow

$$\omega_x = \frac{1}{2}\left[\frac{\partial w}{\partial y} - \frac{\partial v}{\partial z}\right] \quad \textbf{(D-9)}$$

$$\omega_y = \frac{1}{2}\left[\frac{\partial u}{\partial z} - \frac{\partial w}{\partial x}\right] \quad \textbf{(D-10)}$$

This may be expressed mathematically as

$$\underleftarrow{\omega} = \frac{1}{2} curl \underleftarrow{v} = \frac{1}{2}\nabla x \underleftarrow{v} \quad \textbf{(D-11)}$$

$$\underleftarrow{v} = u\underleftarrow{i} + v\underleftarrow{j} + w\underleftarrow{k} \quad \textbf{(D-12)}$$

where the $\underleftarrow{v}$ is the velocity vector at x, y. For the rotation vector $\underleftarrow{\omega}$ equal zero, then the flow is said to be irrotational and hence,

$$\frac{\partial w}{\partial y} = \frac{\partial v}{\partial z} \quad \textbf{(D-13)}$$

$$\frac{\partial u}{\partial z} = \frac{\partial w}{\partial x} \quad \textbf{(D-14)}$$

$$\frac{\partial v}{\partial x} = \frac{\partial u}{\partial y} \quad \textbf{(D-15)}$$

The line integral of the velocity vector around an enclosed contour is used to define the circulation region of the fluid.

$$\Gamma = \oint \underleftarrow{v} \cdot \underleftarrow{dl} \quad \textbf{(D-16)}$$

Using Strokes' theorem, this is also

$$\Gamma = \iint_A \nabla x \underset{\leftarrow}{v} \cdot \underset{\leftarrow}{ds} \quad \textbf{(D-17)}$$

$$\underset{\leftarrow}{ds} = \underset{\leftarrow}{n} \cdot ds \quad \textbf{(D-18)}$$

where $\underset{\leftarrow}{ds}$ is a vector normal to the enclosed region with a magnitude, *ds*, of the elemental area, as show in Figure D-3.

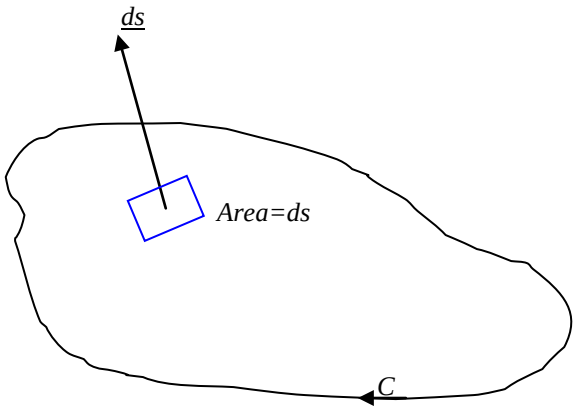

Figure D-3, Circulation of fluid in an enclosed area (Source: Post, D. [74])

Substituting equation (D-12) into (D-17), and with equation (D-13), (D-14) and (D-15)

$$\oint \underset{\leftarrow}{v} \cdot dl = \oint u dx + v dy + w dz \quad \textbf{(D-19)}$$

$$\oint \underset{\leftarrow}{v} \cdot dl = \iint \left[\frac{\partial v}{\partial x} - \frac{\partial u}{\partial y}\right] dxdy + \iint \left[\frac{\partial w}{\partial y} - \frac{\partial v}{\partial z}\right] dydz + \iint \left[\frac{\partial u}{\partial z} - \frac{\partial w}{\partial x}\right] dxdz \quad \textbf{(D-20)}$$

$$\oint \underset{\leftarrow}{v} \cdot dl = \iint 2w_z dxdy + \iint 2w_x dydz + \iint 2w_y dzdx \quad \textbf{(D-21)}$$

The vorticity vector is defined as

$$\underset{\leftarrow}{G} = 2\underset{\leftarrow}{\omega} \quad \textbf{(D-22)}$$

$$\Delta\Gamma = G_n \Delta s \quad \textbf{(D-23)}$$

where G_n is the vorticity vector component normal to the surface element *ds* as shown in Figure D-3. Since the flux of vorticity through the given surface of interest is equal to the circulation along the core enclosing the surface. From equations (D-13), (D-14) and (D-15),

$$G_x = \frac{\partial w}{\partial y} - \frac{\partial v}{\partial z} \quad \textbf{(D-24)}$$

$$G_y = \frac{\partial u}{\partial z} - \frac{\partial w}{\partial x} \quad \textbf{(D-25)}$$

$$G_z = \frac{\partial v}{\partial x} - \frac{\partial u}{\partial y} \quad \textbf{(D-26)}$$

Hence,

$$\frac{\partial G_x}{\partial x} + \frac{\partial G_y}{\partial y} + \frac{\partial G_z}{\partial z} = 0 \quad \textbf{(D-27)}$$

$$\nabla \cdot \underleftarrow{G} = 0 \quad \textbf{(D-28)}$$

Therefore, by the divergence theorem, this is often referred to as the principle of the conservation of vorticity.

$$\iiint_V \nabla \cdot \underleftarrow{G} dv = \iint_s \underleftarrow{G} \cdot \underleftarrow{ds} = 0 \quad \textbf{(D-29)}$$

Assuming the tangential line to the local vorticity vector is a vortex line, and a vortex tube is a surface made up of the vortex lines, the component of the vorticity vector normal to the vortex tube G_z, is zero **[74]**. Therefore, there is no vorticity flux through the surface of a vortex tube. Hence for any cross-section of an elementary vortex tube with uniformly distributed vorticity,

$$\Gamma = G_n s = const \quad \textbf{(D-30)}$$

Since no vorticity can leave the vortex tube, the product of the angular velocity and the area of the vortex tube remain constant along the vortex tube. By substituting equation (D-22), hence

$$\omega_n \cdot s = const \quad \textbf{(D-31)}$$

In a rotational fluid, if the vorticity is due to potential vortex motion, only a single line may exist along the centre of the potential vortices within an infinite set of vortex lines. The vortex tube cannot begin or end inside a fluid which is shown by equation (D-30); therefore a

vortex filament must start and end at the boundaries of the fluid, or close into a ring, or extend to infinity **[74]**.

D-1.4 The Generalised Bernoulli Equation

Assuming the flow is irrotational, Bernoulli's equation can be applied between any two points in the flow that are not necessarily along the same streamline. Furthermore, assuming the fluid is inviscid, there will be no shear stress acting and only the surface stress will be due to pressure. Therefore, for an incompressible fluid, the Navier-Strokes equation (D-6) can then reduced to

$$\frac{\partial u}{\partial t} + u\frac{\partial u}{\partial x} + v\frac{\partial u}{\partial y} + w\frac{\partial u}{\partial z} = B_x - \frac{1}{\rho}\frac{\partial P}{\partial z} \qquad \textbf{(D-32)}$$

Assuming the flow is irrotational, then with equation (D-13), (D-14), and (D-15) substituted into (D-32), hence, for steady flow,

$$\frac{\partial}{\partial x}(\frac{1}{2}u^2 + \frac{1}{2}v^2 + \frac{1}{2}w^2) = B - \frac{1}{\rho}\frac{\partial P}{\partial x} \qquad \textbf{(D-33)}$$

Let $B_x = gh$, then

$$\frac{\partial}{\partial x}(\frac{1}{2}|\underset{\leftarrow}{v}|^2 + \frac{P}{\rho} + gh) = 0 \qquad \textbf{(D-34)}$$

$$\frac{1}{2}|\underset{\leftarrow}{v}|^2 + \frac{P}{\rho} + gh = const \qquad \textbf{(D-35)}$$

D-1.5 Incompressible Potential Flow, Stream Function & Complex Potential

For irrotational flow, a sufficient and necessary condition which will be explained later on, are required to represent the velocity vector field as a scalar potential function φ. Mathematically, if

$$\nabla x \underset{\leftarrow}{v} = 0 \qquad \textbf{(D-36)}$$

$$\underset{\leftarrow}{v} = \nabla\varphi \qquad \textbf{(D-37)}$$

and for

$$\underset{\leftarrow}{G} = \underset{\leftarrow}{w} = 0 \quad \textbf{(D-38)}$$

$$u = \frac{\partial \varphi}{\partial x} \quad \textbf{(D-39)}$$

$$v = \frac{\partial \varphi}{\partial y} \quad \textbf{(D-40)}$$

$$w = \frac{\partial \varphi}{\partial z} \quad \textbf{(D-41)}$$

only in the absence of shear stress, is potential or irrotational flow possible. Hence if the above condition holds, $d\varphi$ is an exact differential and hence the integral

$$\int_1^2 \underset{\leftarrow}{v} dl = \int_1^{22} u dx + v dy + w dz = \int_1^2 d\varphi = \varphi_2 - \varphi_1 \quad \textbf{(D-42)}$$

Equation (D-42) can be seen to be independent of the path joining the two points. Assuming continuity as equation (D-3), φ is a solution to Laplace's equation,

$$\nabla \cdot \underset{\leftarrow}{v} = 0 \quad \textbf{(D-43)}$$

$$\frac{\partial^2 \varphi}{\partial x^2} + \frac{\partial^2 \varphi}{\partial y^2} + \frac{\partial^2 \varphi}{\partial z^2} = \nabla^2 \varphi = 0 \quad \textbf{(D-44)}$$

The contour C surrounds must be a singularity, hence equation (D-16) become

$$\oint_C \underset{\leftarrow}{v} \cdot dl = 0 \quad \textbf{(D-45)}$$

and the scalar potential, $\underline{v}$ can be described in the spherical polar coordinates as follow,

$$v_r = \frac{\partial \varphi}{\partial r} \quad \textbf{(D-46)}$$

$$v_\theta = \frac{\partial \varphi}{\partial \theta} \quad \textbf{(D-47)}$$

$$v_\psi = \frac{\partial \varphi}{r \sin \psi} \frac{\partial \varphi}{\partial \psi} \quad \textbf{(D-48)}$$

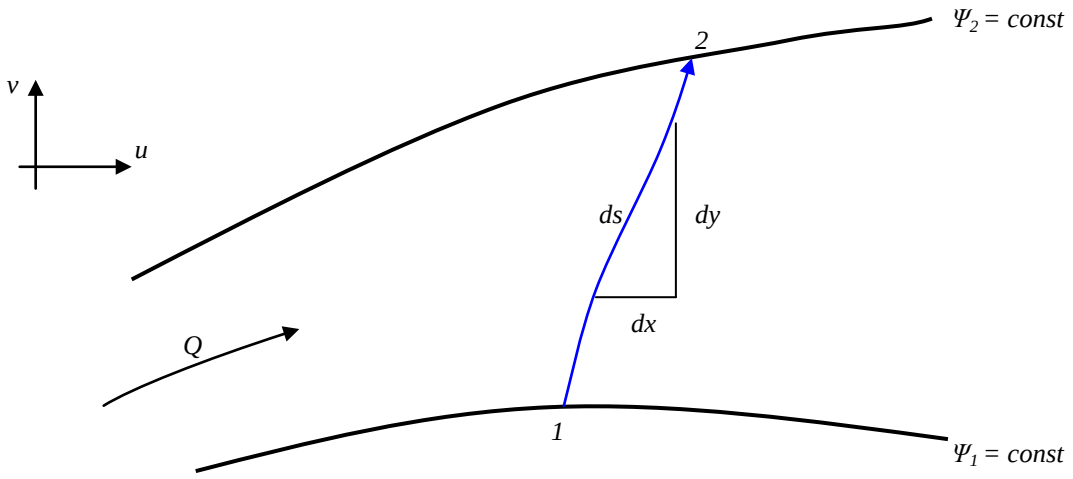

Figure D-4, 2-D Flow across streamlines (Source: Post, D. [74])

For any 2-D flow regardless of the flow condition, a stream function ψ can be used to define it. Hence, the flowrate between the streamlines is equal to the numerical difference between two streamlines. Since the flow can cross a streamline, as shown in Figure D-4, the total flow is therefore

$$dQ = \underset{\leftarrow}{v} \cdot \underset{\leftarrow}{n} ds = udy - vdx \quad \textbf{(D-49)}$$

$$Q_{12} = \int_C udy - vdx \quad \textbf{(D-50)}$$

Substitute (D-38) and (D-39) into (D-48), with minor corrections on the sign convention, then

$$Q_{12} = \int_1^2 d\psi = \psi_2 - \psi_1 \quad \textbf{(D-51)}$$

which is independent of the flow path C, hence expressed in the polar coordinates,

$$v_r = \frac{1}{r}\frac{\partial \psi}{\partial \theta} \quad \textbf{(D-52)}$$

$$v_\theta = -\frac{\partial \psi}{\partial r} \quad \textbf{(D-53)}$$

Equations (D-37), (D-39) and (D-40) are the Cauchy-Riemann conditions, and are sufficient and necessary for a complex function to be analytic (i.e., differentiable over the domain except perhaps at a few singular points) and thus they can represent the real and imaginary

parts of a complex variable [xx]. Hence, for two real valued functions $\varphi(x,y)$ and $\psi(x,y)$ of two real variables x and y have continuous first derivatives that satisfy the Cauchy-Riemann equations in the domain D, then the complex function is,

$$F(z) = \varphi(x, y) + i\psi(x, y) \quad \textbf{(D-54)}$$

where $z = x + iy$. Moreover, the real and imaginary part of a complex function that is analytic in D is the solutions of Laplace's equation, which can be easily proved as follows:

$$\frac{\partial u}{\partial x} = \frac{\partial^2 \varphi}{\partial x^2} = \frac{\partial^2 \psi}{\partial x \partial y} \quad \textbf{(D-55)}$$

$$\frac{\partial v}{\partial y} = \frac{\partial^2 \varphi}{\partial y^2} = -\frac{\partial^2 \psi}{\partial x \partial y} \quad \textbf{(D-56)}$$

From equations (D-55) and (D-56), then

$$\frac{\partial^2 \varphi}{\partial x^2} + \frac{\partial^2 \varphi}{\partial y^2} = \frac{\partial^2 \psi}{\partial x^2} - \frac{\partial^2 \psi}{\partial y^2} = 0 \quad \textbf{(D-57)}$$

Two important Cauchy's theorems used in Complex analysis are listed below,

(1) $\oint_C f(z)dz = 0$, Cauchy's Integral Theory. **(D-58)**

(2) $\oint_C \frac{f(z)}{z - z_0} dz = 2\pi i f(z_o)$, Cauchy's Integral Formula. **(D-59)**

The complex velocity is derived from

$$\frac{dF}{dz} = \frac{\partial \varphi}{\partial x} + i\frac{\partial \psi}{\partial x} = u - iv \quad \textbf{(D-60)}$$

for the limit $\Delta y \rightarrow 0$ and then $\Delta x \rightarrow 0$, and

$$\frac{dF}{dz} = \frac{\partial \psi}{\partial y} - i\frac{\partial \varphi}{\partial y} = u - iv \quad \textbf{(D-61)}$$

for the limit $\Delta x \rightarrow 0$.

Since both (D-60) and (D-61) satisfy the Cauchy-Riemann equations, and let the complex velocity be,

$$\frac{d\overline{F}}{dz} = u + iv \qquad \textbf{(D-62)}$$

Hence,

$$\frac{dF}{dz} \cdot \frac{d\overline{F}}{dz} = (u - iv)(u + iv) = u^2 + v^2 \qquad \textbf{(D-63)}$$

$$|v|^2 = \left|\frac{dF}{dz}\right|^2 \qquad \textbf{(D-64)}$$

With $|\,v\,|^2$ determined, the generalised Bernoulli equation can then be used to obtain the pressure in the flow.

D-1.6 Variation of Velocity in Vortex Flow

The Free Vortex region is considered in the variation of velocity in vortex motion. As shown in Figure D-5, consider a thin shell of air distance *r* away from the centre of rotation.

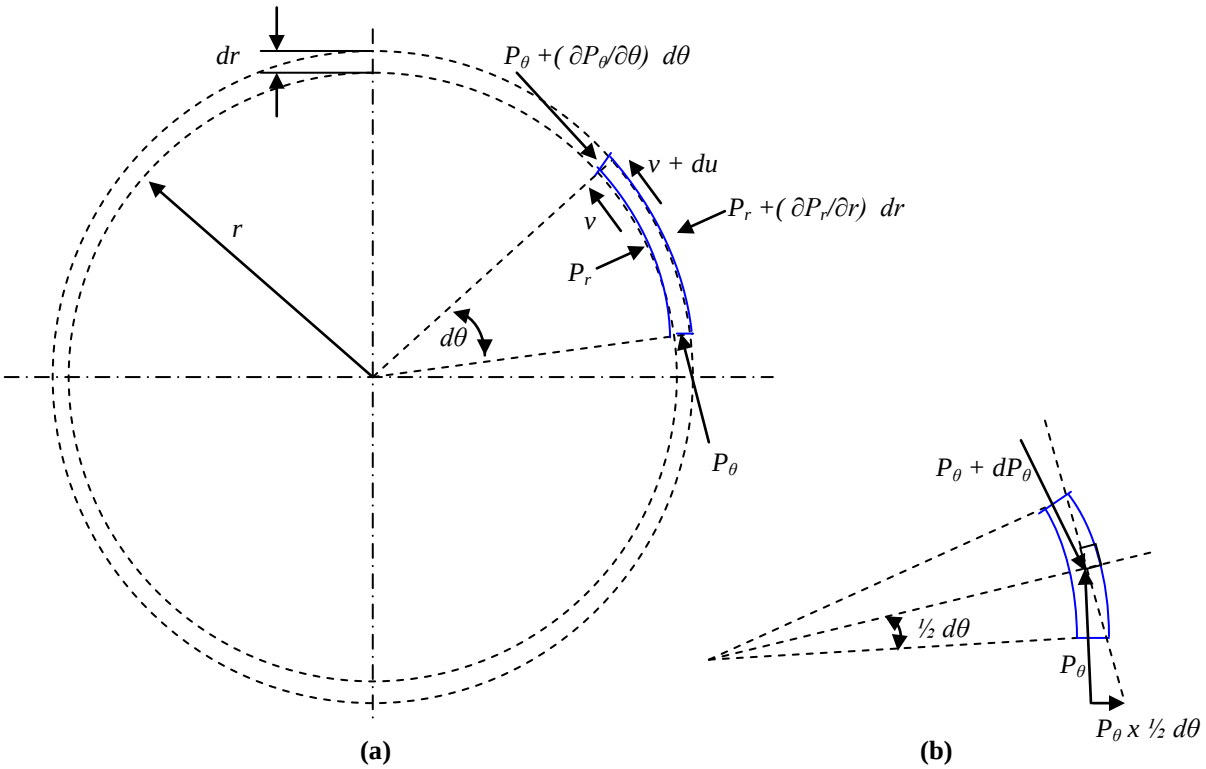

Figure D-5, Pressure in a free vortex, (a) at the distance *r* away from centre, (b) very small θ (Source: Post, D. [74])

Assuming that the flow condition depends only on *r*, then

$$\frac{\partial P_\theta}{\partial \theta} = 0 \qquad \textbf{(D-65)}$$

and assuming the average of the radial pressure P_r and $P_r + dP_r$ as the tangential pressure acting over the width *dr*, then

$$P_\theta = P_r + \frac{1}{2} dP_r \qquad \textbf{(D-66)}$$

Hence, for steady circulation, the radial forces balance is,

$$\sum F = P \cdot r d\theta - (P + dP)(r + dr)d\theta + 2(P + \frac{1}{2} dP) Sin \frac{d\theta}{2} dr = ma \qquad \textbf{(D-67)}$$

For small θ, sin θ = θ, hence

$$r dP d\theta - \frac{1}{2} dP dr d\theta = ma \qquad \textbf{(D-68)}$$

The centripetal acceleration of the fluid at steady circulation is

$$a = \frac{v^2}{r} \qquad \textbf{(D-69)}$$

The mass of the fluid element is

$$m = \rho\, r\, dr\, d\theta \qquad \textbf{(D-70)}$$

hence (D-65) can then be reduced to

$$dP(r - \frac{1}{2} dr) d\theta = (\rho r dr d\theta) \frac{v^2}{r} \qquad \textbf{(D-71)}$$

Assume ½ *dr* is negligible, then (D-71) is reduced to

$$r\,dP = \rho\, v^2\, dr \qquad \textbf{(D-72)}$$

From Bernoulli's equation, for an incompressible flow

$$P + \frac{1}{2}\rho v^2 = P + dP + \frac{1}{2}\rho(v + dv)^2 = P + dP + \frac{1}{2}\rho(v^2 + 2v\,dv + dv^2) \qquad \textbf{(D-73)}$$

which gives

$$dP = -\rho\, v\, dv \qquad \textbf{(D-74)}$$

and hence,

$$r\,dP = \rho\, v^2\, dr = -r\,\rho\, v\, dv$$
$$v\, dr + r\, dv = 0 \qquad \textbf{(D-75)}$$

Therefore, for a free vortex,

$$vr = const = C$$
$$v = \frac{C}{r} \qquad \textbf{(D-76)}$$

Since there is a singularity at the origin, therefore it is assumed that the air within the core rotates as a solid cylinder rotating at a uniform angular velocity. Hence the velocity profile of the simplified vortex can be seen as in Figure D-6.

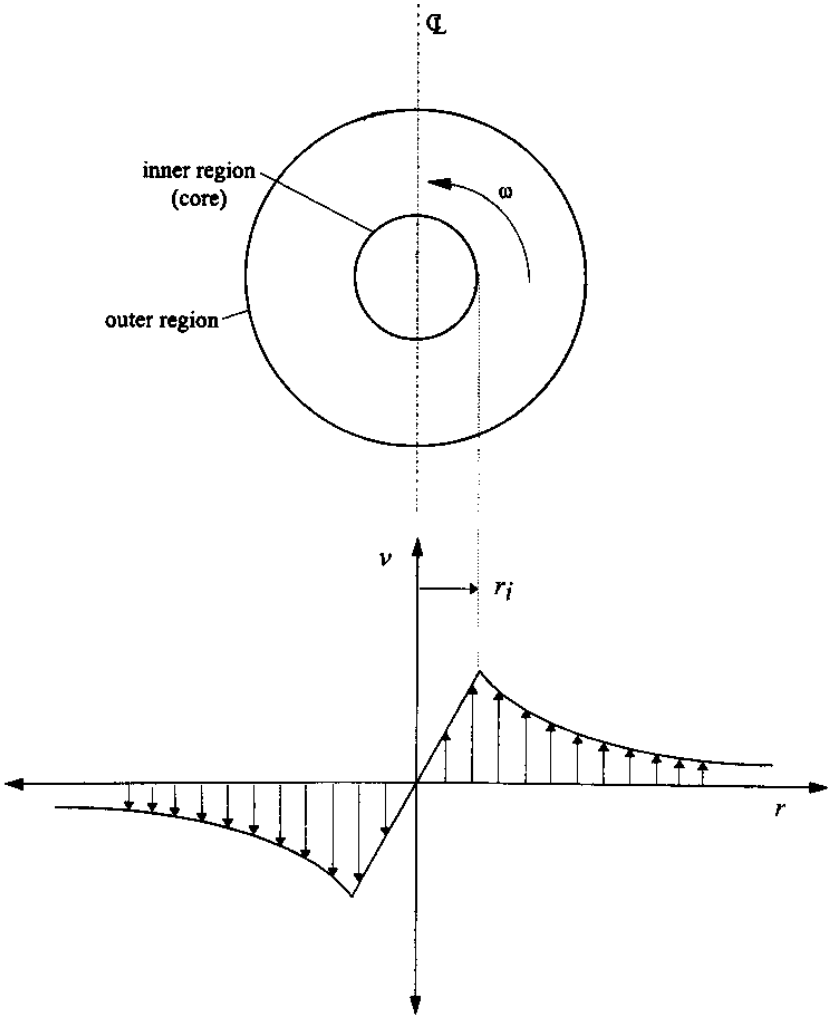

Figure D-6, Typical velocity distribution in a simplified vortex (Source: Patel, R. [72])

D-2 Vortex Motion

D-2.1 Free Vortex

From **Post, D. [74]**, in a free vortex, from equation (D-76),

$$v_r = 0 \tag{D-77}$$

$$v_\theta \propto \frac{1}{r} = \frac{1}{r}\frac{\partial \varphi}{\partial \theta} = \frac{C}{r} \tag{D-78}$$

From **Post, D. [74]**, for Cauchy's Integral Theorem and equation (D-45) considering the complex velocity, the circulation about any contours which do not enclose the origin is

$$\Gamma = \oint_{C_1} \underset{\leftarrow}{v} \cdot dl$$

$$\Gamma = \sum \oint_{C_i} v_\theta dl = \sum \oint_{C_i} v_\theta dl$$

$$\Gamma = \sum \oint_{C_i} v_{\theta_2} r_2 d\theta - v_{\theta_1} r_1 d\theta = \sum \oint_{C_i} \left(\frac{C}{r_2} r_2 - \frac{C}{r_1} r_1\right) = 0 \tag{D-79}$$

Hence, for a contour that encloses the origin (where there is a singularity)

$$\Gamma = \oint_C v_\theta dl = \int_0^{2\pi} v_\theta r d\theta = \int_0^{2\pi} C d\theta$$

$$\Gamma = 2\pi C \tag{D-80}$$

However,

$$\oint \underset{\leftarrow}{v} \cdot \underset{\leftarrow\leftarrow}{ds} = \iint \underset{\leftarrow}{G} \cdot \underset{\leftarrow\leftarrow}{dA} \tag{D-81}$$

therefore, the vorticity is zero everywhere except at $r = 0$, where it is indeterminate. As from equation (D-78),

$$\varphi = C\theta = \frac{\Gamma}{2\pi}\theta \tag{D-82}$$

where $C = \Gamma / 2\pi$ is called the strength of the vortex.

The complex potential of a free vortex is

$$F = \frac{i\Gamma}{2\pi}\ln z = \frac{i\Gamma}{2\pi}\ln r l^{i\theta}$$

$$F = \frac{i\Gamma}{2\pi}\left[\ln r + i\theta\right] = -\frac{\Gamma\theta}{2\pi} + \frac{i\Gamma}{2\pi}\ln r \qquad \textbf{(D-83)}$$

Hence,

$$\varphi = -\frac{\Gamma\theta}{2\pi} \qquad \textbf{(D-84)}$$

$$\psi = \frac{\Gamma}{2\pi}\ln r \qquad \textbf{(D-85)}$$

$$\left|\underset{\leftarrow}{v}\right|^2 = \left|\frac{dF}{dz}\right|^2 = \left|\frac{i\Gamma}{2\pi z}\right|^2 = \left\{\left|\frac{i\Gamma}{2\pi}\right|\left|\frac{1}{z}\right|\right\}^2 = \left(\frac{\Gamma}{2\pi r}\right)^2 \qquad \textbf{(D-86)}$$

Since the flow is irrotational, therefore the Bernoulli's equation (D-35) can be applied, and hence,

$$P = \frac{1}{2}\rho v^2 = P_o$$

$$P = P_o - \frac{1}{2}\rho\frac{\Gamma^2}{4\pi^2 r^2} = P_o - \frac{\rho\Gamma^2}{8\pi^2 r^2} \qquad \textbf{(D-87)}$$

D-2.2 Forced Vortex

Figure D-7 shows that the fluid within the forced vortex region was considered as a rigid body, i.e. $v_\theta = \omega r$.

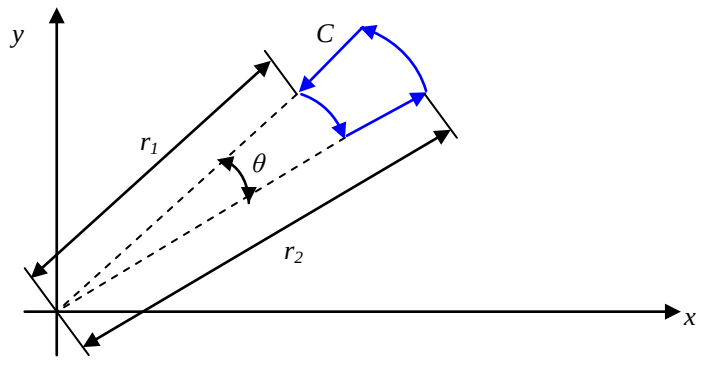

Figure D-7, Element of fluid in forced vortex (Source: Post, D. [74])

and can be expressed as follows,

$$\oint_C \underset{\leftarrow}{v} \cdot \underset{\leftarrow}{ds} = \int (v_{\theta_2} r_2 - v_{\theta_1} r_1) d\theta \quad \textbf{(D-88)}$$

$$\Gamma = \omega\theta(r_2^2 - r_1^2) \quad \textbf{(D-89)}$$

then the area enclosed by the contour is

$$A = \int_{r_1}^{r_2} (\theta r) dr = \frac{\theta}{2}(r_2^2 - r_1^2) \quad \textbf{(D-90)}$$

Substituting equation (D-90) into (D-89), then

$$\Gamma = 2\omega A \quad \textbf{(D-91)}$$

and for

$$\underset{\leftarrow}{G} = G_z \quad \textbf{(D-92)}$$

$$u = -\omega y \quad \textbf{(D-93)}$$

$$v = \omega x \quad \textbf{(D-94)}$$

then from equation (D-22) and (D-26), hence

$$G_z = \frac{\partial v}{\partial x} - \frac{\partial u}{\partial y} = 2\omega \quad \textbf{(D-95)}$$

In a physical vortex such as a tornado, the air circulating in the core in a circular path by due to the effect of the radial pressure gradient in the forced vortex **[73,74]**. Therefore a minimum pressure must be at the centre and increase outward. Hence the velocity must be zero at the centre, which contradicts Bernoulli's equation. For the equilibrium of an element with volume per unit length *V*,

$$V = r\, dr\, d\theta \quad \textbf{(D-96)}$$

The inward force due to the radial pressure gradient on the element is $dP\ (r - \frac{1}{2}\, dr)\, d\theta$, and assuming $\frac{1}{2}\, dr$ is insignificant compared to *r*, then equation (D-68) can be reduced to

$$rdPd\theta = ma \tag{D-97}$$

and for

$$dP = (\frac{\partial P}{\partial r})dr \tag{D-98}$$

$$\omega = \frac{v}{r} \tag{D-99}$$

$$r\omega^2 = \frac{v^2}{r} \tag{D-100}$$

and substitute (D-98) and (D-100)into (D-97)

$$r(\frac{\partial P}{\partial r})drd\theta = \rho rdrd\theta\frac{v^2}{r}$$
$$\frac{dP}{dr} = \rho\omega^2 r$$
$$P = \frac{1}{2}\rho\omega^2 r^2 + C \tag{D-101}$$

With equation (D-87), the pressure on the boundary of the free vortex can determine which is the outer surface of the core, and from this the constant C can then be determined. Let *a* be the distance from the origin to the outer surface of the core, hence from equations (D-101) and (D-87)

$$P_a = P_o - \frac{\Gamma^2\rho}{8\pi^2 a^2} = \frac{1}{2}\rho\omega^2 a^2 + C$$
$$C = P_o - \frac{\rho\Gamma^2}{8\pi^2 a^2} - \frac{1}{2}\rho\omega^2 a^2 \tag{D-102}$$

therefore, inside the core

$$P = P_o - \frac{\rho\Gamma^2}{8\pi^2 a^2} - \frac{1}{2}\rho\omega^2(a^2 - r^2) \tag{D-103}$$

Since $\Gamma = 2\pi rv$ is on or outside of the vortex core, Γ can be evaluated on the core surface from the flow condition within the core, where $r = a$, hence

$$\Gamma = 2\pi a v = 2\pi a(\omega a) = 2\pi\omega a^2 \quad \textbf{(D-104)}$$

$$\omega = \frac{\Gamma}{2\pi a^2} \quad \textbf{(D-105)}$$

Substituted back into (D-103), then

$$P = P_o - \frac{\rho\Gamma^2}{8\pi^2 a^2}\left[2 - (\frac{r}{a})^2\right] \quad \textbf{(D-106)}$$

a minimum occurs at r = 0, i.e.

$$P_{\min} = P_o - \frac{\rho\Gamma^2}{4\pi^2 a^2} \quad \textbf{(D-107)}$$

From Figure D-8, the pressure drop between infinity and the centre of the vortex, half occurs from infinity to the core surface and the other half occurs in the core itself.

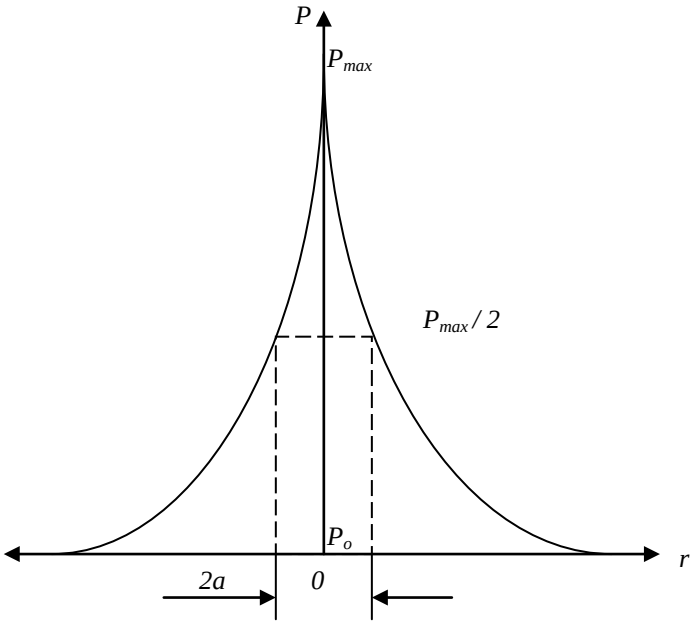

Figure D-8, Pressure distribution across a vortex.

D-3 Lifting Force within a Vortex

From **Lee, C. R. A. [73] and Post, D. [74],** the force acting on a finite particle can be obtained from the findings from pressure distribution in equation (D-106). Consider a particle of radius r_p situated at the foot of the vortex

$$F = \int_0^{r_p} P 2\pi r dr \qquad \textbf{(D-108)}$$

Substituting for *P* from equation (C-106) and

$$F = \int_0^{r_p} (P_o - \frac{\rho\Gamma^2}{4\pi^2 a^2}(2 - (\frac{r}{a})^2))2\pi r dr = P_o \pi r_p^2 - \frac{\rho\Gamma^2 r_p^2}{4\pi a^2} + \frac{\rho\Gamma^2 r_p^4}{16\pi a^4} \qquad \textbf{(D-109)}$$

When the particle is at the point of being lifted by the vortex, from **Post, D. [74]**, the following equality holds.

Force on the lower surface of the particle due to ambient conditions - *Force on upper surface of particle due to vortex* = *Weight of particle.*

Hence,

$$P_o \pi r_p^2 - F = \frac{4}{3}\pi r_p^3 \rho_p g \qquad \textbf{(D-110)}$$

Equating vertical forces on the particle

$$\frac{\rho_p g r_p}{\rho_a \omega_p^2 r_p^2} = \frac{3}{4}(1 - \frac{r_p^2}{4r_i^2})\frac{r_i^2}{r_p^2} \qquad \textbf{(D-111)}$$

APPENDIX E – Process Selection

Process Selection Chart

Swarf Transportation Methods

Sheet 1 of 2

Concept No.	*Functional (geometry, motion, load paths, compatibility, control)*	*Manufacturing, Quality, & Life Cycle (Production, purchase, assembly, waste)*	*Ergonomic, Ecological, & Safety (user, environment, appeal)*	*Feasibility (potential, confidence)*	*Economics & Timing (materials, manufacturing, operational)*	*Information (cooperation, expertise, experience)*	*Comments*	*Score*	*Develop Further*	*Eliminate*	*Get more Information*
P1		+	+		+	+	ADV: simple and easy to use and easy to maintain. DAV: magnetic surrounding ferric base components	**4**	+		
P2		+	+		+	+	ADV: simple and easy to use and easy to maintain. DAV: complete de-magnetise of swarf takes time and may not be successful.	**4**	+		
P3	+	+	+	+	+	+ +	ADV: simple easy construction. DAV: bulky.	**7**	+		
P4	+	+	+	+	+	+ +	ADV: simple easy construction. DAV: bulky.	**7**		+	
P5	+ +	+	+	+	+	+ +	ADV: portable and easy to use. DAV: only allow flow velocity otherwise filter medium may be damaged.	**8**	+		
P6	+ +	+ +		+	+	+ +	ADV: simple and easy to use, and easy to maintain. DAV: hopper swinging when suspended.	**8**		+	
P7	+ +	+ +	+	+	+	+ +	ADV: simple and easy to use, and easy to maintain. DAV: hard to control when rotating over 90°	**9**		+	
P8	+ +	+ +	+ +	+ +	+	+ +	ADV: simple and easy to use, and easy to maintain. DAV: complex analysis.	**11**	+		
P9	+ +	+ +	+ +	+ +	+	+ +	ADV: simple and easy to install. DAV: more complex piping.	**11**	+		
P10	+	-		+	-	+ +	ADV: simple and easy to install. DAV: large torque required high change of gear ratio.	**2**		+	
P11	+ +	+ +	+ +	+ +		+ +	ADV: simple to construct no requirement to lift the hopper. DAV: large area to cover.	**10**	+		

Key: (+) yes + 1, (-) no -1, ( ) neutral 0, (?) insufficient information
ADV: Advantage, DAV: Disadvantage.

Figure E1, Process selection for the various transportation methods.

Process Selection Chart

Swarf Transportation Methods

Sheet 2 of 2

Concept No.	*Functional (geometry, motion, load paths, compatibility, control)*	*Manufacturing, Quality, & Life Cycle (Production, purchase, assembly, waste)*	*Ergonomic, Ecological, & Safety (user, environment, appeal)*	*Feasibility (potential, confidence)*	*Economics & Timing (materials, manufacturing, operational)*	*Information (cooperation, expertise, experience)*	*Comments*	*Score*	*Develop Further*	*Eliminate*	*Get more Information*
P12		+	+	-		-	ADV: deeper penetration of the swarf from the surface. DAV: insufficient knowledge.	**0**		+	
P13	+	-	+	+		+	ADV: simple to construct. DAV: requires large modification on existing equipments.	**3**		+	
P14	+	+ +	+ +	+ +		+	ADV: simple and easy to construct. DAV: bulky and requires long operation time.	**8**	+		
P15	+	+ +	+ +	-	- -	+	ADV: simple to construct. DAV: separation efficiency largely depends on particle size, high wear on equipments.	**3**		+	
P16	+	+ +	+ +		- - -	+	ADV: high separation efficiency can be achieved. DAV: an additional drying process may be required to prevent rusting to occur.	**3**		+	
P17	+	+	+	+		+	ADV: prevent damage on fan unit. DAV: an absolute requirement in pneumatic transportation method.	**5**	+		

Key: (+) yes + 1, (-) no -1, ( ) neutral 0, (?) insufficient information
ADV: Advantage, DAV: Disadvantage.

Figure E2, Concept selection for various transportation methods.

Since for a complete transportation method requires 4 essential steps: lifting (hopper and / or particles), separating, discharging, and filtering, therefore the weighting for the most feasible transportation method will grades base on the summation of best process scored in each steps, as shown in Table E1. However, since for the pneumatic transportation method, there is an additional filtering process required to prevent damage on fan unit, therefore the score for the additional process will not be considered in the weighting.

Table E1, Overall weighting of various transportation methods.

Steps	**Transportation Method**		
	Electromagnetic	Mechanical	Pneumatic
Lifting	4	11	10
Separating	4	11	8
Discharging	7	7	7
Filtering	8	8	8
Total Score	23	37	33

APPENDIX F – Concept Selection

Concept Selection Chart

Sub-System 1&2: Lifting / Rotating & Interlock Mechanism

Sheet 1 of 1

Concept No.	*Functional (geometry, motion, load paths, compatibility, control)*	*Manufacturing, Quality, & Life Cycle (Production, purchase, assembly, waste)*	*Ergonomic, Ecological, & Safety (user, environment, appeal)*	*Feasibility (potential, confidence)*	*Economics & Timing (materials, manufacturing, operational)*	*Information (cooperation, expertise, experience)*	*Comments*	*Score*	*Develop Further*	*Eliminate*	*Get more Information*
A1	+	-	-	+	+	+	ADV: very low manufacturing cost. DAV: poor utilisation of factory facility, and man power. Note: this was the original process within the company.	**2**		+	
A2	+	+ +	-	+	+	+	ADV: low manufacturing cost and easy to use. DAV: swinging motion occur when suspended in air.	**5**		+	
B1	+	+		+ +	+	+ +	ADV: easy to manufacture and operate. DAV: safety concern associate with the access area.	**7**		+	
B2	+		+	+	+	+ +	ADV: kept the load away from the possible access area. DAV: complex hydraulic control, and manufacturing difficulty.	**6**			+
B3	+	+		+ +		+ +	ADV: easy to manufacture and operate. DAV: safety concern associate with the access area.	**6**		+	
C1	+	+ +	+ +	+ +	+	+ +	ADV: kept the load away from the possible access area. DAV: additional load on structure due to deflection.	**10**	+		
C2	+	+ +	+ +	+ +		+ +	ADV: kept the load away from the possible access area. DAV: additional load on structure due to deflection.	**9**		+	
D1			+	+		+	ADV: simple spring control mechanism. DAV: poor control and feedback, high machining cost involves	**3**		+	
D2		+ +	+	+	+ +	+	ADV: simple solenoid control mechanism, easy construction. DAV: insufficient feedback to indicates the status.	**7**		+	
D3	+ +	+ +	+ +	+	+	+	ADV: multi-stage feed and control ensure high safety requirement has reached. DAV: high material cost.	**9**	+		
E1	+	+ +	+ +	+ +	+ +	+	ADV: simple construction and easy adjustment. DAV: damage may occur due to heavy impacts.	**10**	+		

Key: (+) yes + 1, (-) no -1, ( ) neutral 0, (?) insufficient information
ADV: Advantage, DAV: Disadvantage.

Figure F1, Concept selection for the lifting / rotating & interlock mechanism.

Concept Selection Chart

Sub-System 3,4, & 5: Lid, Lid Lock, Discharge Control Valve, & Filter Mechanism

Sheet 1 of 1

Concept No.	*Functional (geometry, motion, load paths, compatibility, control)*	*Manufacturing, Quality, & Life Cycle (Production, purchase, assembly, waste)*	*Ergonomic, Ecological, & Safety (user, environment, appeal)*	*Feasibility (potential, confidence)*	*Economics & Timing (materials, manufacturing, operational)*	*Information (cooperation, expertise, experience)*	*Comments*	*Score*	*Develop Further*	*Eliminate*	*Get more Information*
F1		+	+	+	+	+ +	ADV: simple construction. DAV: bulky, hard to keep the thickness down which might interfere with other structures.	**6**		+	
F2	-	+	+	+	+	+ +	ADV: simple construction, very robust. DAV: structure interferences may occur.	**5**		+	
F3	+	+	+	+	+	+ +	ADV: simple construction, very robust DAV: smaller area available to create an opening tube connection.	**7**	+		
G1	+	+	+	+	+	+ +	ADV: simple and easy to operates DAV: requires additional tools to operate.	**7**		+	
G2	+	+	+ +	+	+	+ +	ADV: simple and easy to operate DAV: bulky.	**8**	+		
H1	+	+	+	+	+	+	ADV: easy to control DAV: possible damage on pneumatic actuator, and leakage.	**6**		+	
H2		+	+		+	+	ADV: good valve mechanism protection DAV: possible blockage in the retraction stroke.	**4**		+	
H3	+ +	+	+	+ +	+	+	ADV: easy to control DAV: possible damage on pneumatic actuator.	**8**	+		
I1	+	+ +	+	+ +	+	+ +	ADV: large settlement space. DAV: bulky.	**9**		+	
I2	+ +	+	+ +	+ +	+	+ +	ADV: small compact size. DAV: more machining requires.	**10**	+		

Key: (+) yes + 1, (-) no -1, ( ) neutral 0, (?) insufficient information
ADV: Advantage, DAV: Disadvantage.

Figure F2, Concept selection for lid, lid lock, control valve and filter mechanism.

Conceptual design work sheet

The transportation mechanism

Requirements	Contributing Factors	Current Status: Good	Current Status: Marginal	Current Status: Poor	Required Action: Proceed	Required Action: Revise	Required Action: N/A
Functional	Overall geometry	■	□	□	■	□	□
	Motion of parts	■	□	□	■	□	□
	Forces involved	■	□	□	■	□	□
	Energy needed	■	□	□	■	□	□
	Materials to be used	□	□	□	□	□	■
	Control system	□	□	□	□	□	■
	Information flow	□	□	□	□	□	■
Safety	Operational	■	□	□	■	□	□
	Human	■	□	□	■	□	□
	Environmental	■	□	□	■	□	□
Quality	Quality assurance	□	■	□	■	□	□
	Quality control	□	■	□	■	□	□
	Reliability	■	□	□	■	□	□
Manufacturing	Production of components	□	■	□	■	□	□
	Purchases of components	■	□	□	■	□	□
	Assembly	□	■	□	■	□	□
	Transport	□	■	□	■	□	□
Timing	Design schedule	□	■	□	■	□	□
	Development schedule	□	■	□	■	□	□
	Production schedule	□	□	■	□	■	□
	Delivery schedule	□	□	■	□	■	□
Economic	Marketing costs	□	□	□	□	□	■
	Design costs	□	□	□	□	□	■
	Development costs	□	■	□	■	□	□
	Manufacturing costs	□	■	□	■	□	□
	Distribution costs	□	□	□	□	□	■
Ergonomic	User needs	□	■	□	■	□	□
	Ergonomic design	□	■	□	■	□	□
	Cybernetic design	□	□	■	□	■	□
Ecological	Material selection	■	□	□	■	□	□
	Working fluid selection	■	□	□	■	□	□
Aesthetic	Customer appeal	□	■	□	■	□	□
	Fashion	□	□	□	□	□	■
	Future expectation	□	□	□	□	□	■
Life cycle	Distribution	□	□	□	□	□	■
	Operation	□	■	□	■	□	□
	Maintenance	■	□	□	■	□	□
	Disposal	□	□	□	□	□	■

Figure F3, Conceptual design worksheet for the transportation system design, (Source: Hales, C. [88])

Embodiment design work sheet

The transportation mechanism

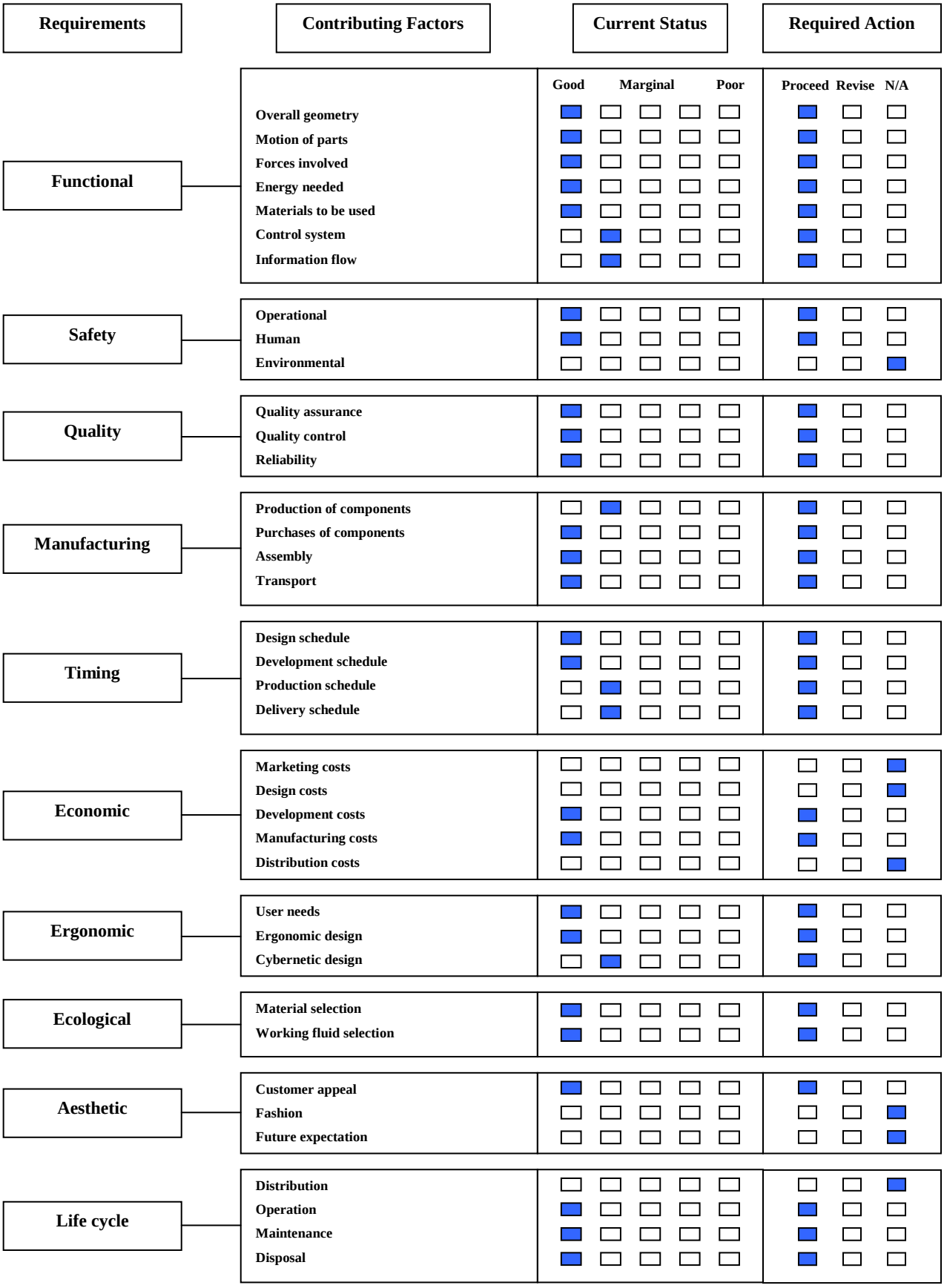

Figure F4, Embodiment design worksheet for the transportation system design, (Source: Hales, C. [88])

Detail design work sheet

The transportation mechanism

Requirements	Contributing Factors	Current Status: Good	Marginal	Poor	Required Action: Proceed	Revise	N/A
Functional	Overall geometry	■	□	□	□	□	■
	Motion of parts	■	□	□	□	□	■
	Forces involved	■	□	□	□	□	■
	Energy needed	■	□	□	□	□	■
	Materials to be used	■	□	□	□	□	■
	Control system	■	□	□	□	□	■
	Information flow	■	□	□	□	□	■
Safety	Operational	■	□	□	□	□	■
	Human	■	□	□	□	□	■
	Environmental	□	□	□	□	□	■
Quality	Quality assurance	■	□	□	□	□	■
	Quality control	■	□	□	□	□	■
	Reliability	■	□	□	□	□	■
Manufacturing	Production of components	■	□	□	□	□	■
	Purchases of components	■	□	□	□	□	■
	Assembly	■	□	□	□	□	■
	Transport	■	□	□	□	□	■
Timing	Design schedule	■	□	□	□	□	■
	Development schedule	■	□	□	□	□	■
	Production schedule	□	□	□	□	□	■
	Delivery schedule	□	□	□	□	□	■
Economic	Marketing costs	□	□	□	□	□	■
	Design costs	■	□	□	□	□	■
	Development costs	■	□	□	□	□	■
	Manufacturing costs	□	□	□	□	□	■
	Distribution costs	□	□	□	□	□	■
Ergonomic	User needs	■	□	□	□	□	■
	Ergonomic design	■	□	□	□	□	■
	Cybernetic design	□	■	□	□	□	■
Ecological	Material selection	■	□	□	□	□	■
	Working fluid selection	■	□	□	□	□	■
Aesthetic	Customer appeal	■	□	□	□	□	■
	Fashion	□	□	□	□	□	■
	Future expectation	□	□	□	□	□	■
Life cycle	Distribution	□	□	□	□	□	■
	Operation	■	□	□	□	□	■
	Maintenance	■	□	□	□	□	■
	Disposal	■	□	□	□	□	■

Figure F5, Detail design worksheet for the transportation system design, (Source: Hales, C. [88])

APPENDIX G – Operating Procedure

The hopper is aboard on the trolley after the oil recycling process, and it is required to be manually guided to the transportation system, as shown in Figure G-1.

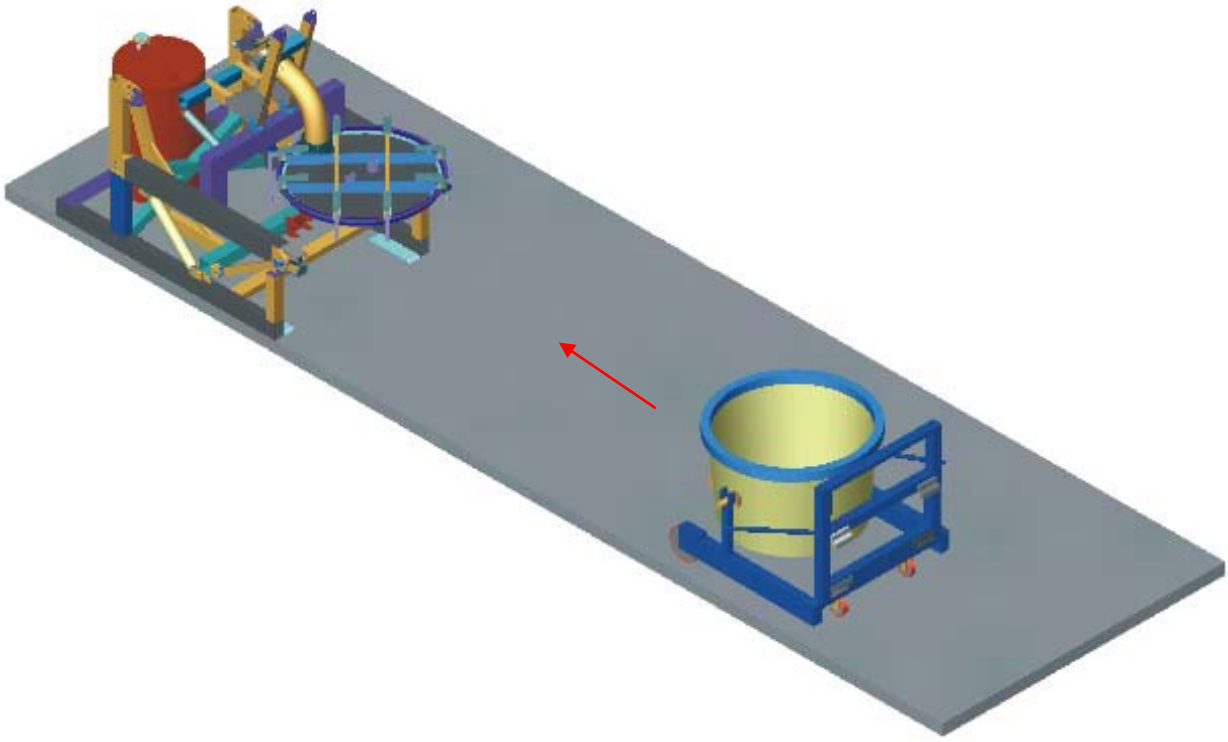

Figure G-1, Hopper aboard on trolley moving towards transportation system

The operating procedures are as follow:

1) Power up the transportation system before the trolley and hopper is engaged. The support rods on the hopper make contacts with the limit switches at different positions as they move through the interlock (Refer to Chapter 5.2).
2) Once the hopper and trolley is in position, the support rods are now well secured by the interlock system, and the hopper lid can then be lowered by operating the 8" hydraulic actuator; however the lid is required to be manually guided to fit onto the hopper.
3) Disengage the chains which is attached on the lid joints, then fully retracts the 8" hydraulic actuator, as shown in Figure G-2.
4) Manually set the lid locks to locking position.
5) Attach the filter onto the outlet hole of the drum, and adjust the support legs to make the filter stand up well.

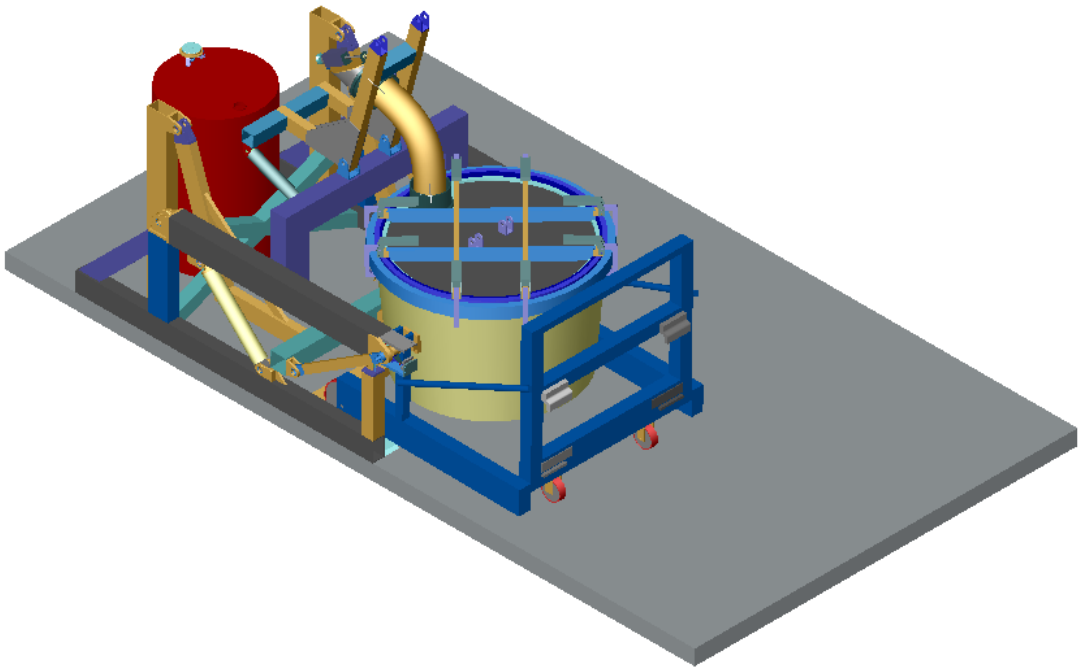

Figure G-2, Hopper engaged into the transportation system with lid attached.

6) Operate the 14” hydraulic actuators to lift the hopper up from the trolley, and the hopper undergoes 135° rotation when the actuator is fully extended, as shown in Figure G-3.

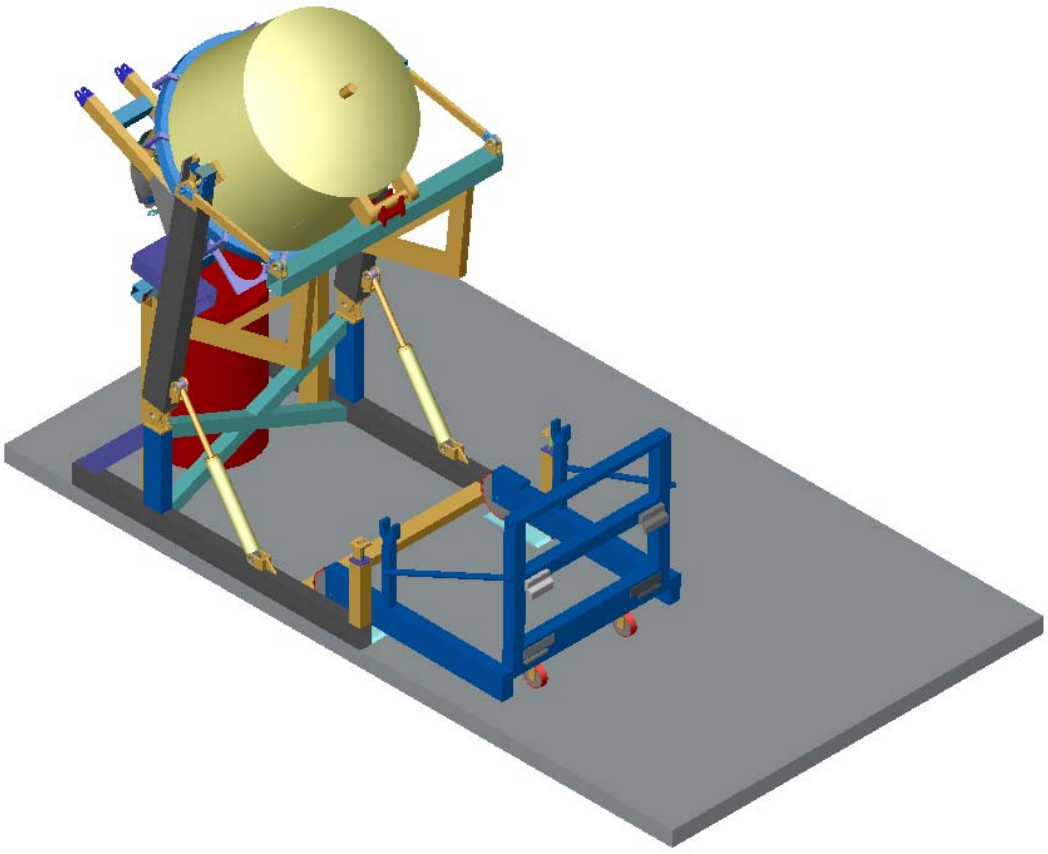

Figure G-3, Hopper rotate 135° when 14” hydraulic actuator is fully extended

6) Manually attach the discharge valve to the inlet port of the barrel, and start the discharging process.
7) Disengage the connection between the valve and inlet port of the barrel when change of barrel takes place. Lower the hopper down slightly and then manually move the barrel out of the loading zone.
8) Reposition the hopper back to discharge position when a new empty barrel is in place.

APPENDIX H – Logic Control System

By combining the flow diagram from Interlock system (Refer to Chapter 5.2), the hydraulic circuit (Refer to Chapter 5.6), and the Pneumatic circuit (Refer to Chapter 5.4), an overall control flow diagram can be formed, as shown in Figure H-1.

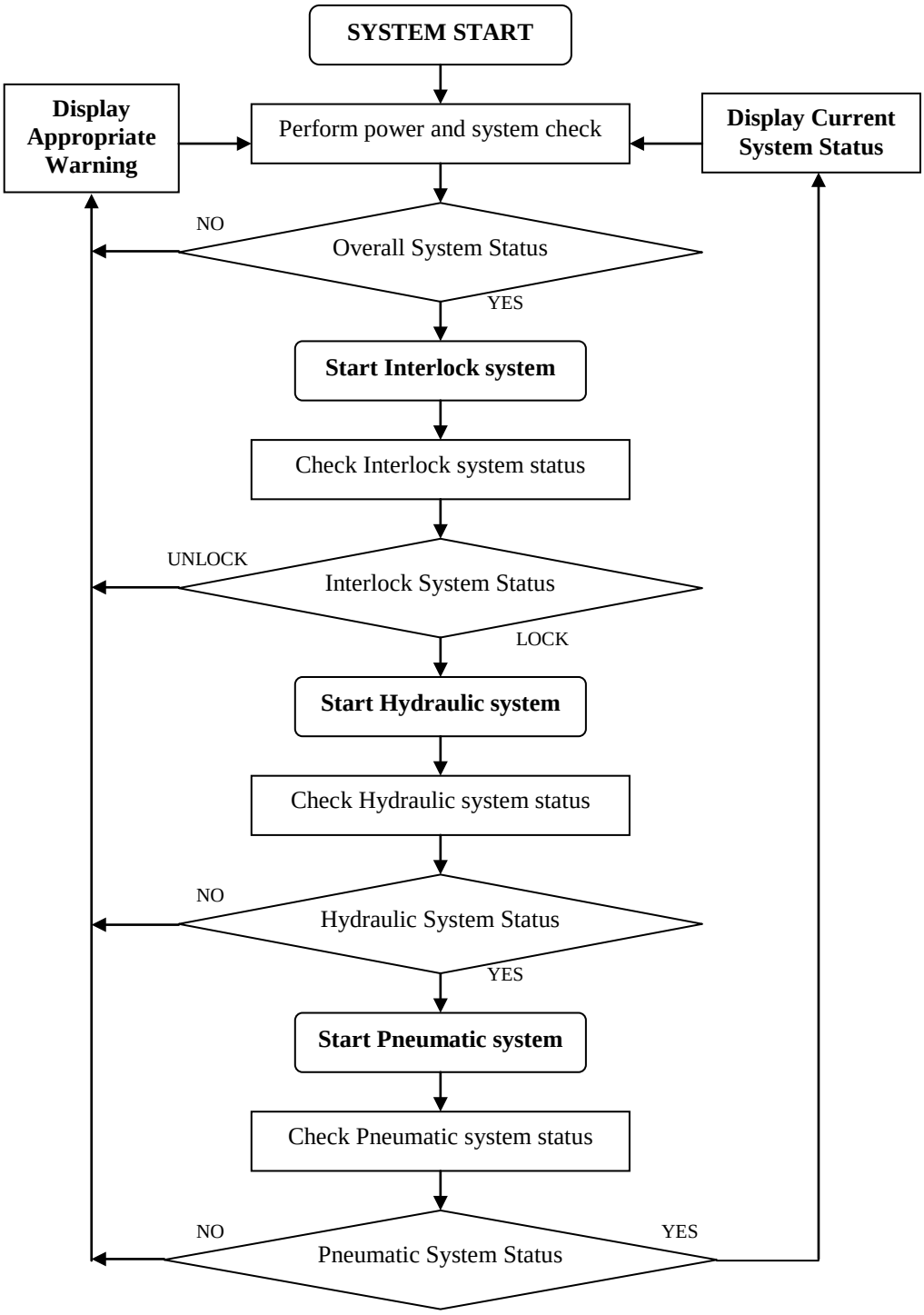

Figure H-1, Logic flow diagram of the overall system

APPENDIX I – Detail Drawing of Test Rig

Appendix I: Detail Drawing of the Test Rig

Appendix I: Detail Drawing of the Test Rig

Appendix I: Detail Drawing of the Test Rig

Appendix I: Detail Drawing of the Test Rig

Appendix I: Detail Drawing of the Test Rig

Appendix I: Detail Drawing of the Test Rig

APPENDIX J – Detail Drawing of Transportation System